Viral evasion of the MHC class I antigen presentation pathway

Patrique Praest

Viral evasion of the MHC class I antigen presentation pathway

Patrique Praest

Viral evasion of the MHC class I antigen presentation pathway
PhD thesis, Utrecht University, the Netherlands

Author: Patrique Praest
Cover design: Patrique Praest and Stijn Nering Bögel (https://www.stijnneringbogel.nl)
Lay-out: Patrique Praest
Printed by: Proefschriftmaken (https://www.proefschriftmaken.nl)
ISBN: 978-94-6380-800-2

Printing of this thesis was financially supported by the Infection and Immunity Utrecht and the University Medical Center Utrecht.

Viral evasion of the MHC class I antigen presentation pathway

It's a T(r)AP

Het ontwijken van MHC klasse I-gemedieerde antigeenpresentatie door virussen
(met een samenvatting in het Nederlands)

Proefschrift

ter verkrijging van de graad van doctor aan de Universiteit Utrecht
op gezag van de rector magnificus, prof.dr. H.R.B.M. Kummeling,
ingevolge het besluit van het college voor promoties
in het openbaar te verdedigen op

woensdag 13 mei 2020 des middags te 12.45 uur

door

Thomas Patrique Praest

geboren op 15 oktober 1991
te Bocholt, Duitsland

Promotor:
Prof. dr. E.J.H.J. Wiertz

Copromotor:
Dr. ir. R.J. Lebbink

Commissie:
Prof. dr. F.G. Förster
Prof. dr. J.A. Killian
Prof. dr. W. Stoorvogel
Prof. dr. I. Drexler
Dr. A.M. Liaci

Paranimfen:
Hendrik de Buhr, MSc
Lisette Scheepmaker

Table of Contents

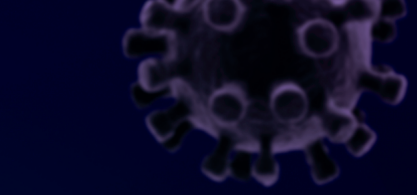

1 General Introduction

P. Praest

Herpesviruses

While the origin of viruses is still under debate up to now, it is assumed that the family of herpesviridae evolved approximately 200 million years ago [1]. This virus family is composed of more than 130 viruses. Based on their biological and phylogenetical properties, they are divisible into three subfamilies: α-, β- and γ-herpesviridae [2]. Currently, nine herpesviruses have been identified whose natural host is the human: herpes simplex virus type 1 and 2 (HSV-1 and HSV1, also referred to as human herpesvirus 1 and 2 (HHV-1 and HHV-2)), varicella-zoster virus (VZV or HHV-3), Epstein-Barr virus (EBV or HHV-4), human cytomegalovirus (HCMV or HHV-5), human herpesvirus 6A, 6B and 7 (HHV-6A/B and HHV-7) and Kaposi's sarcoma-associated herpesvirus (KSHV or HHV-8) [3].

The worldwide seroprevalence of these nine human herpesviruses in the population ranges from 60-95% [4], but may vary depending on the geographic location, age and socioeconomic status. For example, while HCMV is carried by approximately 36-77% of the population in the US, Australia and Europe, the seroprevalence in developing countries can reach up to 100% in adults [5]. In developing countries, a high percentage of children is infected with VZV, EBV and HHV-6 at an early age. This high rate is explained by overcrowding, early attendance at kindergarten and low hygiene standards aiding in earlier transmission of herpesviruses [6].

These human herpesviruses are associated with a large variety of diseases [7]. Usually, primary infections remain asymptomatic and are often unnoticed in healthy individuals. However, reactivations in healthy individuals as well as infections of immunocompromised people can lead to severe diseases. HSV-1 is commonly known for herpes simplex labialis (cold sores), but this virus may also cause keratitis and encephalitis [8]. HSV-2 mostly causes genital herpes, although both HSV types may infect any region of the human body [8, 9]. During primary infection, varicella zoster virus can lead to acute varicella or "chickenpox", whereas during reactivation it can result in herpes zoster or "shingles" [10]. Diseases associated with EBV infections are mononucleosis or 'kissing disease', but also malignancies like Hodgkin's Lymphoma (HL), Burkitt's Lymphoma (BL), Gastric Carcinoma (GC) or Post-Transplant Lymphoproliferative Disorder (PTLD) [11, 12]. Primary HCMV infections during pregnancy can cause serious complications in newborns, leading to extensive damage to the liver and the brain [13]. HHV-6, a virus sharing genetic similarities with HCMV, is causing exanthema subitum or roseola infantum in young children and in rare cases it can also lead to meningitis or encephalitis [14, 15]. HHV-7 causes skin conditions like roseola infantum, but with a lower frequency compared to HHV-6. There are some indications that HHV-7 may play a role in encephalopathy and hepatitis, but further research is needed to confirm this [16, 17].

KSHV can cause several tumors, including Kaposi's sarcoma (KS), mostly occurring in immunocompromised patients [18].

Available treatments for herpesvirus infections predominantly target the productive phase of infection. These drugs are mainly nucleoside analogs that block replication of *herpesviridae*, but can therefore not tackle the latent virus and cannot clear the infection from the human body entirely [19, 20]. Resistance to these nucleoside analogs is an emerging problem for a successful treatment of herpesvirus infections [21, 22]. Most nucleoside analogues have the same target (DNA polymerases) and therefore mutant viruses resistant to one nucleoside analogue are also resistant to others [23]. An alternative to the current treatments could be to target the virus with the CRISPR/Cas9 genome editing system. With specific guide RNAs targeting essential viral genes it was proven that this system is able to block viral replication effectively or to eradicate the virus from infected cells entirely in some cases [24]. This new genome-engineering technique requires more research, but opens new possibilities for the development of new treatments [25].

Herpesvirus biology

All herpesviruses share a four-layered structure. They are comprised of the core, holding the large double-stranded (ds) DNA genome, which is surrounded by an icosahedral capsid. The capsid in turn is surrounded by the tegument that is ultimately encapsulated by a lipid bilayer called the viral envelope (see Figure 1a) [26]. Herpesviruses share key characteristics, but they also differ to a great extent. Their genomic size ranges from 125 kbp in the case of VZV to about 240 kbp for HCMV, and their nucleotide composition varies between 32% and 75% G+C content, depending on the virus species [27–29].

The life cycle of herpesviruses remains an important research topic due to its complexity and uniqueness among the different species of *herpesviridae*. The first crucial step in the life cycle of a virus is its entry into cells. For this, the virion needs to attach to its target cell. The tropism of the human herpesviruses differs, as do their entry receptors and replication steps. Hereunder, solely the life cycle of HCMV is discussed, as this virus is of particular interest for this thesis (see Figure 1b).

During the process of viral entry, HCMV glycoproteins interact with host receptors (stage 1 in Figure 1b) (e.g. NRP2 for epithelial cells or PDGFRα for fibroblasts), and ensure viral fusion or endocytosis into the cell (stage 2) [30, 31]. Like other herpesviruses, HCMV depends on the fusion proteins gB and gL for virus entry [32–34]. HCMV lacking either gB or gL were shown to be impaired in entering cells [32, 35]. After entry and uncoating, the virions are transported to the nucleus via the host microtubule machinery (3) [36].

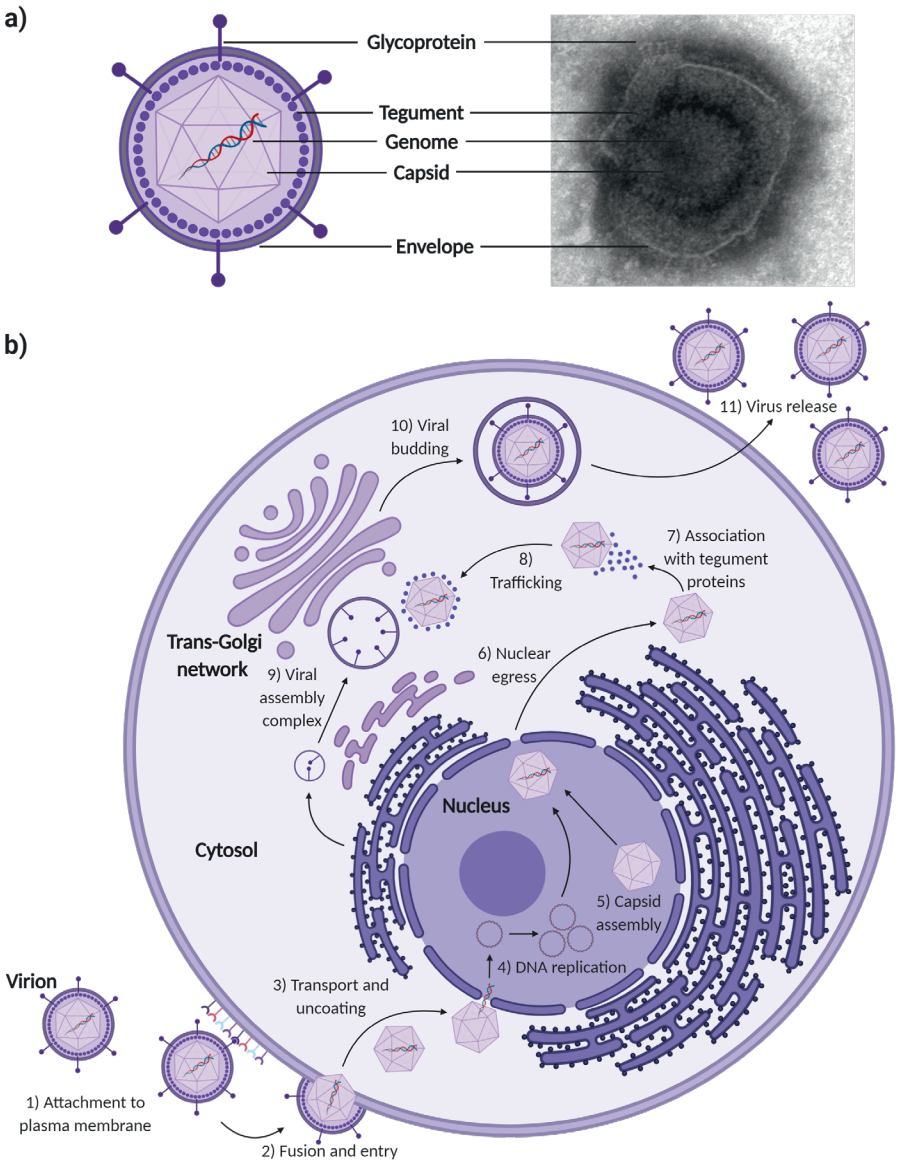

Figure 1: Herpesvirus architecture and life cycle (HCMV). A) All herpesviruses are built up by four structural components. The core of each virion consists of the double-stranded DNA genome that is surrounded by the capsid. The space between the capsid and the viral envelope is comprised of an amorphic protein substance called the tegument. The surface of a virion is covered by glycoproteins. Electron microscopy Image: courtesy of Marco Viveen (Medical Microbiology UMC Utrecht). B) The life cycle of HCMV. The first step of the life cycle is the binding of viral glycoproteins to cell surface receptors (1) after which the virion fuses to the cell membrane (2) or enters via endocytosis. After fusion, the viral capsid carrying the viral genome is transported from the membrane to the cell nucleus via cellular structures such as microtubules (3). At the nuclear membrane, the viral genome enters through the nuclear pores.

Figure 1 (continued). Next, viral gene transcription and translation is initiated for DNA replication (4) and capsid assembly (5). Capsids containing the viral genome then leave the nucleus (6) and tegument proteins associate with the capsids (7). Particles will be then transferred to the viral assembly complex (8). The assembly complex consists of components from the endoplasmic reticulum (ER), the Golgi apparatus and the endosomal machinery (9). The capsids acquire their viral envelope by budding through intracellular vesicles at the assembly complex (10) before these fully infectious particles are released from the cell via exocytosis (11).

Once the viral genome reaches the nucleus, viral transcription and genome replication are initiated (4). Tegument proteins regulate proper viral gene expression [37]. Newly synthesized virus-encoded proteins will hijack host cell-signaling pathways as well as the cellular metabolism to ensure viral replication [38, 39]. Viral capsids are then assembled in the nucleus (5). Subsequently, the viral genome is integrated into the capsids, before they egress through the nuclear membrane (6) into the cytosol where they associate with tegument proteins (7). These capsids are transported to the viral assembly complex (AC) (8). The AC is composed of the Golgi apparatus, the endosomal machinery and the endoplasmic reticulum (ER) (9). By budding, capsids acquire their viral envelope derived from intracellular vesicles (10) [40]. As a final step in the life cycle of HCMV, fully infectious particles are released via exocytosis (11).

Herpesvirus immune evasion

Herpesviruses are experts in tricking the human immune system, which is underlined by the fact that almost the entire adult population is infected with multiple herpesviruses [41, 42]. A considerable part of the large genome of herpesviruses is spent on genes that encode for proteins that manipulate the host's immune system by interfering with crucial steps of innate and adaptive immunity.

As part of the adaptive immune response, $CD8^+$ T-cells recognize peptides presented on the cell surface via the major histocompatibility complex class I (MHC class I) pathway, whereas $CD4^+$ T-cells recognize peptides presented via the MHC class II pathway. While MHC class II molecules are located mostly on antigen presenting cells and are loaded with exogenous peptide fragments in endolysosomal compartments, MHC class I molecules are expressed on nearly every nucleated cell and mostly present peptides from endogenous origin. In this thesis, the focus lies on the classical MHC class I antigen presentation pathway.

This pathway promotes the assembly and expression of MHC class I-peptide complexes at the cell surface. In uninfected cells, misfolded proteins are degraded by the proteasome. The resulting peptides enter the ER and are loaded onto MHC class I molecules by means of the peptide loading complex (PLC). These MHC I-peptide complexes travel via the Golgi

to the cell surface. Scanning by $CD8^+$ T cells allows detection of altered and/or foreign peptides. Upon infection, a fraction of viral proteins enters this route; when viral peptides are detected by $CD8^+$ T cells, the infected cell is destroyed.

Virtually every single step of this pathway is compromised by different herpesvirus proteins (see Chapter 3 Figure 1). The general outcome is a decrease in presentation of viral antigens at the cell surface, with cells escaping $CD8^+$ T-cell recognition and the virus ultimately being able to "hide". These interference mechanisms include the suppression of MHC class I synthesis, the retrotranslocation of MHC class I molecules to the cytosol for degradation by proteasomes, interference with proteasomal degradation of protein substrates, inhibition of peptide transport into the ER via the protein transporter associated with antigen processing (TAP), interference with MHC class I trafficking, the redirection of MHC class I molecules to lysosomes, an increase in endocytosis and lysosomal degradation of cell surface MHC class I, as well as interference with recognition of peptide-loaded MHC class I molecules on the cell surface by T cell receptors of $CD8^+$ T cells [43–45].

The PLC – a key factor in the MHC I pathway

The PLC is often referred to as the bottleneck of the MHC class I antigen presentation pathway. A defect in this complex results in empty MHC class I molecules and subsequently no antigen presentation on the cell surface. This highly important protein complex consists of the TAP heterodimer (TAP1 and TAP2), beta$_2$m (β_2m), MHC class I, Tapasin, endoplasmic reticulum-resident protein 57 (ERp57) and Calreticulin. The PLC is responsible for transporting peptide fragments from the cytosol into the ER and further loading these onto freshly synthesized MHC class I molecules [46, 47]. Due to the importance and complexity of the PLC, it has long been the focus of research. Cryo-electron microscopy (cryo-EM) structures of the single components have been solved over time [48, 49]. Recently, the ER-luminal part of the PLC, including the proteins Tapasin, ERp57, Calreticulin, ß2m and MHC class I, was elucidated [50]. Calreticulin, Tapasin and ERp57 are chaperones acting on the ER-luminal side. Their function is to install and stabilize freshly synthesized MHC class I molecules at the PLC for further loading of peptides into the peptide binding groove of these MHC class I molecules. The central component of the PLC on the cytosolic side is the transporter TAP.

The transporter associated with antigen processing - TAP

The function of TAP in the MHC class I pathway is to transport peptide fragments from the cytosol into the ER lumen [51]. The importance of this transporter is highlighted by a drastic reduction of surface MHC class I levels in TAP-deficient cells resulting in empty

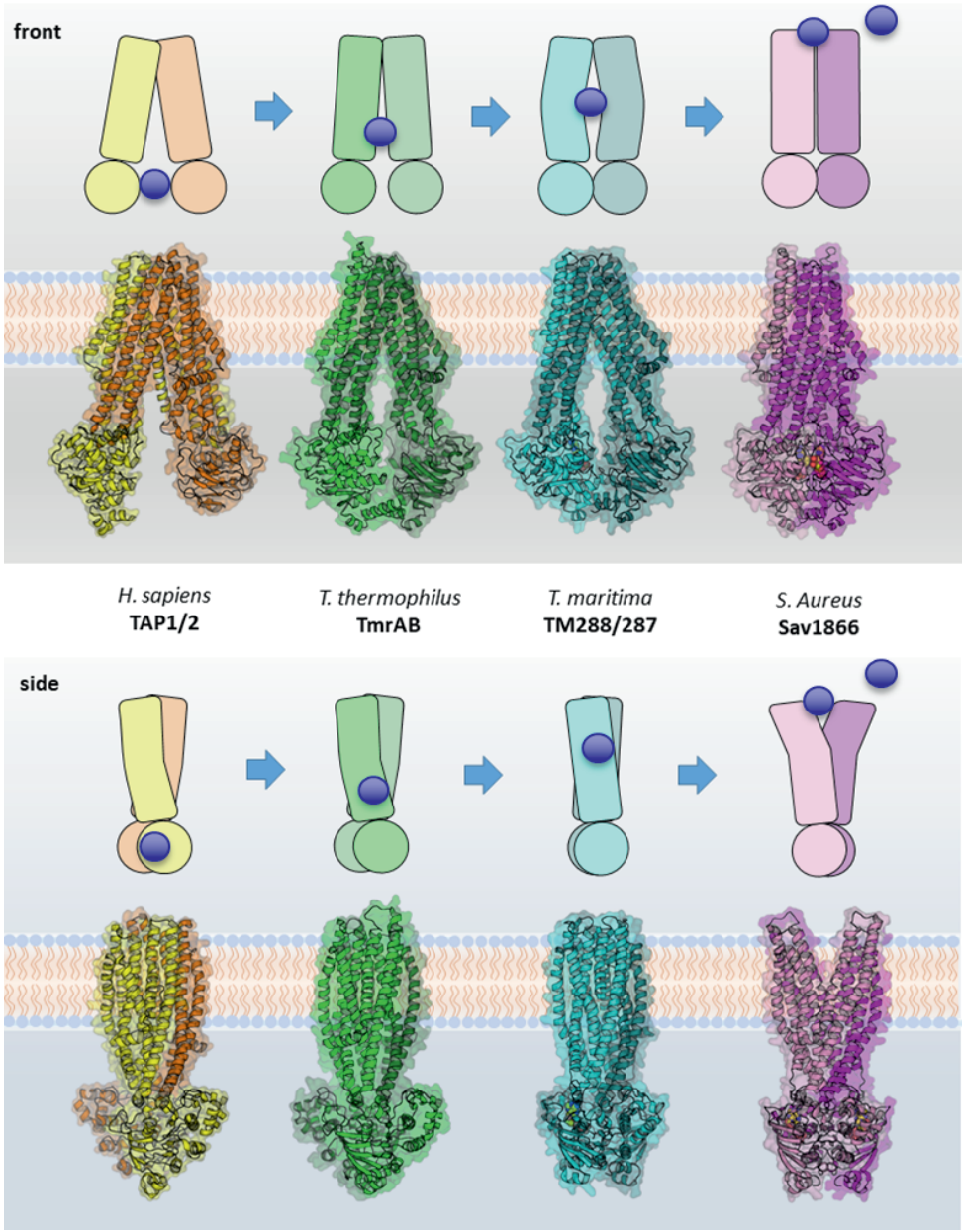

Figure 2: TAP mediated peptide transport cycle. Structural information on the peptide transport cycle of TAP was extrapolated from homologous ABC transporter structures. The TAP1/2 model is based on the structural data of Oldham et al.. The transporter is in an inward- or cytosol-facing, peptide- and ATP-receptive state where the NBDs are physically separated (PDB-ID 5U1D) [49, 56]. inding of both ATP and peptide (dark blue dot) putatively triggers the closure of the cytosol-facing NBD domains. from Thermogata maritima (4Q4A) represent putative intermediate stages of the peptide transport cycle [57, 58].

Figure 2 (continued). The closed ER-facing conformation is based on structural information from Dawson et al. (2ONJ, Staphylococcus aureus Sav1866) and shows interacting NBDs and a cavity formed by the transmembrane domains (TMDs) towards the ER [59]. Peptide release and subsequent ATP hydrolysis take place after the transporter was opened to the ER lumen. The different panels display the four transporter structures from different angles (top: front view; bottom: side view).

MHC class I molecules, which will be retained in the ER and are subsequently degraded [52]. Consequently, these cells can escape T-cell recognition.

TAP is a heterodimer consisting of the two subunits TAP1 (ABCB2) and TAP2 (ABCB3), that both belong to the ATP binding cassette (ABC) transporter family [53]. Common to all ABC transporters, each subunit is composed of a cytosol-facing nucleotide binding domain (NBD) and N-terminal transmembrane helices (ten in TAP1 and nine in TAP2, respectively) [54]. The NBDs are responsible for ATP binding and hydrolysis. These processes mediate conformational changes of the heterodimer that lead to the transport of the peptides from the cytosol across the ER membrane as well as to peptide release, followed by the return of the TAP heterodimer to the cytosolfacing state (see Figure 2). The structural features of the complete peptide transport cycle of TAP remain to be elucidated. Nonetheless, eight high-resolution structures of the ABC transporter TmrAB, a heterodimeric ABC exporter with high homology to TAP, have given insight into the peptide translocation and ATP-hydrolysis cycle [55].

TAP inhibition

Due to the crucial role of TAP in the classical MHC class I antigen presentation pathway, it is not surprising that multiple herpesviruses independently acquired proteins that efficiently block TAP-mediated peptide transport from the cytosol into the ER. The currently identified TAP inhibitors have no structural homology and therefore use unique ways to block TAP function [45].

Herpesviruses

Herpesvirus-encoded TAP-inhibitors hamper ATP and/or substrate binding whereas others do not. Some inhibitors bind to TAP from the ER luminal side, others from the cytosolic side, and they can either be soluble or membrane proteins (see Figure 3). These inhibitors include the proteins BNLF2a derived from EBV, Infected Cell Protein 47 (ICP47) from HSV-1 and HSV-2, US6 from HCMV, and multiple variants of the Unique Long 49.5 (UL49.5) gene product from bovine herpes virus types 1 and 5 (BoHV1/5), equine herpesvirus types 1 and 4 (EHV1/4) and Pseudorabies virus.

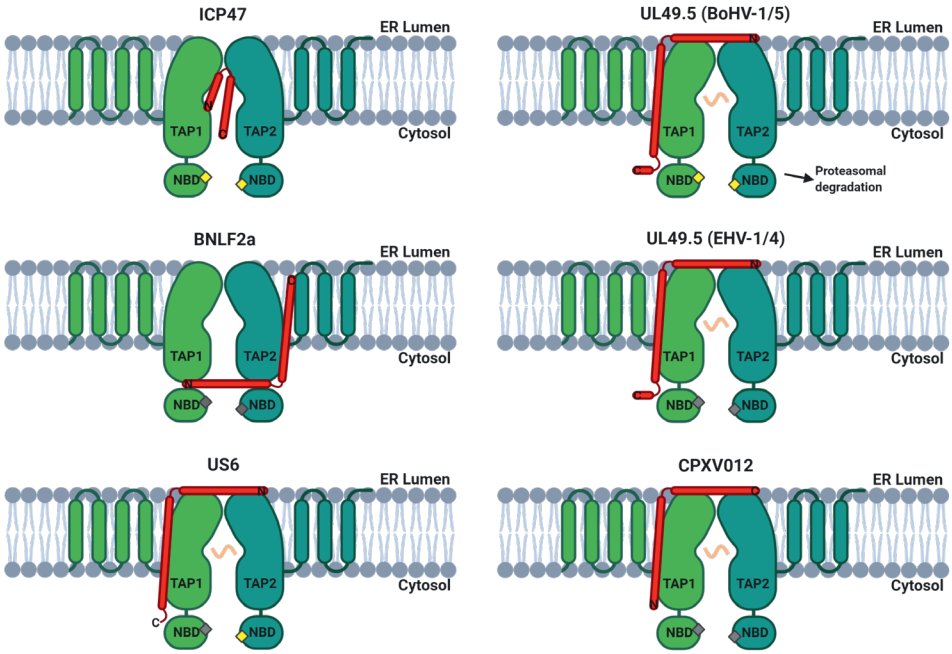

Figure 3: Herpes- and Poxvirus mediated TAP inhibition. All known TAP inhibitors act in a unique way by blocking TAP's function to ensure immune evasion. In addition, the UL49.5 protein from BoHV-1/5 targets TAP for proteasomal degradation. Red bars: viral inhibitor; yellow peptide: TAP substrate; grey diamond: no ATP binding; yellow diamond: ATP binding; C: C-terminus; N: N-terminus.

The EBV encoded protein BNLF2a is a tail-anchored protein. BNLF2a inserts its C-terminus into the ER membrane post-translationally and subsequently interacts with the cytosolic regions of TAP [60]. Since neither substrate nor ATP binding occurs, no further conformational changes can arise [61]. In contrast to BNLF2a, ICP47 interferes with peptide binding to TAP while allowing ATP-binding [62]. This soluble protein acts from the cytosolic side and binds to TAP inside the inward-facing binding cavity. It was shown that correct peptide binding to TAP is a mandatory event in the peptide translocation cycle and crucial for conformational rearrangements as well as ATP hydrolysis [63]. The HCMV protein US6, an ER-resident type I transmembrane protein, blocks binding of ATP to TAP but allows peptide binding to the NBDs. Since US6 is located on the ER-luminal side, inhibition of ATP binding occurs through allosteric crosstalk across the ER membrane [64]. Like US6, the different variants of UL49.5 are type I transmembrane proteins. UL49.5 proteins are encoded by different varicelloviruses and block peptide transport across the ER membrane by inhibiting conformational alterations of TAP while allowing peptide binding to the NBDs of TAP [65]. Furthermore, BoHV-1 and -5 allow ATP binding to TAP but target both subunits of the transporter for proteasomal degradation via an unknown pathway [66]. EHV-1 and -4 on the other hand do not induce degradation of TAP but block ATP binding to TAP.

Cowpox Virus

Cowpox Viruses (CPXV) belong to the orthopoxvirus genus of the poxviridae family and are closely related to vaccinia virus [67]. CPXV have a large genome that allows them to encode a large variety of immune evasion genes [68]. One of these genes, CPXV203, interferes with the MHC I antigen presentation pathway [69]. CPXV203 was shown to hamper the intracellular trafficking of MHC class I molecules by retaining them in the ER and blocking trafficking to the Golgi [69]. A CPXV203-deficient virus cannot restore normal MHC class I levels on the cell surface, indicating that the virus encodes more proteins interfering with this pathway.

TAP inhibition was believed to a unique feature of herpesviruses. However, a poxvirus protein, CPXV012, has also been found to block TAP function [70]. This type II membrane protein CPXV012 interferes with ATP binding to TAP at the cytosolic NBDs while allowing peptide binding [71]. The exact mechanism of how this protein abrogates TAP-mediated peptide transport remains elusive.

Herpesviruses hijacking ERAD

A large proportion of all proteins synthesized in the cell is directed towards the ER lumen via the transporter complex SEC61 co- or post-translationally [72]. In the ER, these proteins will undergo modifications until they ultimately fold into their correct mature conformations with the help of chaperones, like calreticulin or calnexin [73]. In the case of a misfolded protein, the ER quality control (QC) chaperones will initiate another folding attempt [74]. If a protein cannot be folded correctly, it will be removed from the ER by ER-associated protein degradation (ERAD) (see Figure 4). After recognition of these misfolded proteins by the ER QC, these proteins will be dislocated back to the cytosol, ubiquitinated and eventually degraded by the proteasome.

To date, the channel(s) for protein export from the ER still remain to be determined. The ubiquitination process is facilitated by a cascade of E1, E2 and E3 enzymes [75]. On the cytosolic side, the AAA+ ATPase p97 recognizes the ubiquitinated proteins and is believed to provide the pulling force to extract the proteins from the ER [76, 77]. The last crucial step of this pathway is the ubiquitin-dependent degradation of the substrates by the proteasome. This process can be mediated either via direct association of the proteasome to the ERAD complex or alternatively, a chaperone complex could guide the substrate to the proteasome [78, 79].

Under normal cellular conditions, this highly sophisticated pathway prevents accumulation and aggregation of misfolded proteins. A defective ERAD can be associated with major

pathological consequences like Parkinson's disease (due to loss of ERAD function) but also cystic fibrosis (upregulated premature degradation of CFTR) [80, 81]. HCMV hijacks this protein degradation pathway to ensure MHC class I downregulation via its immune evasion proteins US2 and US11. Under regular conditions, only a fraction of newly synthesized MHC class I molecules is targeted for ERAD, due to misfolding, failure to associate with $ß_2$m or the absence of antigenic peptides [82]. The half-life of these misfolded MHC class I molecules is approximately 90 minutes [83], whereas MHC class I molecules targeted by HCMV US2 or US11 will be degraded within approximately five minutes and one minute, respectively [84, 85].

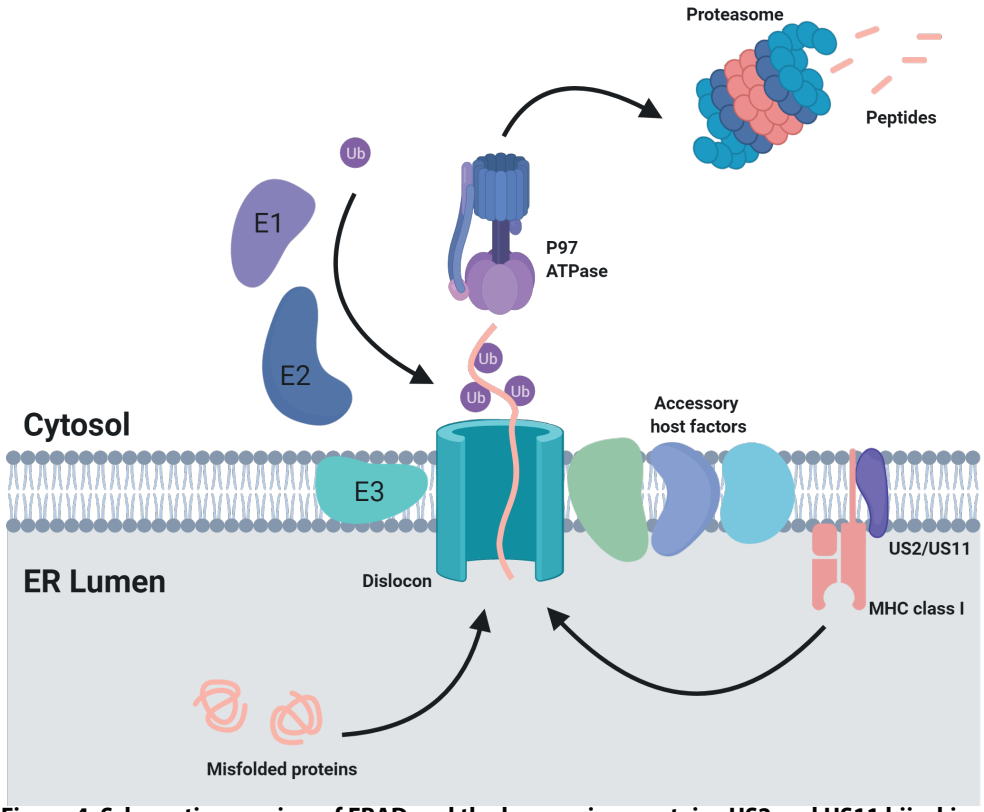

Figure 4: Schematic overview of ERAD and the herpesvirus proteins US2 and US11 hijacking ERAD for MHC class I degradation. Terminally misfolded proteins are targeted for ERAD and will be transported by an unknown protein complex out of the ER (dislocation). HCMV US2 and US11 hijack this pathway for MHC class I degradation. The pathway is comprised of a protein channel ("dislocon") and different accessory proteins to stabilize the complex and to further recruit crucial ERAD proteins. Upon arrival of the substrate at the cytosolic side, the substrate will be ubiquitinated by the respective E1, E2 and E3 ligases. An ATPase recognizes these ubiquitinated proteins and provides the pulling force to extract the substrate from the ER membrane followed by transport to the proteasome for degradation.

US2 and US11 are type I membrane glycoproteins consisting of 199 (US2) or 215 amino acid residues (US11) length, respectively [86, 87]. Both viral immune evasins were identified already decades ago and have served as a paradigm for ERAD since. The mechanism underlying MHC class I degradation by US2 and US11 is not fully understood due to the complexity of ERAD. It is assumed that the components of ERAD for dislocation of proteins differ, depending on the context. Interestingly, both proteins utilize different ERAD proteins for MHC class I degradation. One example is that misfolded MHC class I molecules depend on the E3 ligase Hrd1 for degradation [83], whereas degradation in the context of US2 involves the E3 TRC8 [88] and degradation via US11 involves TMEM129 [89, 90]. In contrast, QC-related ERAD as well as US2 and US11-dependent degradation of MHC class I are all depending on the AAA+ ATPase p97 as the presumed pulling force from the cytosolic side [91].

A structural solution?

Molecular and biochemical methods are essential to identify interaction partners of proteins, key players in different pathways and confirm phenotypes of altered genes. However, they lack the ability to elucidate the architecture of (heterogeneous) protein complexes, as well as the dynamics behind their mode of action. New imaging techniques like Cryo-EM allow for structures of single proteins as well as protein complexes to be solved at a near atomic resolution. The development of Cryo-EM already began in the 1970's, but in the last decade the possibility to resolve structures with near atomic resolution (<4Å) was drawing worldwide attention to this technique [92]. Both advances in software algorithms and detector technology and the redundancy of protein crystallization made Cryo-EM to a powerful alternative to X-ray crystallography and NMR spectroscopy. A detailed summary with all steps involved in structure determination by single-particle cryo-EM is described in Cheng *et al.* [92]. Structural insights into the PLC, TAP inhibition and the ERAD machinery would be of significant importance to the field.

Scope of the thesis

Unravelling the exact mechanisms of how viruses interact with and hide from the human immune system has been a widely studied subject for a long time. Herpesviruses have developed unique ways of evading key steps of antigen presentation. Yet, the exact mechanisms behind these evasive strategies have remained largely unsolved. This thesis aims to shed more light on the mechanisms employed by herpesviruses and poxviruses to elude MHC class I-mediated antigen presentation.

In **chapter 2** we evaluate the effect of several naturally occurring single nucleotide polymorphisms (SNPs) in the heterodimeric ABC-transporter TAP on its function, as well as on its inhibition by several herpesvirus-encoded immune evasion proteins. We test if certain combinations of these naturally occurring SNPs rescue peptide translocation by TAP from the inhibiting effect of the viral proteins, and therefore lead to a higher antigen presentation on the cell surface.

TAP is not the only target in the classical MHC I antigen presentation pathway that is hijacked by viruses. Therefore, we describe a flow cytometry-based approach to assess viral interference with the MHC I antigen processing and presentation pathway in **chapter 3**. This approach can help in identifying viral proteins responsible for interference, and may aid in solving the mode of action of these proteins.

Molecular and biochemical approaches have been instrumental in defining interactions between viral proteins and host factors, and how these viral proteins hinder the immune response. Still, elucidating structural details of these interactions is of major importance, not only to understand dynamic processes, but, potentially, to provide the basis for specific therapeutic strategies. In **chapter 4** we propose the structure for the human peptide-loading complex and model the interactions amongst the key players within this complex. In addition, we put forward a full peptide transport cycle by extrapolating information from the structures resolved for other known homologous ABC transporter.

All herpes- and poxvirus-encoded TAP inhibitors target the transporter at different stages of the peptide transport cycle. Unravelling the structures of these TAP inhibitors in complex with TAP might provide a full picture of the transport cycle and would confirm our proposed models. Therefore, in **chapter 5** we describe a method aimed at obtaining Cryo-EM high-resolution structures of TAP in complex with the viral inhibitors.

While investigating how the TAP inhibitor CPXV012 interferes with TAP function, we discovered a peptide derived from the full-length protein that possesses antiviral activity. In **chapter 6** we propose how this peptide blocks infection of viruses by binding to phosphatidylserine in their viral envelope.

As previously discussed, the ER-associated protein degradation is a quality control system in the ER that targets misfolded proteins for degradation. In **chapter 7** we shed light on protein-protein interactions amongst important components of this system. Furthermore, we have studied the role that the HCMV proteins US2 and US11 play in this pathway and how they might hijack it.

Chapter 8 summarizes all the findings of this thesis and discusses how future research could lead to a better understanding of herpesvirus immune evasion and the development of novel treatment methods. Our findings will be discussed in the context of recently published articles in the field.

References

1. McGeoch DJ, Cook S, Dolan A, et al (1995) Molecular phylogeny and evolutionary timescale for the family of mammalian herpesviruses. J Mol Biol 247:443–458. https://doi.org/10.1006/jmbi.1995.0152
2. Brown JC, Newcomb WW (2011) Herpesvirus capsid assembly: Insights from structural analysis. Curr Opin Virol 1:142–149. https://doi.org/10.1016/j.coviro.2011.06.003
3. Roizmann B, Pellet PE (2001) The Family Herpesviridae: A brief introduction. In: Fields, Knipe, Howley (eds) Fields Virology, 4th ed. Lippincott, Williams & Wilkins
4. E G, V C, Rocca MT D, et al (2018) Seroprevalence of Herpes viruses in a retrospective study in Southern Italy. Arch Clin Microbiol 09:1–5. https://doi.org/10.4172/1989-8436.100074
5. Adland E, Klenerman P, Goulder P, Matthews PC (2015) Ongoing burden of disease and mortality from HIV/CMV coinfection in Africa in the antiretroviral therapy era. Front Microbiol 6:1–9. https://doi.org/10.3389/fmicb.2015.01016
6. Kangro HO, Osman HK, Lau YL, et al (1994) Seroprevalence of antibodies to human herpesviruses in England and Hong Kong. J Med Virol 43:91–96. https://doi.org/10.1002/jmv.1890430117
7. Pertel P, Spear P (2008) Sexually Transmitted Diseases. In: Holmes K. (ed) The Yale Journal of Biology and Medicine, Fourth Edi. YJBM, pp 381–397
8. Chayavichitsilp P, Buckwalter J V, Krakowski AC, Friedlander SF (2009) Herpes Simplex. Pediatr Rev 30:119–130. https://doi.org/10.1542/pir.30-4-119
9. Gupta R, Warren T, Wald A (2007) Genital herpes. Lancet 370:2127–2137. https://doi.org/10.1016/S0140-6736(07)61908-4
10. Pergam S, Limaye A (2010) Varicella Zoster Virus (VZV) : EPIDEMIOLOGY AND RISK FACTORS. Am J Transpl 9:1–12. https://doi.org/10.1111/j.1600-6143.2009.02901.x.Varicella
11. Flavell KJ (2000) Hodgkin's disease and the Epstein-Barr virus. Mol Pathol 53:262–269. https://doi.org/10.1136/mp.53.5.262
12. Gottschalk S, Rooney CM, Heslop HE (2005) Post-Transplant Lymphoproliferative Disorders. Annu Rev Med 56:29–44. https://doi.org/10.1146/annurev.med.56.082103.104727
13. Griffiths P, Baraniak I, Reeves M (2015) The pathogenesis of human cytomegalovirus. J Pathol 235:288–297. https://doi.org/10.1002/path.4437
14. Weber J, Wilson G (1994) Disease association and diagnosis of human herpesvirus 6. Can J Infect Dis 5:184–185. https://doi.org/10.1155/1994/298540
15. Salahuddin SZ, Ablashi D V, Markham PD, et al (1986) Isolation of a new virus, HBLV, in patients with lymphoproliferative disorders. Science (80-) 234:596 LP – 601. https://doi.org/10.1126/science.2876520
16. van den Berg JSP, van Zeijl JH, Rotteveel JJ, et al (1999) Neuroinvasion by human herpesvirus type 7 in a case of exanthem subitum with severe neurologic manifestations. Neurology 52:1077 LP – 1077. https://doi.org/10.1212/WNL.52.5.1077
17. Hashida T, Komura E, Yoshida M, et al (1995) Hepatitis in Association With Human Herpesvirus-7 Infection. Pediatrics 96:783 LP – 785
18. Goncalves PH, Ziegelbauer J, Uldrick TS, Yarchoan R (2017) Kaposi sarcoma herpesvirus-associated cancers and related diseases. Curr Opin HIV AIDS 12:47–56. https://doi.org/10.1097/COH.0000000000000330

19. Sharma V, Luker GD, Piwnica-Worms D (2002) Molecular imaging of gene expression and protein function in vivo with PET and SPECT. J Magn Reson Imaging 16:336–351. https://doi.org/10.1002/jmri.10182

20. Sundaram GSM, Harpstrite SE, Kao JLF, et al (2012) A new nucleoside analogue with potent activity against mutant sr39 Herpes Simplex Virus-1 (HSV-1) Thymidine Kinase (TK). Org Lett 14:3568–3571. https://doi.org/10.1021/ol300728a

21. Crumpacker C (1988) Resistance of Herpes Viruses to Nucleoside Analogues --- Mechanisms and Clinical Importance. In: De Clercq E (ed) Clinical Use of Antiviral Drugs. Springer US, Boston, MA, pp 207–222

22. Piret J, Boivin G (2011) Resistance of herpes simplex viruses to nucleoside analogues: Mechanisms, prevalence, and management. Antimicrob Agents Chemother 55:459–472. https://doi.org/10.1128/AAC.00615-10

23. Coen DM, Schaffer PA (2003) Antiherpesvirus drugs: A promising spectrum of new drugs and drug targets. Nat Rev Drug Discov 2:278–288. https://doi.org/10.1038/nrd1065

24. van Diemen FR, Kruse EM, Hooykaas MJG, et al (2016) CRISPR/Cas9-Mediated Genome Editing of Herpesviruses Limits Productive and Latent Infections. PLoS Pathog 12:e1005701. https://doi.org/10.1371/journal.ppat.1005701

25. de Buhr H, Lebbink RJ (2018) Harnessing CRISPR to combat human viral infections. Curr Opin Immunol 54:123–129. https://doi.org/10.1016/j.coi.2018.06.002

26. Whitley RJ (1996) Herpesviruses. In: Baron S (ed) Medical Microbiology. University of Texas Medical Branch at Galveston

27. Honess RW (1984) Herpes Simplex and 'The Herpes Complex': Diverse Observations and A Unifying Hypothesis. J Gen Virol 65:2077–2107. https://doi.org/ https://doi.org/10.1099/0022-1317-65-12-2077

28. Dolan A, Cunningham C, Hector RD, et al (2004) Genetic content of wild-type human cytomegalovirus. J Gen Virol 85:1301–1312. https://doi.org/10.1099/vir.0.79888-0

29. Peters GA, Tyler SD, Grose C, et al (2006) A Full-Genome Phylogenetic Analysis of Varicella-Zoster Virus Reveals a Novel Origin of Replication-Based Genotyping Scheme and Evidence of Recombination between Major Circulating Clades. J Virol 80:9850–9860. https://doi.org/10.1128/jvi.00715-06

30. Nishimura M, Mori Y (2019) Entry of betaherpesviruses, 1st ed. Elsevier Inc.

31. Martinez-Martin N, Marcandalli J, Huang CS, et al (2018) An Unbiased Screen for Human Cytomegalovirus Identifies Neuropilin-2 as a Central Viral Receptor. Cell 174:1158-1171.e19. https://doi.org/10.1016/j.cell.2018.06.028

32. Isaacson MK, Compton T (2009) Human Cytomegalovirus Glycoprotein B Is Required for Virus Entry and Cell-to-Cell Spread but Not for Virion Attachment, Assembly, or Egress. J Virol 83:3891–3903. https://doi.org/10.1128/JVI.01251-08

33. Spear PG, Longnecker R (2003) Herpesvirus entry: an update. J Virol 77:10179–85. https://doi.org/10.1128/jvi.77.19.10179-10185.2003

34. Connolly SA, Jackson JO, Jardetzky TS, Longnecker R (2011) Fusing structure and function: a structural view of the herpesvirus entry machinery. Nat Rev Microbiol 9:369–381. https://doi.org/10.1038/nrmicro2548

35. Bowman JJ, Lacayo JC, Burbelo P, et al (2011) Rhesus and Human Cytomegalovirus Glycoprotein L Are Required for Infection and Cell-to-Cell Spread of Virus but Cannot Complement Each Other. J Virol 85:2089–2099. https://doi.org/10.1128/JVI.01970-10

36. Ogawa-Goto K, Tanaka K, Gibson W, et al (2003) Microtubule network facilitates nuclear targeting of human cytomegalovirus capsid. J Virol 77:8541–7. https://doi.org/10.1128/jvi.77.15.8541-8547.2003

37. Li T, Chen J, Cristea IM (2013) Human Cytomegalovirus Tegument Protein pUL83 Inhibits IFI16-Mediated DNA Sensing for Immune Evasion. Cell Host Microbe 14:591–599. https://doi.org/10.1016/j.chom.2013.10.007

38. Yurochko AD (2008) Human Cytomegalovirus Modulation of Signal Transduction. In: Current topics in microbiology and immunology. pp 205–220

39. Yu Y, Clippinger AJ, Alwine JC (2011) Viral effects on metabolism: changes in glucose and glutamine utilization during human cytomegalovirus infection. Trends Microbiol 19:360–367. https://doi.org/10.1016/j.tim.2011.04.002

40. Jean Beltran PM, Cristea IM (2014) The life cycle and pathogenesis of human cytomegalovirus infection: lessons from proteomics. Expert Rev Proteomics 11:697–711. https://doi.org/10.1586/14789450.2014.971116

41. Wylie KM, Mihindukulasuriya KA, Zhou Y, et al (2014) Metagenomic analysis of double-stranded DNA viruses in healthy adults. BMC Med 12:1–10. https://doi.org/10.1186/s12915-014-0071-7

42. Wald A, Corey L (2007) Persistence in the population: epidemiology, transmission. In: Arvin A., Campadelli-Fiume G, Mocarski E et al. (ed) Human Herpesviruses: Biology, Therapy. and Immunoprophylaxis. Cambridge University Press

43. Schuren AB, Costa AI, Wiertz EJ (2016) Recent advances in viral evasion of the MHC Class I processing pathway. Curr Opin Immunol 40:43–50. https://doi.org/10.1016/j.coi.2016.02.007

44. Praest P, de Buhr H, Wiertz EJHJ (2019) A Flow Cytometry-Based Approach to Unravel Viral Interference with the MHC Class I Antigen Processing and Presentation Pathway. pp 187–198

45. van de Weijer ML, Luteijn RD, Wiertz EJHJ (2015) Viral immune evasion: Lessons in MHC class I antigen presentation. Semin Immunol 27:125–137. https://doi.org/10.1016/j.smim.2015.03.010

46. Reits EAJ, Vos JC, Grommé M, Neefjes J (2000) The major substrates for TAP in vivo are derived from newly synthesized proteins. Nature 404:774–778. https://doi.org/10.1038/35008103

47. Praest P, Liaci AM, Förster F, Wiertz EJHJ (2019) New insights into the structure of the MHC class I peptide-loading complex and mechanisms of TAP inhibition by viral immune evasion proteins. Mol Immunol 113:. https://doi.org/10.1016/j.molimm.2018.03.020

48. Dong G, Wearsch PA, Peaper DR, et al (2009) Insights into MHC class I peptide loading from the structure of the tapasin-ERp57 thiol oxidoreductase heterodimer. Immunity 30:21–32. https://doi.org/10.1016/j.immuni.2008.10.018

49. Oldham ML, Hite RK, Steffen AM, et al (2016) A mechanism of viral immune evasion revealed by cryo-EM analysis of the TAP transporter. Nature 529:537–40. https://doi.org/10.1038/nature16506

50. Blees A, Januliene D, Hofmann T, et al (2017) Structure of the human MHC-I peptide-loading complex. Nature 551:525–528. https://doi.org/10.1038/nature24627

51. Eggensperger S, Tampé R (2015) The transporter associated with antigen processing: a key player in adaptive immunity. Biol Chem 396:1059–72. https://doi.org/10.1515/hsz-2014-0320

52. Ljunggren H-G, Stam NJ, Öhlén C, et al (1990) Empty MHC class I molecules come out in the cold. Nature 346:476–480. https://doi.org/10.1038/346476a0

53. Dean M, Annilo T (2005) Evolution of the Atp-Binding Cassette (Abc) Transporter Superfamily in Vertebrates*. Annu Rev Genomics Hum Genet 6:123–142. https://doi.org/10.1146/annurev.genom.6.080604.162122

54. Vos JC, Spee P, Momburg F, Neefjes J (1999) Membrane topology and dimerization of the two subunits of the transporter associated with antigen processing reveal a three-domain structure. J Immunol 163:6679–85

55. Hofmann S, Januliene D, Mehdipour AR, et al (2019) Conformation space of a heterodimeric ABC exporter under turnover conditions. Nature 571:580–583. https://doi.org/10.1038/s41586-019-1391-0

56. Oldham ML, Grigorieff N, Chen J (2016) Structure of the transporter associated with antigen processing trapped by herpes simplex virus. Elife 5:. https://doi.org/10.7554/eLife.21829

57. Hohl M, Hurlimann LM, Bohm S, et al (2014) Structural basis for allosteric cross-talk between the asymmetric nucleotide binding sites of a heterodimeric ABC exporter. Proc Natl Acad Sci 111:11025–11030. https://doi.org/10.1073/pnas.1400485111

58. Nöll A, Thomas C, Herbring V, et al (2017) Crystal structure and mechanistic basis of a functional homolog of the antigen transporter TAP. Proc Natl Acad Sci 201620009. https://doi.org/10.1073/pnas.1620009114

59. Dawson RJP, Locher KP (2006) Structure of a bacterial multidrug ABC transporter. Nature 443:180–185. https://doi.org/10.1038/nature05155

60. Horst D, Favaloro V, Vilardi F, et al (2011) EBV Protein BNLF2a Exploits Host Tail-Anchored Protein Integration Machinery To Inhibit TAP. J Immunol 186:3594–3605. https://doi.org/10.4049/jimmunol.1002656

61. Wycisk AI, Lin J, Loch S, et al (2011) Epstein-Barr viral BNLF2a protein hijacks the tail-anchored protein insertion machinery to block antigen processing by the transport complex TAP. J Biol Chem 286:41402–41412. https://doi.org/10.1074/jbc.M111.237784

62. Früh K, Ahn K, Djaballah H, et al (1995) A viral inhibitor of peptide transporters for antigen presentation. Nature 375:415–418. https://doi.org/10.1038/375415a0

63. Gorbulev S, Abele R, Tampé R (2001) Allosteric crosstalk between peptide-binding, transport, and ATP hydrolysis of the ABC transporter TAP. Proc Natl Acad Sci U S A 98:3732–7. https://doi.org/10.1073/pnas.061467898

64. Hewitt EW, Gupta SS, Lehner PJ (2001) The human cytomegalovirus gene product US6 inhibits ATP binding by TAP. EMBO J 20:387–96. https://doi.org/10.1093/emboj/20.3.387

65. Koppers-Lalic D, Verweij MC, Lipińska AD, et al (2008) Varicellovirus UL49.5 Proteins Differentially Affect the Function of the Transporter Associated with Antigen Processing, TAP. PLoS Pathog 4:e1000080. https://doi.org/10.1371/journal.ppat.1000080

66. Koppers-Lalic D, Reits EAJ, Ressing ME, et al (2005) Varicelloviruses avoid T cell recognition by UL49.5-mediated inactivation of the transporter associated with antigen processing. Proc Natl Acad Sci 102:5144–5149. https://doi.org/10.1073/pnas.0501463102

67. Chantrey J, Meyer H, Baxby D, et al (1999) Cowpox: reservoir hosts and geographic range. Epidemiol Infect 122:455–60. https://doi.org/10.1017/s0950268899002423

68. Seet BT, Johnston JB, Brunetti CR, et al (2003) Poxviruses and immune evasion. Annu Rev Immunol 21:377–423. https://doi.org/10.1146/annurev.immunol.21.120601.141049

69. Byun M, Wang X, Pak M, et al (2007) Cowpox virus exploits the endoplasmic reticulum retention pathway to inhibit MHC class I transport to the cell surface. Cell Host Microbe 2:306–15. https://doi.org/10.1016/j.chom.2007.09.002

70. Alzhanova D, Edwards DM, Hammarlund E, et al (2009) Cowpox Virus Inhibits the Transporter Associated with Antigen Processing to Evade T Cell Recognition. Cell Host Microbe 6:433–445. https://doi.org/10.1016/J.CHOM.2009.09.013

71. Luteijn RD, Hoelen H, Kruse E, et al (2014) Cowpox Virus Protein CPXV012 Eludes CTLs by Blocking ATP Binding to TAP. J Immunol 193:1578–1589. https://doi.org/10.4049/jimmunol.1400964

72. Chen X, Karnovsky A, Sans MD, et al (2010) Molecular characterization of the endoplasmic reticulum: insights from proteomic studies. Proteomics 10:4040–52. https://doi.org/10.1002/pmic.201000234

73. Helenius A, Aebi M (2004) Roles of N-linked glycans in the endoplasmic reticulum. Annu Rev Biochem 73:1019–49. https://doi.org/10.1146/annurev.biochem.73.011303.073752

74. Araki K, Nagata K (2011) Protein folding and quality control in the ER. Cold Spring Harb Perspect Biol 3:a007526. https://doi.org/10.1101/cshperspect.a007526

75. Christianson JC, Ye Y (2014) Cleaning up in the endoplasmic reticulum: ubiquitin in charge. Nat Struct Mol Biol 21:325–35. https://doi.org/10.1038/nsmb.2793

76. Rabinovich E, Kerem A, Fröhlich K-U, et al (2002) AAA-ATPase p97/Cdc48p, a cytosolic chaperone required for endoplasmic reticulum-associated protein degradation. Mol Cell Biol 22:626–34. https://doi.org/10.1128/mcb.22.2.626-634.2002

77. Bodnar NO, Rapoport TA (2017) Molecular Mechanism of Substrate Processing by the Cdc48 ATPase Complex. Cell 169:722-735.e9. https://doi.org/10.1016/j.cell.2017.04.020

78. Kalies K-U, Allan S, Sergeyenko T, et al (2005) The protein translocation channel binds proteasomes to the endoplasmic reticulum membrane. EMBO J 24:2284–93. https://doi.org/10.1038/sj.emboj.7600731

79. Wang Q, Liu Y, Soetandyo N, et al (2011) A ubiquitin ligase-associated chaperone holdase maintains polypeptides in soluble states for proteasome degradation. Mol Cell 42:758–70. https://doi.org/10.1016/j.molcel.2011.05.010

80. Omura T, Kaneko M, Okuma Y, et al (2013) Endoplasmic reticulum stress and Parkinson's disease: the role of HRD1 in averting apoptosis in neurodegenerative disease. Oxid Med Cell Longev 2013:239854. https://doi.org/10.1155/2013/239854

81. Meusser B, Hirsch C, Jarosch E, Sommer T (2005) ERAD: the long road to destruction. Nat Cell Biol 7:766–772. https://doi.org/10.1038/ncb0805-766

82. Hughes EA, Hammond C, Cresswell P (1997) Misfolded major histocompatibility complex class I heavy chains are translocated into the cytoplasm and degraded by the proteasome. Proc Natl Acad Sci 94:1896–1901. https://doi.org/10.1073/pnas.94.5.1896

83. Burr ML, Cano F, Svobodova S, et al (2011) HRD1 and UBE2J1 target misfolded MHC class I heavy chains for endoplasmic reticulum-associated degradation. Proc Natl Acad Sci 108:2034–2039. https://doi.org/10.1073/pnas.1016229108

84. Wiertz EJHJ, Tortorella D, Bogyo M, et al (1996) Sec6l-mediated transfer of a membrane protein from the endoplasmic reticulum to the proteasome for destruction. Nature 384:432–438. https://doi.org/10.1038/384432a0

85. Wiertz EJ, Jones TR, Sun L, et al (1996) The human cytomegalovirus US11 gene product dislocates MHC class I heavy chains from the endoplasmic reticulum to the cytosol. Cell 84:769–79

86. Rehm A, Stern P, Ploegh HL, Tortorella D (2001) Signal peptide cleavage of a type I membrane protein, HCMV US11, is dependent on its membrane anchor. EMBO J 20:1573–82. https://doi.org/10.1093/emboj/20.7.1573

87. Gewurz BE, Ploegh HL, Tortorella D (2002) US2, a Human Cytomegalovirus-encoded Type I Membrane Protein, Contains a Non-cleavable Amino-terminal Signal Peptide. J Biol Chem 277:11306–11313. https://doi.org/10.1074/jbc.M107904200

88. Stagg HR, Thomas M, van den Boomen D, et al (2009) The TRC8 E3 ligase ubiquitinates MHC class I molecules before dislocation from the ER. J Cell Biol 186:685–92. https://doi.org/10.1083/jcb.200906110

89. van de Weijer ML, Bassik MC, Luteijn RD, et al (2014) A high-coverage shRNA screen identifies TMEM129 as an E3 ligase involved in ER-associated protein degradation. Nat Commun 5:3832. https://doi.org/10.1038/ncomms4832

90. van den Boomen DJH, Timms RT, Grice GL, et al (2014) TMEM129 is a Derlin-1 associated ERAD E3 ligase essential for virus-induced degradation of MHC-I. Proc Natl Acad Sci 111:11425–11430. https://doi.org/10.1073/pnas.1409099111

91. Soetandyo N, Ye Y (2010) The p97 ATPase Dislocates MHC Class I Heavy Chain in US2-expressing Cells via a Ufd1-Npl4-independent Mechanism. J Biol Chem 285:32352–32359. https://doi.org/10.1074/jbc.M110.131649

92. Inoshima I, Inoshima N, Wilke G, et al (2012) A Primer to Single-Particle Cryo-Electron Microscopy Yifan. 17:1310–1314. https://doi.org/10.1038/nm.2451.A

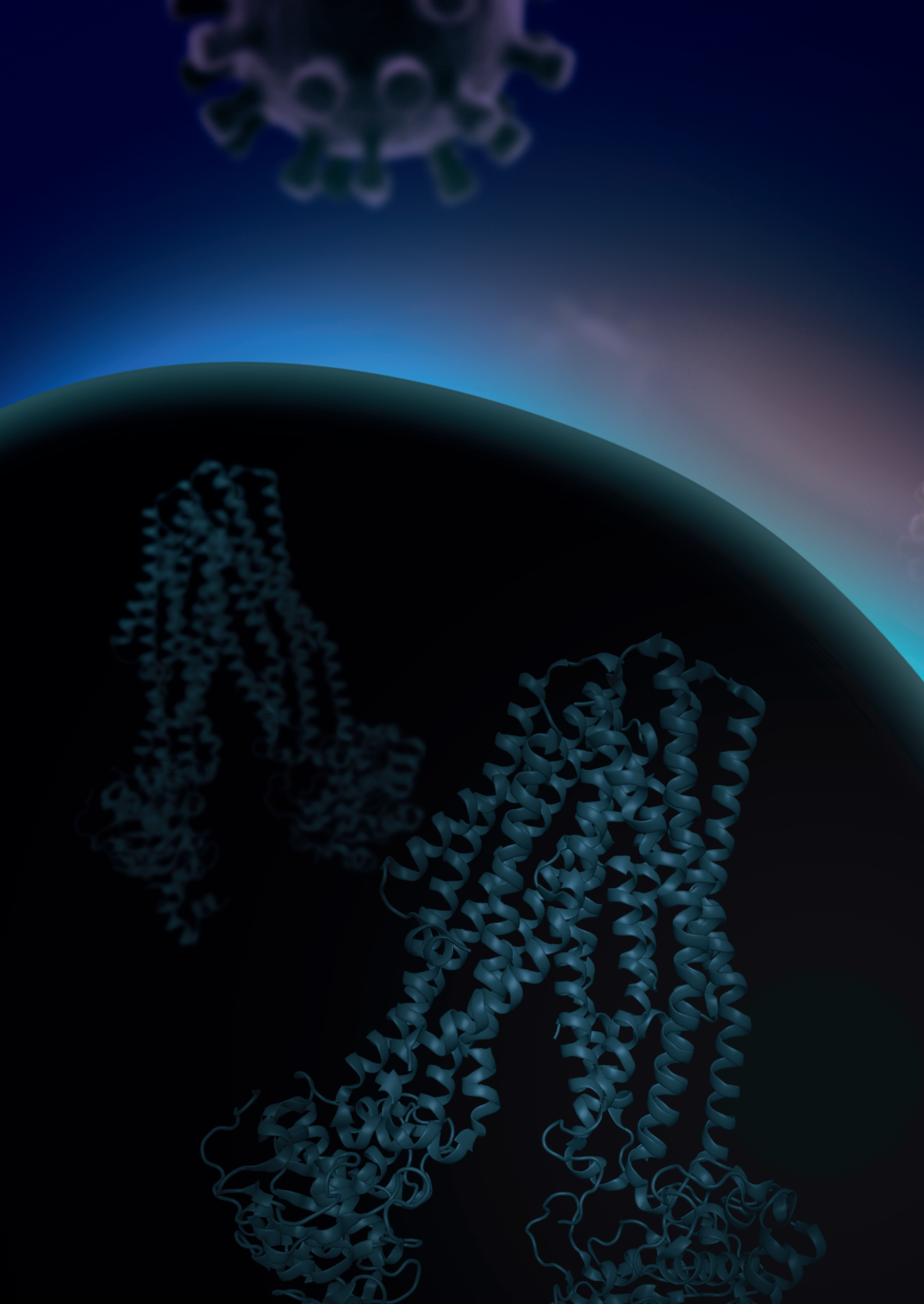

2

The influence of TAP1 and TAP2 gene polymorphisms on TAP function and its inhibition by viral immune evasion proteins

P. Praest, R.D. Luteijn, I.G.J. Brak-Boer, J. Lanfermeijer, H. Hoelen, L. Ijgosse, A.I. Costa, R.D.Gorham Jr., R.J. Lebbink, E.J.H.J. Wiertz

Published in Molecular Immunology (2018) 101 P.55-64

Abstract

Herpesviruses encode numerous immune evasion molecules that interfere with the immune system, particularly with certain stages in the MHC class I antigen presentation pathway. In this pathway, the transporter associated with antigen processing (TAP) is a frequent target of viral immune evasion strategies. This ER-resident transporter is composed of the proteins TAP1 and TAP2, and plays a crucial role in the loading of viral peptides onto MHC class I molecules. Several variants of TAP1 and TAP2 occur in the human population, some of which are linked to autoimmune disorders and susceptibility to infections. Here, we assessed the influence of naturally occurring TAP variants on peptide transport and MHC class I expression. In addition, we tested the inhibitory capacity of three viral immune evasion proteins, the TAP inhibitors US6 from human cytomegalovirus, ICP47 from herpes simplex virus type 1 and BNLF2a from Epstein-Barr virus, for a series of TAP1 and TAP2 variants. Our results suggest that these TAP polymorphisms have no or limited effect on peptide transport or MHC class I expression. Furthermore, our study indicates that the herpesvirus-encoded TAP inhibitors target a broad spectrum of TAP variants; inhibition of TAP is not affected by the naturally occurring polymorphisms of TAP tested in this study. Our findings suggest that the long-term coevolution of herpesviruses and their host did not result in selection of inhibitor-resistant TAP variants in the human population.

1 Introduction

The immune system recognizes altered cells through changes in the peptide repertoire presented by major histocompatibility complex class I (MHC I) molecules. MHC I molecules at the surface of infected cells present antigenic peptides to cytotoxic $CD8^+$ T-cells (CTLs). These adaptive immune cells mount an immune response upon recognition of an antigenic peptide by their T-cell receptor. The majority of peptides presented by MHC I are generated by constant turnover of proteins by the cytosolic proteasome. The resulting peptides are transported into the endoplasmic reticulum (ER) by the transporter associated with antigen processing (TAP). In the ER, TAP and other proteins of the MHC class I peptide-loading complex (PLC) promote folding of MHC I molecules and ensure proper loading of peptides into the MHC I peptide binding groove [1]. Upon stable peptide loading, the peptide-MHC I complex is translocated to the cell surface, where it displays the peptides to $CD8^+$ CTLs.

TAP plays a central role in MHC I antigen presentation, as illustrated by the reduced surface expression of MHC I in cells lacking (functional) TAP. In these cells, empty MHC I molecules are retained in the ER lumen and consequently are unable to display antigens to the immune system [2, 3]. Due to its crucial role in MHC I antigen presentation, TAP has become an attractive target for viral immune evasion strategies. During a long period of virus-host coevolution, herpesviruses independently acquired highly efficient ways to block TAP-mediated peptide transport [4]. The viral TAP-inhibitors identified so far have no structural homology and bind to distinctive domains of the transporter [5].

The TAP heterodimer is composed of TAP1 (ABCB2) and TAP2 (ABCB3), members of the ATP-binding cassette (ABC) family [6]. TAP1 and TAP2 both consist of a nucleotide-binding domain (NBD) and multiple transmembrane domains (TMDs). The core of the TAP heterodimer is comprised of 12 transmembrane domains (six from each TAP subunit), and the cytosolic NBDs. TAP1 and TAP2 have additional transmembrane helices (TMD0 domains) at their N-termini (four in TAP1, three in TAP2), which flank the core region [7]. The core domains of TAP are necessary and sufficient to allow for peptide translocation from the cytosol to the ER to occur. This process requires ATP binding and hydrolysis [8], whereas peptide binding to TAP itself is ATP-independent [9]. TAP contains several domains that are highly conserved throughout the ABC transporter family. These regions are mainly located at the C-terminal NBDs that include the Walker A and B motifs for ATP binding and hydrolysis, the switch domain, and the C-motif [10–12].

Sequence analysis has revealed that for the human TAP (hTAP) 1 and 2 genes several single nucleotide polymorphisms (SNPs) have been maintained within the population.

These SNPs are dispersed throughout the TAP-encoding genes, including regions highly conserved between ABC transporters [11]. Several of these SNPs are more prevalent among certain ethnical groups, whereas others are more equally distributed in the human population [13–15]. In addition, a number of these TAP SNPs have been linked to the susceptibility to or severity of several diseases, including tuberculosis[16, 17], Alzheimer's disease [18], alopecia areata [19], hematological malignancies [20], and cervical intraepithelial neoplasia [21]. Mutational analysis of the rat TAP2 gene revealed that SNPs can result in severe changes in substrate selectivity [22]. In contrast, the few hTAP allelic variants tested thus far did not impact substrate specificity and TAP activity as compared to the most common TAP variants [23, 24]. Therefore, it remains unknown why TAP variants are maintained within the population, and if such polymorphisms have evolved under selective pressure. Evolutionary pressure by viruses, and in particular herpes viruses, has likely driven polymorphism in other components of the immune system, including MHC I [25–28]. Similarly, evolutionary pressure by viral TAP inhibitors may have shaped the SNPs in the TAP-encoding genes, thereby disarming these viral inhibitors.

In this study, we evaluated the influence of TAP polymorphisms on peptide transport. In addition, inhibition of a series of TAP variants by TAP inhibitors encoded by three common human herpesviruses, human cytomegalovirus (HCMV), herpes simplex virus type 1 (HSV-1) and Epstein-Barr virus (EBV), was investigated.

2 Materials and Methods

2.1 Cell culture

The human melanoma cell line MelJuSo (MJS) was cultured in RPMI 1640 (Invitrogen) containing 10% FCS (PAA laboratories), 100 U/ml penicillin, 100 µg/ml streptomycin and 2 mM L-glutamine (complete RPMI medium). HEK293T cells used for lentivirus production were cultivated and maintained in DMEM (Invitrogen) supplemented with 10% FCS (PAA laboratories), 100 U/ml penicillin, 100 µg/ml streptomycin and 2 mM L-glutamine (complete DMEM medium).

2.2 Plasmids

A selectable CRISPR/Cas9 vector based on the pSicoR vector (Addgene plasmid 11579, Tyler Jacks Lab, MIT) was constructed as described previously [29, 30]. This lentiviral vector includes a human codon-optimized *S. pyogenes* Cas9 gene N-terminally fused to a puromycin resistance gene via a T2A ribosome-skipping sequence under control of the human EF1A promoter. In addition, this vector has a human U6 promoter that induces

Table 1: TAP1 alleles used in this study.

Allele	Mutations present in allele
TAP1*01:01	Reference
TAP1*01:01-long	alternative start site at position -60 used
TAP1*02:01	I333V, D637G
TAP1*03:01	I333V
TAP1*01:04	I333V, V458L. D637G, R648Q
TAP1*x	I333V, A370V, V518I, D637G
TAP1-G17R	G17R
TAP1-G247R	G247R
TAP1-S286F	S286F
TAP1-Q728K	Q728K

expression of a guideRNA (gRNA) consisting of a 20 bp target-specific CRISPR RNA (crRNA) fused to the *trans*-activating crRNA (tracrRNA) and a terminator sequence. This vector is called pSicoR-CRISPR-PuroR. For TAP1 overexpression and rescue experiments, a dual promoter lentiviral plasmid expressing puroR and GFP under control of the human PGK promoter was used (pPuroR-GFP; PMID 24807418). TAP1 variants (see Table 1) were introduced downstream of the human EF1a promoter using Gibson assembly (#E2611L, Bioké, New England Biolabs). For TAP2 overexpression and rescue experiments, TAP2 variants were introduced into a dual promoter lentiviral vector expressing the Zeocin resistance gene and mAmetrine (pZeoR-mAmetrine). For overexpression of the viral TAP inhibitors, a dual promoter lentiviral vector expressing a blasticidin resistance gene (pBlastR) was used. Genes encoding viral TAP inhibitors were introduced downstream of an EF1a promoter using Gibson assembly.

2.3 Generation of MJS cells with TAP1 and TAP2 double KO

To generate MJS cells lacking TAP2, cells were transfected with pSico-CRISPR-PuroR containing the TAP2-targeting crRNA sequence 5'-GGAAGAAGAAGGCGGCAACG-3'. After transfection and selection with puromycin (2 µg/ml), cells were cloned by limiting dilution. To prove the absence of TAP2, individual clones were analyzed by (i) immunoblotting (IB), (ii) sequencing of the genomic target site, and (iii) flow cytometry to evaluate cell surface expression of MHC I. A clone lacking TAP2 was subsequently transfected with a pSicoR-CRISPR-PuroR vector containing the TAP1-targeting crRNA sequence 5'-GGGGTCCTCAGGGCAACGGT-3'. After transfection and selection with puromycin, cells were cloned by limited dilution and TAP1 expression was analyzed by IB. Genomic DNA sequence analysis of the TAP2 gRNA target site revealed a deletion of an A nucleotide and

Table 2: TAP2 alleles used in this study.

Allele	Mutations present in allele
TAP2*01:01	Reference
TAP2*01:02	A565S
TAP2*01:03	R651C
TAP2*02:01	T665A, STOP687Q
TAP2*2D	A374T, V467I, T665A, STOP687Q
TAP2*1G	A374T, V379I, R651C
TAP2*2F	V379I, A565S, T665A, STOP687Q
TAP2*BKY	M577V, STOP687Q
TAP2-A513S	A513S

a substitution of a C for a T nucleotide in one allele, and an insertion of an A nucleotide in the other allele. Both mutations induce a frameshift in the reading frame of the TAP2 gene. Genomic DNA sequence analysis of the TAP1 gRNA target site revealed a 31bp deletion. No other mutated or wt sequences were uncovered. A monoclonal cell line lacking TAP1 and TAP2 was used for further experiments.

2.4 Generation of TAP alleles

The TAP1-encoding gene was C-terminally tagged with a streptavidinII-tag using primers 1 and 47. The TAP2-encoding gene was C-terminally tagged with a His-tag using primers 15 and 48. To generate the different TAP variants, the vectors encoding the reference sequences TAP1*01:01-Strep and TAP2*01:01-His were used as templates for PCR amplification. The TAP1*01:01 reference allele with the canonical translation start site was generated using primers 1 and 2. The template for these primers was a vector that encodes the TAP*01:01-long allele. This allele encodes a 5'-extended TAP1*01:01 variant that uses an alternative in frame start site 60bp upstream of the canonical translation start site. This long variant was generated using gBLOCKs (Integrated DNA Technologies). The TAP1*01:01 reference allele was then used to generate the remaining TAP1 alleles. Primers 3-6 for TAP1*02:01, primers 3-4 for TAP1*03:01, primers 3-6 and 33-36 for TAP1*01:04, primers 3-6 and 37-40 for TAP1*x, primers 7-8 for TAP1-G17R, primers 9-10 for TAP1-G247R, primers 11-12 for TAP1-S286F and primers 13-14 for TAP1-Q728K were used. For the generation of the TAP2 alleles, primers 15-16 for TAP2*01:02, primers 17-18 for TAP2*01:03, primers 19-22 for TAP2*02-01, primers 19-26 for TAP2*02D, primers 17, 18, 23, 24, 25 and 26 for TAP2*1G, primers 15,16 and 19-24 for TAP2*2F, primers 21-22 and 29-30 for TAP2*BKY and primers 31 and 32 for TAP2-A513S were used (supplementary table S1).

2.5 Generation of viral inhibitor-constructs

Viral inhibitors were myc-tagged by PCR. The myc tag was added to the C-terminus of US6 [31] (using primers 41 and 42, see supplementary table S2) and BNLF2a [32] (using primers 43 and 44) and to the N-terminus of ICP47 [33] (using primers 45 and 46).

2.6 Lentivirus production and transduction

For the production of replication-deficient recombinant lentiviruses, the lentiviral vectors and third-generation packaging vectors pVSV-G, pMDL and pRSV were co-transfected into HEK293T cells using PEI (1 mg/ml). Lentivirus-containing supernatants were harvested after 3 days and used to transduce MJS cells by spin infection at 2000 rpm for 90 minutes at 33°C in the presence of 4 µg/ml polybrene (Santa Cruz Biotechnology). Selection media containing puromycin (2 µg/ml), blasticidin (20 µg/ml) and zeocin (400 µg/ml) were applied 3 days post infection.

2.7 Immunoblotting (IB)

Cells were harvested and washed with ice-cold PBS, and lysed in 1% Triton X-100 (PanReac) lysis buffer supplemented with 150 mM NaCl and 50 mM Tris-HCl pH 8 for 30 minutes on ice. The cell lysates were centrifuged at 22000 g for 15 minutes at 4°C to remove cellular debris. The supernatants were mixed with Laemmli sample buffer supplemented with 80 mM DTT (Sigma) and loaded on 12% NuPage or 4-12% BOLT SDS gels (Thermo Scientific). The proteins were transferred to Trans-Blot Turbo PVDF membranes (BIO-RAD) using a Trans-Blot Turbo transfer system (BIO-RAD) for 10 minutes at 25 V or using the Mini Trans-Blot Cell system (BIO-RAD) overnight at a constant 12 V at 4°C. The membranes were blocked with 4% milk powder (Campina) in phosphate-buffered saline supplemented with 0.05% Tween 20 (PBST) for 1 h at 4°C. Primary antibodies were diluted in PBST and incubated with the membranes overnight at 4°C. The membranes were washed thoroughly with PBST at 4°C and were then incubated with a labelled secondary antibody for 2 h at 4°C. Membranes were again washed thoroughly at 4°C. Chemiluminescence was detected using Pierce ECL Western Blotting Substrate (Thermo Scientific), followed by exposure of the membranes to Amersham Hyperfilm ECL films (GE Healthcare).

2.8 MHC I surface expression

MHC-I surface expression was assessed by flow cytometry using a FACS Canto II (BD Biosciences). Cells were washed with PBS and stained for 30 minutes with a PE-conjugated antibody (W6/32) at the concentrations indicated in cold PBS supplemented with 0.5% BSA and 0.02% NaN_3 in a total volume of 20 µl. The cells were washed to remove unbound

antibody and then fixed in PBS supplemented with 1% formaldehyde, 0.5% BSA and 0.02% NaN_3. The data were analyzed using FlowJo V10 software.

2.9 Peptide translocation assay

The peptide translocation assay was performed as described previously [34]. Briefly, cells were permeabilized using 2.9 mg/ml of Streptolysin-O (SLO, Murex Diagnostics) at 4°C for 15 minutes, and washed with PBS supplemented with 10mM $MgCl_2$ to remove residual SLO. Permeabilized cells were incubated with 20 nM of a synthetic peptide carrying a fluorescein moiety conjugated to the N-terminal valine residue; the sequence is as follows: (FL)V-N-K-T-E-R-A-Y (kindly provided by Dr. Jan Wouter Drijfhout, Department of Immunohematology and Blood Transfusion, Leiden University Medical Center, Leiden, The Netherlands). Incubation was performed in the presence of 10 mM ATP or 20 mM ADP supplemented with 10 mM $MgCl_2$ for 15 minutes at 37°C in a total volume of 50 µl. Transport was terminated by adding 150 µl PBS supplemented with 20 mM EDTA. The stained cells were analyzed by flow cytometry with a FACS Canto II (BD Biosciences).

2.10 Antibodies

The following primary and secondary antibodies were used for IB: mouse-anti-human TAP1 148.3 C-terminus mAb (1:200)[35], mouse-anti-human TAP2 435.4 mAb (1:200) [9], mouse-anti-myc 9E10 mAb (1:1000), mouse-anti-actin mAb (Millipore MAB1501R, 1:10000), mouse-anti-transferrin receptor mAb (Santa Cruz sc-7327, 1:1000), goat-anti-mouse conjugate-HRP pAb (Jackson #115-035-174, 1:5000) and goat-anti-rat-HRP (Jackson #112-035-175,1:5000). For flow cytometry, the following antibodies were used: PE-conjugated W6/32, anti-HLA-I (Serotec MCA81PE, 1:20).

2.11 Molecular modeling

The molecular structures of the TAP1-TAP2 and TAP1-TAP2-ICP47 complexes were generated using the atomic model based on the high-resolution cryo-EM structure of the TAP1-TAP2-ICP47 complex (PDB code 5U1D)[36]. Missing loops and termini within each molecule were built using Modeller [37]. TAP1 and TAP2 molecules were renumbered according to the numbering scheme in Uniprot entries Q03518 and Q03519, respectively, in order to locate and display all residues affected by SNPs. All SNPs were depicted with the exception of the TAP1 SNP G17R, as it occurs in the N-terminal TMD of TAP1 that was not resolved in the original cryo-EM structure. All figures were rendered using Chimera [38].

3 Results

3.1 Mapping of SNPs in TAP1 and TAP2

In this study, the most common TAP alleles in the human population were investigated (Tables 1 and 2)[39], as well as a number of less frequent alleles with non-synonymous polymorphisms that might affect TAP function. The alleles studied include variants that change the biochemical properties of the amino acid side chains, as well as alleles that carry polymorphisms in highly conserved regions. To highlight the location of these variations within the TAP heterodimer, a molecular model of TAP is displayed in Fig. 1. Three out of the ten TAP1 SNPs are located in the NBD of TAP1, whereas seven out of the nine TAP2 SNPs are located in the NBD of TAP2. The SNPs A374T and V379I are positioned in the TMD of TAP2.

3.2 Generation of a monoclonal TAP1 and TAP2 KO cell line

To investigate the effect of variations within TAP1 and TAP2 on peptide transport and MHC I surface expression, MJS cells lacking TAP1 and TAP2 were generated. As TAP2 is unstable in the absence of TAP1 [40], TAP1/TAP2 double knock-out cells were generated by sequential deletion of TAP2 and TAP1 using the CRISPR/Cas9 technology. The lack of TAP1 and TAP2 expression was confirmed by immunoblotting (Fig. 2A) and sequencing of the TAP alleles (data not shown). As expected, TAP1/TAP2 double KO cells had severely

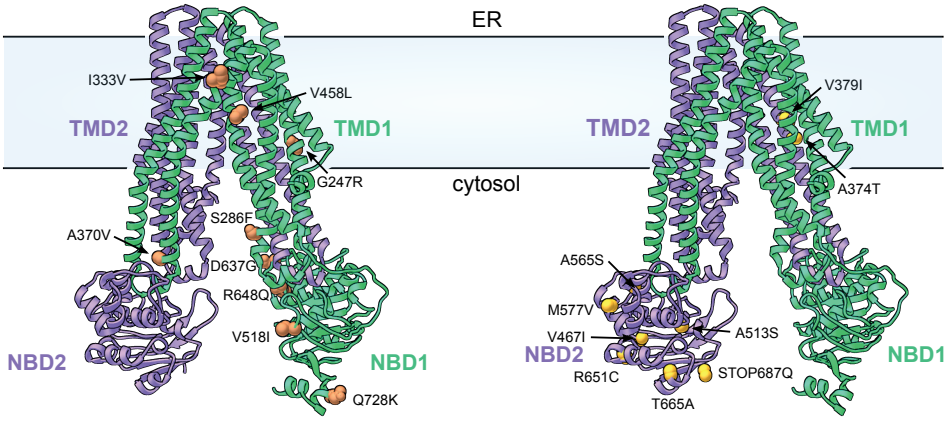

Figure 1: Molecular model of the heterodimeric human TAP complex including SNP's of TAP1 and TAP2. The structure of TAP1 including its cytosolic nucleotide binding domain (NBD1) and its six transmembrane regions forming the core transmembrane domain (TMD1) is depicted in green. The structure of the NBD2 and TMD2 of TAP2 is shown in purple. Non-synonymous SNPs in TAP1 evaluated in this study are shown in orange (left). G17R is not shown because it occurs in the N-terminal TMD not present in the model. The TAP2 SNPs included in this study are shown in yellow (right).

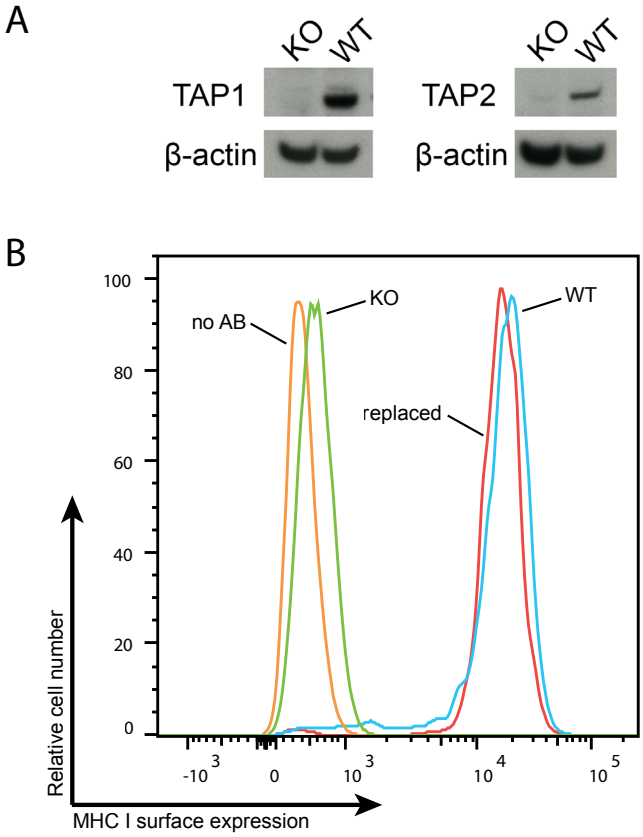

Figure 2: Confirmation of the knock-out phenotype of TAP1/2 KO MJS cells. (A) Lysates from MJS WT cells and TAP1/2 KO MJS cells stained for TAP1 and TAP2 by immunoblotting (IB) with specific antibodies. β-actin was used as a loading control. (B) Surface expression of MHC I molecules of TAP1/2 KO MJS cells (green), TAP1/2 KO MJS cells reconstituted with TAP1/2 (red), MJS WT cells (blue) and unstained MJS WT cells (orange) was assessed by flow cytometry.

reduced MHC I surface expression levels as compared to MJS WT cells (Fig. 2B, green *vs*. blue). MHC I surface expression was restored upon reintroduction of TAP1 and TAP2 (red; shown for the reference genes TAP1*01:01 and TAP2*01:01).

3.3 The effect of TAP1 and TAP2 polymorphisms on TAP function

The TAP variants (Table 1) were expressed in TAP1/TAP2 KO cells as combinations of the TAP1 reference allele and TAP2 variants, or vice versa. Expression of all TAP1 and TAP2 variants was verified by immunoblotting using antibodies specific for TAP1 or TAP2 (Fig. 3A and 3B, respectively). Most variants were expressed at similar levels; TAP1*01-04, TAP1*G247R and TAP2*1G were consistently present at slightly higher levels (Fig. 3A).

To assess TAP function, a peptide transport assay was used. Peptide translocation from the cytosol into the ER was measured using a fluorescein-labelled peptide in the presence of ATP (active transport) or ADP (passive diffusion). The transport activity of the variants and controls was normalized to the levels observed in wild type cells. In the presence of ATP, peptide transport by the TAP1 and TAP2 variants showed some variation, yet it was

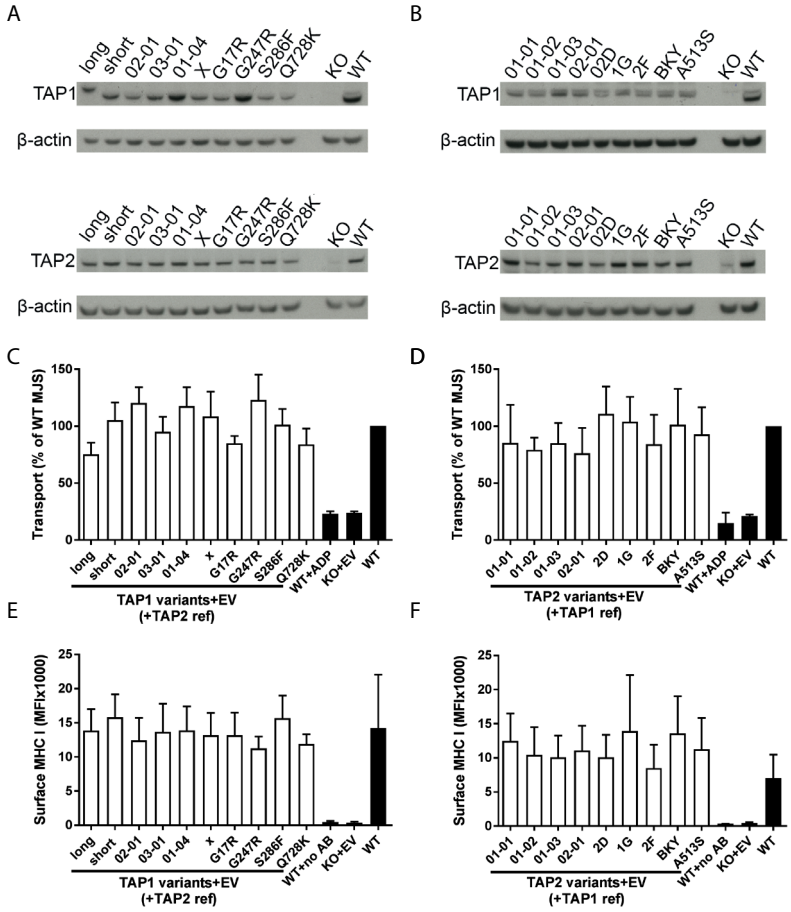

Figure 3: Expression and function of TAP1 and TAP2 variants introduced into TAP1/2 KO MJS cells. Expression of TAP1 variant-TAP2 reference pairs (A) and TAP2 variant-TAP1 reference pairs (B) in MJS cells was analyzed by immunoblotting (IB) of lysates with specific antibodies. TAP expression was compared to that of TAP WT cells; lysates of TAP KO cells served as negative control. β-actin was used as a loading control. (C and D) TAP-dependent peptide translocation in MJS cells transduced with the different variant-reference pairs, displayed as changes in mean fluorescence intensity (MFI), normalized to that of MJS WT cells. MJS WT cells incubated with ADP were used to verify that transport is ATP dependent. TAP1/2 KO cells transduced with an empty vector (EV) were used as a control. (E and F) Relative surface expression levels of MHC I molecules on MJS containing the different TAP variants compared to MJS WT, assessed by flow cytometry. MJS without antibody and TAP1/2 KO MJS were included as controls. Error bars indicate the SD, N=3.

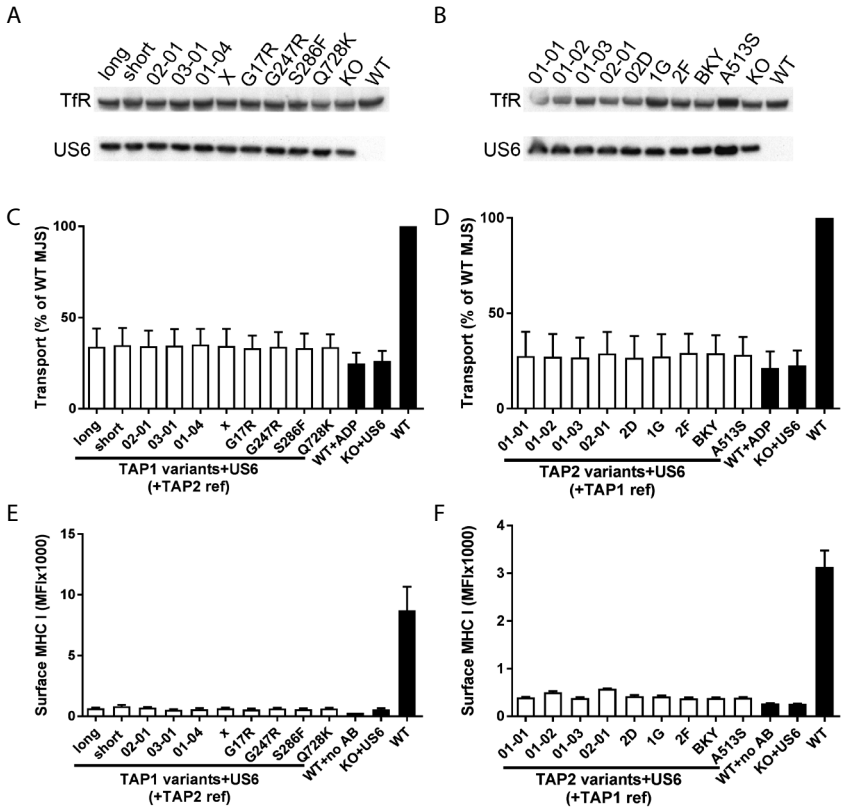

Figure 4: Inhibition of TAP function by the viral inhibitor US6. Expression of US6 in MJS containing the TAP1 variant-TAP2 reference pairs (A) and TAP2 variant-TAP1 reference pairs (B) was analyzed by immunoblotting (IB) of lysates with a mouse-anti-myc antibody. Lysates of TAP KO and untransduced WT cells served as controls. TfR was used as a loading control. (C and D) TAP-dependent peptide translocation in MJS cells transduced with the viral inhibitor US6 and different variant-reference pairs, displayed as changes in MFI, normalized to that of MJS WT cells. MJS WT cells incubated with ADP were used to verify that transport is ATP dependent. TAP1/2 KO cells transduced with the inhibitor US6 were used as a control. (E and F) Relative surface expression levels of MHC I molecules on MJS containing the different TAP variants and US6 compared to MJS WT cells, assessed by flow cytometry. MJS without antibody and TAP1/2 KO MJS cells+US6 were used as controls. Error bars indicate the SD, N=3.

mostly similar to the transport activity of wild-type cells. Upon addition of ADP, almost no transport was observed in wild type cells (Fig. 3C and 3D) or cells expressing TAP variants (data not shown). The level of peptide transport in the presence of ADP was similar to that in TAP1 and TAP2 KO cells.

Next, we assessed the relative MHC I surface expression levels in the presence of the various TAP variants as compared to wild type cells and TAP1/2 KO cells (Fig. 3E and 3F). The TAP variants showed some variation of MHC I surface expression, but the levels did not differ drastically from those observed in wild type cells.

3.4 Inhibition of peptide transport and MHC I surface expression by viral TAP inhibitors in cells expressing TAP1 and TAP2 variants

Next, we tested the ability of these TAP variants to escape inhibition by the TAP inhibitors US6 from HCMV, ICP47 from HSV-1 and BNLF2a from EBV. These viral proteins may affect the TAP variants differently, thereby providing a rationale for the existence of

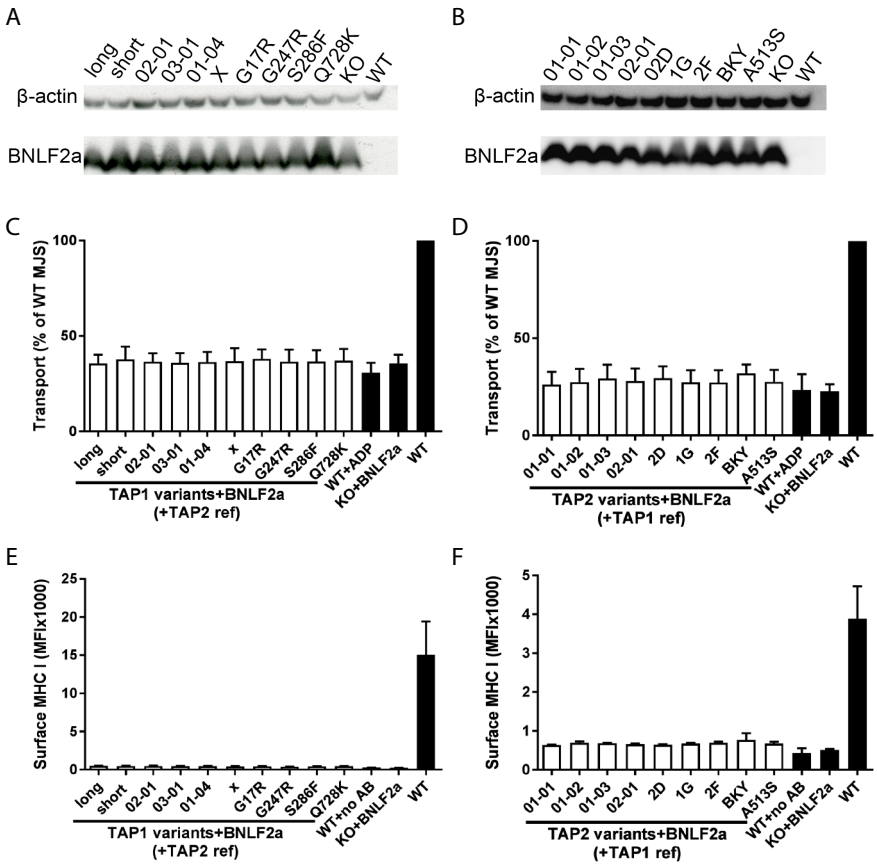

Figure 5: Inhibition of TAP function by the viral inhibitor BNLF2a. Expression of BNLF2a in MJS cells containing the TAP1 variant-TAP2 reference pairs (A) and TAP2 variant-TAP1 reference pairs (B) was analyzed by immunoblotting (IB) of lysates with a mouse-anti-myc antibody. Lysates of TAP KO cells served as negative control. β-actin was used as a loading control. (C and D) TAP-dependent peptide translocation in MJS cells transduced with the viral inhibitor BNLF2a and different variant-reference pairs, displayed as changes in MFI, normalized to that of MJS WT cells. MJS WT cells incubated with ADP were used to verify that transport is ATP dependent. TAP1/2 KO cells transduced with the inhibitor BNLF2a were used as a control. (E and F) Relative surface expression levels of MHC I molecules on MJS containing the different TAP variants and BNLF2a compared to MJS WT cells, assessed by flow cytometry. MJS without antibody and TAP1/2 KO MJS cells+BNLF2a were used as controls. Error bars indicate the SD, N=3.

TAP polymorphisms in the human population. The viral inhibitors and the various TAP alleles were introduced in the TAP1/TAP2 KO cells through lentiviral transduction. Peptide transport was evaluated in the resulting cell lines using a functional assay; in addition, MHC I surface expression was quantified (Fig 4-6).

The presence of the myc-tagged viral inhibitor US6 was confirmed by immunoblotting using a myc tag-specific antibody. The cells showed similar expression levels of US6 (Fig. 4A and 4B). The peptide translocation activity was normalized to the activity of MJS wild type cells (Fig. 4C and 4D). In the presence of US6, peptide translocation via the TAP variants was strongly inhibited, to levels similar to those in the presence of ADP, or in the absence of TAP1 and TAP2. In addition, the TAP variants tested did not differ in translocation activity. Next, MHC I surface levels were assessed in the presence of US6. The reduction of MHC I surface expression confirmed the inhibition of TAP by the viral US6 protein (Fig. 4E and 4F). All TAP1 and TAP2 variants showed an equally strong reduction of cell surface MHC I levels that was comparable to cells containing the viral inhibitor yet lacking TAP1 and TAP2.

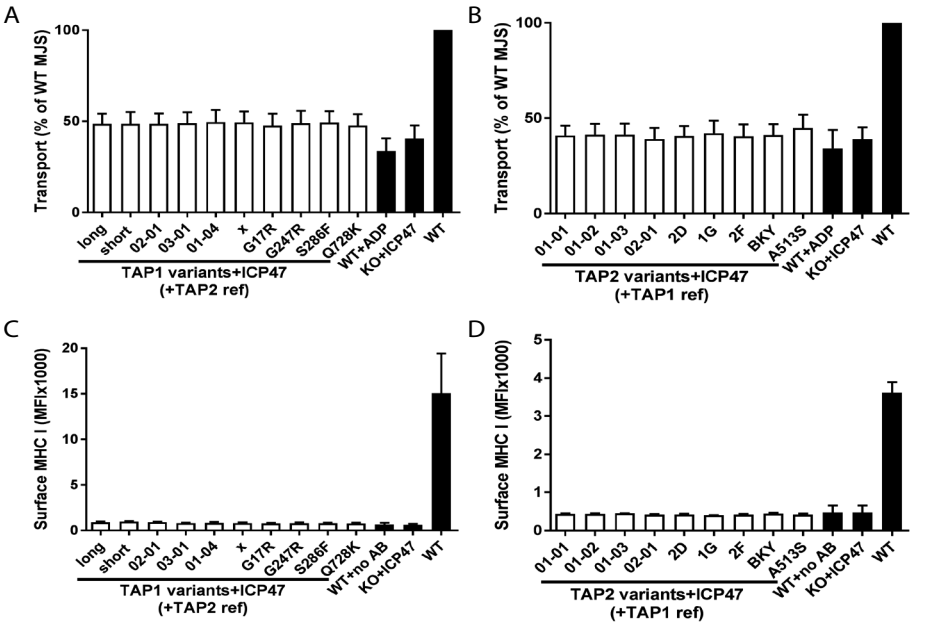

Figure 6: Inhibition of TAP function by the viral inhibitor ICP47. (A and B) TAP-dependent peptide translocation in MJS cells transduced with the viral inhibitor ICP47 and different variant-reference pairs, displayed as changes in MFI, normalized to that of MJS WT cells. MJS WT cells incubated with ADP were used to verify that transport is ATP dependent. TAP1/2 KO cells transduced with the inhibitor ICP47 were used as a control. (C and D) Relative surface expression levels of MHC I molecules on MJS containing the different TAP variants and ICP47 compared to MJS WT cells, assessed by flow cytometry. MJS without antibody and TAP1/2 KO MJS cells+ICP47 were used as controls. Error bars indicate the SD, N=3.

Next, the inhibitory effect of the viral inhibitors BNLF2a and ICP47 on the TAP1/TAP2 variants was analyzed. The presence of the inhibitors was confirmed by immunoblotting for BNLF2a (Fig. 5A and 5B), and by sequencing for ICP47 (data not shown; no antibody with sufficient sensitivity is available for immunoblotting of ICP47). BNLF2a and ICP47 were found to inhibit all TAP variants equally well, reducing peptide transport levels to those observed in TAP1 and TAP2 KO cells (Fig. 5C,D and Fig. 6A,B, respectively). In agreement with this, MHC I surface expression was reduced to background levels in the presence of both inhibitors (Fig. 5E,F and Fig. 6C,D, respectively).

In conclusion, all TAP1 and TAP2 variants were inhibited to a similar extent by the three herpesvirus-encoded TAP inhibitors.

4 Discussion

In this study, we addressed the functional consequences of TAP1 and TAP2 SNPs for peptide transport activity. In addition, we evaluated whether these SNPs influence inhibition of TAP by viral TAP inhibitors. Our results suggest that the SNPs present in a diverse collection of TAP variants have little or no effect on the peptide transport activity of the complex. Furthermore, the different TAP SNPs did not influence the inhibitory capacity of the viral immune evasion proteins ICP47, US6 and BNLF2a.

For some of the variants, expression was consistently higher compared to the other variants tested, for example for TAP1*01:04, TAP1*G247R and TAP2*1G. Possibly, certain SNPs influence the stability of TAP. However, higher or lower expression levels do not seem to correlate with increased or decreased transport activity. Over all, variation in TAP1 and TAP2 protein expression did not correlate with TAP activity *in vitro*.

Our findings are in agreement with a previous study comparing the peptide transport capacity of the TAP1 alleles 01-01, 02-01, and 03-01, and the TAP2 alleles 01-01, 02-01, and 01-02 [23, 24]. No major differences in TAP transport activity or MHC I surface levels were observed for these TAP alleles.

Several polymorphisms are located in, or in close proximity to, highly conserved regions known to be important for TAP function [11]. The polymorphism D637G present in the TAP alleles TAP1*02:01, TAP1*01:04 and TAP1*x results in a change in biochemical properties, as a negatively charged aspartic acid is replaced by a non-polar uncharged glycine. This polymorphism is in close proximity to the C-loop and Walker B domain. Both regions play a role in the binding and hydrolysis of ATP [41]. Nevertheless, the transport activity of the variants carrying this SNP was not very different from that measured in WT cells. The TAP alleles TAP1*02:01,TAP1*01:04 and TAP1*x, as well as TAP1*03:01 contain the SNP

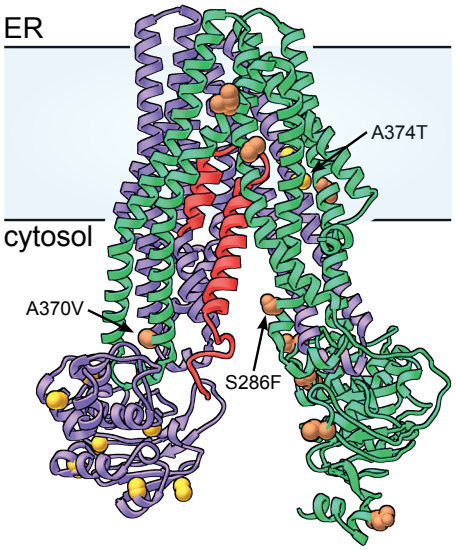

Figure 7: Molecular model of the TAP1-TAP2-ICP47 complex. The viral inhibitor ICP47 (red) forms a helix-loop-helix structure and blocks TAP by obstructing the peptide translocation pathway with a helical hairpin. The SNPs S286F and A370V from TAP1 and A374T from TAP2 are located in close proximity to ICP47.

I333V. The polymorphism I333V is associated with a higher risk of cervical intraepithelial neoplasia after infection of HPV [21]. In the present study, the TAP1*03:01 allele did not exhibit dramatic changes in MHC I surface expression nor did it affect peptide translocation in absence or presence of the viral inhibitors in comparison to the other alleles and the WT cells. It remains possible that peptides highly specific for certain diseases are better transported by certain TAP variants. This may not be reflected by assays measuring overall transport activity or MHC I surface expression.

Regions comprising residues 375-420 and 453-487 of TAP1 and residues 301-389 and 414-433 of TAP2 form part of the peptide binding site [42]. Interestingly, several TAP variants have SNPs in or in close proximity to the peptide binding site, including TAP1 SNPs I333V, A370V and S286F and TAP2 SNPs A374T and V379I. However, the transport activity of TAP proteins containing these polymorphisms is within the same range.

Certain TAP alleles show differences in frequency amongst Africans, Caucasians and Brazilians [13]. These polymorphisms may have emerged within populations due to evolutionary pressure exerted by certain pathogens occurring in these geographically distinct regions [15]. US6, BNLF2a and ICP47 block different TAP-variants equally well and are therefore unlikely to have caused selection pressure on the different SNPs of TAP evaluated in this study. Although it remains possible that certain combinations of

SNPs in TAP1 and TAP2 could influence peptide transport by TAP and its resistance to viral inhibition, no consistent linkage disequilibrium has been found between TAP1 and TAP2 alleles [43, 44].

Recent studies have revealed the mechanism that is used by the viral inhibitor ICP47 to block peptide transport by TAP [45–47]. ICP47 affects peptide binding to TAP by trapping TAP in an inward-facing conformation[36](Oldham et al., 2016a). The molecular structure of TAP1-TAP2-ICP47 presented in these studies reveals that only the TAP1 SNPs S286F and A370V, and the TAP2 SNP A374T are located within potential interacting distance (8 Å) of ICP47 (fig. 7). The most likely interaction would involve the TAP1 residue S286 that, when changed to phenylalanine, would create a more hydrophobic environment around the flexible C-terminal tail of ICP47. However, inhibition of TAP by ICP47 seems not to be influenced by any of the SNPs tested. The TAP1 SNPs V458L and I333V and the TAP2 SNP V379I are located in close proximity to the binding site of ICP47, yet do not directly interact with ICP47. Therefore, these SNPs are unlikely to affect the inhibitory capacity of ICP47.

In contrast to ICP47, HCMV US6 interacts with TM domains 7-10 of TAP1 and TM 1-4 of TAP2 to interfere with ATP binding to TAP1 [48] (fig 8B). Since the exact binding site nor the structure of US6 and BNLF2a have been elucidated, assumptions about the specific mode of interaction of these inhibitors with TAP remain speculative. Furthermore, it is unknown if US6 and BNLF2a also arrest the TAP-complex in a stable conformation as does ICP47 [49]. It has been suggested that US6 interacts with the TAP1 and TAP2 TMDs and occupies the translocation pore from the luminal side [48]. Moreover, ICP47 and US6 cannot simultaneously bind to TAP [50]. Therefore, it is likely that ICP47 and US6 bind to

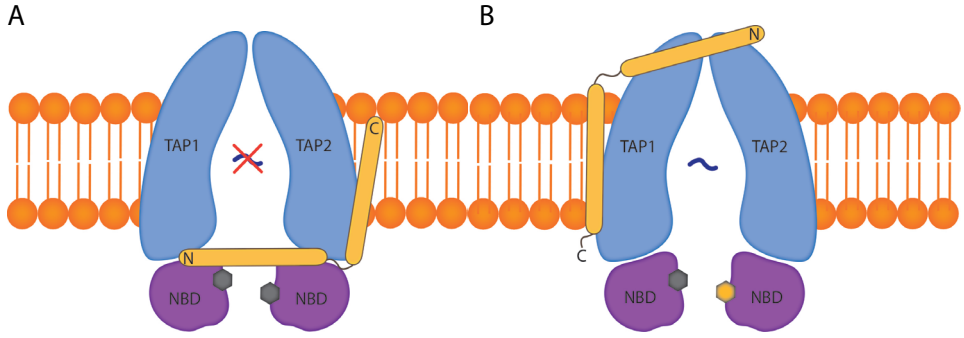

Figure 8: Schematic representation of the interaction between the TAP complex and the viral inhibitors BNLF2a and US6. (A) Upon binding of the tail anchored transmembrane protein BNLF2a to TAP, peptide binding as well as ATP binding are inhibited. (B) In contrast to BNLF2a, the inhibitor US6 interferes with ATP binding to TAP1 while interacting with the ER-luminal loops of TAP1 and TAP2.

TAP at different stages during the peptide translocation cycle and thus target distinct conformations of TAP (reviewed in Praest *et al*., manuscript submitted).

A recent structural study has made clever use of ICP47 to isolate the fully assembled PLC [45]. This study has provided crucial insights into the overall structure and stoichiometry of the PLC. However, the cytosolic part of the TAP heterodimer and the inhibitor ICP47 are resolved in a low resolution. Isolation of the PLC in the presence of US6 or BNLF2a will be instrumental to uncover the mechanisms by which these viral immune evasion proteins interfere with TAP function. Additionally, these studies may provide new insights into the structure of the PLC, in particular of those parts that remain to be resolved at high resolution.

Acknowledgements

We thank Dr. Jan Wouter Drijfhout from the Department of Immunohematology and Blood Transfusion at the Leiden University Medical Center, Leiden, The Netherlands, for generously providing reagents. This work was funded by the European Commission under the Horizon2020 program H2020 MSCA-ITN GA 675278 EDGE.

References

1. Sadasivan B, Lehner PJ, Ortmann B, et al (1996) Roles for calreticulin and a novel glycoprotein, tapasin, in the interaction of MHC class I molecules with TAP. Immunity 5:103–14
2. Townsend A, Öhlén C, Bastin J, et al (1989) Association of class I major histocompatibility heavy and light chains induced by viral peptides. Nature 340:443–448. https://doi.org/10.1038/340443a0
3. Ljunggren H-G, Stam NJ, Öhlén C, et al (1990) Empty MHC class I molecules come out in the cold. Nature 346:476–480. https://doi.org/10.1038/346476a0
4. Verweij MC, Horst D, Griffin BD, et al (2015) Viral inhibition of the transporter associated with antigen processing (TAP): a striking example of functional convergent evolution. PLoS Pathog 11:e1004743. https://doi.org/10.1371/journal.ppat.1004743
5. van de Weijer ML, Luteijn RD, Wiertz EJHJ (2015) Viral immune evasion: Lessons in MHC class I antigen presentation. Semin Immunol 27:125–137. https://doi.org/10.1016/j.smim.2015.03.010
6. Dean M, Annilo T (2005) Evolution of the Atp-Binding Cassette (Abc) Transporter Superfamily in Vertebrates*. Annu Rev Genomics Hum Genet 6:123–142. https://doi.org/10.1146/annurev.genom.6.080604.162122
7. Koch J, Guntrum R, Heintke S, et al (2004) Functional Dissection of the Transmembrane Domains of the Transporter Associated with Antigen Processing (TAP). J Biol Chem 279:10142–10147. https://doi.org/10.1074/jbc.M312816200
8. Neefjes JJ, Momburg F, Hämmerling GJ (1993) Selective and ATP-dependent translocation of peptides by the MHC-encoded transporter. Science 261:769–71

9. van Endert PM, Tampé R, Meyer TH, et al (1994) A sequential model for peptide binding and transport by the transporters associated with antigen processing. Immunity 1:491–500. https://doi.org/10.1016/1074-7613(94)90091-4
10. Walker JE, Saraste M, Runswick MJ, Gay NJ (1982) Distantly related sequences in the alpha- and beta-subunits of ATP synthase, myosin, kinases and other ATP-requiring enzymes and a common nucleotide binding fold. EMBO J 1:945–51
11. McCluskey J, Rossjohn J, Purcell AW (2004) TAP genes and immunity. Curr Opin Immunol 16:651–9. https://doi.org/10.1016/j.coi.2004.07.016
12. Gaudet R, Wiley DC (2001) Structure of the ABC ATPase domain of human TAP1, the transporter associated with antigen processing. EMBO J 20:4964–72. https://doi.org/10.1093/emboj/20.17.4964
13. Tang J, Freedman DO, Allen S, et al (2001) TAPI polymorphisms in several human ethnic groups: characteristics, evolution, and genotyping strategies. Hum Immunol 62:256–68
14. Tang J, Freedman DO, Allen S, et al (2001) Genotyping TAP2 variants in North American Caucasians, Brazilians, and Africans. Genes Immun 2:32–40. https://doi.org/10.1038/sj.gene.6363731
15. Lajoie J, Zijenah LS, Faucher MC, et al (2003) Novel TAP1 polymorphisms in indigenous Zimbabweans: their potential implications on TAP function and in human diseases. Hum Immunol 64:823–9
16. Wang D, Zhou Y, Ji L, et al (2012) Association of LMP/TAP gene polymorphisms with tuberculosis susceptibility in Li population in China. PLoS One 7:e33051. https://doi.org/10.1371/journal.pone.0033051
17. Naderi M, Hashemi M, Aminia S (2016) Association of TAP1 and TAP2 Gene Polymorphisms with Susceptibility to Pulmonary Tuberculosis. Iran J Allergy Asthma Immunol 15:62–8
18. Bullido MJ, Martínez-García A, Artiga MJ, et al (2007) A TAP2 genotype associated with Alzheimer's disease in APOE4 carriers. Neurobiol Aging 28:519–23. https://doi.org/10.1016/j.neurobiolaging.2006.02.011
19. Kim HK, Lee H, Lew BL, et al (2015) Association between TAP1 gene polymorphisms and alopecia areata in a Korean population. Genet Mol Res 14:18820–18827. https://doi.org/10.4238/2015.December.28.31
20. Ozbas-Gerceker F, Bozman N, Gezici S, et al (2013) Association of TAP1 and TAP2 gene polymorphisms with hematological malignancies. Asian Pac J Cancer Prev 14:5213–7
21. Natter C, Polterauer S, Rahhal-Schupp J, et al (2013) Association of TAP gene polymorphisms and risk of cervical intraepithelial neoplasia. Dis Markers 35:79–84. https://doi.org/10.1155/2013/368732
22. Powis SJ, Young LL, Joly E, et al (1996) The rat cim effect: TAP allele-dependent changes in a class I MHC anchor motif and evidence against C-terminal trimming of peptides in the ER. Immunity 4:159–65
23. Obst R, Armandola EA, Nijenhuis M, et al (1995) TAP polymorphism does not influence transport of peptide variants in mice and humans. Eur J Immunol 25:2170–2176. https://doi.org/10.1002/eji.1830250808
24. Daniel S, Caillat-Zucman S, Hammer J, et al (1997) Absence of functional relevance of human transporter associated with antigen processing polymorphism for peptide selection. J Immunol 159:2350–7
25. Borghans JAM, Beltman JB, De Boer RJ (2004) MHC polymorphism under host-pathogen coevolution. Immunogenetics 55:732–9. https://doi.org/10.1007/s00251-003-0630-5

26. Potts WK, Slev PR (1995) Pathogen-based models favoring MHC genetic diversity. Immunol Rev 143:181–97

27. Kubinak JL, Ruff JS, Cornwall DH, et al (2013) Experimental viral evolution reveals major histocompatibility complex polymorphisms as the primary host factors controlling pathogen adaptation and virulence. Genes Immun 14:365–72. https://doi.org/10.1038/gene.2013.27

28. Carrillo-Bustamante P, Keşmir C, de Boer RJ (2015) A Coevolutionary Arms Race between Hosts and Viruses Drives Polymorphism and Polygenicity of NK Cell Receptors. Mol Biol Evol 32:2149–60. https://doi.org/10.1093/molbev/msv096

29. van de Weijer ML, Bassik MC, Luteijn RD, et al (2014) A high-coverage shRNA screen identifies TMEM129 as an E3 ligase involved in ER-associated protein degradation. Nat Commun 5:3832. https://doi.org/10.1038/ncomms4832

30. van Diemen FR, Kruse EM, Hooykaas MJG, et al (2016) CRISPR/Cas9-Mediated Genome Editing of Herpesviruses Limits Productive and Latent Infections. PLoS Pathog 12:e1005701. https://doi.org/10.1371/journal.ppat.1005701

31. Hewitt EW, Gupta SS, Lehner PJ (2001) The human cytomegalovirus gene product US6 inhibits ATP binding by TAP. EMBO J 20:387–96. https://doi.org/10.1093/emboj/20.3.387

32. Horst D, van Leeuwen D, Croft NP, et al (2009) Specific Targeting of the EBV Lytic Phase Protein BNLF2a to the Transporter Associated with Antigen Processing Results in Impairment of HLA Class I-Restricted Antigen Presentation. J Immunol 182:2313–2324. https://doi.org/10.4049/jimmunol.0803218

33. Ahn K, Meyer TH, Uebel S, et al (1996) Molecular mechanism and species specificity of TAP inhibition by herpes simplex virus ICP47. EMBO J 15:3247–55

34. Fischbach H, Döring M, Nikles D, et al (2015) Ultrasensitive quantification of TAP-dependent antigen compartmentalization in scarce primary immune cell subsets. Nat Commun 6:6199. https://doi.org/10.1038/ncomms7199

35. Plewnia G, Schulze K, Hunte C, et al (2007) Modulation of the Antigenic Peptide Transporter TAP by Recombinant Antibodies Binding to the Last Five Residues of TAP1. J Mol Biol 369:95–107. https://doi.org/10.1016/j.jmb.2007.02.102

36. Oldham ML, Grigorieff N, Chen J (2016) Structure of the transporter associated with antigen processing trapped by herpes simplex virus. Elife 5:. https://doi.org/10.7554/eLife.21829

37. Webb B, Sali A, Webb B, Sali A (2014) Comparative Protein Structure Modeling Using MODELLER. In: Current Protocols in Bioinformatics. John Wiley & Sons, Inc., Hoboken, NJ, USA, pp 5.6.1-5.6.32

38. Pettersen EF, Goddard TD, Huang CC, et al (2004) UCSF Chimera?A visualization system for exploratory research and analysis. J Comput Chem 25:1605–1612. https://doi.org/10.1002/jcc.20084

39. Powis SH, Tonks S, Mockridge I, et al (1993) Alleles and haplotypes of the MHC-encoded ABC transporters. Immunogenetics 37:373–380

40. Keusekotten K, Leonhardt RM, Ehses S, Knittler MR (2006) Biogenesis of functional antigenic peptide transporter TAP requires assembly of pre-existing TAP1 with newly synthesized TAP2. J Biol Chem 281:17545–51. https://doi.org/10.1074/jbc.M602360200

41. Parcej D, Tampé R (2010) ABC proteins in antigen translocation and viral inhibition. Nat Chem Biol 6:572–80. https://doi.org/10.1038/nchembio.410

42. Nijenhuis M, Hämmerling GJ (1996) Multiple regions of the transporter associated with antigen processing (TAP) contribute to its peptide binding site. J Immunol 157:5467–77

43. Alvarado-Guerri R, Cabrera CM, Garrido F, López-Nevot MA (2005) TAP1 and TAP2 polymorphisms and their linkage disequilibrium with HLA-DR, -DP, and -DQ in an eastern Andalusian population. Hum Immunol 66:921–30. https://doi.org/10.1016/j.humimm.2005.06.009

44. Klitz W, Stephens JC, Grote M, Carrington M (1995) Discordant patterns of linkage disequilibrium of the peptide-transporter loci within the HLA class II region. Am J Hum Genet 57:1436–44

45. Blees A, Januliene D, Hofmann T, et al (2017) Structure of the human MHC-I peptide-loading complex. Nature 551:525–528. https://doi.org/10.1038/nature24627

46. Oldham ML, Hite RK, Steffen AM, et al (2016) A mechanism of viral immune evasion revealed by cryo-EM analysis of the TAP transporter. Nature 529:537–40. https://doi.org/10.1038/nature16506

47. Luteijn RD, Wiertz EJHJ (2016) Exploiting the exploiter: a viral inhibitor stabilizes TAP for cryo-EM. Nat Struct Mol Biol 23:95–97. https://doi.org/10.1038/nsmb.3168

48. Halenius A, Momburg F, Reinhard H, et al (2005) Physical and Functional Interactions of the Cytomegalovirus US6 Glycoprotein with the Transporter Associated with Antigen Processing. J Biol Chem 281:5383–5390. https://doi.org/10.1074/jbc.M510223200

49. Herbring V, Bäucker A, Trowitzsch S, Tampé R (2016) A dual inhibition mechanism of herpesviral ICP47 arresting a conformationally thermostable TAP complex. Sci Rep 6:36907. https://doi.org/10.1038/srep36907

50. Matschulla T, Berry R, Gerke C, et al (2017) A highly conserved sequence of the viral TAP inhibitor ICP47 is required for freezing of the peptide transport cycle. Sci Rep 7:2933. https://doi.org/10.1038/s41598-017-02994-5

Supplementary Material

Table S1: Primers used for the generation of the TAP1 and TAP2 alleles.

Primer No.	Sequence 5'-3'
1	ccggtgcatgactaagctagtaccggttaggatgcatgctcaggagcccttctcgaactgtggatgggaccaagacccttttc-tcaaactgagggtgactccaagatcctttctcgaactggggatggctccattctggagcatctgcaggagcctgc
2	gtcgtgagctagcagtattaattaaccaccatggctagctctaggtgtcccg
3	cagaggcagggtgaccagggtgacc
4	ggtcaccctggtcaccctgcctctg
5	cagaggtagccgaggctgg
6	ccagcctcggctacctctg
7	gctgcctccccagagcttctctcgc
8	gcgagagaagctctggggaggcagc
9	gagttcgtgggtgacaggatctataacaacaccatg
10	catggtgttgttatagatcctgtcacccacgaactc
11	caggtaacatcatgtttcgggtaacagagg
12	cctctgttacccgaaacatgatgttacctg
13	ggaacccaccagaagctcatggagaaaaag
14	ctttttctccatgagcttctggtgggttcc
15	gtcagtaccggttaggatgcatgcttaatggtgatggtgatggtggagctgggcaagcttctgc
16	gctctgcagcccataagaaatgttgttcctcac
17	gtgaggaacaacatttcttatgggctgcagagc
18	ctgtgcgatccccacaggaattccagtc
19	gactggaattcctgtggggatcgcacag
20	cacaggctgcaggcagttcagcgcgc
21	gcgcgctgaactgcctgcagcctgtg
22	ctagtaccggttaggatgcatgcttaatggtgatggtgatggtggtccatcagccgctgctgaaccaggcgggaatag-aggtcctgtccctcctggagctgggcaagcttctgcag
23	gcggagagacctggaacgcgccttgtacctgctcgtaagg
24	ccttacgagcaggtacaaggcgcgttccaggtctctccgc
25	gcccccaccactctgcaggggggttgtgaaattccaagacg
26	cgtcttggaatttcacaacccccctgcagagtggtgggggc
27	cagcaccctccttatgagcaggtacaag
28	cttgtacctgctcataaggagggtgctg
29	ctgggcagccgccaccaccttatcatc
30	gatgataaggtggtggcggctgcccag
31	ctgcagcagggcagacactgtgctcttc
32	gaagagcacagtgtctgccctgctgcag

33	gagcagtacctccaaagcctgggtgaac
34	gttcacccaggctttggaggtactgctc
35	gccactgcctgttgctgacccctg
36	caggggtcagcaacaggcagtggc
37	gccgacagaacctcaatgg
38	ccattgaggttctgtcggc
39	gtagcactaagatatctgggcgg
40	ccgcccagatatcttagtgctac

Table S2: Primers used for adding a myc- to the viral TAP inhibitors or a streptavidin-tag to the TAP variants.

Primer No.	Sequence 5'-3'
41	gctagtaccggttaggatgcatgcttagaggtcctcttcagagatgagcttctgctccacgtgggagccacaacgtcgaatcc
42	cgtgagctagcagtattaattaaaccaccatggatctcttgattcgtctcg
43	gctagtaccggttaggatgcatgcttagaggtcctcttcagagatgagcttctgctccacgtggatgaggagcaggca-taaaag
44	cgtgagctagcagtattaattaaaccaccatggtacacgtcctggagcg
45	gctagtaccggttaggatgcatgcttaacgggttaccggattacg
46	gtgagctagcagtattaattaaaccaccatggagcagaagctcatctctgaagaggacctccacgtgtcgtgggccctg-gaaatgg
47	ctgctagctcacgacacctgaaatgg
48	ctagctcacgacacctgaaatg

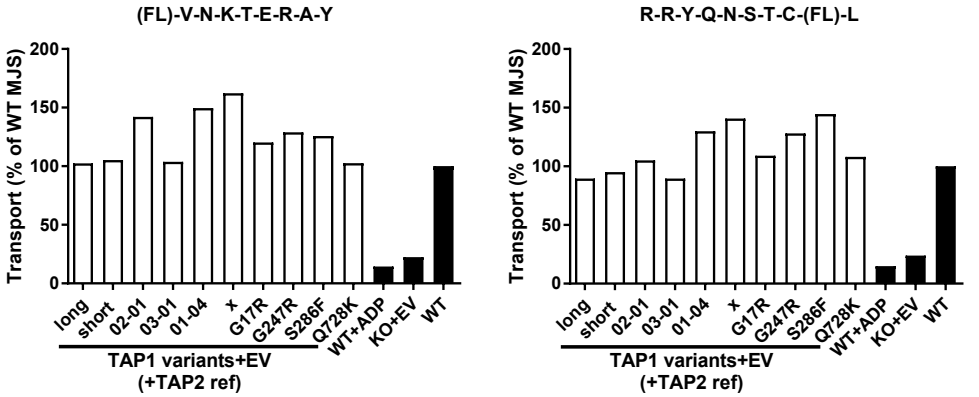

Figure S1: TAP-dependent peptide translocation determined using two different fluorescent peptide substrates. TAP-dependent peptide translocation in MJS cells transduced with the different variant-reference pairs, displayed as changes in mean fluorescence intensity (MFI), normalized to that of MJS WT cells. MJS WT cells incubated with ADP were used to verify that transport is ATP dependent. TAP1/2 KO cells transduced with an empty vector (EV) were used as a control. Transport efficiency of the peptides (FL)-V-N-K-T-E-R-A-Y and R-R-Y-Q-N-S-T-C-(FL)-L were compared.

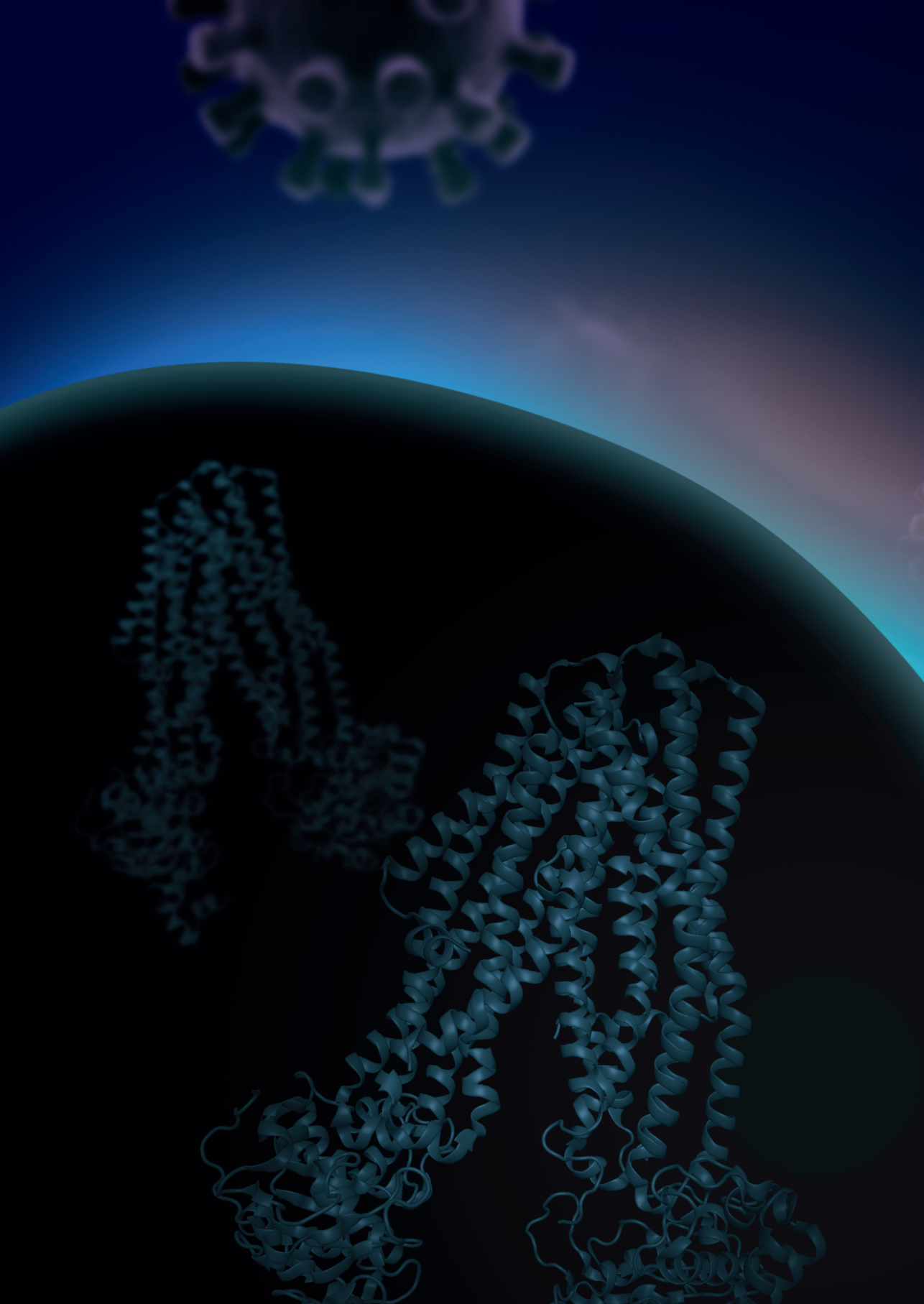

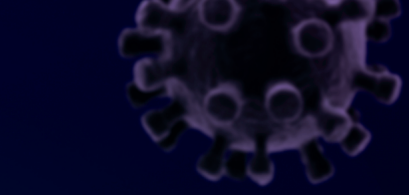

3

A flow cytometry-based approach to unravel viral interference with the MHC class I antigen presentation pathway

P. Praest, H. de Buhr, E.J.H.J. Wiertz

Methods in Molecular Biology,
Antigen Processing, 2nded (2019) P.187-198

Summary

MHC class I molecules are an important component of the cell-mediated immune defense, presenting peptides to surveilling $CD8^+$ cytotoxic T cells. During viral infection, MHC class I molecules carry and display viral peptides at the cell surface. $CD8^+$ T cells that recognize these peptides will eliminate the virus-infected cells. Viruses counteract this highly sophisticated host detection system by downregulating cell surface expression of MHC class I molecules.

In this chapter, we describe a flow cytometry-based method that can be used for the identification of viral gene products potentially responsible for evasion from MHC class I-restricted antigen presentation. The gene(s) of interest are expressed constitutively through lentiviral transduction of cells. Subsequently, MHC I surface expression is monitored using MHC class I-specific antibodies. Once the viral gene product responsible for MHC I downregulation has been identified, the same cells can be used to elucidate the mechanism of action. The stage at which interference with antigen processing occurs can be identified using specific assays. An essential step frequently targeted by viruses is the translocation of peptides into the ER by the transporter associated with antigen processing, TAP. TAP function can be measured using a highly specific *in vitro* assay involving flow cytometric evaluation of the import of a fluorescent peptide substrate.

The protocol described in this chapter enables the identification of virus-encoded MHC class I inhibitors that hinder antigen processing and presentation. Subsequently, their mechanism of action can be unraveled; this knowledge may help to rectify their actions.

1 Introduction

The MHC class I-restricted antigen presentation pathway is a crucial host immune defense mechanism to counter viral infection. Viruses hijack the host's cellular machinery for their own protein synthesis and, ultimately, their replication in the host cell. As part of the normal protein turnover, cytosolic proteasomes degrade a proportion of these viral proteins. The transporter associated with antigen processing (TAP) translocates the resulting peptides into the ER lumen, where they are loaded onto MHC class I molecules. Subsequently, the MHC class I/peptide complexes are displayed at the cell surface, where they can be recognized by $CD8^+$ cytotoxic T lymphocytes (CTLs). This ultimately leads to the cell's destruction and thereby restriction of viral infection.

Viruses have evolved highly specific countermeasures to avert cellular immunosurveillance. Every step of the MHC class-1 restricted antigen presentation pathway can be impacted by viral proteins. Especially, large DNA viruses like herpesviruses, poxviruses and adenoviruses, but also other viruses like HIV impede immunosurveillance (**Figure 1**) [1]–[6]. Viruses employ a great diversity of strategies to interfere with MHC I antigen presentation, including inhibition of MHC class I protein synthesis, obstruction of MHC class I/peptide complex trafficking, and the induction of cytosolic or lysosomal degradation of MHC class I molecules. In addition, viruses can restrict MHC class I peptide binding by inhibiting proteasomal degradation or by interfering with TAP-mediated peptide transport into the ER. Finally, certain viruses prevent CTL recognition of MHC class I molecules at the cell surface.

Flow cytometry is a fast and efficient method to assess viral interference with MHC class I-restricted antigen presentation and the subsequent identification of the viral peptides responsible. Viral genes of interest can either be expressed transiently from a plasmid through transfection, or can be expressed constitutively through lentiviral transduction. Cell surface expression of MHC class I molecules can be evaluated using specific antibodies. Transient transfection is faster and can result in adequate gene expression levels. However, lentiviral transduction is superior to transient transfections due to the integration of DNA into the host genome and thereby lead to stable expression of viral genes. Transfection for transient gene expression can be executed in various ways, commonly through lipofection or nucleofection (electroporation). Various lipofection reagents are commercially available (e.g. PEI, Lipofectamine, etc.) to engulf and deliver the DNA (plasmid) to the cell in a lipid complex. This is less harmful to the cell compared to electroporation-based methods like nucleofection, which utilize electric fields to permeabilize cell membranes for DNA uptake. Transfection efficiencies may vary between methods and cell lines.

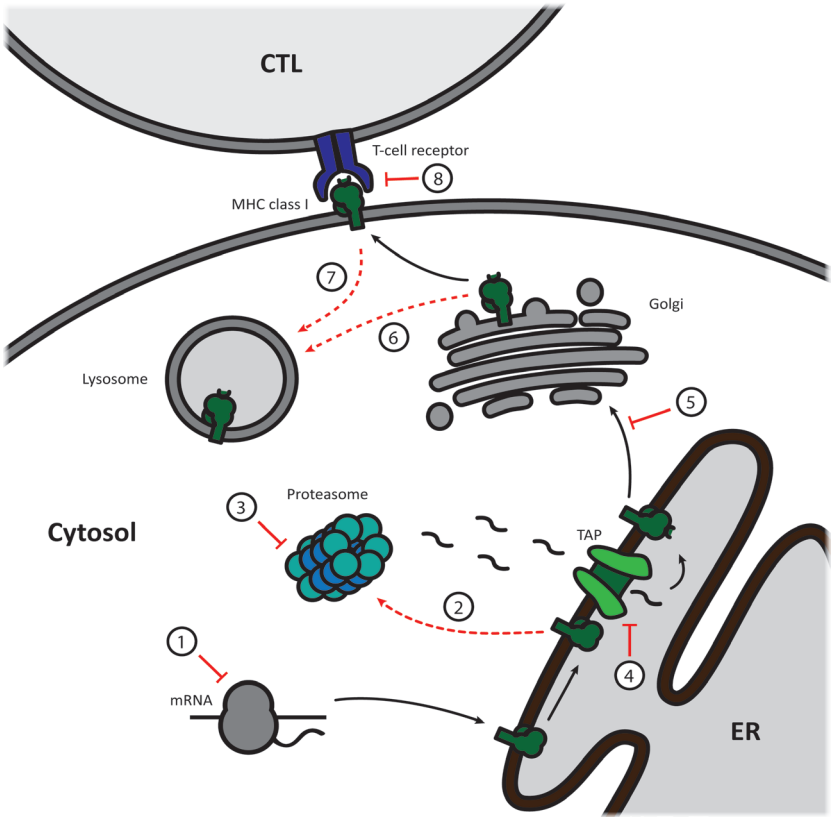

Figure 1: Viral interference with MHC class I-restricted antigen presentation. Viruses virtually subvert every step of the MHC class I-restricted antigen presentation pathway: (1) inhibition of MHC class I synthesis, (2) degradation of MHC class I by cytosolic proteasomes, (3) interference with proteasomal degradation of protein substrates, (4) obstruction of peptide transport into the ER via TAP, (5) inhibition of MHC class I trafficking, (6) redirection of MHC class I to lysosomes, (7) increase in endocytosis and lysosomal degradation of cell surface MHC class I, and (8) interference with recognition of cell surface MHC class I by T cell receptors of CTLs.

Lentiviruses are very suitable for the delivery of DNA into cells and its permanent integration into the host's genome. Subsequent antibiotic selection guarantees cell lines constitutively expressing the gene(s)-of-interest. For the protocol described here, lentiviral transduction is the method of choice to ensure proper viral gene expression. DNA delivery methods and their respective (dis)advantages have been reviewed by Kim & Eberwine [7].

Irrespective of the DNA delivery method, we recommend a vector co-expressing the protein(s)-of-interest and a fluorescent marker and/or an antibiotic selection marker. In transfected cells, the expression levels of the viral proteins should correlate to the expression of the fluorescent marker.

Subsequently, we describe a protocol for surface staining of MHC class I molecules. Viral immune evasion strategies naturally vary and thus their ability to downregulate the expression of MHC class I alleles differ as well (Figure 1). In contrast to interfering with MHC class I display on the cell surface, viral genes might obstruct immunosurveillance at different levels not detectable by FACS analysis. One striking example is the murine cytomegalovirus (MCMV) gp34 protein, that inhibits the recognition of MHC class I/peptide complexes by T cell receptors on $CD8^+$ T cells [8]. Consequently, unless they interfere with antibody binding, such viral genes evade detection with the screening method described here. Nevertheless, they can be identified using CTL recognition assays or TCR-like antibodies as described elsewhere in this volume (see chapters by Dolan and Lemonnier, and by Canaday in the previous edition of this book).

Alternatively to expression of specific viral genes, cells can be infected with a virus. This will allow for the assessment of MHC class I downregulation. Should this be observed, individual orfs can be expressed to identify the responsible viral gene product(s). After identification of a viral protein interfering with MHC class I-restricted antigen presentation, cell lines stably expressing this viral protein can aid investigations into its mechanism of action. Approaches that may be used for this purpose have been described in detail in this volume (see chapters by Giuliano & Antoniou, Jongsma & Neefjes, Wearsch & Cresswell, Ghanem & Springer in the previous edition of this book). In addition, metabolic labelling experiments can be useful, for instance to examine whether the viral protein interferes with MHC class I synthesis or trafficking, or if it rather induces degradation of MHC class I molecules via cytosolic proteasomes or through endosomal proteases [9]–[11] (Guiliano & Antoniou, previous edition).

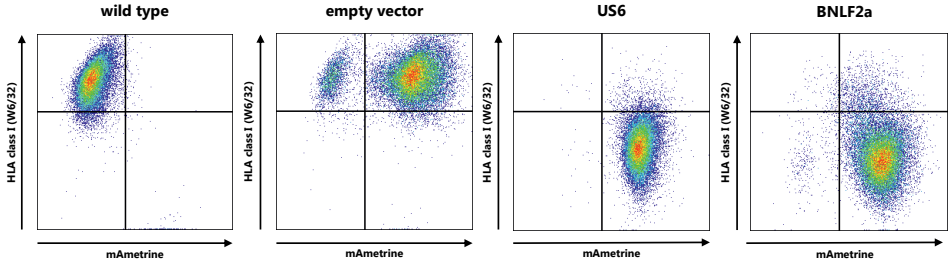

Figure 2: Downregulation of MHC class I cell surface expression by the TAP inhibitors US6 from HCMV and BNLF2a from EBV. RAJI cells were lentivirally transduced and selected for zeomycin resistance, resulting in a high number of cells expressing the fluorescent control protein mAmetrine or co-expressing mAmetrine and the viral TAP inhibitor US6 or BNLF2a. Seven days post transduction, cells were stained for cell surface expression of total HLA class I (PE-conjugated W6/32, Serotec MCA81PE, 1:20). Subsequently, the cells were analyzed by flow cytometry using FlowJo v10 software.

Another frequent target of viral immune evasion proteins is the peptide transporter TAP [3],[12]. Assays to analyze TAP function have been described by Jongsma & Neefjes (previous edition and by Fischbach *et al.* [13]). The latter developed an ultrasensitive flow cytometry-based approach to quantify TAP activity by measuring fluorescent antigenic peptides (protocol included in this chapter). Peptide transport assays have been employed successfully to characterize viral TAP inhibitors, e.g. the ICP47 protein of herpes simplex virus 1 and 2, the UL49.5 protein encoded by certain varicelloviruses, the US6 protein of human cytomegalovirus, and the BNLF2a protein of Epstein-Barr virus [14]–[18].

Taken together, the MHC class I antigen presentation pathway represents a frequent target for viral immune evasion strategies. We describe a protocol for flow cytometry-based detection of viral interference with MHC class I-restricted antigen processing and presentation. Subsequent to detection of MHC class I downregulation, individual viral gene products can be evaluated to identify viral orf(s) responsible for the observed phenotype. This method employs stable lentiviral transduction for simultaneous expression of the viral gene products, a fluorescent reporter and/or a selection marker. Although transient transfection presents an alternative for this protocol, we highly recommend lentiviral

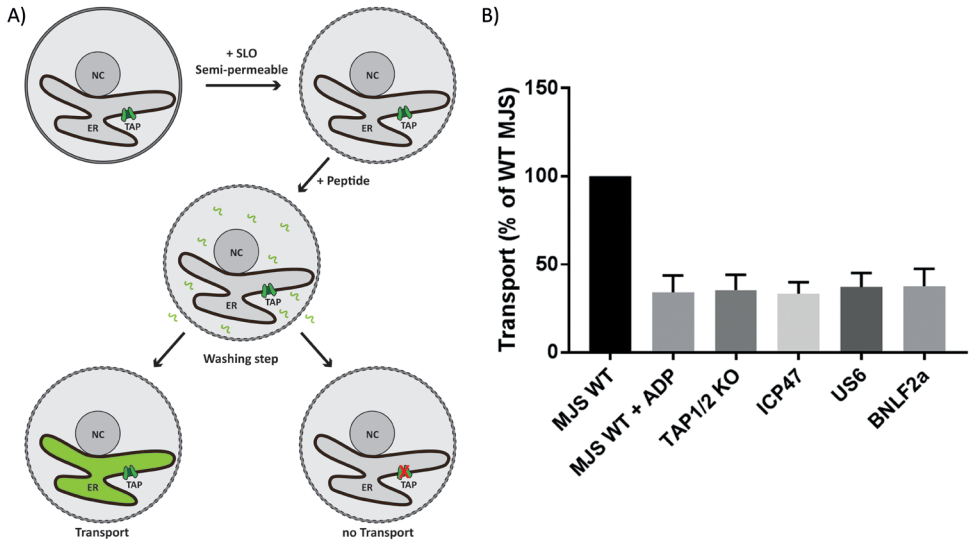

Figure 3: TAP dependent peptide translocation assay. A) Schematic overview. Cells are semi-permeabilized using SLO followed by incubation with a peptide carrying an N-linked glycosylation consensus sequence and fluorescein. The N-linked glycan facilitates ER-retention of the peptide. After washing, the cells are analyzed by flow cytometry. Transport efficiency correlates with the mean fluorescence intensity. NC= nucleus; ER= endoplasmic reticulum; TAP= transporter associated with antigen processing. B) Peptide transport in MelJuSo wildtype (MJS WT) cells was set at 100% and compared to MJS WT cells treated with ADP instead of ATP, cells lacking TAP1/2 and cell lines expressing herpesvirus TAP inhibitors.

transduction. Thus, viral genes will be expressed stably in every cell. Consequently, the constitutive expression of viral gene(s) of interest allows for evaluating their mode of action.

2 Materials

2.1 Lentiviral transduction

1. Cells expressing MHC class I (*see* **note 1**).
2. 24-well plate for cell culture.
3. Complete culture medium. Medium used depends on cell line of interest.
4. Lentiviruses expressing gene(s)-of-interest, a fluorescent marker and/or a selection marker (*see* **note 2 and 3**).
5. Polybrene (10 mg/ml stock).

2.2 Transient transfection using PEI (or alternative lipofection reagent)

1. Cells expressing MHC class I (*see* **note 1**).
2. 12-well plate for cell culture.
3. Complete culture medium without antibiotics. Medium depends on the cell line of interest.
4. Plasmid expressing the gene(s)-of-interest and a fluorescent marker (*see* **note 3**).
5. PEI solution: dissolve PEI powder (Polyethylenimine "Max", (nominally Mw 40,000*) - High Potency Linear PEI (Equivalent to Mw 25,000 in Free Base Form) Polysciences, Inc.) to a concentration of 1 mg/ml in high purity water. This might take a couple of hours during which the solution should be shaken vigorously (additionally, the reaction can be facilitated by heating the solution to 80°C). Allow the solution to cool to room temperature, adjust the pH to 7.4 with HCl and filter sterilize it. Aliquot the PEI solution and store at –80°C. The working aliquot can be stored temporary at 4°C.
6. 150 mM NaCl solution, filter sterilized. Store at room temperature.
7. Polypropylene tubes.

2.3 Cell surface staining and flow cytometry

1. PBS.
2. PBA: PBS with 0.5% bovine serum albumin (BSA) and 0.02% sodium azide (*see* **note 4 and 5**). Store at 4°C.
3. 1% paraformaldehyde in PBS (preferably prepared freshly before usage).

4. Primary antibody (*see* **note 6**). Dilute in PBA to appropriate concentration (*see* **note 7**).

5. Fluorescently-labeled secondary antibody. Dilute in PBA to appropriate concentration (*see* **note 7**) and store at 4°C in the dark to prevent bleaching of the fluorophore (if not prepared directly before use).

6. 15 ml falcon tubes.

7. 96-well plate, V-bottom.

8. FACS tubes or 96-wells plate (V-bottom).

9. Flow cytometer and appropriate analysis software (e.g. FlowJo v10).

2.4 TAP transport assay

1. Cells expressing MHC class I (*see* **note 1**).

2. 96-well plate (V-bottom).

3. Wash solution (PBS supplemented with 10 mM $MgCl_2$).

4. ATP buffer consisting of wash solution supplemented with 10 mM ATP (Sigma A7699-1G).

5. ADP buffer consisting of wash solution supplemented with 10 mM ADP (Sigma A2754).

6. SLO (Streptolysin-O, Murex diagnostics) (*see* **note 8**).

7. Fluorescently labelled peptide that is known to be transported by TAP. Here, we used the peptide (FL) V-N-K-T-E-R-A-Y. The peptide R-R-Y-Q-N-S-T-C-(FL)-L has been used by Fischbach *et al*. [13].

8. EDTA solution (PBS supplemented with 20 mM EDTA).

3 Methods

3.1 Lentiviral transduction

1. Harvest and count cells.

2. Thaw unconcentrated lentiviruses encoding the gene(s)-of-interest.

3. Seed cells (~30.000/well) in a 24-well plate in 500 µl of complete culture medium supplemented with 8 µg/ml polybrene immediately before transduction.

4. Add complete medium to the wells that receive less than the maximal amount of virus, in order to equalize total volume in all wells.

5. Add 10-150 µl of the unconcentrated lentivirus to the cells (*see* **note 9)**.

6. Cover the plate with a lid and spin in plate-centrifuge for 90 minutes at 800 x g at 33°C.

7. Incubate plate for one hour at 37°C in CO_2 incubator.

8. Add 500 µl of complete medium (without polybrene) to wells to dilute polybrene concentration (*see* **note 10**).

9. Incubate the plate at 37°C in CO_2 incubator.

10. Optionally: Add the appropriate selection marker (e.g. puromycin) in according concentration to the complete cell culture medium to enrich for cells containing the lentiviral plasmid.

11. Transgene expression can be monitored after 3-4 days.

3.2 Transient transfection using PEI

1. Seed cells (~100.000–200.000/well) in 1 ml of culture medium without antibiotics in a 12-well plate. Cells should be approximately 70% confluent the next day.

2. Incubate overnight at 37°C in CO_2 incubator (*see* **note 11**).

3. Refresh culture medium without antibiotics before transfection.

4. Prepare transfection mixture in polypropylene tubes (*see* **note 12**). Amounts indicated below have been optimized for MelJuSo cells.

    - Add 0.8 µg of DNA (*see* **note 13**) to 80 µl of 150 mM NaCl solution, vortex carefully during DNA addition.
    - Add 5.2 µl of PEI to 80 µl of 150 mM NaCl solution, vortex carefully during addition of PEI.
    - Add PEI solution to the DNA solution and vortex for 10 seconds.
    - Incubate transfection mixture at room temperature for 15-30 minutes.

5. Add transfection mixture drop-wise to the cells.

6. Gently shake culture plate to ensure transfection mixture is equally distributed throughout the medium.

7. Incubate for 24-72 hours at 37°C in CO_2 incubator.

3.3 Cell surface staining and flow cytometry

Perform work according to the local restrictions for handling virus-transduced cells. All steps should be performed at 4°C/on ice unless indicated otherwise.

1. Collect cells in a 15 ml falcon tube (100.000 cells / staining) (*see* **note 14**).

2. Wash cells with PBS.

3. Add PBA to cell pellet (100 µl PBA/staining).
4. Pipet 100 µl of cell suspension per well in a 96-wells plate (V-bottom).
5. Spin down cells (300 x *g*, 2 min).
6. Discard supernatant.
7. Resuspend cells.
8. Add 20 µl of primary antibody solution (*see* **note 15**).
9. Mix gently.
10. Incubate for 30 min.
11. Wash cells twice with PBA.
12. Add 20 µl of the fluorescently-labeled secondary antibody solution (*see* **note 16**).
13. Mix gently.
14. Incubate for 30 min in the dark.
15. Wash cells twice with PBA.
16. Add 100 µl of 1% paraformaldehyde solution (*see* **note 17**).
17. Incubate for 15 min in the dark.
18. Transfer cells to a FACS tube (if flow cytometer devoid of plate reader).
19. Analyze the cells using a flow cytometer and appropriate software (*see* **note 18**).

3.4 TAP transport assay

1. Collect cells in a 15 ml falcon tube (200.000 cells / well) and spin down cells (300 x g, 3 min, 4°C) (*see* **note 19**).
2. Wash cells with wash solution (see **2.4.3**) and transfer 200.000 cells / well to a 96-well plate (V-bottom).
3. Spin down cells and discard supernatant.
4. Add 100 µl SLO (final concentration of 3 mg /ml) to each sample and incubate for 15 min at 4°C.
5. Spin down cells and discard supernatant.
6. Add 50 µl wash solution supplemented with 10 nM ATP or 10 mM ADP and 20 nM fluorescently labelled peptide (*see* **note 20**).
7. Incubate for 15 min at 37°C in CO_2 incubator.
8. Add 150 µl EDTA solution.

9. Analyze cells using a flow cytometer and appropriate software.

4 Notes

1. We regularly use RAJI and MelJuSo (MJS) cells [19]; these cells can be transduced or transfected with high efficiency and express both MHC class I and MHC class II molecules at the cell surface. MJS cells have been particularly useful for studies on viral immune evasion [14]–[16],[20]. Other cells can be employed provided they express MHC class I and offer efficient transduction or transfection rates.

2. For lentivirus production we refer to a recently published method by Sena-Esteves and Gao [21].

3. To facilitate analysis, it is recommended to use a plasmid that co-expresses the gene-of-interest, a fluorescent marker (here: mAmetrine) and/or a resistance gene (here: the zeomycin resistance 'bleo'). We regularly use plasmids derived from a dual promotor lentiviral vector (BIC-PGK-Zeo-T2a-mAmetrine) derived from no.2025. pCCLsin.PPT.pA.CTE.4×-scrT.eGFP.mCMV.hPGK.NG-FR.pre (kindly provided by L. Naldini, San Raffaele Scientific Institute, Milan, Italy) as described previously [22]. This vector yields high expression levels in various cell lines including MelJuSo and RAJI cells. This vector can be used to produce lentiviruses with high titers, allowing for fast generation of cell lines stably expressing the gene(s)-of-interest.

4. BSA blocks non-specific antibody binding and sodium azide prevents internalization of surface antigens.

5. Sodium azide is highly toxic, handle with care and according to the local restrictions.

6. For most applications, mAbs with pan reactivity for MHC class I molecules (i.e. irrespective of the HLA typing) will suffice, such as W6/32 [23].

7. Optimal concentration of the antibodies should be determined by titration.

8. Used to permeabilize the cell membrane to permit the uptake of the fluorescently labelled peptides.

9. Optimal amount of lentivirus demands determination through titration experiments.

10. Polybrene strongly increases the transduction efficiency but can only be used in low concentrations ranging from 5 to 10 ug/ml (differs between cell lines) and only over a limited amount of time due to its cellular toxicity [24].

11. Alternatively, cells can be seeded immediately prior to transfection.

12. Optimal ratios of DNA and PEI should be determined in a pilot experiment and are cell line dependent.

13. Appropriate controls should be taken along in each experiment; e.g. negative control protein without effect on MHC class I levels and positive control protein with known downregulation capacity of cell surface MHC class I levels.

14. Appropriate controls should be taken along in each experiment; e.g. secondary antibody only, isotype control, antibody against a cell surface protein unaffected by the protein-of-interest.

15. For intracellular staining, the cells should be fixed and permeabilized before addition of primary antibody.

16. In case a directly-conjugated primary antibody is used, **steps 12-15** should be omitted.

17. Alternatively, cells can be fixed before antibody staining. However, certain antibodies lose reactivity after fixation, so this should be tested anteriorly.

18. The methods described in this paper may also be used to evaluate viral evasion of MHC class II-restricted antigen presentation [20], as well as viral subversion of other forms of adaptive and innate immunity [25], provided antibodies against the potential cellular target proteins are available.

19. Appropriate controls should be taken along in each experiment; e.g. negative control protein without effect on TAP mediated peptide translocation and positive control protein with known downregulating capacity of TAP peptide translocation.

20. As a negative control each sample can be incubated with ADP instead of ATP. TAP is an ATP dependent peptide transporter; therefore, background fluorescence should be observed in the presence of ADP. A further control may be incubation with ATP without prior semi-permeabilization of the cell membrane.

Acknowledgements

This work was funded by the European Commission under the Horizon2020 program H2020 MSCA-ITN GA 675278 EDGE.

References

1. Hansen, T. H. & Bouvier, M. MHC class I antigen presentation: learning from viral evasion strategies. *Nat. Rev. Immunol.* **9**, 503–13 (2009).
2. Horst, D., Ressing, M. E. & Wiertz, E. J. H. J. Exploiting human herpesvirus immune evasion for therapeutic gain: potential and pitfalls. *Immunol. Cell Biol.* **89**, 359–66 (2011).
3. Horst, D., Verweij, M. C., Davison, A. J., Ressing, M. E. & Wiertz, E. J. H. J. Viral evasion of T cell immunity: ancient mechanisms offering new applications. *Curr. Opin. Immunol.* **23**, 96–103 (2011).
4. Schuren, A. B., Costa, A. I. & Wiertz, E. J. Recent advances in viral evasion of the MHC Class I processing pathway. *Curr. Opin. Immunol.* **40**, 43–50 (2016).
5. Verweij, M. C. *et al.* Viral inhibition of the transporter associated with antigen processing (TAP): a striking example of functional convergent evolution. *PLoS Pathog.* **11**, e1004743 (2015).
6. Praest, P., Liaci, A. M., Förster, F. & Wiertz, E. J. H. J. New insights into the structure of the MHC class I peptide-loading complex and mechanisms of TAP inhibition by viral immune evasion proteins. *Mol. Immunol.* **113**, 103–114 (2019).
7. Kim, T. K. & Eberwine, J. H. Mammalian cell transfection: the present and the future. *Anal. Bioanal. Chem.* **397**, 3173–3178 (2010).
8. Doom, C. M. & Hill, A. B. MHC class I immune evasion in MCMV infection. *Med. Microbiol. Immunol.* **197**, 191–204 (2008).

9. Reusch, U. *et al.* A cytomegalovirus glycoprotein re-routes MHC class I complexes to lysosomes for degradation. *EMBO J.* **18**, 1081–91 (1999).
10. Wiertz, E. J. H. J. *et al.* Sec6l-mediated transfer of a membrane protein from the endoplasmic reticulum to the proteasome for destruction. *Nature* **384**, 432–438 (1996).
11. Wiertz, E. J. *et al.* The human cytomegalovirus US11 gene product dislocates MHC class I heavy chains from the endoplasmic reticulum to the cytosol. *Cell* **84**, 769–79 (1996).
12. Griffin, B. D., Verweij, M. C. & Wiertz, E. J. H. J. Herpesviruses and immunity: the art of evasion. *Vet. Microbiol.* **143**, 89–100 (2010).
13. Fischbach, H. *et al.* Ultrasensitive quantification of TAP-dependent antigen compartmentalization in scarce primary immune cell subsets. *Nat. Commun.* **6**, 6199 (2015).
14. Koppers-Lalic, D. *et al.* Varicelloviruses avoid T cell recognition by UL49.5-mediated inactivation of the transporter associated with antigen processing. *Proc. Natl. Acad. Sci.* **102**, 5144–5149 (2005).
15. Hislop, A. D. *et al.* A CD8+ T cell immune evasion protein specific to Epstein-Barr virus and its close relatives in Old World primates. *J. Exp. Med.* **204**, 1863–73 (2007).
16. Koppers-Lalic, D. *et al.* Varicellovirus UL49.5 Proteins Differentially Affect the Function of the Transporter Associated with Antigen Processing, TAP. *PLoS Pathog.* **4**, e1000080 (2008).
17. Matschulla, T. *et al.* A highly conserved sequence of the viral TAP inhibitor ICP47 is required for freezing of the peptide transport cycle. *Sci. Rep.* **7**, 2933 (2017).
18. Wycisk, A. I. *et al.* Epstein-Barr viral BNLF2a protein hijacks the tail-anchored protein insertion machinery to block antigen processing by the transport complex TAP. *J Biol Chem* **286**, 41402–41412 (2011).
19. van Ham, S. M. *et al.* HLA-DO is a negative modulator of HLA-DM-mediated MHC class II peptide loading. *Curr. Biol.* **7**, 950–7 (1997).
20. Ressing, M. E. *et al.* Interference with T cell receptor-HLA-DR interactions by Epstein-Barr virus gp42 results in reduced T helper cell recognition. *Proc. Natl. Acad. Sci. U. S. A.* **100**, 11583–8 (2003).
21. Sena-Esteves, M. & Gao, G. Production of High-Titer Retrovirus and Lentivirus Vectors. *Cold Spring Harb. Protoc.* **2018**, pdb.prot095687 (2018).
22. van de Weijer, M. L. *et al.* A high-coverage shRNA screen identifies TMEM129 as an E3 ligase involved in ER-associated protein degradation. *Nat. Commun.* **5**, 3832 (2014).
23. Barnstable, C. J. *et al.* Production of monoclonal antibodies to group A erythrocytes, HLA and other human cell surface antigens-new tools for genetic analysis. *Cell* **14**, 9–20 (1978).
24. Aubin, R. J., Weinfeld, M. & Paterson, M. C. Factors influencing efficiency and reproducibility of polybrene-assisted gene transfer. *Somat. Cell Mol. Genet.* **14**, 155–67 (1988).
25. van Gent, M. *et al.* EBV lytic-phase protein BGLF5 contributes to TLR9 downregulation during productive infection. *J. Immunol.* **186**, 1694–702 (2011).

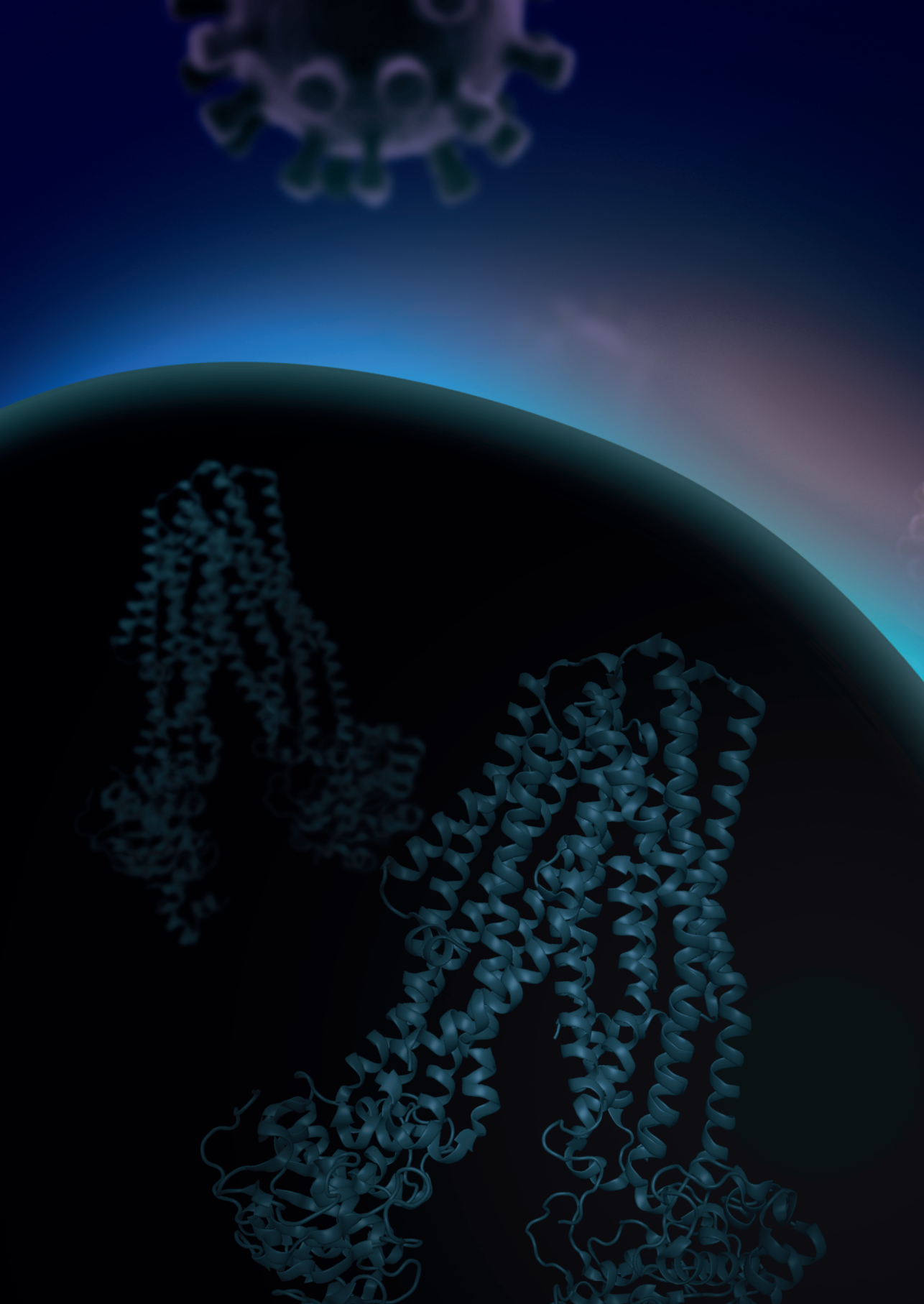

4

New insights into the structure of the MHC class I peptide-loading complex and mechanisms of TAP inhibition by viral immune evasion proteins

P. Praest, A.M. Liaci, F. Förster, E.J.H.J. Wiertz

Molecular Immunology (2019) 113 P.103-114

Abstract

Several hundred million years of co-evolution of vertebrates and invading pathogens have shaped the adaptive immune system to fight back the unwanted invaders through highly sophisticated defense mechanisms. Herpesviruses manage to dodge this immune response by hampering one of the central hinges of human adaptive immunity, the major histocompatibility complex (MHC) class I antigen presentation pathway. One of the bottlenecks of this pathway is the loading of pathogen-derived peptides onto MHC-I molecules in the endoplasmic reticulum (ER). This task is accomplished by the MHC class I peptide-loading complex (PLC), of which the transporter associated with antigen-processing (TAP) is a central component. In this review, we summarize recent structural and functional insights into the molecular architecture of the PLC, how TAP accomplishes the transport of peptides across the ER membrane, and how herpes- and poxviruses inhibit TAP-mediated peptide translocation and subsequent antigen presentation.

1 Introduction – MHC class I-mediated antigen presentation

Major histocompatibility complex class I (MHC-I) restricted T-cells constitute one of the main effector branches of the human adaptive immune system, protecting the organism against intracellular pathogens. MHC class I molecules occur at the surface of every nucleated cell and present peptides to patrolling, primed $CD8^+$ cytotoxic T-cells (CTLs). Upon detection of pathogen-derived peptides, the CTLs will induce cell death of the infected cell. The MHC class I-restricted antigen presentation pathway thus plays a central role in anti-viral immunity. Its importance is reflected by the observation that many viruses, especially large DNA viruses such as herpesviruses, have acquired dedicated immune evasion proteins that specifically interfere with MHC-I dependent antigen presentation. These immune evasins likely contribute to the life-long persistence of herpesviruses in their hosts. Peptide loading of MHC class I molecules is accomplished by the ER-resident MHC class I peptide-loading complex (PLC), a multisubunit complex consisting of a central peptide transporter and a luminal modular network of co-chaperones for MHC-peptide association. The PLC also performs quality control for newly assembled MHC-I/peptide complexes (Figure 1).

A pool of peptides representing the protein landscape within the cell is continuously generated by the cytosolic proteasome-ubiquitin system. The resulting peptides are transported into the ER lumen by the transporter associated with antigen-processing (TAP, a member of the ATP-binding cassette (ABC) transporter family). On the luminal face of the PLC, the chaperones tapasin, calreticulin, and ERp57 stably install and stabilize nascent MHC molecules in the proximity of TAP. This arrangement facilitates the proper loading of peptides with sufficient affinity into the MHC-I peptide binding groove [1]–[3]. Once peptides are stably associated with MHC-I molecules, the MHC I-peptide complexes are released from the PLC and shuttled to the cell surface for antigen presentation [4].

Due to its central role in antigen presentation it is not surprising that TAP is a frequent target for viral inhibition, especially among viruses that develop life-long infections. This viral 'lifestyle' requires elaborate ways of molecular camouflage. Through a long period of coevolution with their hosts, DNA viruses such as herpes-, and poxviruses have independently acquired highly efficient means of blocking TAP-mediated peptide transport and/or subsequent peptide loading onto MHC-I [5]–[8]. These viral TAP-inhibitors have no structural similarity and all bind TAP at different sites [7]. An increasing body of functional studies and recent advances in structural biology now allow a much more detailed understanding of the peptide transport cycle of TAP and the different inhibition strategies employed by the various immune evasins. This review outlines the current knowledge about the structure of the PLC and the peptide transport cycle, highlights

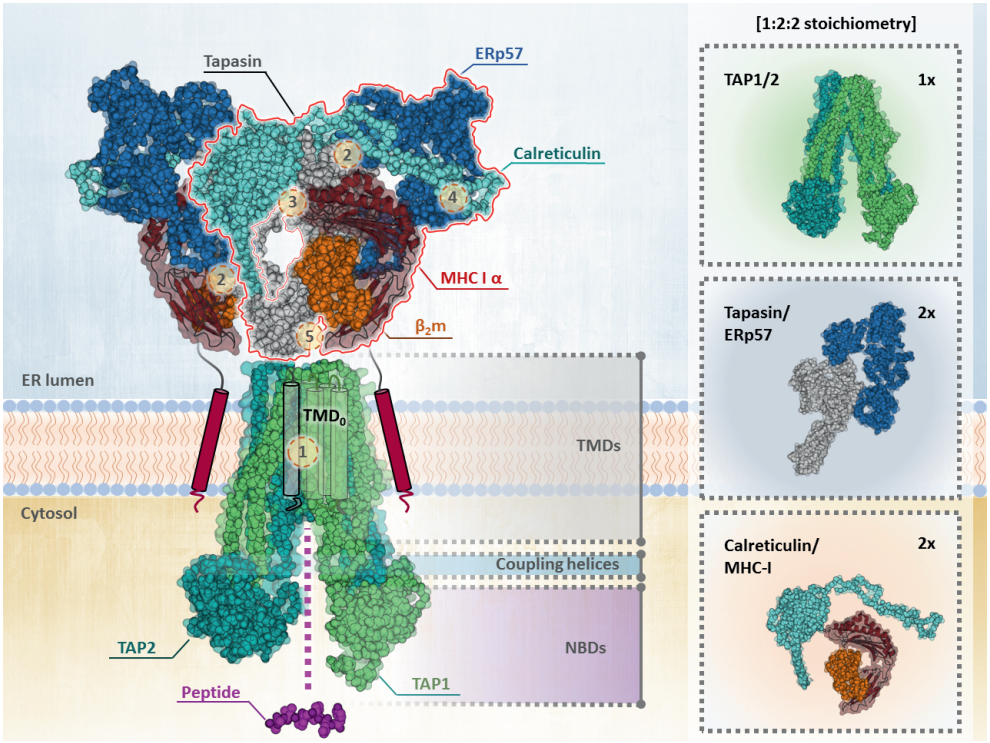

Figure 1: Model of the MHC-I peptide loading complex (PLC). Current structural information (PDB-IDs 6ENY, 5U1D, 3F8U) was combined into a model with a 1:2:2 stoichiometry (one TAP heterodimer per two of each other compound). In this model, two sets of MHC-I and its interacting chaperones (one of the two editing modules outlined in red) can be docked independently to the two TMD0 platforms of TAP. TAP1 is shown in green, TAP2 in teal, Tapasin in grey, ERP57 in blue, Calreticulin in cyan, and MHC-I in red/orange. Interfaces in the model that are substantiated by independent experimental evidence are marked in circles (1 TAP/Tapasin [25]; 2 tapasin/ERp57 [24]; 3 MHC-I/Calreticulin [24],[40]; 4 Calreticulin/ERp57 [29],[34],[39], 5 Tapasin/MHC-I [24],[25],[40]). TAP1/2 (5U1D) was docked into the electron density for the PLC (EMDB-ID 3905), but with low confidence and has to be considered purely contextual. The NBDs and different TMD segments of TAP are indicated. The proposed route of peptide transport is sketched in magenta. TAP is displayed in an 'inward' cytosol-facing orientation with separated NBDs. The right panels show the stable sub-complexes of the PLC and their relative stoichiometry.

recent findings about the differences and similarities between the various modes of TAP inhibition, and summarizes what viral immune evasion can teach us about the mechanism of antigen transport by TAP.

2 Assembly of the MHC class I peptide-loading complex

TAP, MHC-I and the chaperones tapasin, calreticulin, and ERp57 have been unambiguously identified as components of the PLC. However, our understanding about the structure and mode of action of the PLC and its stoichiometry is far from complete [9]–[11]. The

functionally and structurally central constituent of the PLC is a single TAP heterodimer. Since TAP links the cytosolic peptide pool and the ER-resident MHC-I molecules, TAP is of critical importance for the MHC-I antigen presentation pathway. Its significance is reflected by the fact that cells lacking functional TAP display severe defects in MHC-I-dependent antigen presentation [12]–[14]. In these cells, MHC-I molecules are unable to leave the ER and consequently the display of antigens to the immune system is impaired.

TAP is composed of the two structurally closely related proteins TAP1 (ABCB2) and TAP2 (ABCB3) [15]. Like all ABC transporters, both proteins contain an N-terminal transmembrane domain (TMD) and and a C-terminal nucleotide-binding domain (NBD) facing the cytosol. The core part of the TMD domains of both TAP1 and TAP2 consist of 2 x 6 transmembrane helices (numbered 1 to 6 according to a general convention for ABC transporters). In similarity to several other ABC transporters, the two monomers each swap two of them (Figure 2) [16]. These domains are responsible for peptide binding [17] and form the channel that mediates the translocation of peptides. In addition to the six 'core' transmembrane helices, the TMD domains of both TAP1 and TAP2 possess a non-canonical extension at their extreme N-terminus: a four-helix transmembrane bundle called TMD_0. The two TMD_0 extensions function as an assembly platform for the remaining PLC components (explained in more detail below). The NBDs carry out the crucial task of ATP binding and hydrolysis. These processes are thought to power conformational changes of the TMDs that enable peptide transport into the lumen [18]–[20].

The architecture of the luminal portion of the PLC has been controversially discussed for decades. It is now widely accepted that the chaperones tapasin, ERp57, and calreticulin form a stable 'editing module' that recruits, stabilizes and proof-reads MHC-I molecules [11]. Several stoichiometric models have been proposed, the most popular suggesting that two such editing modules can be accommodated by TAP per PLC. Very recently, a single-particle cryo-EM structure of natively expressed human PLC in combination with crosslinking-mass spectrometry (XL-MS) data have provided a wealth of new information on the molecular organization of the PLC [21]. Although the inherent flexibility of the complex limits the resolution and information content concerning the relative positioning of TAP to the other PLC components, the complex structure provides unprecedented insights into the architecture of the luminal chaperone network of the complex. The structure shows that indeed up to two MHC-I editing modules can be accommodated per PLC to form a slightly skewed pseudo-C2 symmetrical structure.

The only contacts between TAP and the rest of the PLC are formed at an intra-membrane interface between TAP and tapasin. The chaperone tapasin then acts as a scaffold for assembling all the other components. Recent publications agree that TAP1 and TAP2 each

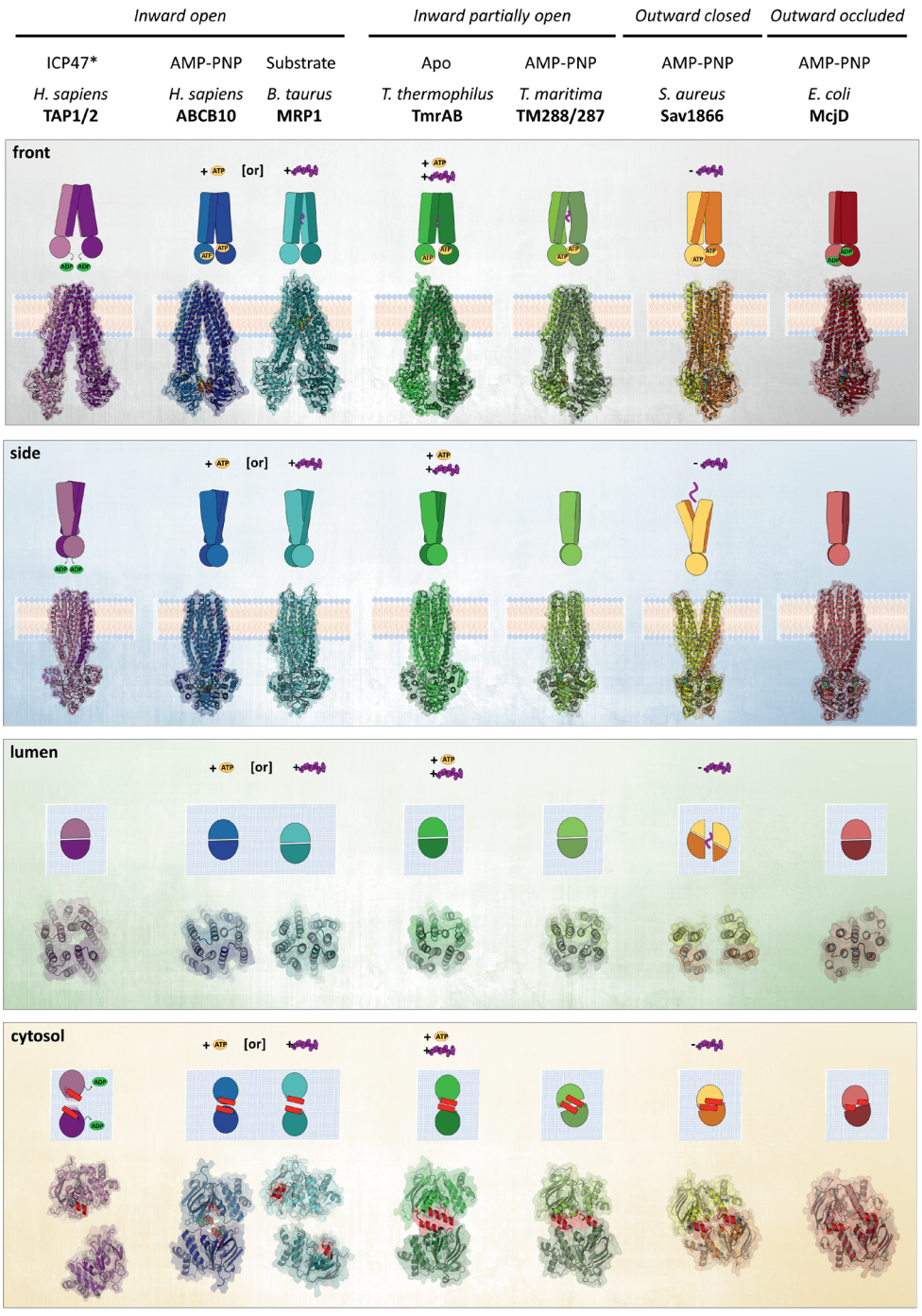

Figure 2: Structural information on the transport cycle of TAP extrapolated from homologous ABC transporter structures. The crystal structures of homologous type III/B-family ABC exporters allow for the reconstruction of a putative TAP transport cycle.

Figure 2 (continued). The inward- or cytosolic-facing TAP model is based on the structural data of Oldham et al. where the NBDs are physically separated (PDB-ID 5U1D) [16],[57]. The transporter is blocked by the HSV-1 protein ICP47 (not shown) in a peptide- and ATP-receptive state. Peptide- and substrate binding might occur independently from each other and lead to a partial closure of the transporter, similarly to the conformations of human ABCB10 (4AYT, nucleotide-bound) and bovine MRP1 (5UJA, substrate-bound, the two transporter subunits are coded on one polypeptide chain). Binding of both ATP and peptide putatively triggers the closure of the cytosol-facing NBD domains. The crystal structures of TmrAB from Thermus thermophilus. (5MKK) and TM287/288 from Thermogata maritima (4Q4A) represent putative intermediate stages of the peptide transport cycle [84],[85]. The closed ER-facing conformation is based on structural information from Dawson et al. (2ONJ, Staphylococcus aureus Sav1866) and shows interacting NBDs and a cavity formed by the TMDs towards the ER [91]. Cargo release and subsequent ATP hydrolysis take place after the transporter is opened to the ER lumen. McjD from E. coli is present in an outward-occluded state (4PL0) [83]. The different panels show the four transporter structures from different angles (from top to bottom: front-, side-, top- and bottom-view), the grey arrows indicate the putative conformational flow. The zipper helices in the NBD domains are colored red. The zipper helix of TAP2 was left out of the construct for experimental reasons [16].

recruit one tapasin molecule through a single binding site located in their respective TMD_0 transmembrane helix bundle [11],[22],[23]. Thus, the TMD_0 helices of TAP form an assembly hub for the PLC chaperone modules. The association of a single tapasin moiety to one of the TAP subunits is already sufficient for peptide translocation [22].

According to the XL-MS data reported by Blees *et al*., two isoforms of tapasin can be incorporated into the PLC. The L-shaped tapasin protein consists of an N-terminal fusion domain (formed by a seven-stranded beta barrel adjacent to an immunoglobin fold), a second, membrane-proximal immunoglobulin domain, and a single transmembrane helix [24]. A conserved intra-membrane ionic 'lock-switch'-interaction between the tapasin transmembrane helix and either TMD_0 domain of TAP has been proposed to act as one of the central PLC interfaces (point 1 in Figure 1) [25]. Unexpectedly, a third tapasin binding site has been found in the transmembrane domain segment of TAP1. However, tapasin recruitment to this site seems to be dispensable for peptide translocation, and indeed the binding site is occluded in fully assembled TAP heterodimers. Instead, the additional tapasin functions as an assembly chaperone for TAP and is lost upon assembly of the TAP1/2 heterodimer [26].

The luminal portion of tapasin forms a structural and functional unit with ERp57, to which it is stably associated through a disulfide bridge [27]. The complex structure of tapasin and ERp57 has been solved by X-ray crystallography [24]. The soluble protein disulfide isomerase ERp57 consists of four globular thioredoxin-like domains (called a, b, b', and a' from N-to C-terminus) that form a 'U'-shape around two contact points with tapasin (point 2 in Figure 1), as well as a C-terminal region. Of the four thioredoxin-like domains,

only the N/C terminal a/a' domains have retained their redox activity [28]. This redox activity is dispensable for the functionality of the PLC [29],[30], and instead the main role of ERp57 within the PLC seems to be the maintenance of structural integrity of the individual editing modules, in conjunction with tapasin [31]. Together, ERp57 and tapasin also ensure that MHC-I stably binds high-affinity peptides before dissociating from the PLC (reviewed extensively in Hulpke *et al*.[32]). Two unexpected additional interfaces between opposing editing modules have been found in the cryo-EM structure and accompanying XL-MS studies [21]. One interface is located between ERp57 and tapasin from the opposing editing module, the other one between the two tapasins, suggesting an additional stabilizing role for the PLC quarternary arrangement. As a result, the two tapasin molecules in the fully assembled PLC bend over by about 30° to form an arc with a potential outlet window for peptides emerging from TAP. As a note of caution, Blees et al. used gradient fixation (GraFix) in order to conformationally stabilize the complex for cryo-EM. GraFix is a cross-linking technique which might potentially influence the observed interface.

Within each editing module, TAP and the tapasin/ERp57 subcomplex stably associate to a static 'core' complex that transiently associates with one or two copies of MHC-I/calreticulin at two independent binding sites [11]. The two tapasin/ERp57 subcomplexes in the PLC independently each recruit one MHC-I molecule (pre-associated with calreticulin) [33]. A charged interface with a fast off-rate was observed for the interaction between calreticulin and ERp57, which might reflect a dynamic 'screening' of calreticulin/MHC-I sub-complexes by the PLC [34],[35]. The percentage of fully occupied PLCs (associated with 2 MHC-I/calreticulin subcomplexes) varies depending on the involved MHC-I alleles and as a function of peptide supply [11],[36]. In the single particle dataset of Blees et al. consisting of approximately 620,000 particles, one of the editing modules is always fully assembled, while some subpopulations miss one calreticulin and/or one MHC-I substrate in the second module, which is in line with previous reports [11]. The authors conclude that due to peptide editing, the off-rate of MHC-I association is slower than the on-rate, which might lead to a relatively high occupation with MHC-I [21]. However, the use of the viral inhibitor ICP47 for purification has an additional influence on MHC-I occupation. Moreover, such variable complex composition also occurs for the 26S proteasome, which generates the peptides in the cytosol [37], suggesting that variable complex stoichiometry is a general means to buffer capacity of the peptide degradation and MHC display system.

MHC-I consists of a heavy α chain and the small soluble immunoglobulin β_2 microglobulin (β_2m). The α chain consists of two domains forming the peptide binding cleft (called α1 and α2), an immunoglobulin domain (α3), and a single transmembrane helix. In addition

to the more classical HLA alleles, HLA-E, F, and G are also incorporated into the PLC [21]. The conformational plasticity observed in the N-terminal β-sheet of tapasin appears to be a crucial factor for receptor promiscuity.

Nascent MHC-I heavy chains depend on the chaperone activity of the ER-resident lectin calnexin and its soluble homolog calreticulin for folding and association with β_2m. The characteristic hook shape of calreticulin is formed by three parts. A globular part formed by its N- and C-terminal domains contains the carbohydrate-binding site and is essential for chaperone activity. Besides that, calreticulin contains an unusual proline-rich hairpin protrusion in between N- and C-terminal domains called the P domain, which at its very tip contains a binding site for ERp57, and a C-terminal helical domain. Upon association with β_2m, MHC-I is passed from calnexin to calreticulin, which then facilitates its association with the PLC. Calreticulin binds the mono-glucosylated N-linked glycan chain of MHC-I, as it does with many other proteins in the ER lumen (point 3 in Figure 1) [21]. In their cryo-EM structure, the hairpin-domain of calreticulin exhibits considerable flexibility as it hovers over the peptide binding groove of MHC-I. Calreticulins extended alpha-helical C-terminal acidic domain is facing towards the membrane, potentially contacting tapasin. This observation is in line with a potential lipid-sensing function of this helix [38].

Within the PLC, the MHC-I/calreticulin unit engages in several contacts with the ERp57/tapasin subcomplex. Experimentally verified contacts are formed between MHC-I and tapasin, as well as between calreticulin and ERp57. As determined by transverse relaxation optimized spectroscopy NMR (TROSY-NMR), the tip of the calreticulin P domain forms a contact with ERp57, thereby stabilizing interactions between the three functional PLC subunits [34]. It is assumed that this is the only interface between calreticulin and ERp57 [28]. According to a study investigating the ability of calreticulin to bind to specific point mutants of ERp57, the P domain tip of calreticulin is engaged at the b' domain of ERp57, (point 4 in Figure 1) [39]. According to this assay, the redox-active a and a' domains are dispensable for the binding, whereas a deletion of the C-terminal region reduces the binding by about 50%. A newer heteronuclear single quantum coherence (HSQC) NMR study has mapped the binding site to two residues located in close proximity at the interface of the b and b' domains [35], concomitant with the cryo-EM structure [21].

Co-Immunoprecipitation experiments with mutant tapasin revealed an extended MHC-I binding site in the N-terminal domain [24]. Furthermore, the deletion of a loop located on the same side of tapasin, but within the C-terminal domain, abrogated the binding (point 5 in Figure 1) [40], although a corresponding interface was not observed in the single particle structure [21]. Two recently solved crystal structures of human TAPBPR (TAP binding protein, related) in complex with a murine MHC-I molecule seem to confirm this

interface [41],[42]. TAPBPR has a similar function and interface as tapasin, but does not associate with the PLC and instead seems to additionally act in the Golgi compartment [43]. According to a homology model based on the complex structure, tapasin could insert a loop into the MHC-I peptide binding groove. This loop could compete with the C-terminus of peptides and thus account for peptide editing. In contrast, the transmembrane domains of both MHC-I and tapasin/TAPBPR seem to be dispensable for the interaction, as soluble tapasin mutants still stably associate with MHC-I [40].

The model presented in Figure 1 is based on the single particle structures of the human TAP and PLC, respectively. The model is in agreement with propositions from other authors [24],[32],[44]. Interfaces that have been verified in independent experiments are marked in the figure. In the original publication describing the PLC architecture [21], TAP has not been modelled. Here, the TAP structure has been docked into the PLC electron density, but with low confidence, and thus intra-membrane interfaces and the relative orientations of TAP and the chaperone network are contextual.

Additional factors that are functionally coupled to the PLC, such as the two closely related ER aminopeptidases associated with antigen processing (ERAP1/2), interact with the peptides *en route* [45],[46], but there is no *in vivo* evidence for binding to the PLC to date [47]–[49]. In addition, TAPBPR appears to functionally complement MHC-I binding by tapasin [41],[50]. How these factors interact with the PLC is not yet understood. Further, it is unknown which conformational changes TAP undergoes upon peptide translocation, and how the peptide is then delivered to the MHC-I peptide binding groove.

3 Current understanding of the TAP peptide transport cycle

The central task accomplished by the peptide-loading complex is the unidirectional transportation of peptides from the cytosol into the ER by TAP. Substantial effort has been made to understand in detail how peptides are translocated by the transporter. Over decades, a host of biochemical data have identified the structural motifs involved in nucleotide binding, roughly mapped the peptide binding region, and revealed secondary structures that are responsible for the crosstalk between ATP hydrolysis in the NBDs and conformational changes in the transmembrane helices (reviewed extensively in Seyffer *et al.*[51]). A special feature of TAP among ABC transporters is the presence of its TMD_0 domains, whose function and importance have already been discussed. It is generally agreed that TAP and other ABC transporters undergo alternating cycles of opening towards the cytosol ('inward') or the lumen/extracellular space ('outward') powered by ATP hydrolysis of the NBDs and executed by motions of the TMDs (reviewed in Locher *et al.*[52]). However, the picture is not complete, as of yet this wealth of information has

not been conclusively integrated into a robust trajectory of how TAP and its substrates move during the transport cycle. Furthermore, the precise conformational changes that are induced by the binding of either substrate or nucleotides remain uncharted.

TAP is classified as a type III/B-family exporter and shows a common fold with all structurally characterized ABC exporters [52],[53]. Human TAP1/2 exhibits remarkable structural similarity to several related peptide or multidrug exporters within this class, occurring in both eu- and prokaryotes (with root mean square deviations in the low Ångstrom range). In recent years, several new high-resolution structures of these transporters have been solved, sampling the transporters in different conformations. This has tempted many authors to calculate TAP homology models and to develop transport models of a 'general ABC transporter' [16],[51],[53]–[56]. The current (structural) understanding of the TAP transport cycle is largely based on such extrapolations, and for this reason we have summarized the novel insights these new structures can (and cannot) provide (Fig. 2). However, it has to be noted that an extrapolation across species and experimental methods has to be interpreted with caution, as the transporters most likely do not undergo the same structural cycles and no common mechanism has been proposed [52].

3.1 Resting state

A high resolution cryo-EM structure of human TAP trapped in an inward-facing state was solved in 2016 [16],[57]. In the resting state visualized by the structure, TAP is trapped by the viral immunoevasin ICP47 in a cytosol-facing V-shape conformation with two wide-open NBDs, supposedly mimicking the peptide- and ATP-receptive resting state of the transporter [16],[57],[58].

Without ICP47, however, TAP appears to display a degree of flexibility that is prohibitive for structural studies [16], raising the question whether this broad separation would occur without the inhibitor as well. Several models exist to interpret the functional role of NBD separation. In the case of TAP, the most conclusive model is the so-called processive clamp or 'switch' model. This model implies that the NBDs dimerize upon binding of two ATP molecules and completely separate after sequential ATP hydrolysis; this model is in line with the structures mentioned above [59],[60]. An alternative model (called the constant contact model) suggests that the NBDs stay associated at all times, involving an asymmetric opening of one of the nucleotide binding sites at a time [52].

However, confirming a correct model proved difficult to address experimentally. Complicating factors are the replacement of the lipid membrane environment by detergents (common to most studies), crystal packing (crystallographic studies), and

the complete absence of nucleotides, all of which might force the transporters into non-physiological conformations. Given the high concentration of ATP and ADP in the cytosol (mM range), it seems likely that apo states are very short-lived, if present at all. Therefore, structural studies and data based on methods such as Foerster resonance energy transfer (FRET) / luminescence resonance energy transfer (LRET), cross-linking mass spectrometry (XLMS), or double electron-electron resonance pulsed electron paramagnetic resonance (DEER-EPR) experiments might be intrinsically flawed.

In the absence of substrate and nucleotide analogues, several other structures have been found to persist in inward-open conformations, including homologues of the multidrug resistance transporter P-glycoprotein (P-gp) from different organisms [58],[61],[62] as well as the mitochondrial iron-sulfur cluster exporter Atm1 from *S. cerevisiae* [63]. All these structures display varying degrees of NBD separation, and in some cases, this variation can even be observed in different structures of the same transporter. Indeed, a recently published cryo-EM study on human P-gp shows that without substrate or peptide, P-gp can adopt several states with differing degrees of NBD closure [64]. Similarly, several different structures of the LPS exporter MsbA exhibit considerable differences in NBD separation in the absence of nucleotides or substrate [65],[66]. However, extremely wide-spread conformations such as the one found for MsbA or the oligosaccharide flippase PglK from *C. jejuni* are most likely not physiologically relevant [67].

Further, there might be differential behavior of homo- and heterodimeric transporters. For example, while a complete separation of the NBDs has been proposed for the homodimeric MsbA based on spin labeling and EPR spectroscopy [68], mechanistic and structural studies of mammalian P-gp and BmrCD from *B. subtilis* suggest a constant contact between NBDs during transport that is only possible in heterodimers [69]–[71]. Consequently, some authors suggest a model in which heterodimeric transporters constantly associate their NBDs in a way reminiscent of the constant contact model, while homodimeric transporters such as MsbA completely separate their NBDs according to the switch model [69]. The structure of TAP however shows the heterodimeric transporter in a state with wide-open NBDs. In this light, it remains to be determined to which extent the separation of the NBDs is induced by the viral inhibitor and the deletion of a C-terminal helix in TAP2, or to which extent the conformational cycles of ABC transporters can be unified into simplified models at all. Further aspects of NBD separation are discussed in George *et al.* [72].

3.2 Binding of Substrate and ATP

Binding of both the substrate and ATP is thought to provide the trigger for conformational changes that ultimately lead to a complete closure of the NBD domains and a rearrangement of the channel. TAP is able to bind both peptides and ATP independently from each other [17],[73],[74], but exhibits no peptide translocation without ATP [17],[18],[75],[76] and no basal ATP hydrolysis without peptide [77]. Thus, clearly both substrates need to be bound for this movement to happen.

It appears possible that binding of either substrate or ATP might make the transporter adopt a 'primed' conformation that shows signs of TMD closure. This is reflected by the human mitochondrial orphan transporter ABCB10, the structure of which was solved in the presence of several ATP analogues, but without the (yet unidentified) substrate [78]. The nucleotide-bound transporter is still present in the 'inward' facing open conformation with open nucleotide binding pockets, although the separation of the NBDs varies between different crystals and is not as pronounced as in the TAP structure. ATP binding introduces a slight conformational change compared to the unliganded ('apo') structure, but is not sufficient to trigger NBD occlusion.

The ABCB10 structure shows that nucleotides are capable of binding to ABC transporters before the substrate, but there are also *vice versa* examples that show substrate binding independently of nucleotides. In one such example, substrate-bound bovine P-gp (MRP1) adopts a conformation very similar to that of nucleotide-bound ABCB10 and also lacks NBD closure [79]. Hence, it seems plausible also for TAP that although there is no fixed order to peptide and ATP binding, slight structural rearrangements might occur upon engagement of one component that make the transporter more receptive for the missing component.

3.3 Formation of active sites for ATP hydrolysis

In order to reach the ATP-hydrolysis competent 'outward'-facing state, ABC transporters need to bring together their cytosolic part and dimerize their NBD domains. Since the active sites for ATP hydrolysis are both formed by residues from both TAP chains, NBD closure is an essential part of the catalytic mechanism. Accordingly, many transporters are inactivated when NBD closure is physically inhibited [80],[81].

The conformational flow necessary to accomplish the closing motion and formation of the catalytic centers is a topic of intense research. The conserved power stroke for the movement is generally thought to be generated by the consolidation of the cytoplasmic TMD segments (Figure 1&2) [72],[82]. An important role in this process is attributed to the

so-called coupling helices that lie at the interface between the NBD and transmembrane domains and are thought to allosterically transmit information on ATP binding (in the form of conformational changes in the NBDs) to the TMDs (indicated in Figure 1) [83]. Recently, structures of *T. thermophilus* TmrAB and *T. maritima* TM287/288 were solved in novel conformations raising questions about on-pathway intermediate states [84],[85]. Contacts between the NBD domains are formed in both structures, but the cytosolic parts of the TMD domains providing the power stroke remain separated.

TmrAB is a multidrug resistance protein with a broad substrate specificity that can functionally substitute TAP in human cells. Although it was crystallized in the presence of AMP-PNP, TmrAB is present in an unliganded state with a unique asymmetric conformation. It possesses approaching NBD domains, whose nucleotide and peptide binding pockets remain open towards the solvent. As an intriguing feature, contacts between the two NBDs are present, but largely restricted to their C-terminal helices. It is currently unclear whether this conformation represents an intermediate state, or whether the TmrAB transporter is simply not separating its NBDs as much as is observed for TAP in the 'inward-facing' resting state due to the C-terminal helices preventing a complete separation of the NBDs. In many structures containing nucleotides mimicking 'outward-occluded' or post-hydrolysis states (such as AMP-PNP or ADP vanadate, respectively), the C-terminal helices are rearranged and swapped between NBD domains to tightly lock the interface. It appears conceivable that such a swapping movement is one of the steps leading to the firm occlusion of NBD domains. However, these helices are subject to considerable evolutionary variation, and it remains to be determined how common their role among ABC transporters turns out to be [63],[85].

TM287/288 is present in a semi-closed state that is not open towards the 'outside'. The structure shows one open nucleotide pocket, but a more extensive NBD interface reminiscent of that found in the structure of Sav1688 (see below). Like TAP and TmrAB, TM287/288 contains a single consensus ATP-binding site, whereas the second site contains degenerate motifs with decreased ATP binding or hydrolysis. The TM287/288 structure is complexed with AMP-PNP bound only to the non-canonical, high ATP affinity site, not to the catalytic site. It seems that the NBDs are not fully closed yet, which might possibly represent a functional intermediate, but a definitive role of this asymmetry for substrate transport has not been proven yet. The structural aspects of NBD asymmetry is even more minimally explored for TAP. Upon NBD closure, TAP forms a 'canonical' binding site and a 'non-canonical' nucleotide binding site, the latter of which is formed by an atypical Walker B motif and H-switch in TAP1 and an unusual C-loop in TAP2 [86],[87]. Both of its ATP binding sites seem to have similar affinities for ATP and ADP, but mutations in the

canonical and non-canonical binding site, respectively, seem to be tolerated to different degrees [87]–[90].

3.4 Peptide release

The AMP-PNP-bound multidrug transporter Sav1688 from *S. aureus* represents the 'outward'-facing, NBD-closed state from which substrates are most likely released [91]. After the NBD domains have approached to adopt an occluded conformation, the transmembrane helices open up outwards and orthogonally to the movement of the NBD domains. Adapting this state is sufficient for the release of peptides [92]. It is currently unknown whether these movements also affect the positioning of the TMD_0 domains and the other PLC constituents. In contrast to other transporters, which usually allow a certain degree of retrograde transport, TAP is a 'diode' and strictly unidirectional. The underlying structural determinants of TAP unidirectionality are unclear, but it seems likely that a strongly reduced substrate affinity in the outward-facing state plays a key role in the process [92].

3.5 ATP hydrolysis

After peptide release, ATP hydrolysis likely triggers the return of TAP to an inward-facing orientation. A recent structure of the antibacterial peptide transporter McjD from *E. coli* shows an outward-facing, occluded state that likely exists after peptide release, but before ATP hydrolysis [83]. The homodimeric MsbA trapped with ADP vanadate is present in a similar conformation but with completely closed NBDs [66], similar to the recently solved structure of the peptide transporter PrtD from *A. aeolicus* [93]. As for TAP, it is possible that an asymmetric ADP-bound state might exist, as became apparent with experiments involving ADP-agarose and the viral inhibitor US6 [94]. To complete the cycle, ADP release brings the transporter back into the resting state. It has so far not been excluded that the two ATP hydrolysis events occur independently from each other, and they may even separately trigger different stages of the transport cycle.

3.6 General remarks

Although this mechanistic deduction allows for a general idea of how type III/B-family peptide or multidrug exporters might work, several inconsistencies and complications are subject to controversies in the field [52]. Thus, it remains questionable whether the structures of different transporters can accurately reflect the transport cycle of TAP. In 2015, Moeller *et al.* presented a population-oriented negative stain EM based approach, in which sensible classification schemes of MsbA and P-gp in either an apo, substrate,

ATP, or ADP-vanadate bound state revealed the full spectrum of conformations observed after solubilization in a bilayer-mimicking environment [95]. Upon incubation with a given combination of substrate and nucleotide, both transporters show a range of different conformational populations. Although the resolution was modest, this study showed that (i) even in a purified state with a defined amount of nucleotides and substrates, there is substantial conformational heterogeneity, and (ii) the two exporters are occupying strikingly different conformational states in different stages of their transport cycle and behave very differently upon nucleotide binding. Indeed, the differences in catalytic activity, transport function, and local concentration of substrates on both sides of the membrane might dictate differential uses of the available conformational landscapes.

For these reasons, it is relevant to structurally characterize human TAP in distinct conformations within the transport cycle. The many viral Inhibitors of TAP could be useful tools in this respect, as they trap TAP in different conformations.

4 TAP-inhibition

Among all DNA viruses, the *Herpesviridae* have acquired the most extensive arsenal of genes to mitigate antigen surface presentation. *Herpesviridae* express numerous immune evasion molecules that (i) cause degradation of MHC-I [96]–[98], (ii) lead to retention of immature molecules in the cis-Golgi [99], (iii) induce enhanced endocytosis of MHC-I [100],[101] and (iv) block MHC-1 protein synthesis to reduce its surface expression [102]–[104]. The PLC and especially TAP appear to be prominently targeted components of the pathway.

Herpesviruses independently developed distinct methods to block TAP. TAP-inhibitors can be identified in all three herpesvirus subfamilies [5]. To date, four herpesvirus-encoded TAP-inhibitors have been identified: (i) ICP47 encoded by herpes simplex virus (HSV) 1 and 2, (ii) BNLF2a encoded by Epstein-Barr virus (EBV), (iii) US6 encoded by human and rhesus cytomegalovirus (HCMV and RhCMV), and (iv) UL49.5 encoded by a broad range of varicelloviruses. Here, we highlight novel findings mainly concerning ICP47 and the poxvirus-encoded TAP inhibitor CPXV012, for both of which substantial new findings have been published recently. For reviews on the function of the other herpesvirus inhibitors, we refer to Verweij *et al* [5]. and Van de Weijer *et al*. [7].

4.1 ICP47

The first viral protein found to inhibit TAP function is the HSV-1 (and HSV-2)-encoded Infected Cell Protein 47 (ICP47) [105],[106]. ICP47 is an 88-amino acid cytosolic protein and the only known soluble TAP inhibitor [107],[108]. ICP47 causes retention of MHC-I

molecules in the ER by competitively blocking the binding of cytosolic peptides to TAP [107]. A number of studies have identified the key residues within the ICP47 sequence. Using synthetically produced or recombinantly expressed ICP47 truncation mutants, the active domain of ICP47 was mapped to the first 34 residues [109],[110]. Fragments of this length were able to efficiently block peptide binding. In addition, a recently published study showed that the highly conserved residues 50-52 (coined the 'PLL-motif' by the authors) in the central region of ICP47 are responsible for freezing TAP in the 'inward'-facing conformation [111]. This study demonstrates that the previously described active residues of ICP47 are not sufficient for full inhibition of TAP. Only a combination of the active N-terminal region with the PLL-motif leads to complete TAP inhibition. In line with these findings, a study from Herbring *et al*. suggests a dual interaction mechanism of ICP47 with a destabilizing active domain of ICP47 that inhibits the function of TAP, whereas a conserved C-terminal region next to the active domain of ICP47 is essential for the complete stabilization of the TAP-ICP47 complex [112].

The cryo-EM structure of TAP in complex with ICP47 revealed the molecular details of this dual inhibition mechanism [57]. As mentioned above, ICP47 indeed traps the transporter in an 'inward'-facing resting state. The first 43 amino acids of ICP47 form a helix-turn-helix motif that wedges itself into the TAP pore and directly clogs its peptide binding region. Presumably, the interface generated by the first 34 amino acids is large enough to provide efficient competitive inhibition. The residues of the 'PLL' motif precisely locate to one of the two pairs of coupling helices (formed by coupling helix 2 of TAP1 and coupling helix 1 of TAP2) and presumably prevent the transmission of the power stroke from the NBDs to the TMDs, which leads to the observed freezing of the transporter.

4.2 CPXV012

For a long time, inhibition of TAP was thought to be unique for herpesviruses. Recently however, a protein from cowpox viruses (CPXVs) was identified as a powerful TAP-inhibitor. CPXVs are part of the *orthopoxvirus* family. In healthy humans, an infection with CPXVs causes local skin lesions and is self-limiting [113], but an infection of immune compromised patients may be lethal [114]. An enlarging animal host range and growing numbers of CPXV infections in Europe and parts of Asia recently led to an increasing worldwide awareness of this public health concern [115].

CPXVs encode a cluster of sophisticated immune-evasion proteins, including the proteins CPXV203 and CPXV012, that evade CTL recognition by hampering the MHC-I antigen presentation pathway [116],[117]. CPXV203 was found to target fully assembled MHC-I molecules and to retain them in the ER. A deletion of CPXV203 did not fully restore MHC-I

surface expression, indicating that a second protein might be involved in the inhibition of this pathway [118].

Subsequently, CPXV012 was identified as the second CPXV protein that interferes with MHC-I-mediated antigen presentation [119],[120]. The 70 amino acid type II transmembrane (TM) protein CPXV012 consists of a short cytosolic N-terminal domain (mapped to residues 1-11), a single transmembrane helix (12-26), and a C-terminal luminal domain (27-70) [121],[122]. It impedes TAP-mediated peptide transport via its ER-luminal domain, blocking ATP binding to the NBDs of TAP [122]. More precisely, the amino acid residues 41-65, all located in the ER-luminal domain, appear to be sufficient for inhibition, whereas the TM domain and cytosolic N-terminal tail could possibly enhance the efficiency of inhibition [122]. In contrast, a different study showed that an isolated C-terminal 10mer CPXV012 fragment (residues 60-70) is sufficient for blocking ATPase activity of TAP, indicating that the extreme C-terminus of CPXV012 is the inhibitory fragment of the viral protein [121]. Notably, the two identified active regions only overlap by six amino acids.

The CPXV012 ortholog D10L of the CPX strains GRI-90 and GER 91-3 does not inhibit TAP function [119]. CPXV012 and D10L have a high degree of sequence identity within their cytosolic and TM regions, but have a very different ER-luminal C-terminal region [123]. The finding that the C-terminal domain of CPXV012 is necessary for inhibition of TAP supports the conclusion that the lack of inhibitory capacity of D10L is related to the sequence of its C-terminal domain [119].

The underlying genetic background for this abrupt decline in sequence identity is likely a deletion of 5 nucleotides that results in a frameshift of the gene segment that encodes the ER-luminal domain of the protein. The resulting alternative protein sequence is leading to a stop codon 25 residues after the gene segment encoding for the TMD, resulting in a shorter C-terminal reading frame. The domain formed by this alternative sequence was described to mimic a TAP substrate bound to the outward-facing TAP before release into the ER lumen [121].

CPXV012 blocks ATP binding to TAP, but does not interfere with peptide binding [121]. Co-immunoprecipitation studies showed that CPXV012 directly associates with the TAP complex [121]. This interaction seems to be restricted to TAP, as CPXV012 did not co-precipitate with TAP-like (TAPL), a homodimeric peptide translocation complex located in lysosomes, sharing 38% amino acid sequence identity with TAP1 and 40% with TAP2 [121],[124],[125].

In 2014, a model of CPXV012 was proposed by Luteijn *et al*. in which the C-terminal part of CPXV012 'snorkels' the ER-membrane in parallel to the lipid-water interface. The latter is likely related to the strong affinity of this domain for phospholipids [122]. Evidence for this theory was provided by an assay that measured the surface pressure of Langmuir lipid monolayers in the presence or absence of CPXV012. A rapidly and strongly increasing surface pressure after incubation with the viral inhibitor indicated that the ER-luminal domain can penetrate lipid monolayers [122].

The affinity for a lipid environment was taken as an indicator to presume a direct interaction of the viral protein with the TM helices of TAP was [122]. The constant binding of the inhibitor to the low-affinity release site of outward-facing TAP is thought to simulate a high luminal peptide concentration, resulting in a negative feedback mechanism of the TAP-mediated peptide translocation machinery [121],[122]. This indicates that the inhibition mechanism of CPXV012 is unique amongst the viral TAP inhibitors identified so far, but the conformational state(s) in which CPXV012 interacts with TAP remains unknown.

4.3 Functional orthogonality of TAP inhibitors could elucidate the TAP transport cycle

The different mechanisms of inhibition employed by the individual TAP inhibitors are functionally intertwined with the transport cycle of the ABC transporter. Since all viral TAP inhibitors interact with TAP in a very specific manner, they all are likely to trap the transporter in distinct conformational stages of the transport cycle. In this sense, viral compounds may provide unique insights into specific steps of the TAP-transport cycle, but it is challenging to assign the herpesvirus inhibitors to specific states of the TAP-transportation cycle only based on the presence or absence of substrate or nucleotide binding. Here, we briefly summarize the current notion of when and where the viral inhibitors could bind during the peptide translocation cycle.

ICP47 and BNLF2a are the only known TAP-inhibitors that act on the cytosolic side of TAP; all other inhibitors most likely lead to inhibition via the ER-luminal side. The only known complex structure of human TAP is the one of ICP47 that binds in an 'inward-facing' resting state. BNLF2a is a tail-anchored protein that is targeted to the ER membrane post translationally and a substitution of the hydrophobic C-terminal transmembrane region was shown not to be essential for inhibition of TAP [126]. Since BNLF2a has no functional residues on the luminal side and the N-terminal domain was identified to be sufficient for interfering with the binding of both peptides and ATP [126], it most likely also clogs the pore of TAP, like ICP47.

In contrast to the cytosolically acting viral inhibitors ICP47 and BNLF2a, the HCMV-encoded TAP inhibitor US6 binds from the luminal side and does not interfere with peptide binding, which implies that this inhibitor locks TAP in a different state. Seyffer *et al.* speculate that US6 indeed binds in a post-hydrolysis state, since US6 competes with ATP, but not ADP binding [51], suggesting that US6 interferes somewhere between an inward open and a substrate-bound state during the translocation cycle. In line with these findings, a study from Hewitt *et al.* demonstrated that US6 inhibits ATP binding to TAP1 and that conformational changes of TAP caused by peptide binding are inhibited. In this publication, it is assumed that US6 traps TAP in an intermediate conformational state occurring shortly after peptide binding, potentially locking it in a 'primed' state [127].

As already mentioned, the conformational state in which CPXV012 binds to TAP is unknown. Since the inhibitor is interfering with ATP binding but not with peptide binding, CPXV012 may bind between an outward, occluded and a substrate-bound state of TAP. An allocation for the varicellovirus-encoded inhibitor UL49.5 appears to be even more intricate. Different variants of UL49.5 are encoded by the equine herpesvirus types 1 and 4 (EHV-1 and 4), bovine herpesvirus types 1 and 5 (BoHV-1 and 5), pseudorabiesvirus (PRV), and many other varicelloviruses. These UL49.5 variants inhibit TAP in distinct ways; all mentioned variants inhibit conformational rearrangements that would follow peptide and ATP binding. In addition, UL49.5 of EHV-1 and 4 interfere with ATP binding to TAP. UL49.5 of BohV-1 strongly reduces TAP protein levels by targeting both subunits for proteasomal degradation [128].

A number of recent studies explores the functional orthogonality of different TAP inhibitors [111],[121], which might be exploited to elucidate different TAP conformations and assign them to different states of the transport cycle.

A recent study demonstrates that US6 is unable to bind TAP that is already locked in a distinct conformation by ICP47, and *vice versa* [111]. This would fit well with the current idea of US6 inhibiting TAP from the luminal side. However, further experiments are necessary to solidify this notion. A similar finding about unique conformational arrests of TAP during the peptide transportation cycle was reported by Lin *et al*. in 2014, who have shown that US6 or BNLF2a both can prevent the formation of TAP/CPXV012 complexes [121]. Furthermore, Wycisk *et al.* show that BNLF2a and US6 are also mutually exclusive [129].US6-inhibited TAP is peptide-receptive and therefore likely to be open to the cytosol, but in a conformation that precludes association with ICP47.

These findings, combined with further structural studies, could help to elucidate the conformational details of the TAP mediated peptide transportation cycle.

5 Concluding remarks / future perspectives

This review highlights the key function of TAP in antigen presentation and, based on recent new insights, sheds new light on TAP function and its inhibition by viral immune evasion proteins. Detailed structural studies into the PLC will be required for the elucidation of the interactions between the proteins involved in MHC-I restricted antigen presentation. Studies performed on PLCs complexed with viral TAP inhibitors reveals the nature of the interaction between these viral inhibitors and TAP and will uncover their mode of action.

Acknowledgements

Patrique Praest is supported by the European Commission under the Horizon2020 program H2020 MSCA-ITN GA 675278 EDGE. A. Manuel Liaci and Friedrich Förster are funded by the ERC Consolidator Grant 724425 (Biogenesis and Degradation of Endoplasmic Reticulum Proteins).

References

1. Pamer, E. & Cresswell, P. MECHANISMS OF MHC CLASS I–RESTRICTED ANTIGEN PROCESSING. *Annu. Rev. Immunol.* **16**, 323–358 (1998).
2. Hewitt, E. W. The MHC class I antigen presentation pathway: strategies for viral immune evasion. *Immunology* **110**, 163–9 (2003).
3. Antoniou, A. N., Powis, S. J. & Elliott, T. Assembly and export of MHC class I peptide ligands. *Curr. Opin. Immunol.* **15**, 75–81 (2003).
4. Spiliotis, E. T., Manley, H., Osorio, M., Zúñiga, M. C. & Edidin, M. Selective export of MHC class I molecules from the ER after their dissociation from TAP. *Immunity* **13**, 841–51 (2000).
5. Verweij, M. C. *et al.* Viral inhibition of the transporter associated with antigen processing (TAP): a striking example of functional convergent evolution. *PLoS Pathog.* **11**, e1004743 (2015).
6. Schuren, A. B., Costa, A. I. & Wiertz, E. J. Recent advances in viral evasion of the MHC Class I processing pathway. *Curr. Opin. Immunol.* **40**, 43–50 (2016).
7. van de Weijer, M. L., Luteijn, R. D. & Wiertz, E. J. H. J. Viral immune evasion: Lessons in MHC class I antigen presentation. *Semin. Immunol.* **27**, 125–137 (2015).
8. Windheim, M., Hilgendorf, A. & Burgert, H. G. Immune evasion by adenovirus E3 proteins: exploitation of intracellular trafficking pathways. *Curr. Top. Microbiol. Immunol.* **273**, 29–85 (2004).
9. Ortmann, B. A Critical Role for Tapasin in the Assembly and Function of Multimeric MHC Class I-TAP Complexes. *Science (80-.).* **277**, 1306–1309 (1997).
10. Rufer, E., Leonhardt, R. M. & Knittler, M. R. Molecular architecture of the TAP-associated MHC class I peptide-loading complex. *J. Immunol.* **179**, 5717–27 (2007).
11. Panter, M. S., Jain, A., Leonhardt, R. M., Ha, T. & Cresswell, P. Dynamics of major histocompatibility complex class I association with the human peptide-loading complex. *J. Biol. Chem.* **287**, 31172–84 (2012).

12. Spies, T. & DeMars, R. Restored expression of major histocompatibility class I molecules by gene transfer of a putative peptide transporter. *Nature* **351**, 323–324 (1991).

13. Spies, T. *et al.* Presentation of viral antigen by MHC class I molecules is dependent on a putative peptide transporter heterodimer. *Nature* **355**, 644–646 (1992).

14. de la Salle, H. *et al.* Asymptomatic deficiency in the peptide transporter associated to antigen processing (TAP). *Clin. Exp. Immunol.* **128**, 525–31 (2002).

15. Dean, M. & Annilo, T. Evolution of the Atp-Binding Cassette (Abc) Transporter Superfamily in Vertebrates*. *Annu. Rev. Genomics Hum. Genet.* **6**, 123–142 (2005).

16. Oldham, M. L. *et al.* A mechanism of viral immune evasion revealed by cryo-EM analysis of the TAP transporter. *Nature* **529**, 537–40 (2016).

17. van Endert, P. M. *et al.* A sequential model for peptide binding and transport by the transporters associated with antigen processing. *Immunity* **1**, 491–500 (1994).

18. Neefjes, J. J., Momburg, F. & Hämmerling, G. J. Selective and ATP-dependent translocation of peptides by the MHC-encoded transporter. *Science* **261**, 769–71 (1993).

19. Spies, T. *et al.* A gene in the human major histocompatibility complex class II region controlling the class I antigen presentation pathway. *Nature* **348**, 744–747 (1990).

20. Van Kaer, L., Ashton-Rickardt, P. G., Ploegh, H. L. & Tonegawa, S. TAP1 mutant mice are deficient in antigen presentation, surface class I molecules, and CD4-8+ T cells. *Cell* **71**, 1205–14 (1992).

21. Blees, A. *et al.* Structure of the human MHC-I peptide-loading complex. *Nature* **551**, 525–528 (2017).

22. Hulpke, S., Baldauf, C. & Tampe, R. Molecular architecture of the MHC I peptide-loading complex: One tapasin molecule is essential and sufficient for antigen processing. *FASEB J.* **26**, 5071–5080 (2012).

23. Hulpke, S. *et al.* Direct evidence that the N-terminal extensions of the TAP complex act as autonomous interaction scaffolds for the assembly of the MHC i peptide-loading complex. *Cell. Mol. Life Sci.* **69**, 3317–3327 (2012).

24. Dong, G., Wearsch, P. A., Peaper, D. R., Cresswell, P. & Reinisch, K. M. Insights into MHC class I peptide loading from the structure of the tapasin-ERp57 thiol oxidoreductase heterodimer. *Immunity* **30**, 21–32 (2009).

25. Blees, A. *et al.* Assembly of the MHC I peptide-loading complex determined by a conserved ionic lock-switch. *Sci. Rep.* **5**, 17341 (2015).

26. Leonhardt, R. M., Abrahimi, P., Mitchell, S. M. & Cresswell, P. Three Tapasin Docking Sites in TAP Cooperate To Facilitate Transporter Stabilization and Heterodimerization. *J. Immunol.* **192**, 2480–2494 (2014).

27. Vigneron, N., Peaper, D. R., Leonhardt, R. M. & Cresswell, P. Functional significance of tapasin membrane association and disulfide linkage to ERp57 in MHC class I presentation. *Eur J Immunol* **39**, 2371–2376 (2009).

28. Frickel, E. M. *et al.* ERp57 Is a Multifunctional Thiol-Disulfide Oxidoreductase. *J. Biol. Chem.* **279**, 18277–18287 (2004).

29. Zhang, Y. *et al.* ERp57 does not require interactions with calnexin and calreticulin to promote assembly of class I histocompatibility molecules, and it enhances peptide loading independently of its redox activity. *J. Biol. Chem.* **284**, 10160–10173 (2009).

30. Peaper, D. R. & Cresswell, P. The redox activity of ERp57 is not essential for its functions in MHC class I peptide loading. *Proc Natl Acad Sci U S A* **105**, 10477–10482 (2008).

31. Stepensky, D., Bangia, N. & Cresswell, P. Aggregate formation by ERp57-deficient MHC class I peptide-loading complexes. *Traffic* **8**, 1530–1542 (2007).

32. Hulpke, S. & Tampé, R. The MHC I loading complex: a multitasking machinery in adaptive immunity. *Trends Biochem. Sci.* **38**, 412–20 (2013).

33. Wearsch, P. a, Peaper, D. R. & Cresswell, P. Essential glycan-dependent interactions optimize MHC class I peptide loading. *Proc. Natl. Acad. Sci.* **108**, 4950–4955 (2011).

34. Frickel, E.-M. *et al.* TROSY-NMR reveals interaction between ERp57 and the tip of the calreticulin P-domain. *Proc. Natl. Acad. Sci. U. S. A.* **99**, 1954–9 (2002).

35. Kozlov, G. *et al.* Crystal Structure of the bb??? Domains of the Protein Disulfide Isomerase ERp57. *Structure* **14**, 1331–1339 (2006).

36. Neisig, A., Wubbolts, R., Zang, X., Melief, C. & Neefjes, J. Allele-specific differences in the interaction of MHC class I molecules with transporters associated with antigen processing. *J. Immunol.* **156**, 3196–206 (1996).

37. Asano, S. *et al.* A molecular census of 26S proteasomes in intact neurons. *Science (80-.).* **347**, 439–442 (2015).

38. Wijeyesakere, S. J., Bedi, S. K., Huynh, D. & Raghavan, M. The C-Terminal Acidic Region of Calreticulin Mediates Phosphatidylserine Binding and Apoptotic Cell Phagocytosis. *J. Immunol.* **196**, 3896–3909 (2016).

39. Russell, S. J. *et al.* The primary substrate binding site in the b' domain of ERp57 is adapted for endoplasmic reticulum lectin association. *J. Biol. Chem.* **279**, 18861–9 (2004).

40. Simone, L. C., Georgesen, C. J., Simone, P. D., Wang, X. & Solheim, J. C. Productive association between MHC class I and tapasin requires the tapasin transmembrane/cytosolic region and the tapasin C-terminal Ig-like domain. *Mol. Immunol.* **49**, 628–39 (2012).

41. Thomas, C. & Tampé, R. Structure of the TAPBPR-MHC I complex defines the mechanism of peptide loading and editing. *Science* eaao6001 (2017) doi:10.1126/science.aao6001.

42. Jiang, J. *et al.* Crystal structure of a TAPBPR-MHC-I complex reveals the mechanism of peptide editing in antigen presentation. *Science* eaao5154 (2017) doi:10.1126/science.aao5154.

43. Boyle, L. H. *et al.* Tapasin-related protein TAPBPR is an additional component of the MHC class I presentation pathway. *Proc. Natl. Acad. Sci.* **110**, 3465–3470 (2013).

44. Fisette, O., Wingbermühle, S. & Schäfer, L. V. Partial Dissociation of Truncated Peptides Influences the Structural Dynamics of the MHCI Binding Groove. *Front. Immunol.* **8**, 408 (2017).

45. Saveanu, L. *et al.* Concerted peptide trimming by human ERAP1 and ERAP2 aminopeptidase complexes in the endoplasmic reticulum. *Nat. Immunol.* **6**, 689–697 (2005).

46. Chen, H. *et al.* ERAP1-ERAP2 dimers trim MHC I-bound precursor peptides; implications for understanding peptide editing. *Sci. Rep.* **6**, 28902 (2016).

47. Serwold, T., Gonzalez, F., Kim, J., Jacob, R. & Shastri, N. ERAAP customizes peptides for MHC class I molecules in the endoplasmic reticulum. *Nature* **419**, 480–483 (2002).

48. Kanaseki, T., Blanchard, N., Hammer, G. E., Gonzalez, F. & Shastri, N. ERAAP Synergizes with MHC Class I Molecules to Make the Final Cut in the Antigenic Peptide Precursors in the Endoplasmic Reticulum. *Immunity* **25**, 795–806 (2006).

49. Kanaseki, T. *et al.* ERAAP and Tapasin Independently Edit the Amino and Carboxyl Termini of MHC Class I Peptides. *J. Immunol.* **191**, 1547–1555 (2013).

50. Hermann, C., Strittmatter, L. M., Deane, J. E. & Boyle, L. H. The binding of TAPBPR and Tapasin to MHC class I is mutually exclusive. *J. Immunol.* **191**, 5743–50 (2013).

51. Seyffer, F. & Tampé, R. ABC transporters in adaptive immunity. *Biochim. Biophys. Acta* **1850**, 449–60 (2015).

52. Locher, K. P. Mechanistic diversity in ATP-binding cassette (ABC) transporters. *Nat. Struct. Mol. Biol.* **23**, 487–493 (2016).

53. Parcej, D. & Tampé, R. ABC proteins in antigen translocation and viral inhibition. *Nat. Chem. Biol.* **6**, 572–80 (2010).

54. Mayerhofer, P. U. & Tampé, R. Antigen Translocation Machineries in Adaptive Immunity and Viral Immune Evasion. *J. Mol. Biol.* **427**, 1102–1118 (2015).

55. Eggensperger, S. & Tampé, R. The transporter associated with antigen processing: a key player in adaptive immunity. *Biol. Chem.* **396**, 1059–72 (2015).

56. Abele, R. & Tampé, R. The TAP translocation machinery in adaptive immunity and viral escape mechanisms. *Essays Biochem.* **50**, 249–64 (2011).

57. Oldham, M. L., Grigorieff, N. & Chen, J. Structure of the transporter associated with antigen processing trapped by herpes simplex virus. *Elife* **5**, (2016).

58. Jin, M. S., Oldham, M. L., Zhang, Q. & Chen, J. Crystal structure of the multidrug transporter P-glycoprotein from Caenorhabditis elegans. *Nature* **490**, 566–569 (2012).

59. van der Does, C. & Tampé, R. How do ABC transporters drive transport? *Biol. Chem.* **385**, 927–933 (2004).

60. Higgins, C. F. & Linton, K. J. The ATP switch model for ABC transporters. *Nat. Struct. Mol. Biol.* **11**, 918–926 (2004).

61. Kodan, A. *et al.* Structural basis for gating mechanisms of a eukaryotic P-glycoprotein homolog. *Proc. Natl. Acad. Sci.* **111**, 4049–4054 (2014).

62. Aller, S. G. *et al.* Structure of P-Glycoprotein Reveals a Molecular Basis for Poly-Specific Drug Binding. *Science (80-.).* **323**, 1718–1722 (2009).

63. Srinivasan, V., Pierik, A. J. & Lill, R. Crystal structures of Nucleotide-Free and Glutathione-Bound Mitochondrial ABC Transporter Atm1. *Science (80-.).* **343**, 1137–1140 (2014).

64. Frank, G. A. *et al.* Cryo-EM Analysis of the Conformational Landscape of Human P-glycoprotein (ABCB1) During its Catalytic Cycle. *Mol. Pharmacol.* **90**, 35–41 (2016).

65. Ward, A., Reyes, C. L., Yu, J., Roth, C. B. & Chang, G. Flexibility in the ABC transporter MsbA: Alternating access with a twist. *Proc. Natl. Acad. Sci.* **104**, 19005–19010 (2007).

66. Mi, W. *et al.* Structural basis of MsbA-mediated lipopolysaccharide transport. *Nature* **549**, 233–237 (2017).

67. Perez, C. *et al.* Structure and mechanism of an active lipid-linked oligosaccharide flippase. *Nature* **524**, 433–438 (2015).

68. Zou, P., Bortolus, M. & Mchaourab, H. S. Conformational Cycle of the ABC Transporter MsbA in Liposomes: Detailed Analysis Using Double Electron-Electron Resonance Spectroscopy. *J. Mol. Biol.* **393**, 586–597 (2009).

69. Mishra, S. *et al.* Conformational dynamics of the nucleotide binding domains and the power stroke of a heterodimeric ABC transporter. *Elife* **3**, e02740 (2014).

70. Siarheyeva, A., Liu, R. & Sharom, F. J. Characterization of an asymmetric occluded state of P-glycoprotein with two bound nucleotides: Implications for catalysis. *J. Biol. Chem.* **285**, 7575–7586 (2010).

71. Tombline, G. & Senior, A. E. The occluded nucleotide conformation of P-glycoprotein. *J. Bioenerg. Biomembr.* **37**, 497–500 (2005).

72. George, A. M. & Jones, P. M. Perspectives on the structure–function of ABC transporters: The Switch and Constant Contact Models. *Prog. Biophys. Mol. Biol.* **109**, 95–107 (2012).

73. Muller, K. M., Ebensperger, C. & Tampe, R. Nucleotide binding to the hydrophilic C-terminal domain of the transporter associated with antigen processing (TAP). *J Biol Chem* **269**, 14032–14037 (1994).

74. Russ, G. *et al.* Assembly, intracellular localization, and nucleotide binding properties of the human peptide transporters TAP1 and TAP2 expressed by recombinant vaccinia viruses. *J. Biol. Chem.* **270**, 21312–21318 (1995).

75. Meyer, T. H., Endert, P. M. Van, Uebel, S., Ehring, B. & Tamp, R. Functional expression and purification of the ABC transporter complex associated with antigen processing (TAP) in insect cells. **351**, 443–447 (1994).

76. Shepherd, J. C. *et al.* TAP1-dependent peptide translocation in vitro is ATP dependent and peptide selective. *Cell* **74**, 577–584 (1993).

77. Herget, M. *et al.* Purification and reconstitution of the antigen transport complex TAP. A prerequisite determination of peptide stoichiometry and ATP hydrolysis. *J. Biol. Chem.* **284**, 33740–33749 (2009).

78. Shintre, C. A. *et al.* Structures of ABCB10, a human ATP-binding cassette transporter in apo-and nucleotide-bound states. doi:10.1073/pnas.1217042110.

79. Johnson, Z. L. & Chen, J. Structural Basis of Substrate Recognition by the Multidrug Resistance Protein MRP1. *Cell* **168**, 1075-1085.e9 (2017).

80. Gerber, S., Comellas-Bigler, M., Goetz, B. A. & Locher, K. P. Structural Basis of Trans-Inhibition in a Molybdate/Tungstate ABC Transporter. *Nat. Struct. Mol. Biol.* **321**, 246–251 (2008).

81. Ward, A. B. *et al.* Structures of P-glycoprotein reveal its conformational flexibility and an epitope on the nucleotide-binding domain. *Proc. Natl. Acad. Sci.* **110**, 13386–13391 (2013).

82. Oldham, M. L., Davidson, A. L. & Chen, J. Structural insights into ABC transporter mechanism. *Curr. Opin. Struct. Biol.* **18**, 726–733 (2008).

83. Choudhury, H. G. *et al.* Structure of an antibacterial peptide ATP-binding cassette transporter in a novel outward occluded state. *Proc. Natl. Acad. Sci.* **111**, 9145–9150 (2014).

84. Hohl, M. *et al.* Structural basis for allosteric cross-talk between the asymmetric nucleotide binding sites of a heterodimeric ABC exporter. *Proc. Natl. Acad. Sci.* **111**, 11025–11030 (2014).

85. Nöll, A. *et al.* Crystal structure and mechanistic basis of a functional homolog of the antigen transporter TAP. *Proc. Natl. Acad. Sci.* 201620009 (2017) doi:10.1073/pnas.1620009114.

86. Chen, M., Abele, R. & Tampé, R. Functional non-equivalence of ATP-binding cassette signature motifs in the transporter associated with antigen processing (TAP). *J. Biol. Chem.* **279**, 46073–81 (2004).

87. Zaitseva, J. *et al.* The role of CAPS buffer in expanding the crystallization space of the nucleotide-binding domain of the ABC transporter haemolysin B from Escherichia coli. *Acta Crystallogr. D. Biol. Crystallogr.* **60**, 1076–84 (2004).

88. Procko, E. & Gaudet, R. Functionally Important Interactions between the Nucleotide-Binding Domains of an Antigenic Peptide Transporter †. *Biochemistry* **47**, 5699–5708 (2008).

89. Karttunen, J. T., Lehner, P. J., Gupta, S. S., Hewitt, E. W. & Cresswell, P. Distinct functions and cooperative interaction of the subunits of the transporter associated with antigen processing (TAP). *Proc. Natl. Acad. Sci. U. S. A.* **98**, 7431–6 (2001).

90. Saveanu, L., Daniel, S. & van Endert, P. M. Distinct functions of the ATP binding cassettes of transporters associated with antigen processing: a mutational analysis of Walker A and B sequences. *J. Biol. Chem.* **276**, 22107–13 (2001).

91. Dawson, R. J. P. & Locher, K. P. Structure of a bacterial multidrug ABC transporter. *Nature* **443**, 180–185 (2006).

92. Grossmann, N. *et al.* Mechanistic determinants of the directionality and energetics of active export by a heterodimeric ABC transporter. *Nat Commun* **5**, 5419 (2014).

93. Morgan, J. L. W., Acheson, J. F. & Zimmer, J. Structure of a Type-1 Secretion System ABC Transporter. *Structure* **25**, 522–529 (2017).

94. Kyritsis, C. *et al.* Molecular Mechanism and Structural Aspects of Transporter Associated with Antigen Processing Inhibition by the Cytomegalovirus Protein US6. *J. Biol. Chem.* **276**, 48031–48039 (2001).

95. Moeller, A. *et al.* Distinct Conformational Spectrum of Homologous Multidrug ABC Transporters. *Structure* **23**, 450–460 (2015).

96. Park, B., Spooner, E., Houser, B. L., Strominger, J. L. & Ploegh, H. L. The HCMV membrane glycoprotein US10 selectively targets HLA-G for degradation. *J. Exp. Med.* **207**, 2033–41 (2010).

97. Wiertz, E. J. H. J. *et al.* Sec6l-mediated transfer of a membrane protein from the endoplasmic reticulum to the proteasome for destruction. *Nature* **384**, 432–438 (1996).

98. Wiertz, E. J. *et al.* The human cytomegalovirus US11 gene product dislocates MHC class I heavy chains from the endoplasmic reticulum to the cytosol. *Cell* **84**, 769–79 (1996).

99. Ziegler, H. *et al.* A mouse cytomegalovirus glycoprotein retains MHC class I complexes in the ERGIC/cis-Golgi compartments. *Immunity* **6**, 57–66 (1997).

100. Zuo, J. *et al.* The Epstein-Barr virus G-protein-coupled receptor contributes to immune evasion by targeting MHC class I molecules for degradation. *PLoS Pathog.* **5**, e1000255 (2009).

101. Lehner, P. J., Hoer, S., Dodd, R. & Duncan, L. M. Downregulation of cell surface receptors by the K3 family of viral and cellular ubiquitin E3 ligases. *Immunol. Rev.* **207**, 112–125 (2005).

102. Glaunsinger, B., Chavez, L. & Ganem, D. The exonuclease and host shutoff functions of the SOX protein of Kaposi's sarcoma-associated herpesvirus are genetically separable. *J. Virol.* **79**, 7396–401 (2005).

103. Fenwick, M. L. & Clark, J. Early and Delayed Shut-off of Host Protein Synthesis in Cells Infected with Herpes Simplex Virus. *J. Gen. Virol.* **61**, 121–125 (1982).

104. Zuo, J. *et al.* The DNase of Gammaherpesviruses Impairs Recognition by Virus-Specific CD8+ T Cells through an Additional Host Shutoff Function. *J. Virol.* **82**, 2385–2393 (2008).

105. Früh, K. *et al.* A viral inhibitor of peptide transporters for antigen presentation. *Nature* **375**, 415–418 (1995).

106. Hill, A. *et al.* Herpes simplex virus turns off the TAP to evade host immunity. *Nature* **375**, 411–5 (1995).

107. Tomazin, R. *et al.* Stable binding of the herpes simplex virus ICP47 protein to the peptide binding site of TAP. *EMBO J.* **15**, 3256–66 (1996).

108. Ahn, K. *et al.* Molecular mechanism and species specificity of TAP inhibition by herpes simplex virus ICP47. *EMBO J.* **15**, 3247–55 (1996).

109. Galocha, B. *et al.* The active site of ICP47, a herpes simplex virus-encoded inhibitor of the major histocompatibility complex (MHC)-encoded peptide transporter associated with antigen processing (TAP), maps to the NH2-terminal 35 residues. *J. Exp. Med.* **185**, 1565–72 (1997).

110. Neumann, L., Kraas, W., Uebel, S., Jung, G. & Tampé, R. The active domain of the herpes simplex virus protein ICP47: a potent inhibitor of the transporter associated with antigen processing. *J. Mol. Biol.* **272**, 484–92 (1997).

111. Matschulla, T. *et al.* A highly conserved sequence of the viral TAP inhibitor ICP47 is required for freezing of the peptide transport cycle. *Sci. Rep.* **7**, 2933 (2017).

112. Herbring, V., Bäucker, A., Trowitzsch, S. & Tampé, R. A dual inhibition mechanism of herpesviral ICP47 arresting a conformationally thermostable TAP complex. *Sci. Rep.* **6**, 36907 (2016).

113. Bourquain, D., Dabrowski, P. W. & Nitsche, A. Comparison of host cell gene expression in cowpox, monkeypox or vaccinia virus-infected cells reveals virus-specific regulation of immune response genes. *Virol. J.* **10**, 61 (2013).

114. Czerny, C. P., Eis-Hübinger, A. M., Mayr, A., Schneweis, K. E. & Pfeiff, B. Animal poxviruses transmitted from cat to man: current event with lethal end. *Zentralbl. Veterinarmed. B* **38**, 421–31 (1991).

115. Vorou, R. M., Papavassiliou, V. G. & Pierroutsakos, I. N. Cowpox virus infection: an emerging health threat. *Curr. Opin. Infect. Dis.* **21**, 153–156 (2008).

116. Alzhanova, D. & Früh, K. Modulation of the host immune response by cowpox virus. *Microbes Infect.* **12**, 900–9 (2010).

117. Seet, B. T. *et al.* P OXVIRUSES AND I MMUNE E VASION. *Annu. Rev. Immunol.* **21**, 377–423 (2003).

118. McCoy, W. H., Wang, X., Yokoyama, W. M., Hansen, T. H. & Fremont, D. H. Cowpox virus employs a two-pronged strategy to outflank MHCI antigen presentation. *Mol. Immunol.* **55**, 156–158 (2013).

119. Alzhanova, D. *et al.* Cowpox Virus Inhibits the Transporter Associated with Antigen Processing to Evade T Cell Recognition. *Cell Host Microbe* **6**, 433–445 (2009).

120. Byun, M. *et al.* Two Mechanistically Distinct Immune Evasion Proteins of Cowpox Virus Combine to Avoid Antiviral CD8 T Cells. *Cell Host Microbe* **6**, 422–432 (2009).

121. Lin, J. *et al.* A negative feedback modulator of antigen processing evolved from a frameshift in the cowpox virus genome. *PLoS Pathog.* **10**, e1004554 (2014).

122. Luteijn, R. D. *et al.* Cowpox Virus Protein CPXV012 Eludes CTLs by Blocking ATP Binding to TAP. *J. Immunol.* **193**, 1578–1589 (2014).

123. Dabrowski, P. W., Radonić, A., Kurth, A. & Nitsche, A. Genome-Wide Comparison of Cowpox Viruses Reveals a New Clade Related to Variola Virus. *PLoS One* **8**, e79953 (2013).

124. Demirel, O., Bangert, I., Tampé, R. & Abele, R. Tuning the cellular trafficking of the lysosomal peptide transporter TAPL by its N-terminal domain. *Traffic* **11**, 383–93

(2010).

125. Zhang, F. *et al.* Characterization of ABCB9, an ATP binding cassette protein associated with lysosomes. *J. Biol. Chem.* **275**, 23287–94 (2000).

126. Horst, D. *et al.* EBV Protein BNLF2a Exploits Host Tail-Anchored Protein Integration Machinery To Inhibit TAP. *J. Immunol.* **186**, 3594–3605 (2011).

127. Hewitt, E. W., Gupta, S. S. & Lehner, P. J. The human cytomegalovirus gene product US6 inhibits ATP binding by TAP. *EMBO J.* **20**, 387–96 (2001).

128. Koppers-Lalic, D. *et al.* Varicelloviruses avoid T cell recognition by UL49.5-mediated inactivation of the transporter associated with antigen processing. *Proc. Natl. Acad. Sci.* **102**, 5144–5149 (2005).

129. Wycisk, A. I. *et al.* Epstein-Barr viral BNLF2a protein hijacks the tail-anchored protein insertion machinery to block antigen processing by the transport complex TAP. *J Biol Chem* **286**, 41402–41412 (2011).

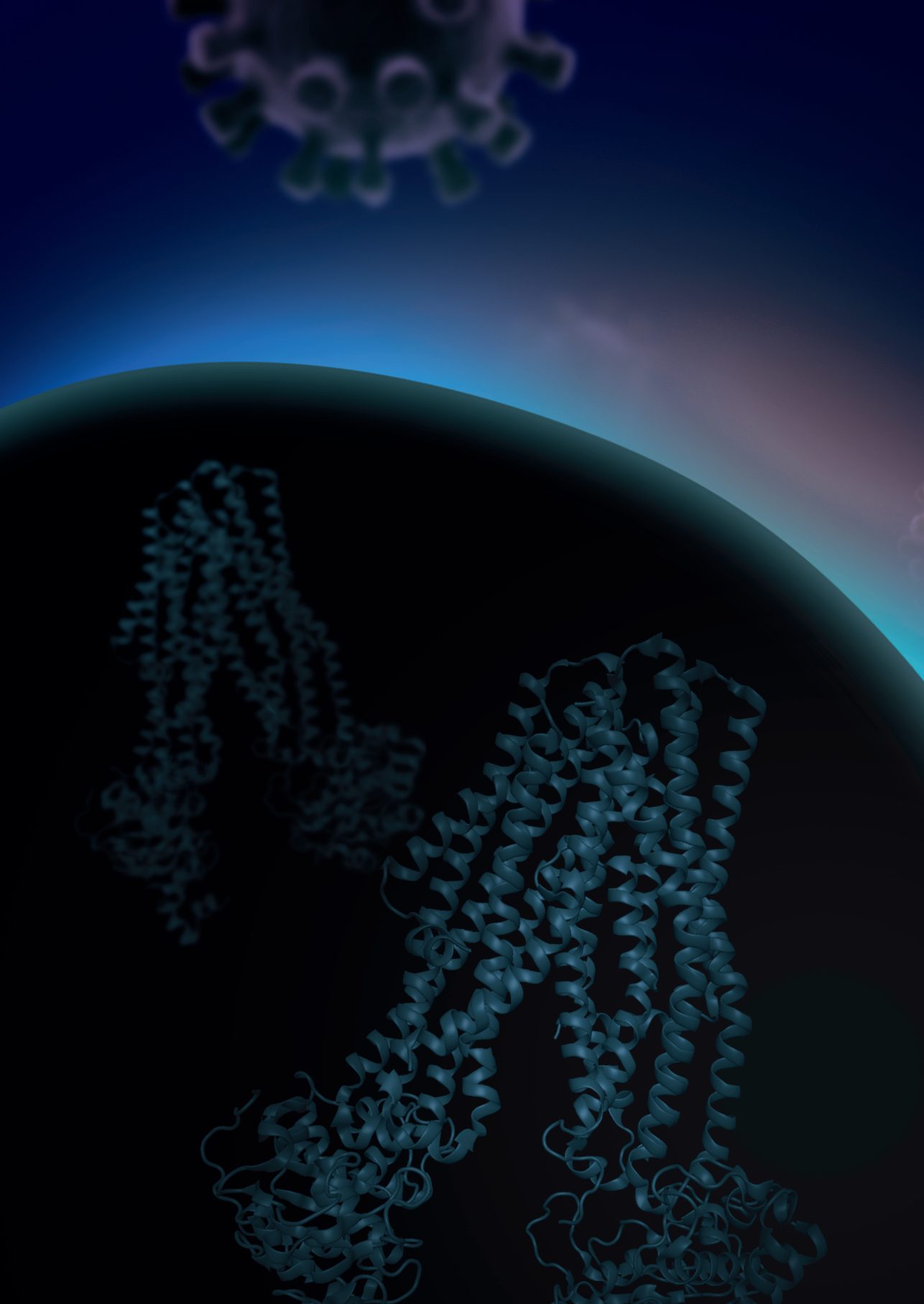

5

Paving the road to a structural elucidation of the TAP mediated peptide transport cycle by Cryo-EM

P. Praest, A.M. Liaci, H. Leegwater, P. Drougkas, R.J. Lebbink, F. Förster, E.J.H.J. Wiertz

Manuscript in preparation

Abstract

In order to establish persistent infections, DNA viruses have evolved multiple strategies to interfere with recognition by the human adaptive immune system. A major cellular target is the MHC class I peptide loading complex (PLC), which facilitates the presentation of peptides on the cell surface of infected cells for recognition by cytotoxic T-lymphocytes. Although the molecular mechanisms underlying viral targeting of the PLC have been studied extensively, detailed structural studies on these interactions are largely lacking. Here, we aim to study the molecular interactions between inhibitors expressed by several large DNA viruses, including ICP47 from the herpes simplex virus 1, BNLF2a from the Epstein-Barr virus, and US6 from the human cytomegalovirus, with the heterodimeric ABC-transporter TAP, a central component of the PLC. Using single particle cryo-electron microscopy (cryo-EM), we intend to assess where these viral inhibitors interact with TAP and how this impacts the peptide transport cycle on a structural level.

1 Introduction

The major histocompatibility complex class I (MHC class I) antigen presentation pathway is crucial in antiviral immunity. MHC class I molecules are expressed on every nucleated cell and are responsible for presenting peptides to $CD8^+$ cytotoxic T-lymphocytes (CTLs). In the event of a viral infection, pathogen-derived peptides will be presented to and recognized by $CD8^+$ CTLs, which induces apoptosis of the infected cell, thereby clearing the infection. However, viruses have evolved multiple strategies to escape this cellular immunosurveillance.

Large DNA viruses, such as poxviruses and herpesviruses, encode multiple viral proteins dedicated to immune evasion (immune evasins). Nearly every step in the MHC class I antigen presentation pathway is targeted by viral immune evasins; interference with peptide transport over the endoplasmic reticulum (ER) membrane mediated by the transporter associated with antigen processing (TAP) is a frequent target [1]. Viral proteins inhibit peptide loading onto MHC class I molecules by binding to the ATP-binding cassette (ABC) transporter TAP, the central component of the PLC. TAP is a heterodimeric complex composed of TAP1 (ABCB2) and TAP2 (ABCB3), each consisting of a nucleotide-binding domain (NBD) and multiple transmembrane domains (TMDs) that intertwine to form the cleft through which peptides are transported [2]. Peptide translocation across the ER-membrane requires ATP binding and hydrolysis; peptide binding itself is ATP-independent [3],[4]. Binding of ATP and peptide to TAP induces extensive conformational rearrangements resulting in peptide release towards the ER lumen and subsequent ATP hydrolysis [5],[6]. Interestingly, long-term virus-host coevolution has resulted in independently acquired TAP inhibitors across different virus species. These inhibitors share no structural homology and bind to distinct domains of the transporter [7]–[9].

Recently, the structures of TAP and the PLC have been solved by exploiting the herpesvirus-encoded TAP inhibitor ICP47 from HSV as a stabilizer to arrest the complex in a peptide-depleted state [10]–[12]. These studies provided a detailed insight into the interface of the PLC and the mechanism of ICP47-mediated TAP inhibition. Furthermore, the heterodimeric ABC exporter TmrAB (*Thermus thermophilus* multidrug-resistance proteins A and B), a homolog of TAP, was used to unravel eight high-resolution structures that comprise the full peptide translocation cycle in a lipid environment [13]. This ABC-transporter is a functional homolog of TAP and can restore the presentation of peptides in human TAP-deficient cells [14],[15]. Different studies propose a model for the TAP mediated peptide transport cycle by extrapolating structural information of other ABC-transporter proteins [13],[16]–[18]. Although these structural studies provide a model for the peptide transport cycle by TAP, the exact mechanism remains to be determined.

Here, we attempt to employ various herpes- and poxvirus-encoded TAP inhibitors to lock TAP in different conformations of the peptide transport cycle. With the use of single particle cryo-electron microscopy (cryo-EM), we aim to gain information about the inhibitors' mode of action and to elucidate the structural arrangements of TAP.

2 Materials and Methods

2.1 Cloning

A vector expressing TAP1-mVenus-10xHis, TAP2, Inhibitor-TwinStrep-HA was constructed (see Figure S1 for vector layout and Table S1 for sequences of the individual elements). The genes of interest were cloned into the U-Protein Express BV (UPE, Utrecht, The Netherlands) backbone vector 2691.

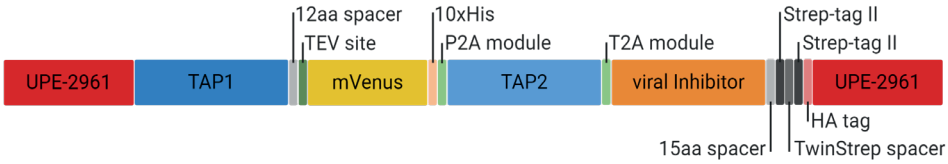

Figure S 1: Layout of the TAP-Inhibitor inserts.

Expression of the genes was under control of a CMV promotor and each gene was separated by a 2A module. A 12 amino acid long flexible linker was cloned between the TAP1 and mVenus genes to ensure proper functionality of the transporter. Depending on the viral inhibitor, the TwinStrep-HA tag was added to either the N- or C-terminus of the construct for immunoprecipitation.

2.2 Fluorescence imaging microscopy

A total of 10 µL human embryonic kidney 293 EBNA1 cells (HEK293E, ± 10.000 cells) were placed in a 15 µ-slide 2 well co-culture plastic object glass (IBIDI) and imaged with a CorrSight fluorescence microscope. Live acquisition (FEI Munich, 2016) was used to operate the microscope. A 63/1.4 oil immersion lens was used for wide-field and fluorescence imaging. Cells were imaged in wide-field mode (transillumination LED illumination) and spinning-disk confocal mode (excitation 488 nm, 50%, no emission filter) with 50 milliseconds exposure times. Images were analyzed with ImageJ and the brightness was adjusted accordingly. Wide-field and confocal image overlays were generated.

Table S 1: Sequences of spacer elements and tags.

Element	Sequence 5'-3'
12aa spacer	GGAGGGTCACCTGGAGGTTCTGGAGGTGGTAGTGCA
15aa spacer	GCGAGCGGCGGAGGGTCACCTGGGGGCTCCGGCGGT GGAAGCGCC
StrepII-tag	TGGTCCCATCCCCAGTTCGAGAAG
TwinStrep Spacer	GGCGGGGGATCCGGCGGTGGAAGCGGTGGCTCCGCC
TEV Site	GAAAACCTGTATTTTCAGGGC
P2A module	GCCACAAACTTCTCTCTGCTAAAGCAAGCAGGTGATGTT GAAGAAAACCCCGGGCCT
T2A module	GAGGGCAGAGGAAGTCTGCTAACATGCGGTGACGTCGA GGAGAATCCTGGCCCA
HA tag	TATCCTTACGACGTGCCAGATTATGCC
10xHIS tag	CATCATCATCATCATCACCACCACCACCAC

2.3 Cell density and viability

HEK293E cells were resuspended, and 10 µL cell suspension were mixed in a 1:1 ratio with Trypan blue. Dual chamber counting slides (Bio-Rad) were filled and cell culture density (cells/mL) and viability (% alive) was analyzed with an automated TC20 cell counter (Bio-Rad).

2.4 MHC I surface expression

HLA class I surface expression was assessed by flow cytometry using a FACS Canto II (BD Biosciences). Cells were washed with PBS and stained for 30 minutes with the PE-conjugated antibody W6/32, anti-HLA-I (Serotec MCA81PE, 1:100) in cold PBS supplemented with 0.5% BSA and 0.02% NaN_3 in a total volume of 20 µl. The cells were washed twice to remove unbound antibody. The data were analyzed using FlowJo V10 software.

2.5 Immunoblotting

SDS-page was performed with 12% NuPage SDS gels (Thermo Scientific). Proteins were transferred to Trans-Blot Turbo PVDF membranes (BIO-RAD) using a Trans-Blot Turbo transfer system (BIO-RAD) for 10 minutes at 25 V. Membranes were blocked with 4% milk powder (Campina) in phosphate-buffered saline supplemented with 0.05% Tween 20 (PBST) for 2 h at 4°C. Primary antibodies (mouse-anti-human TAP1 148.3 C-terminus mAb (1:200) [19], mouse-anti-human TAP2 435.4 mAb (1:200) [4]) were diluted in PBST supplemented with 1% milk powder and incubated with the membranes overnight at

4°C or 2 h at room temperature. Membranes were washed thoroughly with PBST at 4°C and subsequently incubated with HRP-conjugated secondary antibodies for 2 h at 4°C. Membranes were again washed extensively at 4°C and subjected to chemiluminescence using the Pierce ECL Western Blotting Substrate (Thermo Scientific), followed by picture acquisition (ImageQuant LAS 4000, GE Healthcare).

2.6 Tandem affinity purification

Cell pellets were lysed in 15 mL lysis buffer (50 mM HEPES pH 7.8, 300 mM NaCl, 15% Glycerol, 10 mM EDTA, 1 mM Pepstatin, 1% digitonin, ½ complete protease inhibitor tablet per 17.5 mL buffer) for 1h at 4°C in an overhead mixer (15rpm). Lysates were centrifuged at 120,000 g for 30 minutes at 4°C to pellet aggregates and membranes. The supernatant was loaded onto 0.8 mL StrepTactin XT high-capacity gravity flow beads which were previously equilibrated with five column volumes Strep wash buffer (20 mM HEPES pH 7.8, 300 mM NaCl, 15% Glycerol, 1 mM DTT, 0.1% digitonin). The flow-through was collected and re-immobilized twice. Beads were washed with 20 mL Strep wash buffer, resuspended in 2 mL Strep elution buffer (20 mM HEPES pH 7.8, 300 mM NaCl, 15% Glycerol, 1 mM DTT, 0.1% digitonin, 50 mM Biotin) and incubated for 5 minutes before elution. Elution was repeated several times obtaining a total elution volume of ~10 column volumes (cv). The sample was immobilized on a HiTrap Talon crude column (1mL) for 60 minutes and washed with 15 cv His wash buffer (20 mM HEPES pH 7.8, 150 mM NaCl, 15% Glycerol, 0.1% digitonin). The sample was eluted with 3 mL His elution buffer (20 mM HEPES pH 7.8, 300 mM NaCl, 15% Glycerol, 250 mM Imidazole, 0.1% digitonin) and immediately applied to two conjoined prepacked HiTrap desalting columns, previously equilibrated with a total volume of 50 mL desalting buffer (20 mM HEPES pH 7.8, 300 mM NaCl, 15% Glycerol, 0.1% digitonin). The sample was eluted with 4 mL of desalting buffer. For each eluate, protein concentration was measured via NanoDrop.

2.7 Size exclusion chromatography

The sample was concentrated to 25 uL in an Amicon Ultra 100 kDa-cutoff Centrifugal filter Unit (Merck Millipore) and subsequently loaded on a Superose 6 increase 3.2/300 PC column (GE healthcare) on an AKTA micro system equipped with an autosampler (GE healthcare). 22 uL-fractions were collected, and peak fractions were combined and concentrated again for electron microscopy grid preparation.

In the TAP-EHV pilot study, complexes were purified as described in section 2.8. 100 uL Strep-eluate at low concentration (0.23 mg/mL) was applied to a Superdex 200 increase 10/30 GL column (GE Healthcare) on a Shimadzu prominence equipped with an

autosampler and a fluorescence detector unit. Tryptophan fluorescence was measured at excitation/emission wavelengths of 275/354 nm, mVenus fluorescence at 515/528 nm.

2.8 Negative stain

For negative-stain transmission electron microscopy, cell pellets from 800 mL cell culture were lysed and centrifuged as described above. The same buffers as above were used throughout, with the exception of a lower NaCl concentration (150 mM). The supernatant was immobilized three times on a 1 mL TALON gravity flow column, washed with 20 cv of His wash buffer, and eluted with 3 cv His elution buffer. The eluate was loaded on a 1.8 mL Streptactin XT high capacity gravity flow column, washed with 10 cv Strep wash buffer, eluted with 5 cv Strep elution buffer, and concentrated to 0.23 mg/mL for downstream analysis. Strep eluates were diluted 1:10 in strep elution buffer. 3 uL-samples were applied to freshly glow-discharged (25s, 6 mA, 10^{-4} mbar) 200 mesh carbon coated copper grids and incubated for 1 minute. Excess liquid was removed manually using Whatman 1 blotting paper. The grid surface was washed once with a 2% uranyl acetate in milli-q H_2O prior to final staining with 2% uranyl acetate for one minute. After each step, excess liquid was removed manually using Whatman 1 blotting paper. Finally, grids were allowed to air-dry. Grids were imaged on a Tecnai 20 electron microscope (Thermo Fischer) equipped with an Eagle CCD camera operated at 200 kV at a magnification of 100,000x, resulting in a nominal pixel spacing of 1.14 Å.

3 Results

3.1 Localization of the TAP1-mVenus fusion protein

The only existing structure of TAP is as a complex with the soluble inhibitor ICP47. This complex was produced *in vitro* by co-incubating TAP1 and TAP2 expressed from yeast with ICP47 [12]. Since all other inhibitors are membrane proteins and therefore diffusion-limited, we aimed to co-express all components in human cell lines and isolate the assembled complexes by immunoprecipitation. We fused TAP1 to the fluorescent protein mVenus and a His-tag and co-expressed it together with TAP2 and single viral evasion proteins (Table 1) from a transient expression vector (see Figure S1 for details) in HEK293E cells. We could readily detect mVenus fluorescence by confocal microscopy (Figure 1), indicating a high transfection efficiency. Additionally, we observed increased fluorescence intensities in close proximity to the nucleus, suggesting a localization of the TAP1 fusion protein to the endoplasmic reticulum (ER).

All cells transfected with the different viral inhibitor constructs displayed a similar

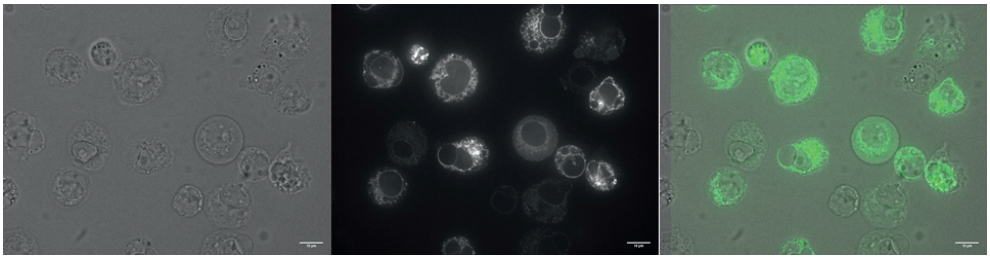

Figure 1: Expression of mVenus-tagged TAP1 in HEK293E cells. Left panel: representative wide-field image of cells expressing the full construct (here with the TAP inhibitor CPXV012) at four days after transfection of 1000 ng DNA. Middle panel: confocal image of the same location (excitation at 488nm). Right panel: Overlay of wide-field and confocal image; fluorescent signal colored in green. Scale bars are 10 µm.

expression pattern of the TAP1 fusion protein, except for cells co-expressing ICP47. These cells displayed fluorescence throughout the cell, potentially due to proteolytic cleavage of the GFP tag *in vivo* (data not shown).

3.2 Screening for optimal expression conditions

We optimized for experimental conditions favoring high expression levels in as many cells as possible, without affecting cell viability. Cell density, cell viability and mVenus expression were analyzed for various DNA concentrations and time points. For example, HEK293E cells were transfected with 2 µg plasmid DNA and cell density and viability were measured over a period of five days (Figure 2). While cell density increased over time, cell viability decreased at day four and five.

To further optimize the conditions of protein expression, we analyzed TAP1-mVenus-10xHis expression by flow cytometry (Figure 3). Higher DNA input resulted in enhanced mVenus expression levels in an increased number of cells (Figure 3A). Also, the expression time affected protein levels where expression of the fusion protein peaked at three days

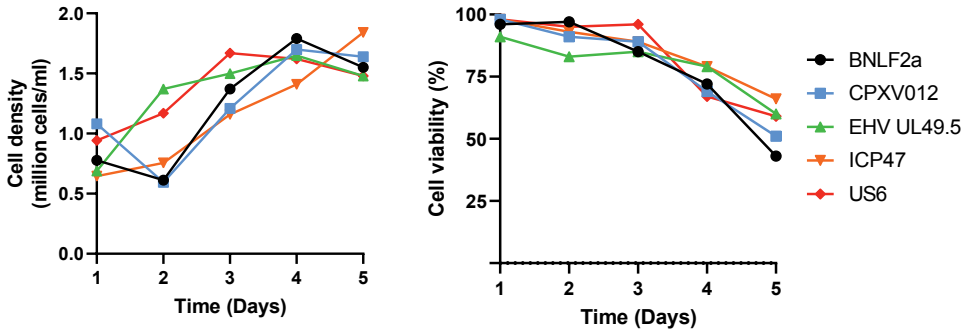

Figure 2: Cell density and viability after transfection. HEK293E cells were transfected with 2 µg of plasmid (TAP1-mVenus-10xHis, TAP2 and a TwinStrep-HA-tagged variant of the indicated viral protein).

post transfection (dpt) but decreased thereafter (Figure 3B). Based on these experiments, we decided to use high amounts of DNA (2 µg/mL) and harvest the cells at three days post transfection.

3.3 Tagged viral inhibitors are able to reduce MHC class I surface expression

We next confirmed the functionality of the tagged viral inhibitors by assessing surface MHC class I expression levels in transfected cells. Under physiological conditions, newly synthesized MHC class I molecules are loaded with peptides in the ER and subsequently migrate to the cell surface. Upon expression of viral TAP inhibitors however, peptide transport is halted resulting in reduced MHC class I surface expression. Wild type (wt) cells showed high levels of surface MHC class I and an absence of mVenus signal (Figure 4a, see quadrant 1, Q1). As expected, cells transfected with the viral inhibitor BNLF2a displayed high mVenus expression (Figure 4b) and strongly reduced MHC class I surface levels (Figure 4b, see Q3 versus Q2). Similar results were obtained for the other viral inhibitors (data not shown).

3.4 Digitonin solubilization results in more stable TAP-Inhibitor complexes

The choice of the detergent used to allow for solubilization of intact protein complexes is an important step to achieve high-resolution structure information. As previous studies have used either N-Dodecyl β-D-maltoside (DDM) [12] or the digitonin-analogue glyco-diosgenin to solubilize TAP complexes [12],[20], we assessed whether these could also effectively solubilize TAP in our experimental setup. For this, DDM- or digitonin-solubilized proteins of interest were immobilized on Streptactin XT affinity resin through

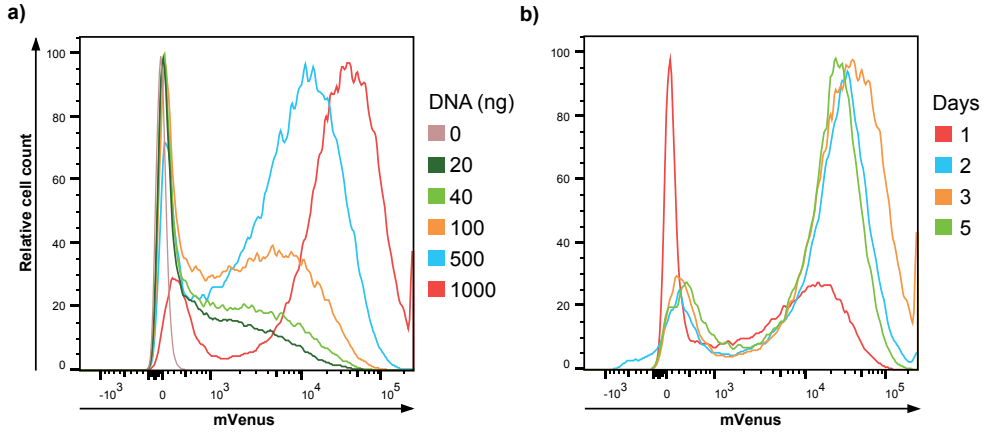

Figure 3: Fluorescence intensity of cells transfected with the construct encoding the viral inhibitor BNLF2a. a) A range of different DNA concentrations (ng/mL) used for transfection was tested. b) Cells were transfected with 2 µg of DNA and the relative mVenus fluorescence was measured over time.

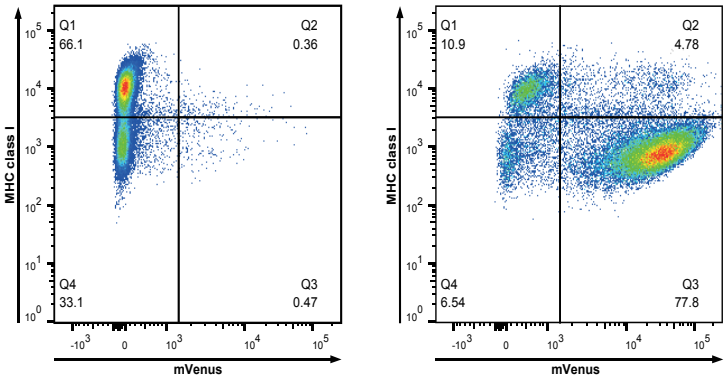

Figure 4: Viral TAP-inhibitor mediated surface MHC class I downregulation. Flow cytometric analysis of surface MHC class I (W6/32-PE) and TAP1-mVenus levels in wt HEK293E cells (left panel) and cells transfected with BNLF2a (right panel) at five days post-transfection. One representative experiment of N=2 is shown.

the TwinStrep tag attached to the inhibitors. As a proxy for the number of TAP-inhibitor complexes, the fluorescence intensity of co-purified mVenus immobilized on the beads was assessed by eye in a small-scale solubilization and purification experiment with five TwinStrep-tagged viral inhibitor constructs (BNLF2a, CPXV012, EHV UL49.5, ICP47 and US6). The lysis and strep-based purification of the full complex were more efficient for digitonin-solubilized samples as compared to DDM solubilization (Figure 5). Only ICP47 could be successfully co-purified with DDM, whereas fluorescence was absent for the other inhibitors (Figure 5D). In contrast to DDM, digitonin solubilization resulted in visible retention of the complex on the beads for all constructs (Figure 5C). Further experiments were therefore performed with digitonin as the detergent of choice.

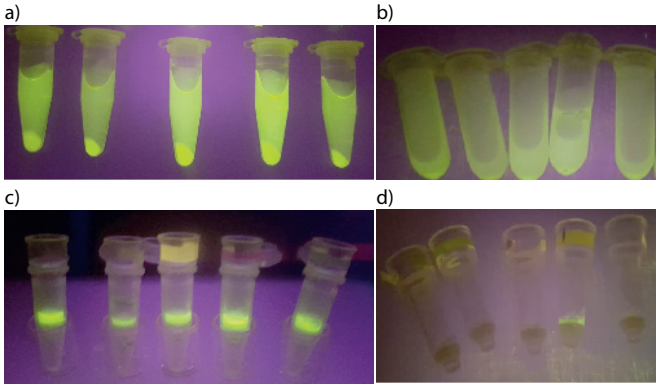

Figure 5: Small-scale purification of TAP-inhibitor complexes with the detergents digitonin and DDM. Lysates of cells expressing the proteins of interest were centrifuged to exclude aggregates and membranes prior to purification (a and b are digitonin- and DDM-solubilized samples, respectively). Tandem affinity purification of digitonin- (c) and DDM-solubilized supernatants (d) in StrepTactin XT high-capacity gravity flow beads. Sample order from left to right for each condition: BNLF2a, EHV UL49.5, ICP47 and US6.

The digitonin-solubilized strep-purified eluates were analyzed by SDS-PAGE (Figure 6). For each sample, five clear bands were observed. Signals at around 110kDa correspond to the expected size of the TAP1-mVenus-10xHis fusion protein, and bands at 70kDa to TAP2. The different viral inhibitors were present in each sample at their respective molecular weights. Additional bands at 250kDa and 45kDa were observed.

Mass spectrometry showed that the 45kDa product was a degradation product of TAP1. The appearance of this proteolysis product was mitigated by the use of a higher concentration of protease inhibitors in subsequent experiments (data not shown). The 250kDa product proved an incompletely denatured complex of TAP1-mVenus, TAP2 and the viral inhibitor. Although a normalized number of cells was used for the purification, the intensity of all bands in the samples of BNLF2a and US6 was higher when compared to the other samples. This might be explained by either higher expression levels of the proteins in the cell, better immobilizability (e.g. by better steric accessibility of the tag), or a better stability of the complex during the purification.

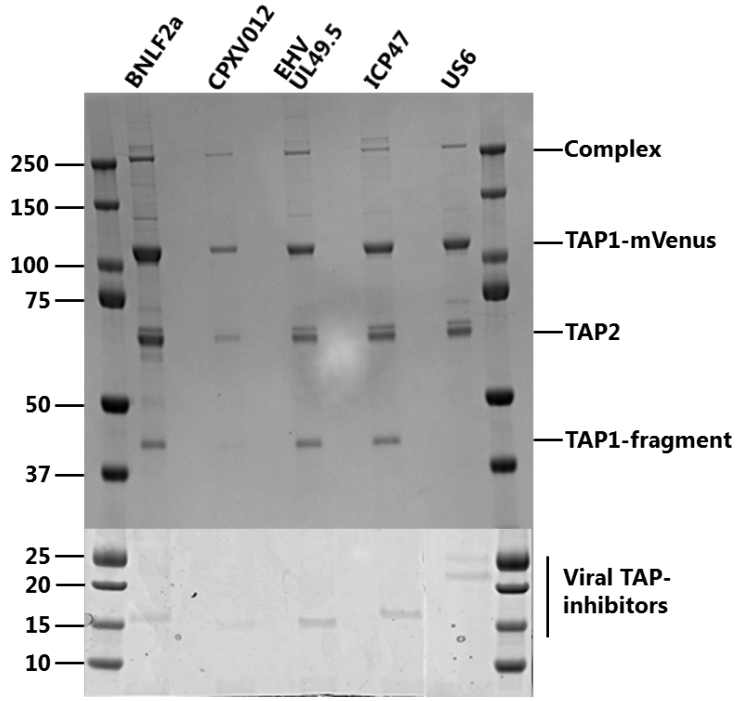

Figure 6: Coomassie staining of digitonin solubilized TAP-inhibitor complexes. For each sample, bands can be observed at around 250kDa, 110kDa, 70kDa, 45kDa and for viral TAP inhibitors, respectively. The bands were identified by immunoblotting (not shown) as TAP1-mVenus (115kDa), TAP2 (75kDa), viral TAP inhibitors (13-25kDa). The signals at 250kDa and 45kDa were determined via mass spectrometry and identified as a TAP1-mVenus-TAP2-Inhibitor complex and a TAP1 fragment, respectively.

3.5 Purification

At the point of writing, a highly reproducible purification protocol has not been established yet. Therefore, this section describes an outline of the general purification procedure. All purifications of TAP-Inhibitor complexes were performed in the presence of 1% digitonin and protease inhibitors. The lysate was cleared by ultracentrifugation and lysed samples were immobilized via the TwinStrep tag on the viral inhibitors, followed by a second immobilization step via the 10xHis-tag on TAP1-mVenus (Figure 7A). Rapid removal of imidazole via a HiTrap desalting column was crucial to prevent protein aggregation.

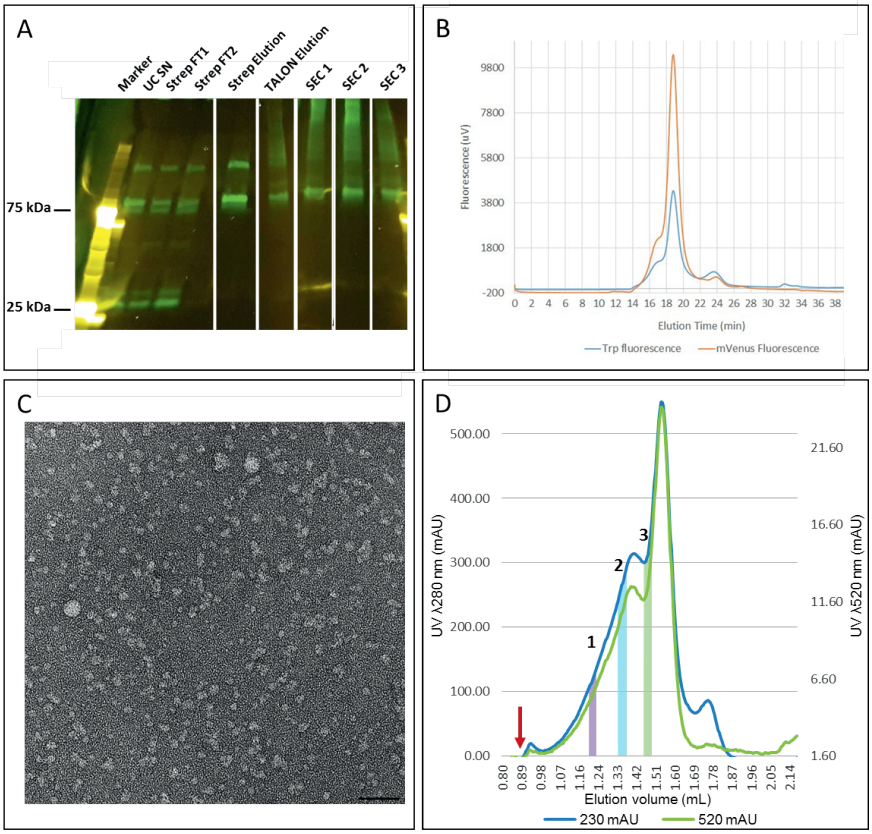

Figure 7: Tandem affinity purification of TAP-inhibitor complexes. a) Purification of 0.5L of cells expressing TAP-US6. In-gel fluorescence after SDS-PAGE shows the appearance of proteolytic products in the lysate and aggregates following TALON purification. SEC 1-3: SEC fractions of aggregates of varying hydrodynamic radius as indicated in e). b) At low concentration (0.23 mg/mL), TAP-EHV UL49.5 forms a nearly monodisperse complex without apparent aggregation. c) Negative stain electron microscopy of TAP-EHV UL49.5 at low concentrations reveals monodisperse particle size distribution even before SEC. d) SEC of a 0.5L purification of TAP-US6. At the current stage, around 45% of the total protein remains monodisperse and can be partially separated from aggregated particles. Red arrow indicates the void volume of the SEC column. Blue line: UV absorption at 230 nm (230 mAU); green line: mVenus signal at 520nm (520 mAU).

A small-scale tandem affinity purification was performed for the construct encoding the UL49.5 inhibitor from EHV and analyzed for sample homogeneity and monodispersity - two of the main prerequisites for successful data collection in cryo-EM (Figures 7B-C). At low protein concentrations, a near-monodisperse size exclusion chromatography (SEC) profile with a single major protein peak at around 18 minutes was observed. mVenus fluorescence strongly overlapped with the protein peak in the chromatogram (Figure 7B). The samples collected after SEC were analyzed via immunoblotting to confirm the presence of the intact EHV UL49.5-TAP complex (data not shown). Negative-stain electron microscopy of the sample before SEC mainly showed particles with a homogeneous size of around 20 nm, interspersed with a few larger particles that may be contaminants or staining artifacts.

Nonetheless, scaling up the protocol for the preparation of cryo-EM samples results in variable yields and the occurrence of protein aggregates following TALON affinity chromatography (Figure 7 A,D). Likely reasons are a chemical incompatibility with imidazole or with the nitrocellulose membrane used for concentrating the protein in intermediate steps. Both are known sources of protein aggregation and occur in many projects. A systematic assessment of protein stability in different conditions, e.g. by differential scanning fluorimetry, will be instrumental for the development of a more robust purification protocol.

4 Discussion

Here, we aimed to obtain structures of different herpes- and poxvirus-encoded TAP-inhibitors in complex with the TAP1 and TAP2 heterodimer. Our approach was to design an expression cassette consisting of TAP1-mVenus, TAP2 and the individual TAP-inhibitors on a lentiviral plasmid. Initial experiments revealed that a single Strep tag purification was insufficient to obtain pure samples and size exclusion chromatography showed considerable heterogeneity across the sample (data not shown). To overcome this issue, we cloned an additional 10xHis tag to the TAP1-mVenus fusion protein. The new tandem affinity purification setup resulted in more homogenous samples (Figure 6 and 7B).

In addition, the choice of the right detergent is crucial in structural biology. A previous study elucidating the structure of HSV ICP47 bound to TAP made use of the detergent DDM [21]. Our results showed that DDM solubilization only allowed successful purification of TAP-ICP47 complexes (Figure 5), but not of the other viral TAP inhibitors. Solubilization using digitonin, however, resulted in efficient downstream immunoprecipitation and purification of intact TAP-Inhibitor complexes for all viral inhibitors. Since the integrity of the TAP-inhibitor complexes appears to be sensitive to the choice of detergents, we

hypothesize that interactions occurring between the transmembrane segments of TAP and the inhibitors play an important role in complex formation. Notably, the structure of DDM-solubilized TAP lacks ordered densities for the TM_0 domains, which are not important for the interaction with the soluble ICP47 but may be crucial for interactions with membrane-integral inhibitors. One important feature of detergents is the curvature their micelles induce around the protein. Harsher detergents tend to form small micelles with higher curvature, forcing the transmembrane parts of proteins into unnatural conformations that often disrupt protein-protein interfaces. Digitonin is one of the mildest detergents available, since it forms large micelles that possess limited curvature. In order to further mimic the ER membrane as closely as possible, digitonin could be exchanged for lipid nanodiscs following initial purification steps. Lipid nanodiscs are composed of a lipid bilayer of phospholipids surrounding the protein, limited in size and shielded from the aqueous environment by a ring of amphiphilic peptides. While the lipid bilayer introduces significantly less curvature than any available detergent, the system cannot be directly used for extracting the complexes from the cells, so an initial extraction step in digitonin is still necessary.

Through thoroughly screening for optimal conditions we were able to obtain relatively pure samples at a moderate protein concentration. Initial screens for optimal expression showed that 3-4 days of expression gave the highest yield. We detected the loss of a considerable amount of fluorescence during purification. We hypothesize that in-cell proteolysis occurs and is responsible for the free mVenus signal. By adding EDTA during the purification process we reduced the amount of free mVenus protein. A shorter expression time post-transfection might also reduce the observed effect.

Understanding the mechanism of the peptide translocation cycle in combination with the structural information from the viral TAP inhibitors may aid in developing new therapeutic approaches: strategies might range from counteracting viral inhibition of TAP and thus exposing infected cells to the immune system, to tailoring novel immune suppressors.

Funding

Patrique Praest was funded by the European Commission under the Horizon2020 program H2020 MSCA-ITN GA 675278 EDGE. A. Manuel Liaci and Friedrich Förster are funded by the ERC Consolidator Grant 724425 (Biogenesis and Degradation of Endoplasmic Reticulum Proteins).

References

1. Sadasivan, B., Lehner, P. J., Ortmann, B., Spies, T. & Cresswell, P. Roles for calreticulin and a novel glycoprotein, tapasin, in the interaction of MHC class I molecules with TAP. *Immunity* **5**, 103–14 (1996).
2. Dean, M. & Annilo, T. Evolution of the Atp-Binding Cassette (Abc) Transporter Superfamily in Vertebrates*. *Annu. Rev. Genomics Hum. Genet.* **6**, 123–142 (2005).
3. Neefjes, J. J., Momburg, F. & Hammerling, G. J. Selective and ATP dependent translocation of peptides by the MHC encoded transporter. *Science (80-.).* **261**, 769–771 (1993).
4. van Endert, P. M. *et al.* A sequential model for peptide binding and transport by the transporters associated with antigen processing. *Immunity* **1**, 491–500 (1994).
5. Grossmann, N. *et al.* Mechanistic determinants of the directionality and energetics of active export by a heterodimeric ABC transporter. *Nat Commun* **5**, 5419 (2014).
6. Mayerhofer, P. U. & Tampé, R. Antigen Translocation Machineries in Adaptive Immunity and Viral Immune Evasion. *J. Mol. Biol.* **427**, 1102–1118 (2015).
7. Schuren, A. B., Costa, A. I. & Wiertz, E. J. Recent advances in viral evasion of the MHC Class I processing pathway. *Curr. Opin. Immunol.* **40**, 43–50 (2016).
8. van de Weijer, M. L., Luteijn, R. D. & Wiertz, E. J. H. J. Viral immune evasion: Lessons in MHC class I antigen presentation. *Semin. Immunol.* **27**, 125–137 (2015).
9. Verweij, M. C. *et al.* Viral inhibition of the transporter associated with antigen processing (TAP): a striking example of functional convergent evolution. *PLoS Pathog.* **11**, e1004743 (2015).
10. Herbring, V., Bäucker, A., Trowitzsch, S. & Tampé, R. A dual inhibition mechanism of herpesviral ICP47 arresting a conformationally thermostable TAP complex. *Sci. Rep.* **6**, 36907 (2016).
11. Blees, A. *et al.* Structure of the human MHC-I peptide-loading complex. *Nature* **551**, 525–528 (2017).
12. Oldham, M. L. *et al.* A mechanism of viral immune evasion revealed by cryo-EM analysis of the TAP transporter. *Nature* **529**, 537–40 (2016).
13. Hofmann, S. *et al.* Conformation space of a heterodimeric ABC exporter under turnover conditions. *Nature* **571**, 580–583 (2019).
14. Zutz, A. *et al.* Asymmetric ATP hydrolysis cycle of the heterodimeric multidrug ABC transport complex TmrAB from Thermus thermophilus. *J. Biol. Chem.* **286**, 7104–15 (2011).
15. Nöll, A. *et al.* Crystal structure and mechanistic basis of a functional homolog of the antigen transporter TAP. *Proc. Natl. Acad. Sci.* 201620009 (2017) doi:10.1073/pnas.1620009114.
16. Geng, J., Sivaramakrishnan, S. & Raghavan, M. Analyses of conformational states of the transporter associated with antigen processing (TAP) protein in a native cellular membrane environment. *J. Biol. Chem.* **288**, 37039–37047 (2013).
17. Seyffer, F. & Tampé, R. ABC transporters in adaptive immunity. *Biochim. Biophys. Acta* **1850**, 449–60 (2015).
18. Praest, P., Liaci, A. M., Förster, F. & Wiertz, E. J. H. J. New insights into the structure of the MHC class I peptide-loading complex and mechanisms of TAP inhibition by viral immune evasion proteins. *Mol. Immunol.* **113**, 103–114 (2019).

19. Plewnia, G., Schulze, K., Hunte, C., Tampé, R. & Koch, J. Modulation of the Antigenic Peptide Transporter TAP by Recombinant Antibodies Binding to the Last Five Residues of TAP1. *J. Mol. Biol.* **369**, 95–107 (2007).

20. Panter, M. S., Jain, A., Leonhardt, R. M., Ha, T. & Cresswell, P. Dynamics of major histocompatibility complex class I association with the human peptide-loading complex. *J. Biol. Chem.* **287**, 31172–84 (2012).

21. Oldham, M. L., Grigorieff, N. & Chen, J. Structure of the transporter associated with antigen processing trapped by herpes simplex virus. *Elife* **5**, (2016).

6

A broad-spectrum antiviral peptide blocks infection of viruses by binding to phosphatidylserine in the viral envelope

R.D. Luteijn, F. Thiele, P. Praest, S.M. Sadasivam, K. Singethan, J.W. Drijfhout, C. Bach, S.M. de Boer, F.J. van Kuppeveld, S. Tao, M. Helfer, N.C. Bach, U. Protzer, A.I. Costa, J.A. Killian, I. Drexler, E.J.H.J. Wiertz

Manuscript submitted

Abstract

The ongoing threat of viral infections and the emergence of antiviral drug resistance warrants a ceaseless search for new antiviral compounds. Broadly-inhibiting compounds that act on elements shared by many viruses are promising antiviral candidates. Here, we identify a peptide derived from the cowpox virus protein CPXV012 as a broad-spectrum antiviral peptide. We found that CPXV012 peptide hampers infection by a multitude of clinically and economically important enveloped viruses, including poxviruses, herpes simplex virus-1, hepatitis B virus, HIV-1, and Rift Valley fever virus. Infections with non-enveloped viruses such as Coxsackie B3 virus and adenovirus are not affected. The results furthermore suggest that viral particles are neutralized by direct interactions with CPXV012 peptide and that this cationic peptide may specifically bind to and disrupt membranes composed of the anionic phospholipid phosphatidylserine, an important component of many viral membranes. The combined results strongly suggest that CPXV012 peptide inhibits virus infections by direct interactions with phosphatidylserine in the viral envelope. These results reiterate the potential of cationic peptides as broadly-acting virus inhibitors.

Importance

New strategies of antiviral treatment are needed to face (re)emerging viral infections and the increase in viral resistance against antiviral agents. Here, we show that a peptide derived from the cowpox virus protein CPXV012 can inhibit the infectivity of several enveloped viruses of clinical and economic relevance. The peptide is shown to target membranes containing phosphatidylserine, a crucial component of the envelope of many viruses, and disrupts these membranes. Additional analyses of the biophysical and physicochemical properties of the peptide can guide pharmacological improvements of this promising broad-spectrum antiviral agent.

1 Introduction

The continuous threat of conventional viruses and emergence of new virus species requires an ongoing search for new antiviral compounds. Broad-spectrum antiviral inhibitors have become promising therapeutic candidates [1]. These compounds act on common elements shared by many groups of viruses, including synthesis of viral RNA and DNA, viral proteases, and glycosylation of viral proteins (reviewed by [2]). An important class of broad-spectrum antivirals targets the lipid envelope of viruses [3]–[7].These include not only antibodies and chemical compounds, but also cationic peptides present as defence peptides in the human host and in other organisms. In essence, the applicability of such peptides as antiviral compounds targeting the envelope of viruses will depend on their ability to discriminate viral from human membranes.

Enveloped viruses, in contrast to non-enveloped ones, have their nucleocapsid surrounded by a lipid membrane. Depending on the virus, this lipid bilayer is derived from the plasma membrane or intracellular organelles. Although the membrane is host cell-derived, it may differ functionally and structurally from the membrane of origin in several aspects, including the lipid composition. Compared to host cell membranes, the envelope of many viruses is enriched for the phospholipid phosphatidylserine (PS). PS is the most abundant anionic lipid in eukaryotic cells. In resting cells, PS is mainly contained within the cell, with only very limited exposure to the extracellular environment. PS is enriched in some intracellular organelles, but the majority of PS is asymmetrically distributed on the inner leaflet of the plasma membrane [8]. This organization results from constantly flipping PS from the outer membrane leaflet to the inner membrane leaflet by ATP-dependent flippases. As a result, the outer exposed membrane leaflet of the cellular plasma membrane is devoid of PS. In apoptotic cells, this organization is lost due to inactivation of flippases and activation of scramblases. The resulting PS exposure on apoptotic cells and cell debris induces uptake by surrounding cells through PS receptors. Many viruses take advantage of this uptake mechanism by exposing PS on their envelope, thereby facilitating virus entry. The increase in PS on the virus membrane may be due to the lack of an active flippase. Alternatively, some viruses actively accumulate PS at sites of virus budding, or bud from subcellular microdomains enriched in PS [9].

Another important aspect of the host membrane is its property of self-renewal upon injury. This fast-acting mechanism involves several events, including the detection of the damaged site, exocytosis of nearby cytosolic vesicles, cytoskeletal remodeling, endocytosis of the damaged membrane, and reconstitution of membrane homeostasis [10],[11]. The lipid membrane loses its self-renewal capacity once surrounding the viral nucleocapsid, thereby becoming particularly prone to membrane damage [5]. The

structural and functional differences between virus and host cell membranes make viral membranes ideal targets for antiviral therapy.

Here, we identify a peptide with broad-spectrum antiviral activity, whose sequence is derived from the cowpox virus protein CPXV012. Within virus-infected cells, this protein helps to evade the immune system by inhibiting the transporter associated with antigen processing (TAP), thereby interfering with MHC I-dependent antigen presentation [12]–[16]. We pinpointed the segment of the CPXV012 protein responsible for blocking TAP: a peptide comprising the C-terminal domain of CPXV012. Interestingly, when doing functional assays with this peptide upon infection, we noticed that the percentage of infected cells decreased significantly. It should be noted that we have no indication that this peptide is actually made upon CPXV infection. This finding was the basis for the current study: here, we show that this peptide inhibits infection of many enveloped viruses by interacting with virus particles. Variants of the CPXV012 peptide revealed that basic residues within the peptide are important for this inhibitory effect. Furthermore, CPXV012 strongly interacts with lipid monolayers and membranes enriched for the anionic phospholipid PS. These results suggest that this CPXV012 peptide disturbs the integrity of viral membranes enriched for PS, and thus may be explored as an antiviral agent against a broad range of enveloped viruses.

2 Materials and Methods

2.1 Cells and viruses

MelJuSo (MJS), and BHK21 cells were cultivated with RPMI 1640 containing 10% FCS, 100U/ml penicillin, 100µg/ml streptomycin and 2 mM L-glutamine (complete medium). HEK293T, HeLa, Huh7.5, and Vero cells were grown in DMEM supplemented with 10% FCS (5% for Vero cells), 100 U/ml penicillin, 100 µg/ml streptomycin, 1% nonessential amino acids, 2mM L-glutamine and 1% sodium pyruvate (complete DMEM). HepRG cells were differentiated in Williams E medium supplemented with 10% FCS (Fetalclone II from Hyclone, Thermo Scientific), 100U/ml penicillin, 100 µg/ml streptomycin, glutaMax, 0.023 IE/ml human insulin (Sanofi Aventis), 4.7 µg/ml hydrocortisone (Pfizer), 80µg/ml Gentamicin and 1.8% DMSO. HepG2.2.15 cells were cultivated in Williams E medium with 10% FCS, 100U/ml penicillin, 100 µg/ml streptomycin and 1% nonessential amino acids. LC5-RIC cells (EASY-HIT assay) were maintained as described previously [17].

Recombinant modified vaccinia virus Ankara (MVA) expressing eGFP under the natural early/late promoter p7.5 was used in this study (MVA-eGFP)[18]. MVA-eGFP was propagated and titrated in chicken embryonic fibroblasts (CEFs) according to standard methodology

[19]. Vaccinia virus expressing eGFP (VACV-eGFP) was a generous gift from Dr. Jon Yewdell (NIH, Bethesda, USA). VACV-eGFP was propagated and titrated on CV-1 cells. Cowpoxvirus strain Brighton Red (CPXV-BR) expressing RFP/eGFP virus was originally obtained from Dr. Karsten Tischer (FU Berlin, Germany). HSV-1 expressing the VP16-eGFP was kindly provided by Dr. Peter O'Hare (Imperial College London, UK). Stocks were prepared and titrated on Vero cells.

HBV particles were concentrated from the supernatant of HepG2.2.15 cells as described previously [20]. Infectious HIV-1 stocks were prepared as described before [17]. Measles virus expressing eGFP (MV-eGFP) was generated as previously described [21]. Vesicular stomatitis virus expressing Luciferase (VSV-deltaG (Luc)) was a kind gift from Dr. Gert Zimmer (Institute of Virology and Immunology, Mittelhäusern, Switzerland). Recombinant adenovirus expressing GFP and ovalbumin (AdGOva) was kindly provided by Dr. Percy Knolle (Institutes of Molecular Medicine and Experimental Immunology, Bonn, Germany) and virus stocks were prepared as previously described [22]. Non-spreading Rift Valley fever virus (RVFV) replicon particles were produced and titrated as described previously [23]. Coxsackie B3 virus expressing Renilla Luciferase (RLuc-CVB3) was produced and titrated as described previously [24].

2.2 Peptides

The inhibitory peptide used in this study comprises amino acids 36-69 of the CPXV012 protein. The sequences of the wild-type (WT) and CPXV012 peptide variants (Ala1-Ala8) are indicated in Fig. 5A. The control peptide is derived from the pseudorabies virus TAP inhibitor UL49.5, and comprises amino acid residues 28-59 of this protein (sequence: STEGPLPLLREESRINFWNAAUAARGVPVDQP). U in amino acid sequence refers to alpha-amino-n-butyric acid, see below.

Synthetic peptides were prepared by normal Fmoc chemistry using preloaded Tentagel resins, using PyBop/N-methylmorpholine for in situ activation and 20% piperidine in N-methylpyrrolidinon for Fmoc removal [25]. Couplings were performed for 75 min. After final Fmoc removal, peptides were cleaved with trifluoroacetic acid/H2O 19:1 v/v containing additional scavengers when C or W residues were present in the peptide sequence. Peptides were isolated by ether/pentane precipitation. Peptides were checked for purity using reversed-phase HPLC–mass spectrometry and for integrity using MALDI-TOF mass spectrometry, showing the calculated molecular masses. All peptides were synthesized with an N-terminal biotin moiety and a C-terminal amide. Cysteines were replaced by the isosteric alpha-amino-n-butyric acid. Lyophilized peptides were dissolved in DMSO. Peptide concentrations were confirmed by the NanoDrop spectrophotometer

(Thermo Scientific) using the absorbance of Trp at 280 nm. Peptides were aliquoted in Eppendorf LoBind microcentrifuge tubes (Sigma-Aldrich) and kept at -20 °C for short-term storage.

2.3 Cell viability assays

Cells were incubated with CPXV012 peptide, control peptide, or DMSO at the indicated concentrations for at 37°C for 20-24h. Thereafter, cell viability was measured using different assays. DAPI staining was performed to discriminate between live and dead cells using flow cytometry. Cell Titer-Blue Cell Viability Assay (Promega) was performed according to manufacturer's instructions. Neutral Red uptake (Applichem) was performed as described previously [26]. WST-1 salt conversion assay (Roche Applied Sciences) was performed according to the manufacturer's instructions at 7h or 20h post exposure to the peptides. No difference was observed between 7h and 20h post exposure.

2.4 Virus inhibition assays

2.4.1 MVA, VACV and Cowpox

MJS, BHK21, HeLa and HEK-293T cells ($1x10^5$) were seeded in 24-well plates in a total volume of 400µl and incubated overnight at 37°C. Cells were infected with MVA-eGFP, VACV-eGFP or CPXV-RFP/eGFP at 37°C for 18-20h in the presence of DMSO vehicle control or peptides at the concentrations indicated. Flow cytometric analysis was performed to quantify the percentage of infected cells as indicated by eGFP or RFP expression.

Where mentioned, MVA-eGFP was pretreated with 50, 100, or 150 µg/ml CPXV012 peptide, control peptide or DMSO vehicle at 37°C for 1h. Thereafter, the virus-CPXV012 peptide mixture was diluted 1:10 by volume and used to infect MJS cells (corresponding to an MOI of 10) resulting in a final concentration of 5, 10, or 15 µg/ml peptide in the culture medium. As a control, MJS cells were incubated with the same concentrations of CPXV012 peptide (5, 10 and 15 µg/ml) during infection with MVA-eGFP that was not pretreated with peptides. After 20h, cytometric analysis was performed to quantify the percentage of infected cells indicated by eGFP-expression.

For qPCR analysis (Fig. 1B), MJS cells were infected with MVA-eGFP (MOI 10) in the presence of 100 µg/ml of CPXV012 peptide, or control peptide or DMSO at 37°C for 20h. RNA was isolated using RNeasy Mini Kit (Qiagen). 3µg of RNA was digested with 10 U of DNase I (Roche) and cDNA synthesis was performed by using 200 U Superscript III RNase H reverse transcriptase (Invitrogen), 7.5 pmol oligo$(dT)_{12-18}$ (Invitrogen), 20 U of RNasin (Promega), and 10 mM each deoxynucleoside triphosphate (Qiagen). For semiquantitative

analysis of viral mRNAs, cDNA was used as the template for a PCR with the indicated primers: *B8R* (fwd ATCCGCATTTCCAAAGAATG, rev ACATGTCACCGCGTTTGTAA), *H3L* (fwd GTCTTGAAGGCAATGCATGA, rev TCCCGATGATAGACCTCCAG) and *G8R* (fwd ATC GAT AAA CTG CGC CAA AT), rev CTC CGC GGT AGA ACA CTG AT). Quantitative RT-PCR analysis was performed by using the LightCycler DNA Master SYBR green I kit (Roche) and LightCycler 1.5 (Roche). Gene expression was determined using the $2^{-\Delta\Delta Ct}$ method. The results are quantified relative to housekeeping gene GAPDH [27],[28].

2.4.2 HSV-1

MJS cells (10^5/well) were seeded in a 24 wells plate and cultured overnight at 37°C. HSV-1-eGFP was mixed with CPXV012 peptide, control peptide or DMSO in complete medium. Medium of cells was replaced with virus/peptide inoculum (MOI 0.1) and cells were incubated for 16h at 37°C. Cells were harvested, fixed using 1% formaldehyde, and the number of eGFP-positive cells was determined using flow cytometry.

2.4.3 HBV

Confluent HepRG cells cultured in 48-well plates were differentiated for two weeks. Medium was removed and cells were left untreated, or CPXV012 peptide or control peptide was added at the concentrations indicated. DMSO was used as vehicle control. Cells were infected with HBV (MOI 200) and incubated for 16h. Medium was removed, cells were washed three times with PBS, fresh medium was added and cultures were incubated for another 12 days with medium change every three days. Thereafter, supernatant was collected after centrifugation to remove cellular debris (5 min, 350g) and HBeAg was quantified using commercial immunoassays as described [20]. HBV DNA was extracted from the supernatant using the BioSprint 96 One-For-All Vet Kit (Qiagen) and was quantified by qPCR.

2.4.4 HIV-1

The EASY-HIT assay was performed as described previously [17]. Briefly, $1x10^4$ LC5-RIC cells were plated in 96-well plates and incubated at 37°C for 24h. Thereafter, cells were treated with CPXV012 peptide, control peptide, or DMSO vehicle control at the concentrations indicated for 1h prior to infection with HIV inoculum. After 48h, cultures were assayed for cellular reporter gene expression by quantification of total fluorescence intensity of each culture using a fluorescence microplate reader (step 1). To assess titers of infectious virus in culture supernatant (virion production in primary infected cells), 20 µl of medium was added to fresh LC5-RIC cells and incubated for another 72h before reporter gene expression was quantified (step 2).

2.4.5 Measles and VSV

Vero cells (1x10^5 cells/well) were plated in 12-well plates and left untreated, or CPXV012 peptide or control peptide was added at the concentrations indicated. DMSO was used as vehicle control. Cells were infected with MV-eGFP (MOI 0.1). Once maximum giant cell formation was observed at 48h post infection, microscopic fluorescence images were taken by using an inverted microscope CKX41 (Olympus) with an LCachN/10X/0.40 Phc/1/FN22 UIS objective. Thereafter, medium was removed and infection was measured based on expression of eGFP. Fluorescence was detected using a Infinite 200 PRO Tecan reader (fluorescence bottom reading for cell-based assays). For VSV infections, Huh7.5 cells (2x10^5 cells/well) were seeded in 12-well plates and peptides were added at the concentrations indicated. DMSO was used as vehicle control. Cells were infected with VSVdeltaG (Luc) (MOI 0.6). At 18h post infection, luciferase was measured using the luciferase assay system (Promega) and normalized to the protein content of the individual sample as determined by a Bradford assay.

2.4.6 Adenovirus

HEK-293 cells (4x10^5 cells/well) were seeded in 12-well plates in a total volume of 1ml and incubated overnight at 37°C. Cells were treated with the indicated concentrations of CPXV012 peptide or DMSO control at 37°C for 1h. Afterwards, cells were infected with an MOI of 10 with AdGOva for 24h. Photometric analysis was performed with the Infinite 200 PRO Tecan to quantify the percentage of infected cells based on GFP-expression.

2.4.7 Rift Valley fever virus

MJS cells (2x10^4 cells/well) were seeded in a 96-well plate and incubated for two days at 37°C. Cells were treated with the indicated peptide concentrations or DMSO as vehicle control. After 15 min, RVFV-eGFP was added to the cells. Twenty-four hours after infection, cells were harvested and the percentage of eGFP-positive cells was determined using flow cytometry.

2.4.8 Coxsackie virus B3

MJS cells (10^4 cells/well) were seeded in a 96 well plate. After overnight incubation at 37°C, cells were infected with RLuc-CVB3 in the presence of the indicated concentrations of peptide or DMSO as vehicle control. After 7h of infection, cells were lysed and renilla luciferase expression levels were quantified using the Renilla Luciferase Assay System kit (Promega).

2.5 Preparation of Large Unilamellar Vesicles (LUVs)

Calcein-encapsulated LUVs were prepared using 1,2-dioleoyl-*sn*-glycero-3-phosphocholine (DOPC) or a mixture of DOPC and 1,2-dioleoyl-*sn*-glycero-3-phospho-L-serine (DOPS) (Avanti Polar Lipids) in a 7:3 molar ratio. Stock solution of DOPC and DOPS in chloroform (10mM) were mixed in a glass tube. The solvent was evaporated with dry nitrogen gas yielding a lipid film that was subsequently kept in a vacuum desiccator for 20 min. Lipid films were hydrated for 30 min in buffer containing 10mM Tris, 50 mM NaCl at pH 7.4 resulting in total lipid concentration of 10 mM. For calcein-encapsulated LUVs, 50 mM of calcein was added during hydration. The lipid suspension was freeze-thawed ten cycles, at temperatures of -80 and +40°C, respectively, and eventually extruded 10 times through 0.2 μM-pore size filters (Anotop 10, Whatman, UK). For the preparation of calcein-encapsulated LUVs, free calcein was separated from calcein-filled LUVs using size exclusion column chromatography (Sephadex G-50 fine) and eluted with 10 mM Tris-HCl, 150 mM NaCl buffer at pH 7.4. Finally, the phospholipid content of lipid stock solutions and vesicle preparations was determined as inorganic phosphate according to Rouser [29].

2.6 Circular Dichroism

Circular dichroism (CD) experiments were performed as described previously [15]. Briefly, the CD spectra of 625 μM LUVs and/or 100 μg/ml peptides diluted in 10 mM MES buffer (pH 6.2) were recorded on a Jasco 810 spectropolarimeter (Jasco, Easton, MD) over a wavelength range of 200-250nm. Each reported spectrum is the average of five independent scans recorded every 1 nm at a scan rate of 20 nm/min at room temperature in cuvettes with a path length of 1.0 mm.

2.7 Langmuir monolayers

Peptide-induced changes in the surface pressure of a monomolecular layer (monolayer) of phospholipids at a constant surface area were measured using a Langmuir Microtrough XL device (Kibron, Helsinki, Finland). A Teflon trough was filled with 16 ml PBS (pH 7.4) and lipid monolayers of DOPC or DOPC/ DOPS (ratio 7:3) were spread from a 0.5 mM stock solution in chloroform at the air–buffer interface. The buffer below the lipid monolayer (subphase) was continuously stirred using a magnetic stirrer. Upon stabilization of the initial surface pressure to 25 mN/m, a freshly prepared stock of peptide in DMSO was injected into the subphase, resulting in a final peptide concentration of 0.25 μM.

Table 1 - Inhibitory effect of CPXV012 peptide on enveloped and non-enveloped viruses of different families.

Virus	Family	Genome	Envelope	Inhibition
MVA	Poxviridae	dsDNA	yes	yes
VACV-WR	Poxviridae	dsDNA	yes	yes
CPXV-BR	Poxviridae	dsDNA	yes	yes
HSV-1	Herpesviridae	dsDNA	yes	yes
HBV	Hepadnaviridae	dsDNA-RT	yes	yes
HIV-1	Retroviridae	ssRNA-RT	yes	yes
RVFV	Bunyaviridae	ssRNA	yes	yes
Measles	Paramyxoviridae	ssRNA	yes	no
VSV	Rhabdoviridae	ssRNA	yes	no
Adenovirus	Adenoviridae	dsDNA	no	no
CVB3	Picornaviridae	ssRNA	no	no

MVA: Modified Vaccinia virus Ankara; VACV-WR: vaccinia virus strain Western Reserve; CPXV-BR: cowpox virus strain Brighton Red; HSV-1: herpes simplex virus-1; HBV: Hepatitis B virus; RVFV: Rift Valley fever virus; VSV: vesicular stomatitis virus (VSV), CVB3: coxsackie virus B3.

2.8 Membrane permeability assay

Membrane permeability was measured in standard 96-wells transparent microtiter plates in a plate reader (Spectrafluor, Tecan, Salzburg, Austria). Peptides (5 µL of 0.2 mM in DMSO) were added to calcein-containing LUVs (195 µL of lipid vesicles [50 µM] in 10mM Tris – HCl, 100 mM NaCl buffer [pH 7.4]). As positive control human islet amyloid polypeptide [hIAPP; Bachem] 5 µL of a 0.2 mM in DMSO) was added to calcein-containing LUVs. As negative control, murine IAPP ([mIAPP; Bachem] 5 µl of 0.2 mM in DMSO) was added to calcein-containing LUVs. For blank only, 5 µL DMSO was added to calcein-containing LUVs. Directly after addition of all components, the microtiter plate was shaken for 10 sec. Fluorescence was measured from the top, every 5 min, using a 485 nm excitation filter and a 535 nm emission filter at 25°C. The maximum leakage at the end of each measurement was determined by adding 1 µL of 10% Triton X-100 to a final concentration of 0.05% (v/v). The release of fluorescent dye was calculated according to equation 1:

$$L(t) = (F_t - F_0)/(F_{100} - F_0)$$

L(t) is the fraction of dye released (normalized to membrane leakage), Ft is the measured fluorescence intensity, and F0 and F100 are the fluorescence intensities at times t = 0 and after addition of Triton X-100, respectively. All membrane leakage assays were performed two times, each in duplicate, on different days, using different IAPP stock solutions.

2.9 Statistical analysis

Statistical significance was analyzed by one-way ANOVA testing, followed by the Dunnett's multiple comparisons test (the mean of each column was compared to that of the DMSO control), using GraphPad Prism 8.0.1. In Figure 1D, statistical analysis was performed on the plotted data transformed as follows: Y= Log(Y). P-values of <0.05 were considered significant (* $p < 0.05$; ** $p < 0.01$, *** $p < 0.001$).

3 Results

3.1 CPXV012 peptide prevents infection by different viruses in cell culture

To assess the effect of CPXV012 peptide on viral infection, different infection inhibition assays were performed using a diversity of viruses and cell types. Cells were treated with CPXV012 peptide (34 amino acids) or a similar-length control peptide derived from the pseudorabies virus protein UL49.5. The viral inoculum was mixed with the peptide at different concentrations and immediately added to cells. After incubation for the indicated times, infection was determined based on viral gene expression, or viral DNA or mRNA synthesis.

Infection of the human melanoma cell line MelJuSo (MJS) with recombinant modified vaccinia virus Ankara (MVA) expressing eGFP (MVA-eGFP) was confirmed via microscopy (Fig. 1A). The cell monolayer showed the typical cytopathic effect upon infection (in the presence of DMSO, peptide vehicle control; bright field) and eGFP fluorescence could be detected. A similar pattern was verified in the presence of the control peptide. In contrast, upon infection and incubation with the CPXV012 peptide (100 µg/ml), the monolayer was microscopically indiscernible from that of the uninfected control. MVA-eGFP infection was inhibited in a concentration-dependent manner (Fig. 1B). Inhibition starts at 50 µg/ml and is stronger upon increasing peptide concentrations, reaching 98.3% (±0.3) at 150 µg/ml CPXV012 peptide (Fig. 1B). To test potential cytotoxicity of the peptides, the amount of DAPI-negative (live, i.e. cells whose membrane was not compromised/permeable) cells was quantified. We did not observe any decrease in live cells up to the highest concentrations (200 µg/ml) (Fig. 1C). To further test any effect on cell viability, other assays were performed. The WST-1 assay measures the net metabolic activity of the cells (it is based on the enzymatic conversion of the WST-1 salt into the colored dye formazan in viable cells), and the Neutral red uptake assay relies on the staining of lysosomes in viable cells upon active transport of the cationic dye. MJS cell viability was not severely impaired upon addition of up to 200 µg/ml CPXV012 peptide using the WST-1 assay (Fig. S1A), and the Neutral Red assay (Fig. S1B). Cell titer blue assays, as the WST-1 assay, also assess

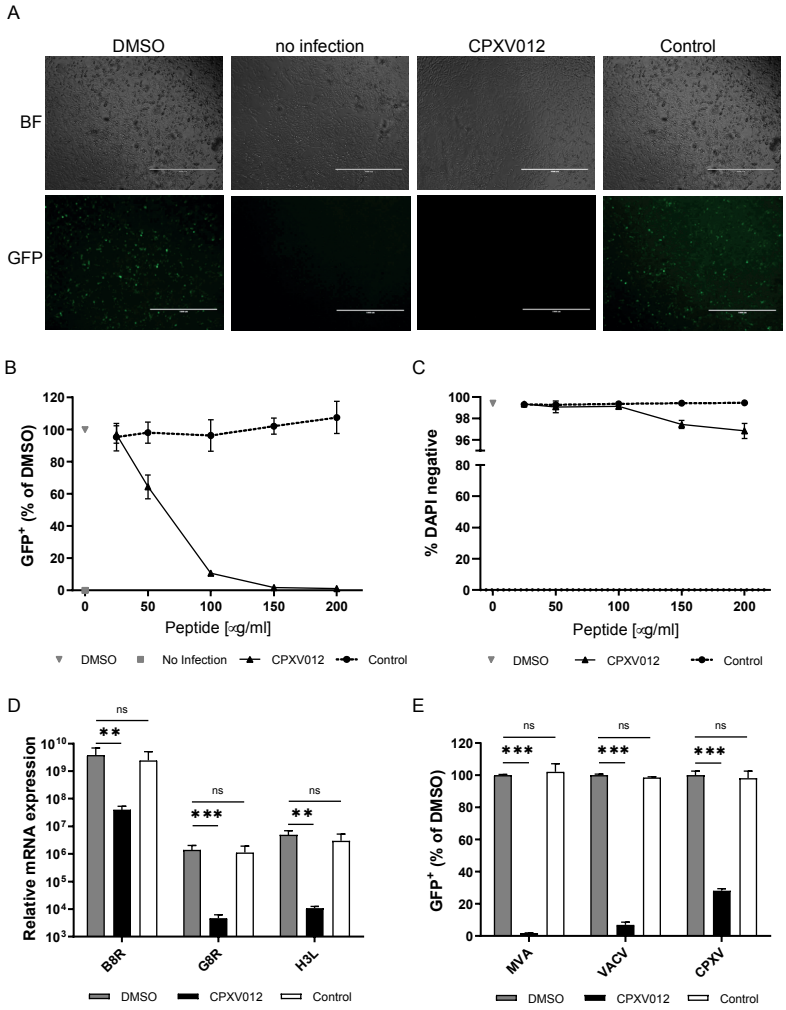

Figure 1: CPXV012 peptide inhibits poxvirus infection. (A) MJS cells were infected with MVA-eGFP (MOI 10) under different conditions (DMSO control, CPXV012 and control peptide). At 20 h.p.i., infection was assessed by fluorescence microscopy (bar size 1 mm). Results are representative of at least 3 independent experiments. BF: Bright field. GFP: Green fluorescent protein (MVA infection). (B) MJS cells were infected with MVA-eGFP (MOI 10) in the presence of DMSO vehicle control, or CPXV012 peptide, or control peptide. 18-20h post infection, cells were harvested and analyzed for viral gene expression. The number of eGFP-positive cells was quantified using flow cytometry. S.E.M. of three independent experiments is shown. (C) MJS cells were treated for 20h with the indicated peptide concentrations. Subsequently, cells were harvested and stained with DAPI for flow cytometric analysis. S.E.M. of three independent experiments is shown. (D) MJS cells infected with MVA-eGFP (MOI 10) in the presence of 100 µg/ml peptide or DMSO control were lysed 20h post infection. RNA was isolated and qPCR was performed for expression of viral genes B8R, H3L, and G8R. S.E.M. of three independent experiments is shown.Log-transformed data were analyzed with one-way ANOVA followed by multiple comparisons Dunnett's test (the mean of each column was compared to that of the DMSO control).

Figure 1 (continued). (E) CPXV012 peptide inhibits infection with the poxviruses MVA-eGFP, VACV-eGFP and CPXV-RFP/eGFP. MJS cells were infected with VACV-eGFP (MOI 10) or CPXV-RFP/eGFP (MOI 10) in the presence of 150µg/ml peptide or DMSO. After 18-20h, infection was quantified by cytometric analysis of fluorescent cells. S.E.M. of three independent experiments is shown using different batches of peptide. Data were analyzed with one-way ANOVA followed by multiple comparisons Dunnett's test (the mean of each column was compared to that of the DMSO control). (* $p < 0.05$; ** $p < 0.01$; *** $p < 0.001$).

the metabolic capacity of living cells (conversion of a redox dye into a fluorescent end product). These were performed to test the viability of other cell lines (Vero and Huh7.5 cells) used in this study in the setting of other viral infections. Again, no significant effect was observed at the highest peptide concentrations (Fig. S1C).

To confirm the inhibitory effect of CPXV012 peptide on infection of MJS with MVA-eGFP, qPCR analysis for expression of viral genes was performed (Fig. 1D). CPXV012 peptide decreased the expression of the early-expressed gene B8R up to 2 logs, relative to its expression upon infection in the presence of DMSO vehicle only. The decrease in expression of the intermediate-expressed gene G8R and and late expressed gene H3L was more pronounced (more than 2 logs). No effect was seen if cells were treated with the control peptide compared to the DMSO sample (Fig. 1D). To assess whether the inhibitory effect on MVA-eGFP infection also occurs in other cell types, HEK-293T, BHK21, and HeLa cells were used (Fig. S2).

Cells were infected with MVA-eGFP in the presence of peptide or DMSO controls. In all cell lines, a strong decrease in infection (87.4-94.2%) was observed. To investigate whether other poxviruses besides MVA were inhibited by CPXV012 peptide, we tested the effect on Vaccinia virus (VACV) strain WR and cowpox virus strain BR (CPXV). Again, infection of MJS with both viruses was inhibited (93±1.7% for VACV and 72±1.1% for CPXV) by CPXV012 peptide (150 µg/ml) while no effect was seen with the control peptide in comparison to the DMSO sample (Fig. 1E). Thus, CPXV012 peptide inhibits infection of different members of the poxvirus family. Cells were infected with MVA-eGFP in the presence of peptide or DMSO controls. In all cell lines, a strong decrease in infection (87.4-94.2%) was observed. To investigate whether other poxviruses besides MVA were inhibited by CPXV012 peptide, we tested the effect on Vaccinia virus (VACV) strain WR and cowpox virus strain BR (CPXV). Again, infection of MJS with both viruses was inhibited (93±1.7% for VACV and 72±1.1% for CPXV) by CPXV012 peptide (150 µg/ml) while no effect was seen with the control peptide in comparison to the DMSO sample (Fig. 1E). Thus, CPXV012 peptide inhibits infection of different members of the poxvirus family.

To further characterize the inhibitory effect of CPXV012, *in vitro* infection inhibition assays

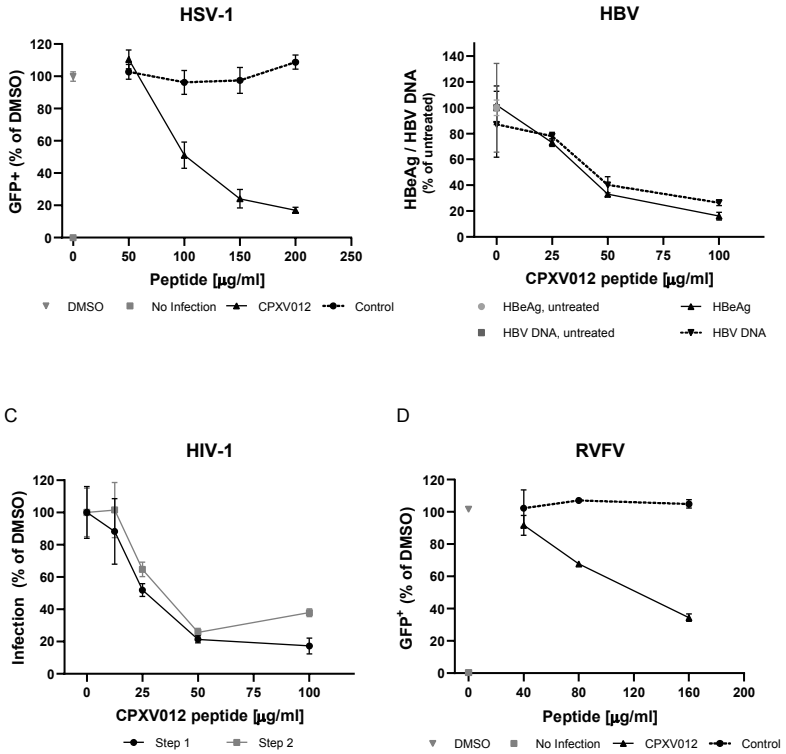

Figure 2: CPXV012 peptide inhibits infection with HSV-1, HBV, HIV, and RVFV. (A) CPXV012 peptide inhibits HSV-1 infection. MJS cells were infected with HSV-1 (MOI 0.1) in the presence of the indicated peptide concentrations or DMSO control. 16h after infection, cells were harvested and the amount of eGFP-positive cells was quantified using flow cytometry. S.E.M. of three independent experiments is shown. (B) Effect of CPXV012 peptide on HBV infection. Differentiated HepRG cells were left untreated or CPXV012 peptide was added using the concentrations indicated and DMSO as control. Cells were infected with HBV (MOI 200) for 16h. Subsequently, cells were washed and fresh medium was added. After 12 days, supernatant was analyzed for HBeAg and HBV DNA. S.E.M. of three independent experiments is shown. (C) CPXV012 peptide inhibits HIV infection. LC5-RIC cells were treated with the indicated concentrations of CPXV012 peptide (DMSO as control) for 1h and infected with HIV for 48h according to the EASY-HIT assay system (17). Cellular reporter expression was quantified using a fluorescence microplate reader to assess ability of HIV to infect LC5-RIC cells (Step 1). 20µl of culture supernatant were added to fresh LC5-RIC cells and incubated for another 72h before fluorescence detection was performed to assess virion production from the first round of infection (Step 2). S.E.M. of three independent experiments is shown. (D) CPXV012 peptide inhibits infection with RVFV. MJS cells were infected with RVFV-eGFP in the presence of the indicated peptide concentrations or DMSO control. After 24h, cells were harvested and the amount of eGFP-positive cells was quantified using flow cytometry. S.E.M. of three independent experiments is shown.

were performed with a collection of viruses that differ in genome content (RNA or DNA) and structural composition (enveloped or non-enveloped). These viruses include herpes simplex virus-1 (HSV-1), Hepatitis B virus (HBV), HIV-1, adenovirus, measles virus, vesicular

stomatitis virus (VSV), coxsackie virus B3 (CVB3), and Rift Valley fever virus (RVFV) (Table 1, Fig. 2 and 3).

The inhibitory effect of CPXV012 peptide on HSV-1-eGFP, a large dsDNA virus from the herpesvirus family, was evaluated upon infection of MJS cells. The cells were infected with HSV-1-eGFP in the presence of peptide or DMSO vehicle control. After 16h, the amount of eGFP-positive cells was determined using flow cytometry (Fig. 2A). As observed for the poxviruses, CPXV012 peptide showed a dose-dependent inhibition of HSV-1 infection (Fig. 2A; 75.9±5.7% when using 150 µg/ml peptide). For HBV, an enveloped dsDNA virus of the hepadnavirus family, infectivity was monitored by quantifying the amount of viral envelope protein (HBeAg) and viral DNA in the supernatant of HepRG-infected cells (Fig. 2B). Both HBeAg and viral DNA were decreased in the supernatant of cells treated with CPXV012 peptide in a concentration-dependent manner. At a peptide concentration of 100 µg/ml, a decrease of 84.0±3.0% of HBeAg and 73.6±2.3% of viral DNA was observed.

The infectivity of HIV-1, an enveloped ssRNA virus, was monitored using the EASY-HIT assay on LC5-RIC reporter cells. In this essay, both early and late phases of HIV replication

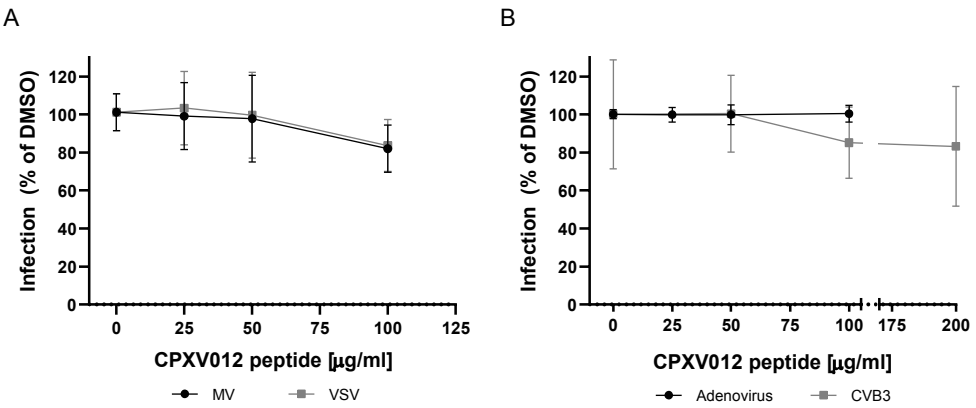

Figure 3: CPXV012 peptide does not inhibit infection with Measles virus, VSV, Adenovirus or Coxsackie B3 virus. (A). Measles virus infection: Vero cells were treated with the indicated concentrations of CPXV012 peptide or DMSO as control, and infected with eGFP-expressing measles virus (MV-eGFP) (MOI 0.1). Once maximum giant cell formation was observed (approximately at 48h post infection), infection was quantified by detection of eGFP with using a microplate reader. VSV infection: Huh7.5 cells were treated with the indicated concentrations of CPXV012 peptide or DMSO, and infected with luciferase-expressing VSV-deltaG (Luc) (MOI 0.6). 18h post infection, luciferase activity was measured to assess VSV infection of the culture. S.E.M. of each three independent experiments is shown. (B) Adenovirus infection: HEK-293 cells were treated with the indicated concentrations of CPXV012 peptide or DMSO for 1h and infected with eGFP-expressing adenovirus (AdGOva) (MOI 10) for 24h. Infection was quantified by cytometric analysis of eGFP expression. Coxsackie virus B3 infection: MJS cells were infected with RLuc-CVB3 in the presence of the indicated concentration of peptide or DMSO as vehicle control. After 7 hours, cells were lysed and Renilla Luciferase expression was quantified. S.E.M. of each three independent experiments are shown.

are assessed: in step 1, the levels of a fluorescent reporter protein induced during the early phase of HIV replication are quantified, and in step 2 the production of infectious virions in primary infected cells is determined. HIV infection was reduced in the presence of CPXV012 peptide, but not in the presence of DMSO vehicle control (Fig. 2C). Both primary viral infection (step 1) and viral replication (step 2) were dose-dependently affected, with an inhibition of 82.7±4.9% (step 1) and 62.2±2.4% (step 2) at the highest peptide concentration (100 µg/ml).

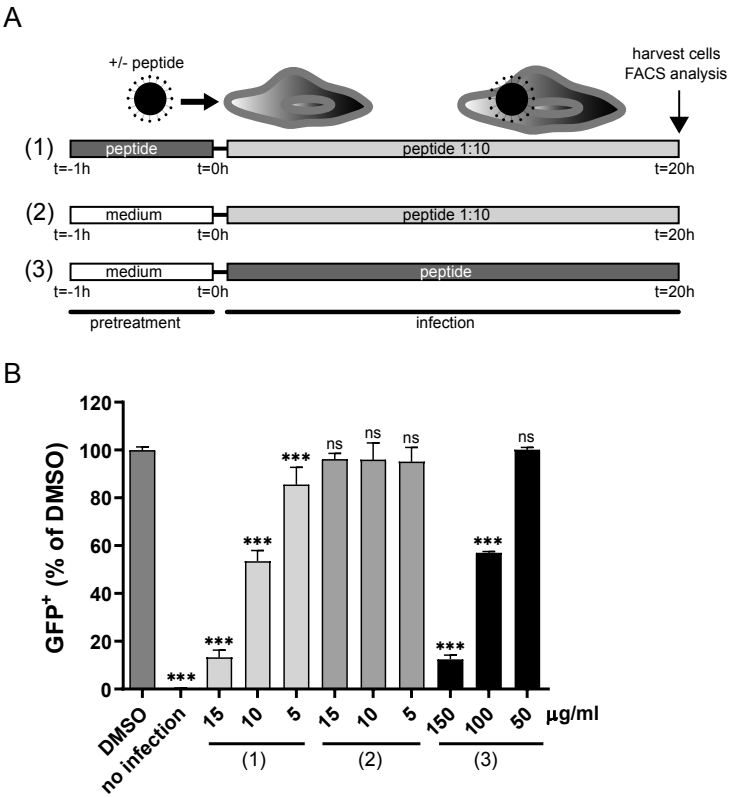

Figure 4: CPXV012 peptide inhibits infection by binding to viral particles. (A) Timeline of infection experiment as shown in (B). (1) MVA-eGFP was pretreated with 50, 100 or 150µg/ml peptide or DMSO in culture medium at 37 °C for 1h. Subsequently, the virus-peptide pre-incubation mixture was diluted ten times and used to infect MJS cells (corresponding to an MOI of 10), resulting in a final concentration of 5, 10 and 15 µg/ml peptide in the culture medium. (2-3) MVA-eGFP was incubated in culture medium only at 37 °C for 1h. The virus mixture was added to MJS cells in the presence of 5, 10, or 15µg/ml peptide (2) or 50, 100, or 150 µg/ml peptide (3) in the culture medium. (B) After 18-20h of infection as shown in (A), the amount of infected eGFP-positive cells was quantified using flow cytometry. S.E.M. of three independent experiments is shown using different batches of peptide. Data were analyzed with one-way ANOVA followed by multiple comparisons Dunnett's test (the mean of each column was compared to that of the DMSO control). (* $p < 0.05$; ** $p < 0.01$; *** $p < 0.001$).

For RVFV, an enveloped ssRNA virus of the Bunyavirus family, infection was monitored by viral eGFP expression 24h post infection (Fig. 2D). Infection was reduced by CPXV012 peptide in a concentration-dependent manner (65.5±2.3% at 160 µg/ml).

In contrast, CPXV012 peptide showed no effect on infection by measles virus, an enveloped ssRNA virus of the paramyxovirus family (Fig. 3A). Formation of measles virus-induced syncytia was unchanged (Fig. S3). Replication of measles virus and cell-to-cell spread was assessed by quantification of viral titers present in infected cultures using plaque assays. No difference was found between CPXV012 peptide-treated samples and the DMSO vehicle control. For VSV, an enveloped ssRNA virus of the rhabdovirus family, virus-encoded Renilla luciferase activity was measured 18h after infection (Fig. 3A). Luciferase activity was unchanged in the presence of CPXV012 peptide.

Next, the effect of CPXV012 on the infection of two non-enveloped viruses was tested. The infectivity of adenovirus, a dsDNA virus, was not altered in the presence of CPXV012 peptide, as measured by viral eGFP expression (Fig. 3B). For coxsackie B3 virus, a non-enveloped ssRNA virus, infection was monitored by the activity of the virus-encoded Renilla luciferase. No change in Renilla luciferase activity was observed in the presence of CPXV012 or control peptide (Fig. 3B).

These results identify the CPXV012 peptide as an antiviral peptide acting on enveloped viruses.

3.2 CPXV012 may bind to viral particles

To find out whether CPXV012 peptide mediates its inhibitory effect by interacting directly with viral particles, we performed a modified inhibition assay using MJS cells and MVA-eGFP. Instead of simultaneously adding CPXV012 peptide and virus to the cells, viral particles were pretreated with CPXV012 peptide for 1h at 37°C. After this preincubation, the virus-CPXV012 peptide mixture was diluted ten times and used to infect cells. Thus, the final peptide concentration during infection was 5-15 µg/ml (Fig. 4A). Pretreating the virus with a high concentration of CPXV012 peptide before infection affected infectivity to a similar level as the presence of a high concentration of CPXV012 peptide during infection (Fig. 4B). This effect was not due to the remaining CPXV012 peptide in the culture medium, as the diluted peptide alone was not sufficient to block infection when added directly to the cells. These data suggest that the peptide can directly act on viral particles.

A

```
WT:   QEGISRFKICPYHWYKQHMSLLFRRYYHKLDSII
Ala1: AAAAARFKICPYHWYKQHMSLLFRRYYHKLDSII
Ala2: QEGISAAAAAPYHWYKQHMSLLFRRYYHKLDSII
Ala3: QEGISRFKICAAAAAKQHMSLLFRRYYHKLDSII
Ala4: QEGISRFKICPYHWYAAAAALLFRRYYHKLDSII
Ala5: QEGISRFKICPYHWYKQHMSAAAAAYYHKLDSII
Ala6: QEGISRFKICPYHWYKQHMSLLFRRAAAAADSII
Ala7: QEGISRFKICPYHWYKQHMSLLFRRYYHKLAAAA
Ala8: QEGISAFAICPYAWYAQAMSLLFAAYYAALDSII
```

B

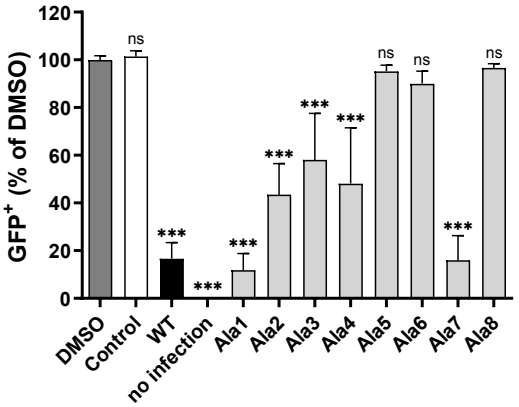

Figure 5: CPXV012 peptide variants differentially affect virus infection. (A) Amino acid sequence of CPXV012 peptide variants used in experiment (B). (B) MJS cells were infected with MVA-eGFP at an MOI of 20 in the presence of 100 µg/ml of the peptide indicated or DMSO as vehicle control. After 20h, cells were harvested and the amount of eGFP-positive cells was quantified using flow cytometry. S.E.M. of three independent experiments is shown using different batches of peptide. Data were analyzed with one-way ANOVA followed by multiple comparisons Dunnett's test (the mean of each column was compared to that of the DMSO control). (* $p < 0.05$; ** $p < 0.01$; *** $p < 0.001$).

3.3 CPXV012 peptide variants differentially affect virus infection

To determine the amino acid residues within the CPXV012 peptide crucial for virus inhibition, alanine substitution variants of the CPXV012 peptide were synthesized. These variants had small stretches of amino acid residues replaced by alanine residues (Fig. 5A). To test the inhibitory capacity of these variants, MJS cells were infected with MVA-eGFP in the presence of 100 µg/ml of each of these peptides (Fig. 5B). CPXV012 variants with the N-terminal five amino acid residues (Ala1) or the C-terminal four amino acid residues substituted by alanine (Ala7) inhibited MVA infection to similar levels as wild type CPXV012 peptide. Substituting amino acid residues 6-20 for alanine (CPXV012-Ala2/Ala3/Ala4) significantly affected the inhibitory capacity of the peptides. Substituting amino acid residues 20-30 for alanine (Ala5 and Ala6) completely abolished the inhibitory effect of

CPXV012 peptide. Interestingly, the CPXV012 peptide variants with lower or no inhibitory capacity also had a lower net positive charge at pH 7.4 compared to the wild type peptide, due to the substitution of the charged amino acid residues lysine, arginine, or histidine. To test the role of these amino acid residues in virus inhibition, a peptide was synthesized with the charged amino acid residues replaced for alanine (Ala8). Indeed, this CPXV012 peptide variant lost its inhibitory capacity, thus confirming the role of basic amino acid residues in inhibiting virus infection.

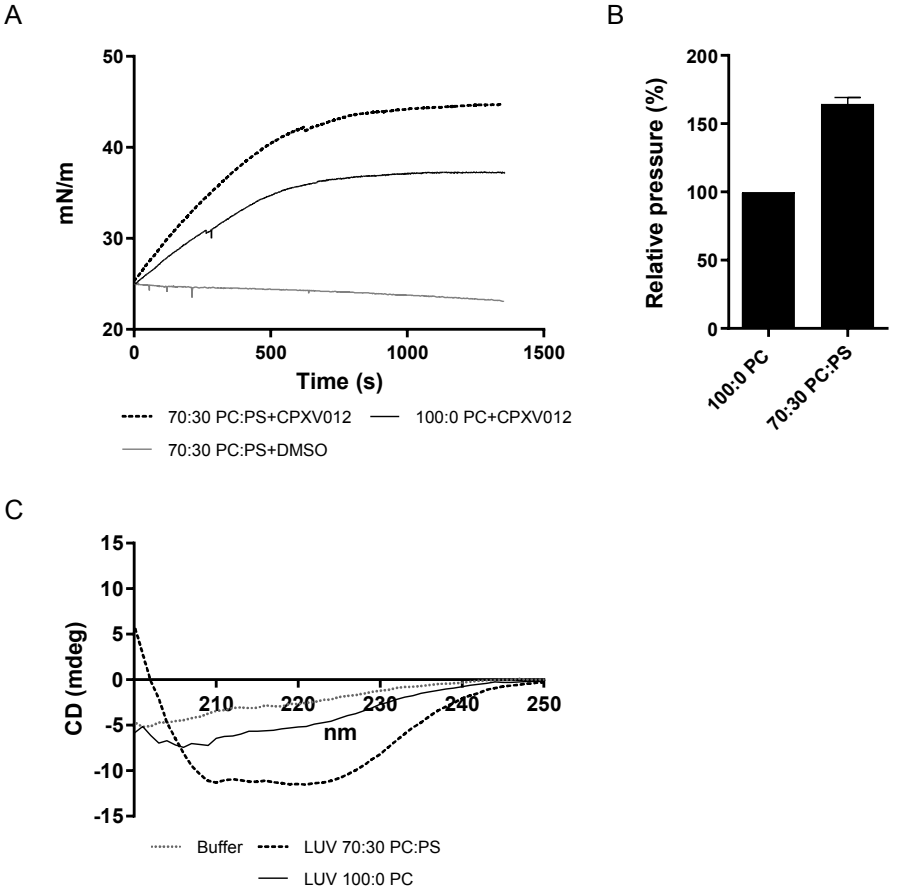

Figure 6: CPXV012 peptide interacts with PS. (A) CPXV012 peptide preferentially integrates into lipid monolayers composed of PC:PS (70:30). Langmuir monolayers of PC or PC:PS (70:30) with an initial surface pressure of 25mN/m were formed over an aqueous subphase. Peptide was injected into the subphase at t = 0s. As vehicle control, DMSO was injected in the subphase of PC:PS (70:30) monolayers. Results are representative of three independent experiments. (B) Quantification of CPXV012 peptide integration into lipid monolayers composed of PC:PS (70:30), as compared to monolayers composed of PC only (set at 100%) . S.E.M. of three independent experiments is shown. (C) CPXV012 peptide adopts different secondary structures depending on the presence of PS. CD spectrum of CPXV012 peptide was determined in the presence of aqueous buffer or LUVs composed of PC or PC:PS (70:30). Results are representative of three independent experiments.

3.4 CPXV012 peptide interacts with charged phospholipids

The preferential inhibition of enveloped viruses suggests that CPXV012 peptide interacts with a common structure within these viral particles. A major constituent of these virions are the phospholipids forming the lipid bilayer of the viral envelope. To test the interaction between CPXV012 peptide and phospholipids, Langmuir monolayers were formed using the zwitterionic phospholipid phosphatidylcholine (PC) and the anionic phosphatidylserine (PS) on an aqueous buffer. Upon stabilization of the monolayer at an initial surface pressure of 25 mN/m, CPXV012 peptide was injected into the monolayer aqueous subphase and the surface pressure was measured for ~25 min (Fig. 6A). A change in surface pressure is interpreted as integration of CPXV012 peptide into the lipid monolayer. Although the surface pressure of monolayers formed by the zwitterionic PC changed rapidly upon the addition of CPXV012 peptide, the shift in surface pressure was much higher for monolayers formed by a 7:3 mixture of PC and the negatively charged PS (Fig. 6B). These data suggest a preferred interaction between CPXV012 and the anionic PS. This is further supported by the circular dichroism (CD) experiments used to determine the secondary structure of CPXV012 peptide (Fig. 6C). The CD spectrum of CPXV012 was measured in the presence of large unilamellar vesicles (LUVs), lipid vesicles consisting of PC only or of PC and PS. In aqueous MES buffer or in the presence of PC, CD spectra of CPXV012 peptide were rather similar and becoming more negative at shorter wavelength, suggesting the presence of a significant amount of random coil structure. However, upon

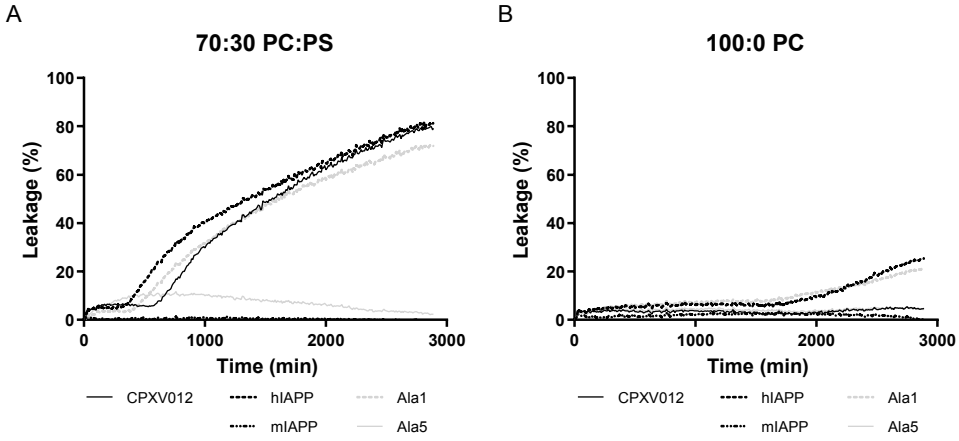

Figure 7: CPXV012 peptide disrupts membranes composed of PS. Calcein-containing PC:PS (7:3) LUVs (A) or PC LUVs (B) were incubated with human IAPP (hIAPP) as positive control, murine IAPP (mIAPP) as negative control, CPXV012 peptide, CPXV012 peptide variants Ala1 or Ala5 (see Fig. 5A for amino acid sequences). Calcein leakage from the vesicle lumen was quantified using a microplate reader. Membrane leakage was compared to fully disintegrated detergent-treated LUVs (set at 100%). Results are representative of three independent experiments.

addition of PS to PC lipids using a similar ratio as for the monolayer experiments, the CPXV012 peptide acquired a different CD spectrum with minima around 208 and 222 nm, typical for an alpha-helical structure. Thus, CPXV012 peptide adopts different secondary structures, depending on the presence of PS.

To gain further insight into the interaction between CPXV012 peptide and lipid membranes, the effect of the peptide on the integrity of lipid membrane vesicles was evaluated by membrane leakage assays using LUVs. These LUVs were composed of PC:PS and contained the self-quenching fluophore calcein in their lumen. As soon as vesicle integrity is compromised, calcein leakage induces an increase in fluorescence, which can be measured in the supernatant using a fluorometer. As described previously, addition of human IAPP, but not murine IAPP, induced leakage of LUVs composed of PC and PS, whereas LUVs composed of PC alone were more resistant to leakage by human IAPP (Fig. 7A and B) [30]. Addition of 25 µg/ml CPXV012 peptide disrupted the LUV membranes composed of both PC and PS, whereas membranes containing PC alone were unaffected. As described for human IAPP [31], membrane leakage by CPXV012 peptide is not instant, but is preceded by a lag phase of approximately 8h.

Two alanine substitution peptides, Ala1 and Ala5 (see Fig. 5), were also tested. CPXV012 peptide variant Ala1, which inhibited virus infection, induced membrane leakage of PC:PS LUVs to similar levels and kinetics as wt CPXV012 peptide. In contrast to CPXV012, this variant was able to induce slight leakage of LUVs composed of PC only. Ala5, which had no effect on virus infection, did not compromise the integrity of either one of the LUV membranes (Fig. 7B).

In conclusion, the capacity of CPXV012 peptide to inhibit virus infections correlates with its ability to disrupt lipid membranes that contain PS.

4 Discussion

In this study, we identified the CPXV012 peptide as a broadly-acting antiviral agent that probably interacts with the anionic phospholipid PS. The antiviral potency of the CPXV012 peptide can be considered modest, yet we believe that this peptide may be a candidate for biochemical improvement. The interaction between the CPXV012 peptide and PS is likely mediated by opposing electrostatic forces determined by cationic residues within the peptide and the anionic head groups of PS. In addition, hydrophobic amino acid residues (which make up more than 30% of CPXV012 peptide) may facilitate penetration of the peptide into the lipid phase of the membrane. As shown for other peptides, such interactions may promote the formation of an alpha-helical secondary structure of

otherwise unstructured peptides [32]. The biophysical properties of CPXV012 peptide are shared with antimicrobial host defense peptides. Antimicrobial peptides form a crucial innate immune barrier by targeting the negatively charged surfaces of bacteria and certain fungi. Like CPXV012 peptide, these small peptides (up to 50 residues) have a net positive charge and high affinity for anionic phospholipids. In addition, these lipid interactions promote the formation of secondary structures including beta-sheets and alpha-helices. These structural rearrangements are crucial for the antimicrobial activity, and can trigger pore formation, membrane depolarization and disruption of the bacterial membrane [33]. Although less studied, antimicrobial peptides may also affect virus infection by different mechanisms. These mechanisms include interference with viral entry (binding to receptors, fusion), inhibition of viral replication, reduction/suppression of viral gene expression, immunomodulation, viral aggregation and disruption of the integrity of the viral membrane (reviewed in[6],[7]). While a list of peptides are reported to disrupt viral envelopes, their mode of action has not been formally tested. Still, a number of them were shown to directly affect viral membranes, although the specific interacting partners remain elusive. Examples include the human cathelicidin LL-37 and its murine equivalent mCRAMP, which disrupt the membranes of RSV, influenza A virus and VACV, and can prevent virus infection *in vivo* [34]–[36]. Although their effect on infectivity of other viruses is not known, the structural similarities between these cationic peptides and CPXV012 peptide may suggest that these and other antimicrobial peptides possess a broader antiviral activity. Electron microscopy has also provided indications of envelope disruption with the cationic peptides Tachyplesin (VSV) [7], Temporin B (HSV-1) [37], and more recently Urumin (H1-bearing influenza A viruses) [38].

Membrane leakage induced by CPXV012 peptide was preceded by a lag phase, as was also observed for human IAPP. For human IAPP, this lag phase originates from the formation of transient oligomeric intermediates prior to the assembly of membrane-disruptive aggregates [31]. Likewise, disruption of membranes by CPXV012 peptides may be linked to the formation of (transient) oligomeric structures. The shorter lag time in the presence of PS is possibly due to a more efficient binding of the peptide to the membrane: upon favorable electrostatic interactions, CPXV012 peptides achieve a higher local concentration and therefore the assembly process is supported.

Our data indicate that CPXV012 peptide neutralizes infectivity of viruses from diverse families. *In vitro* assays indicate that CPXV012 peptide directly interacts with membranes. The disruptive behavior of CPXV012 peptide on artificial membrane vesicles suggests that CPXV012 peptide may similarly affect viral membranes. As viral particles do not have a membrane repair mechanism, this damaging effect may particularly destabilize and

disrupt viral particles. Extensive membrane damage may also hamper virus fusion to the host cell membrane by impacting the fluidity and curvatures of lipid membranes. Lipids including PS play an essential role in the induction of these membrane curvatures and subsequent membrane fusion [39],[40]. Even in the absence of membrane damage, the interaction between CPXV012 peptide and PS in the viral envelope may interfere with virus infectivity by sterically blocking the interaction between viral PS and host cell PS receptors. A similar inhibitory mechanism was observed using the PS-specific antibody Bavituximab [3],[41], or the PS-binding protein Annexin V [42],[43]. CPXV012 peptide may also indirectly affect virus infection by binding to PS on the host cell membrane. Specific microdomains of the host cell plasma membrane are enriched for PS, including lipid rafts [44]. These sites are used by certain viruses as entry point [45]. Although PS typically would reside in the inner leaflet of the plasma membrane, there are indications that some viruses induce redistribution of PS to the outer membrane to promote/facilitate entry [45]. In addition, some viruses use lipid rafts as budding sites when exiting the host cell [46].

The effect of CPXV012 peptide on the viruses used in this study and potential inhibitory mechanism(s) are discussed in more detail.

4.1 Poxviruses

The CPXV012 peptide was able to inhibit infection with different orthopoxviruses (MVA, VACV and CPXV) in several cell lines. In infected cells, poxvirus gene expression occurs sequentially in a cascade-like fashion with three distinct phases orchestrated by viral promoters with early, intermediate or late activity. Given that early expression starts immediately after virus entry and occurs in the virion without the need of cellular RNA-polymerase, the decrease in early transcripts (as shown for the *B8R* promoter, Fig. 1D) indicates a block at the entry step. Viral particles of the *poxviridae* family adopt distinct structures and composition of the outer membrane, such as mature virions (MVs, also named IMVs, intracellular mature virus) [47]. MVs represent the majority of infectious progeny; they are very stable and largely responsible for viral spread. In viral preparations, MVs are the most abundant virion form. Importantly, membranes of MVs have been shown to contain large amounts of PS that is essential for infectivity. Noninfectious virus was converted to infectious forms by incubation with liposomes containing different phospholipids and only PS was able to restore infectivity while other phospholipids (including phosphatidylcholine or phosphatidylinositol) did not [48]. Moreover, VACV MVs also enter cells via macropinocytosis and this entry step is dependent on the presence of exposed PS in the viral membrane – a process called apoptotic mimicry [42]. Of note, when PS was masked by Annexin V, infectivity was strongly decreased [42]. We found that CPXV012 peptide binds to PS and thus likely mediates its inhibitory effect on poxvirus

infection by interacting with PS in the viral membrane. This was confirmed by the observation that pretreating virions with CPXV012 peptide effectively blocked infection.

4.2 HSV-1

Inhibition of HSV-1 by cationic peptides has been previously reported, including the antimicrobial peptide LL-37 that presumably acts by targeting factors within the viral membrane [49]–[51]. It is believed that HSV-1 derives its final envelope from membranes of the late secretory pathway (e.g.: trans-Golgi network) and/or endosomal pathway [52]. The inhibition of HSV-1 by CPXV012 peptide suggests that PS in the HSV-1 envelope is a potent target for antiviral therapy.

4.3 HBV

CPXV012 peptide affected HBV infection as measured by a decrease in viral DNA and viral antigen in the supernatant of infected cultures. HBV particles are thought to acquire their envelope from multivesicular bodies [53], which are rich in PS [54]. The role of PS in HBV infection is underlined by studies showing that antibodies specific for PS block HBV infection [55]. Similar to poxviruses, PS may play a role in virus entry through apoptotic mimicry [56],[57]. PS may also play a role in the proper folding of HBV envelope proteins [58].

4.4 HIV

Given that the EASY-HIT assay relies on the expression of tat and rev induced in the early phase of HIV replication, the results obtained with CPXV012 peptide showing a concentration-dependent decrease of viral infection in Step 1 indicate that CPXV012 peptide acts as an early-phase inhibitor. The presence of PS in the membrane of HIV particles was shown to be an important cofactor for infection and blocking of PS led to a decrease of infection [59],[60]. In addition, HIV infection was inhibited by addition of lipid vesicles composed of PS that competed with the HIV particles for plasma membrane association, while lipid vesicles containing PC had no effect [59]. Therefore, the binding of CPXV012 peptide to PS in the viral envelope could explain the inhibitory effect observed in the EASY-HIT assay.

4.5 RVFV

The inhibition of RVFV infection by CPXV012 peptide suggests that PS is critical for RVFV infection. Although the lipid composition of RVFV is unknown, the viral envelope of Uukuniemi virus, a related member of the bunyavirus family, is enriched for PS [61].

Like Uukuniemi virus, RVFV obtains its membrane by budding into the Golgi membrane, suggesting that PS may also be enriched in these virus particles [62],[63].

4.6 Viruses not affected by CPXV012 peptide

No effects of CPXV012 peptide were observed on infection with adenovirus, coxsackie B3, measles virus and VSV. Although measles virus and VSV are enveloped viruses, the role of PS during infection is limited for these viruses. For measles virus, different phospholipids were tested for their ability to reassemble with the viral envelope glycoproteins and to restore haemolytic activity. Phosphatidylethanolamine was effective in forming active haemolysins while PC was only able to regenerate haemolytic activity at high concentrations. In contrast, PS completely failed to restore haemagglutinating activity [64]. For VSV, phosphatidylserine expressed on the host cell membrane was considered to be important for cell entry [65]. However, this assumption was based on indirect studies with isolated VSV-G protein and peptides [66],[67]. In contrast, a more recent study found no correlation between PS surface levels and VSV binding. Moreover, masking of phosphatidylserine with annexin V during infection did not affect VSV binding to cells, or entry of virus particles pseudotyped with VSV-G [59],[67]. Thus, the limited role of PS during entry of VSV and measles virus may explain the lack of inhibition by CPXV012 peptide.

Both adenovirus and Coxsackie virus B3 are non-enveloped viruses and the nucleocapsid does not contain any phospholipids (nor glycoproteins) CPXV012 peptide could bind to. CPXV012 peptide binding to the host cell membrane might not be sufficient for steric impediment of viral ligand – cellular receptor interaction. Supporting this, the adenoviral elongated fiber protein responsible for binding to the host cell is flexible and large in size (9-30 nm), as is the coxsackie and adenovirus receptor (CAR) on the host cell [68]. The size and flexibility of the fiber protein is important for adenovirus entry and infection [69].

CAR is also important for the infection of free CVB3 particles [70]. In addition, CVB3 may use a PS-dependent entry strategy for bulk transmission of virus particles [71]. Infected cells release clusters of virus particles enwrapped in PS-enriched membranes. These vesicles enhance subsequent virus entry in a process that highly depends on the presence of PS [71]. As CPXV012 peptide had no effect on CVB3 virus infection, PS may not play a significant role in our study. This discrepancy likely results from our virus production protocol that involves repeated freeze-thawing to liberate virus particles. Although necessary to obtain high virus titers, this method also releases CVB3 from PS-enriched vesicles [71].

In conclusion, the CPXV012 peptide-mediated inhibition of virus infection correlates well with the observed interaction between CPXV012 peptide and PS. The broad inhibitory range may thereby be further extended to other viruses for which PS has a crucial function during the viral life cycle. These viruses include clinically and economically important pathogens such as ebola virus, lassa virus, dengue virus and poliovirus [56].

The differences between viral and host membranes makes PS an Achilles' heel that can be targeted by the cationic CPXV012 peptide. It will be worth investigating if other cationic peptides can also target PS within the viral envelope, and perhaps fulfill a similar function as broad-range antiviral agents. Analyses of the peptide's biophysical and physicochemical properties (number of charges, hydrophobicity, aromatic amino acids, density and distribution of these amino acids along the peptide chain, among other) can shed some light on how to improve the moderate efficiency of CPXV012 and other cationic peptides.

Acknowledgements

Patrique Praest is supported by the European Commission under the Horizon2020 program H2020 MSCA-ITN GA 675278 EDGE. SMS was supported by the seventh framework program of the European Union (Initial Training Network "ManiFold," Grant 317371), and ID was supported by the DFG funding GRK 1949.

References

1. Marston, H. D., Folkers, G. K., Morens, D. M. & Fauci, A. S. Emerging viral diseases: confronting threats with new technologies. *Sci Transl Med* **6**, 253ps10 (2014).
2. Zhu, J. D., Meng, W., Wang, X. J. & Wang, H. C. Broad-spectrum antiviral agents. *Front Microbiol* **6**, 517 (2015).
3. Soares, M. M., King, S. W. & Thorpe, P. E. Targeting inside-out phosphatidylserine as a therapeutic strategy for viral diseases. *Nat Med* **14**, 1357–1362 (2008).
4. Vigant, F. *et al.* A mechanistic paradigm for broad-spectrum antivirals that target virus-cell fusion. *PLoS Pathog* **9**, e1003297 (2013).
5. Wolf, M. C. *et al.* A broad-spectrum antiviral targeting entry of enveloped viruses. *Proc Natl Acad Sci U S A* **107**, 3157–3162 (2010).
6. Gwyer Findlay, E., Currie, S. M. & Davidson, D. J. Cationic host defence peptides: potential as antiviral therapeutics. *BioDrugs* **27**, 479–493 (2013).
7. Mulder, K. C. L., Lima, L. A., Miranda, V. J., Dias, S. C. & Franco, O. L. Current scenario of peptide-based drugs: the key roles of cationic antitumor and antiviral peptides. *Front. Microbiol.* **4**, 1–23 (2013).
8. Leventis, P. A. & Grinstein, S. The distribution and function of phosphatidylserine in cellular membranes. *Annu Rev Biophys* **39**, 407–427 (2010).
9. Moller-Tank, S. & Maury, W. Phosphatidylserine receptors: enhancers of enveloped virus entry and infection. *Virology* **468**–**470**, 565–580 (2014).

10. Andrews, N. W., Almeida, P. E. & Corrotte, M. Damage control: cellular mechanisms of plasma membrane repair. *Trends Cell Biol* **24**, 734–742 (2014).
11. Cooper, S. T. & McNeil, P. L. Membrane Repair: Mechanisms and Pathophysiology. *Physiol Rev* **95**, 1205–1240 (2015).
12. Alzhanova, D. *et al.* Cowpox Virus Inhibits the Transporter Associated with Antigen Processing to Evade T Cell Recognition. *Cell Host Microbe* **6**, 433–445 (2009).
13. Byun, M. *et al.* Two Mechanistically Distinct Immune Evasion Proteins of Cowpox Virus Combine to Avoid Antiviral CD8 T Cells. *Cell Host Microbe* **6**, 422–432 (2009).
14. Lin, J. *et al.* A negative feedback modulator of antigen processing evolved from a frameshift in the cowpox virus genome. *PLoS Pathog.* **10**, e1004554 (2014).
15. Luteijn, R. D. *et al.* Cowpox Virus Protein CPXV012 Eludes CTLs by Blocking ATP Binding to TAP. *J. Immunol.* **193**, 1578–1589 (2014).
16. Praest, P., Liaci, A. M., Förster, F. & Wiertz, E. J. H. J. New insights into the structure of the MHC class I peptide-loading complex and mechanisms of TAP inhibition by viral immune evasion proteins. *Mol. Immunol.* **113**, 103–114 (2019).
17. Kremb, S. *et al.* EASY-HIT: HIV full-replication technology for broad discovery of multiple classes of HIV inhibitors. *Antimicrob Agents Chemother* **54**, 5257–5268 (2010).
18. Gasteiger, G., Kastenmuller, W., Ljapoci, R., Sutter, G. & Drexler, I. Cross-Priming of Cytotoxic T Cells Dictates Antigen Requisites for Modified Vaccinia Virus Ankara Vector Vaccines. *J. Virol.* **81**, 11925–11936 (2007).
19. Staib, C., Drexler, I. & Sutter, G. Construction and isolation of recombinant MVA. *Methods Mol Biol* **269**, 77–100 (2004).
20. Lucifora, J. *et al.* Hepatitis B virus X protein is essential to initiate and maintain virus replication after infection. *J Hepatol* **55**, 996–1003 (2011).
21. Duprex, W. P. *et al.* In vitro and in vivo infection of neural cells by a recombinant measles virus expressing enhanced green fluorescent protein. *J Virol* **74**, 7972–7979 (2000).
22. Wohlleber, D. *et al.* TNF-induced target cell killing by CTL activated through cross-presentation. *Cell Rep* **2**, 478–487 (2012).
23. Kortekaas, J. *et al.* Creation of a nonspreading Rift Valley fever virus. *J Virol* **85**, 12622–12630 (2011).
24. Lanke, K. H. *et al.* GBF1, a guanine nucleotide exchange factor for Arf, is crucial for coxsackievirus B3 RNA replication. *J Virol* **83**, 11940–11949 (2009).
25. Hiemstra, H. S. *et al.* The identification of CD4+ T cell epitopes with dedicated synthetic peptide libraries. *Proc Natl Acad Sci U S A* **94**, 10313–10318 (1997).
26. Repetto, G., del Peso, A. & Zurita, J. L. Neutral red uptake assay for the estimation of cell viability/cytotoxicity. *Nat Protoc* **3**, 1125–1131 (2008).
27. Livak, K. J. & Schmittgen, T. D. Analysis of relative gene expression data using real-time quantitative PCR and the 2(-Delta Delta C(T)) Method. *Methods* **25**, 402–408 (2001).
28. Pfaffl, M. W. A new mathematical model for relative quantification in real-time RT-PCR. *Nucleic Acids Res* **29**, e45 (2001).
29. Rouser, G., Kritchevsky, G., Simon, G. & Nelson, G. J. Quantitative analysis of brain and spinach leaf lipids employing silicic acid column chromatography and acetone for elution of glycolipids. *Lipids* **2**, 37–40 (1967).

30. Engel, M. F. *et al.* Membrane damage by human islet amyloid polypeptide through fibril growth at the membrane. *Proc Natl Acad Sci U S A* **105**, 6033–6038 (2008).

31. Buchanan, L. E. *et al.* Mechanism of IAPP amyloid fibril formation involves an intermediate with a transient beta-sheet. *Proc Natl Acad Sci U S A* **110**, 19285–19290 (2013).

32. Eiriksdottir, E., Konate, K., Langel, U., Divita, G. & Deshayes, S. Secondary structure of cell-penetrating peptides controls membrane interaction and insertion. *Biochim Biophys Acta* **1798**, 1119–1128 (2010).

33. Baltzer, S. A. & Brown, M. H. Antimicrobial peptides: promising alternatives to conventional antibiotics. *J Mol Microbiol Biotechnol* **20**, 228–235 (2011).

34. Currie, S. M. *et al.* Cathelicidins Have Direct Antiviral Activity against Respiratory Syncytial Virus In Vitro and Protective Function In Vivo in Mice and Humans. *J Immunol* **196**, 2699–2710 (2016).

35. Howell, M. D. *et al.* Selective killing of vaccinia virus by LL-37: implications for eczema vaccinatum. *J Immunol* **172**, 1763–1767 (2004).

36. Tripathi, S. *et al.* The human cathelicidin LL-37 inhibits influenza A viruses through a mechanism distinct from that of surfactant protein D or defensins. *J Gen Virol* **94**, 40–49 (2013).

37. Marcocci, M. E. *et al.* The Amphibian Antimicrobial Peptide Temporin B Inhibits In Vitro Herpes Simplex Virus 1 Infection . *Antimicrob. Agents Chemother.* **62**, 1–13 (2018).

38. Holthausen, D. J. *et al.* An Amphibian Host Defense Peptide Is Virucidal for Human H1 Hemagglutinin-Bearing Influenza Viruses. *Immunity* **46**, 587–595 (2017).

39. Sanchez-Migallon, M. P., Aranda, F. J. & Gomez-Fernandez, J. C. Role of phosphatidylserine and diacylglycerol in the fusion of chromaffin granules with target membranes. *Arch Biochem Biophys* **314**, 205–216 (1994).

40. Teissier, E. & Pecheur, E. I. Lipids as modulators of membrane fusion mediated by viral fusion proteins. *Eur Biophys J* **36**, 887–899 (2007).

41. Dowall, S. D. *et al.* Effective binding of a phosphatidylserine-targeting antibody to Ebola virus infected cells and purified virions. *J Immunol Res* **2015**, 347903 (2015).

42. Mercer, J. & Helenius, A. Vaccinia virus uses macropinocytosis and apoptotic mimicry to enter host cells. *Science (80-.).* **320**, 531–535 (2008).

43. Moller-Tank, S., Kondratowicz, A. S., Davey, R. A., Rennert, P. D. & Maury, W. Role of the phosphatidylserine receptor TIM-1 in enveloped-virus entry. *J Virol* **87**, 8327–8341 (2013).

44. Pike, L. J., Han, X., Chung, K. N. & Gross, R. W. Lipid rafts are enriched in arachidonic acid and plasmenylethanolamine and their composition is independent of caveolin-1 expression: a quantitative electrospray ionization/mass spectrometric analysis. *Biochemistry* **41**, 2075–2088 (2002).

45. Briggs, J. A., Wilk, T. & Fuller, S. D. Do lipid rafts mediate virus assembly and pseudotyping? *J Gen Virol* **84**, 757–768 (2003).

46. Lorizate, M. & Krausslich, H. G. Role of lipids in virus replication. *Cold Spring Harb Perspect Biol* **3**, a004820 (2011).

47. Roberts, K. L. & Smith, G. L. Vaccinia virus morphogenesis and dissemination. *Trends Microbiol* **16**, 472–479 (2008).

48. Ichihashi, Y. & Oie, M. The activation of vaccinia virus infectivity by the transfer of phosphatidylserine from the plasma membrane. *Virology* **130**, 306–317 (1983).

49. Daher, K. A., Selsted, M. E. & Lehrer, R. I. Direct inactivation of viruses by human granulocyte defensins. *J Virol* **60**, 1068–1074 (1986).

50. Gordon, Y. J. *et al.* Human cathelicidin (LL-37), a multifunctional peptide, is expressed by ocular surface epithelia and has potent antibacterial and antiviral activity. *Curr Eye Res* **30**, 385–394 (2005).

51. Yasin, B. *et al.* Evaluation of the inactivation of infectious Herpes simplex virus by host-defense peptides. *Eur J Clin Microbiol Infect Dis* **19**, 187–194 (2000).

52. Crump, C. Virus Assembly and Egress of HSV. in *Advances in experimental medicine and biology* vol. 1045 23–44 (2018).

53. Jiang, B., Himmelsbach, K., Ren, H., Boller, K. & Hildt, E. Subviral Hepatitis B Virus Filaments, like Infectious Viral Particles, Are Released via Multivesicular Bodies. *J Virol* **90**, 3330–3341 (2016).

54. Gyorgy, B. *et al.* Membrane vesicles, current state-of-the-art: emerging role of extracellular vesicles. *Cell Mol Life Sci* **68**, 2667–2688 (2011).

55. De Meyer, S., Gong, Z., Depla, E., Maertens, G. & Yap, S. H. Involvement of phosphatidylserine and non-phospholipid components of the hepatitis B virus envelope in human Annexin V binding and in HBV infection in vitro. *J Hepatol* **31**, 783–790 (1999).

56. Amara, A. & Mercer, J. Viral apoptotic mimicry. *Nat Rev Microbiol* **13**, 461–469 (2015).

57. Vanlandschoot, P. & Leroux-Roels, G. Viral apoptotic mimicry: an immune evasion strategy developed by the hepatitis B virus? *Trends Immunol* **24**, 144–147 (2003).

58. Gomez-Gutierrez, J., Rodriguez-Crespo, I., Peterson, D. L. & Gavilanes, F. Reconstitution of hepatitis B surface antigen proteins into phospholipid vesicles. *Biochim Biophys Acta* **1192**, 45–52 (1994).

59. Callahan, M. K. *et al.* Phosphatidylserine on HIV envelope is a cofactor for infection of monocytic cells. *J Immunol* **170**, 4840–4845 (2003).

60. Lorizate, M. *et al.* Comparative lipidomics analysis of HIV-1 particles and their producer cell membrane in different cell lines. *Cell Microbiol* **15**, 292–304 (2013).

61. Renkonen, O., Kaariainen, L., Pettersson, R. & Oker-Blom, N. The phospholipid composition of Uukuniemi virus, a non-cubical tick-borne arbovirus. *Virology* **50**, 899–901 (1972).

62. Ellis, D. S., Shirodaria, P. V, Fleming, E. & Simpson, D. I. Morphology and development of Rift Valley fever virus in Vero cell cultures. *J Med Virol* **24**, 161–174 (1988).

63. Kuismanen, E., Hedman, K., Saraste, J. & Pettersson, R. F. Uukuniemi virus maturation: accumulation of virus particles and viral antigens in the Golgi complex. *Mol Cell Biol* **2**, 1444–1458 (1982).

64. Hall, W. W. & Martin, S. J. Structure and function relationships of the envelope of measles virus. *Med Microbiol Immunol* **160**, 143–154 (1974).

65. Schlegel, R., Tralka, T. S., Willingham, M. C. & Pastan, I. Inhibition of VSV binding and infectivity by phosphatidylserine: is phosphatidylserine a VSV-binding site? *Cell* **32**, 639–646 (1983).

66. Carneiro, F. A., Bianconi, M. L., Weissmuller, G., Stauffer, F. & Da Poian, A. T. Membrane recognition by vesicular stomatitis virus involves enthalpy-driven protein-lipid interactions. *J Virol* **76**, 3756–3764 (2002).

67. Coil, D. A. & Miller, A. D. Phosphatidylserine is not the cell surface receptor for vesicular stomatitis virus. *J Virol* **78**, 10920–10926 (2004).

68. Bergelson, J. M. & Coyne, C. B. Picornavirus entry. *Adv Exp Med Biol* **790**, 24–41 (2013).

69. Wu, E. *et al.* Flexibility of the adenovirus fiber is required for efficient receptor interaction. *J Virol* **77**, 7225–7235 (2003).

70. Marjomaki, V., Turkki, P. & Huttunen, M. Infectious Entry Pathway of Enterovirus B Species. *Viruses* **7**, 6387–6399 (2015).

71. Chen, Y. H. *et al.* Phosphatidylserine vesicles enable efficient en bloc transmission of enteroviruses. *Cell* **160**, 619–630 (2015).

Supplemantary data

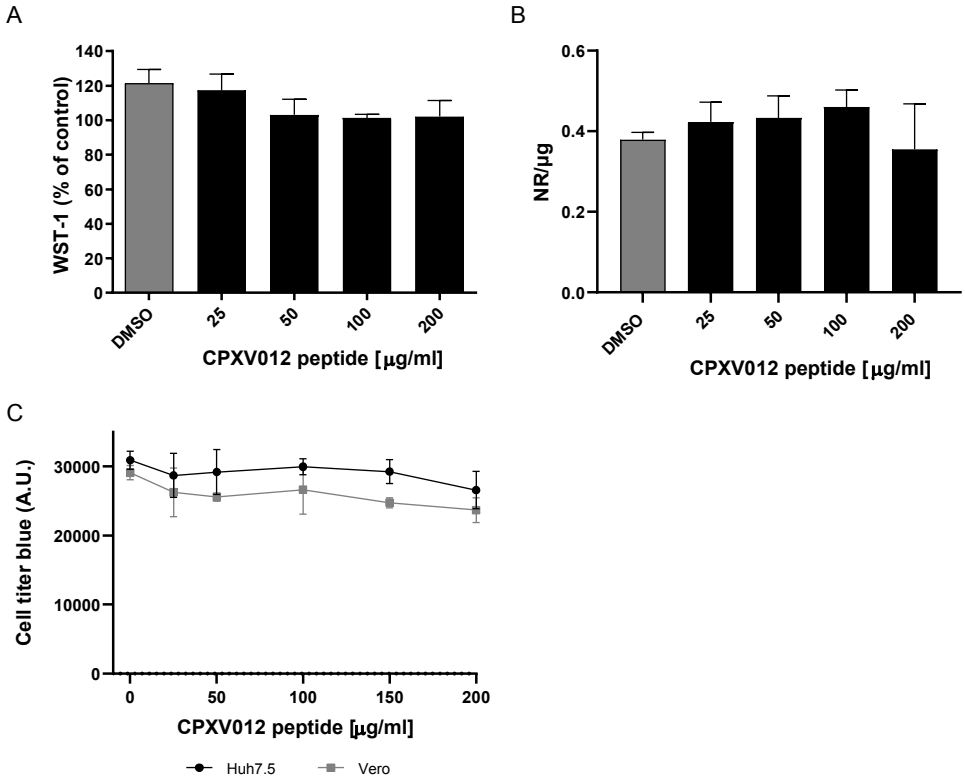

Figure S 1: CPXV012 peptide does not affect cell viability. (A-C) Cells were treated with the indicated concentrations of peptide or DMSO as vehicle control. S.E.M. of three independent experiments is shown. (A) Viability of MJS cells was measured by WST-1 assay or (B) Neutral Red uptake. (C) Viability of Huh7.5 and Vero cells was measured by the cell titer blue assay. A.U.: arbitrary units. S.E.M. of three independent experiments is shown.

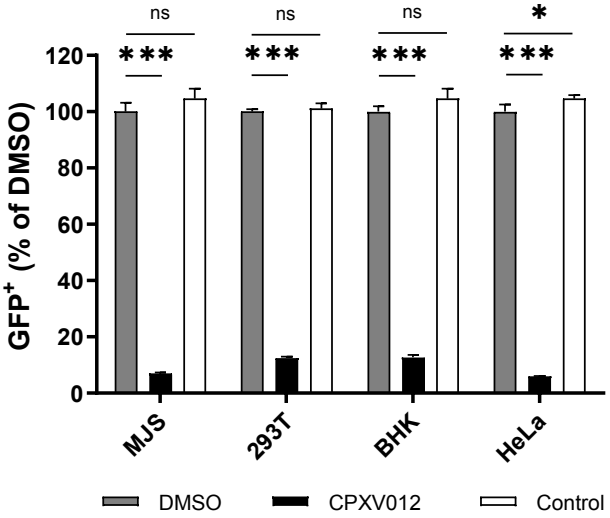

Figure S 2: CPXV012 peptide (CPX) prevents infection with MVA in different cell lines. Indicated cells were infected with MVA-eGFP (MOI 10) in the presence of 100 µg/ml peptide or DMSO. 18-20h after infection the amount of eGFP-positive cells was quantified using flow cytometry. Data were analyzed with one-way ANOVA followed by multiple comparisons Dunnett's test (the mean of each column was compared to that of the DMSO control). (* $p < 0.05$; ** $p < 0.01$; *** $p < 0.001$).

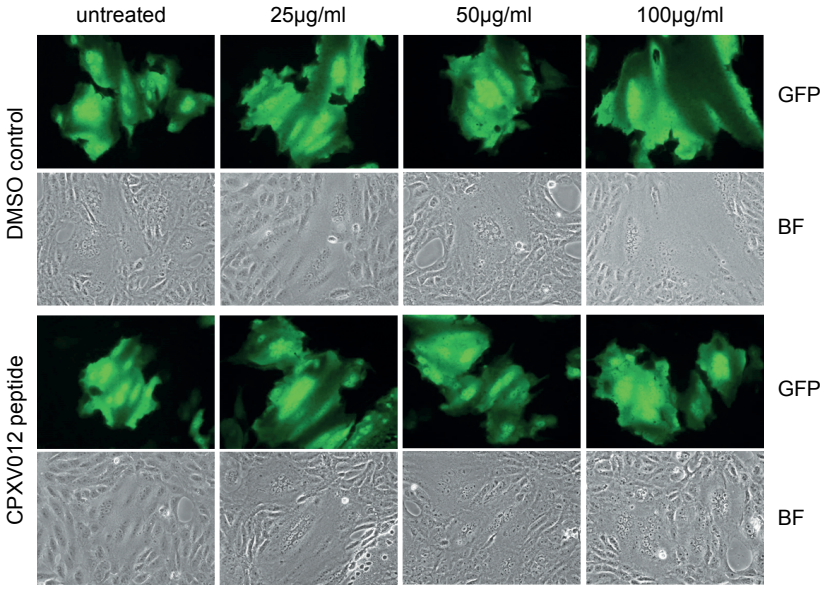

Figure S 3: CPXV012 peptide does not affect infection with measles virus. Vero cells were left untreated or were treated with indicated concentrations of CPXV012 peptide or DMSO. Cells were infected with eGFP-expressing measles virus (MV-eGFP) (MOI 0.1). After maximum giant cell formation was observed (approximately at 48h post infection), fluorescence microscopy images were taken (magnification 10x). Results are representative of three independent experiments. BF: bright field.

7

Identifying SEC61 and TRC8 as components of a dislocation complex involved in ER-associated protein degradation (ERAD)

P. Praest, I.G.J. Brak-Boer, S.L. Blanken, J. Fedry, K. Chappin, A.B.C. Schuren, A.I. Costa, F. Förster, R.J. Lebbink, E.J.H.J. Wiertz

Manuscript in preparation

Abstract

HCMV dedicates an extensive arsenal of proteins to evasion from the human immune system. The HCMV proteins US2 and US11 hijack the ER-associated protein degradation (ERAD) pathway to specifically degrade newly synthesized HLA class I molecules. By interfering with antigen presentation, the virus evades T-cell recognition of virus-infected cells. Multiple cellular proteins are crucial for US2 and US11-mediated HLA class I downregulation, but the protein channel(s) instrumental for retrotranslocation (or dislocation) of HLA-I molecules from the ER to the cytosol have not been identified. Correspondingly, the identity of dislocon channels involved in dislocation of endogenous substrates in a physiological setting remains elusive. In this study, we aim to identify the proteins that compose the dislocon channel by co-immunoprecipitation studies. We identified protein-protein interactions between the SEC translocation complex, P97, HRD1, Derlin1 and the proteasome. These interactions suggest that the SEC61 complex itself could be directly involved in protein dislocation. However, we could not confirm an interaction of SEC61 with HLA class I molecules in the absence or presence of US2. HLA class I molecules, therefore, may exit the ER through an alternative channel. In the presence of US2, ubiquitinated HLA class I was found to interact with the E3 ligase TRC8, the ATPase P97 and the proteasome. A dual role of TRC8 as the E3 ligase as well as a component of the dislocon in US2-dependent HLA class I downregulation may be hypothesized.

1 Introduction

Approximately one third of all proteins in the cell will be secreted or expressed in cellular or organelle membranes [1]. The signal peptide-dependent translocation of nascent and newly synthesized proteins into the endoplasmic reticulum (ER) is facilitated by the heterotrimeric SEC61 complex, which is comprised of the multimembrane-spanning SEC61α1 protein associated with SEC61β and SEC61γ [2] subunits. Furthermore, the SEC61-complex can associate with the dimeric SEC62 and SEC63 complex for post-translational translocation of proteins [3],[4]. On the ER-luminal side, the signal sequence of the translocated protein is cleaved off by the signal peptidase complex [5]. Protein folding is completed with the help of chaperones and glycosylation of the proteins can occur. In the event of misfolding, the proteins will be recognized by ER quality control chaperones for a repeated folding attempt [6].

If a protein fails to acquire its correct mature conformation, it will be removed from the ER by the ER-associated protein degradation (ERAD) machinery. The ERAD pathway is facilitated by a multiprotein complex that is responsible for the recognition of misfolded proteins, their dislocation across the lipid bilayer, ubiquitination and ultimately proteasomal degradation [7],[8]. ERAD prevents the accumulation and aggregation of misfolded proteins in the ER and reduces ER-stress. The importance of the ERAD pathway is highlighted by the continuously growing list of sporadic and genetic human diseases that are associated with this pathway, such as cystic fibrosis and Parkinson's disease [9],[10].

Most of the current knowledge about ERAD was gained by studies in yeast (reviewed in [11]), but the larger proteome and multicellular lifestyle of metazoans hints towards a more complex ERAD system in these species [7]. Over time, an array of proteins involved in ERAD has been identified through genetic and biochemical analyses, but the exact configuration and structure of ERAD complexes is only partially understood. In fact, the landscape of interacting proteins in ERAD is extremely complex. The E3 ligases Hrd1 and gp78 appear to be central in substrate ubiquitination [11]. Substrate extraction is powered by the ATPase P97 and requires recruitment factors, such as UBXD8 [12]. For dislocation, it is crucial that substrates are recognized and ubiquitinated by the ubiquitination system (E1 ubiquitin activating enzyme, E2 ubiquitin conjugating enzyme and E3 ubiquitin ligase), and exit through a given channel. Ultimately, the proteasome machinery proceeds to degradation. The interacting protein network will likely vary depending on the substrate of subject. Under physiological conditions, misfolded HLA class I molecules are the substrate of the E3 ligase Hrd1 prior to degradation [13].

During HCMV infection, multiple proteins of the unique short (US) region of the HCMV

genome are dedicated to interfere with different steps of the classical HLA class I antigen presentation pathway thereby evading $CD8^+$ T cell recognition [14]–[18]. Of these, the immune evasins US2 and US11 are type I membrane glycoproteins localized in the ER membrane [19],[20], which require different E3 ligases to target HLA class I to the proteasome. US2 requires the E3 ligase TRC8 [21] and US11 requires TMEM129 [22],[23].

The dislocon(s) that channel substrates across the ER-membrane still remain(s) to be identified. Several cellular proteins have been implicated to be constituents of a dislocon channel, such as TRC8, Derlin1, Hrd1 and Sec61 [21],[24],[25]. These proteins possess multiple transmembrane domains, that theoretically could adopt a channel conformation. For example, Derlin1 is an ER-membrane protein carrying six transmembrane domains that was shown to associate with multiple ERAD substrates that exit the ER [26],[27]. The protein Hrd1 also has six transmembrane domains and is a E3 ubiquitin ligase involved in US2-independent degradation of ER-resident proteins [28]. The E3-ligase TRC8 possesses twelve transmembrane domains, as does the SEC61α1/β/γ-complex. In this study, we probed if SEC61 and/or TRC8 can act as a dislocation channel for HLA class I molecules in the context of US2-independent and -dependent degradation. We confirm previously proposed protein interactions and key players of these pathways by co-immunoprecipitation analyses. We show that SEC61α1, the proteasome and the ATPase P97 establish stable protein-protein interactions. This finding has led us to investigate the structural framework of these interactions by Cryo-electron microscopy (Cryo-EM). Furthermore, upon inhibition of the ATPase P97, we found that the E3 ligase TRC8 interacts with the ATPase P97, the proteasome and also ubiquitinated HLA class I molecules in US2-expressing cells. Potentially, this discovery points towards TRC8 as a component of the dislocon in US2-mediated HLA class I downregulation.

2 Materials and Methods

2.1 Cell culture

The human monocytic U937 and human embryonic kidney (HEK) 239T cell lines (American Type Culture Collection, ATCC) were cultured in RPMI 1640 (Invitrogen) containing 5% FCS (Sigma), 100 U/ml penicillin, 100 µg/ml streptomycin and 2 mM L-glutamine (complete RPMI medium).

2.2 Plasmids

The C-terminal GFP-tagged HLA-A2 construct was expressed from a lentiviral pHRSin-cPPT-SGW vector (kindly provided by Dr. Paul Lehner and Dr. Louise Boyle, University

of Cambridge). The TwinStrep-HA tagged SEC variants and the TwinStrep-Flag tagged TRC8 were cloned into a bidirectional lentivector expressing the tagged proteins of interest under control of the EF1A promotor, and a Zeocin-resistance cassette under control of the hPGK promotor for selection of transduced cells. Wt-US2 and CD8L-HA-US2 were expressed from the same lentiviral backbone vector as the SEC variants, but under Blasticidin resistance instead of Zeocin. An HA-tag was added to certain constructs (SEC61a1 and CD8L-US2), as endogenous protein concentrations or antibody sensitivity were not sufficient for detection with the currently available antibodies.

2.3 Lentivirus production and transduction

HEK293T cells were seeded the day prior to virus production. The lentiviral vector (250ng) was co-transfected with the third-generation packaging vectors pVSV-G, pMDL and pRSV using PEI (1 mg/ml). Three days post-transfection, the lentivirus-containing supernatants were harvested and either stored at -80°C or directly used to transduce U937 cells by spin infection at 2000 rpm for 90 minutes at 33°C in the presence of 4 µg/ml polybrene (Santa Cruz Biotechnology). Stable transduced cells were selected after 2 days post-infection by means of puromycin (2 µg/ml), hygromycin B (500 µg/ml), blasticidin (20 µg/ml) or zeocin (400 µg/ml) addition.

2.4 Co-Immunoprecipitation (IP)

U937 cells were harvested and washed with ice-cold PBS, and lysed in 1% LMNG (Anatrace) lysis buffer (50 mM Tris-HCl pH 7.4, 150 mM NaCl, 5 mM EDTA) supplemented with 10 µM Leupeptin (Roche) and 10 mM Pefabloc SC (Roche) for 30 minutes on ice. Lysates were centrifuged at 20.000 g for 15 minutes at 4°C to remove cellular debris. Supernatants were either directly mixed with Laemmli sample buffer supplemented with 80 mM DTT (Sigma) or incubated overnight with StrepTactin-Sepharose beads (GE Healthcare) on a rotating device at 4°C. The following day, beads were washed 4 times with 0.1% LMNG lysis buffer and eluted with elution buffer (2.5-10 mM Biotin, 50 mM Tris-HCL, 150 mM NaCl and 1mM EDTA at a pH of 7.4). SpinX filter colums (0.45 µM, Corning Costar) were used to separate the eluate from the beads. After elution, Laemmli sample buffer supplemented with 80 mM DTT (Sigma) was added, samples were boiled for 10 min at 70°C and stored at -80°C until further use.

2.5 Immunoblotting

SDS-page was performed with 4-12% Bolt Bis-Tris Plus SDS gels (Thermo Scientific). Proteins were transferred to Trans-Blot Turbo PVDF membranes (BIO-RAD) using a Trans-Blot Turbo

transfer system (BIO-RAD) for 10 minutes at 25 V. Membranes were blocked with 4% milk powder (Campina) in phosphate-buffered saline supplemented with 0.05% Tween 20 (PBST) for 2 h at 4°C. Primary antibodies were diluted in PBST supplemented with 1% milk powder and incubated with the membranes overnight at 4°C or 2 h at room temperature. Membranes were washed thoroughly with PBST at 4°C and were then incubated with an HRP-labelled secondary antibody (diluted in 1% milk powder in PBST) for 2 h at 4°C. Membranes were again washed thoroughly before detection. Chemiluminescence was detected using Pierce ECL Western Blotting Substrate (Thermo Scientific), followed by image acquisition (Image Quant LAS 4000).

2.6 HLA I surface expression

HLA class I surface expression or HLA-A2-GFP expression were assessed by flow cytometry using a FACS Canto II (BD Biosciences). Cells were washed with PBS and stained for 30 minutes with a PE-conjugated antibody (W6/32) at the concentrations indicated in cold PBS supplemented with 0.5% BSA and 0.02% NaN_3 in a total volume of 20 µl. Cells were washed to remove unbound antibody. The data were analyzed using FlowJo V10 software.

2.7 Antibodies

The following primary and secondary antibodies were used for IB: mouse anti-20S proteasome α6 (MCP20) mAb (Santa Cruz sc-58416, 1:100), Rat anti-HA 3F10 mAb (Roche 11867423001, 1:1000), rabbit anti-human SEC61β pAb (Abcam ab15576, 1:10.000), rabbit anti-human SEC61γ pAb (Proteintech 11147-2-AP, 1:500), mouse anti-FLAG M2 mAb (Sigma-Aldrich F3165, 1:10.000), Mouse anti-VCP (p97) mAb (BD transduction laboratories 612183, 1:1000), rabbit anti-UBXD8 mAb (Cell signaling 34945S, 1:1000), rabbit anti-Derlin pAb (MBL international PM018, 1:1000), mouse-anti-transferrin receptor mAb (Santa Cruz sc-7327, 1:1000), goat-anti-mouse conjugate-HRP pAb (Jackson #115-035-174, 1:10000), mouse-anti-rabbit conjugate-HRP mAb (Jackson #211-032-171, 1:10000) and goat-anti-rat-HRP pAb (Jackson #112-035-175,1:5000). For flow cytometry, the following antibodies were used: PE-conjugated W6/32, anti-HLA-I (Serotec MCA81PE, 1:100).

2.8 Density gradient ultracentrifugation

For fractionation of the immunoprecipitated SEC61α1 samples (all treated with the P97 inhibitor CB5083, Bio-Connect), IP samples were subjected to density gradient ultracentrifugation in a 10-40% glycerol gradient. The samples were centrifuged for 12h at 4°C and 160.000 g (Sorvall TH-641, 30400rpm). The fractions were separated manually and used for further experiments.

3 Results

3.1 HCMV US2-mediated downregulation of HLA-A2 GFP and surface HLA class I

The HCMV protein US2 hijacks the ERAD machinery to promote downregulation of surface HLA class I thereby interfering with the recognition of virus-infected cells by cytotoxic $CD8^+$ T cells. The interaction partners involved in US2-mediated ERAD of HLA class I molecules have not been fully elucidated. As degradation of HLA class I in this context is fast-paced, and there are technical limitations to tracking of the endogenous proteins involved, we use a setup that allows easier detection of the decrease in intracellular and surface expression. We focused on HLA-A2 downregulation, as this HLA-type has been previously reported to be efficiently downregulated by US2 [29]. Cell lines stably expressing HLA-A2-GFP were generated by lentiviral transduction. Next, the immunoevasin US2 was introduced, either as the wildtype protein (wt-US2), or HA-tagged variant cloned downstream the CD8 leader sequence (CD8L-HA-US2). To test different dislocon candidates previously suggested in the literature, TwinStrep- and HA-tagged components of the SEC-complex (SEC61α1/SEC61β/SEC61γ) or TwinStrep-Flag tagged TRC8 were transduced into US2-expressing U937 cells. Surface expression levels of HLA-A2-GFP were analyzed, and are shown for cell lines transduced with SEC61α1 or TRC8 and respective controls (see Table 1 for the set of cell lines analyzed).

The functionality of US2 in the different cell lines was confirmed by assessing HLA-A2-eGFP levels by flow cytometry (shown for SEC61α1 and TRC8 in Figure 1a and b, respectively). In the absence of the viral protein, cells express high levels of HLA-A2-GFP (Figure 1a and 1b, red peaks). Upon introduction of wt-US2 or CD8L-HA-US2, a potent reduction of the

Table 1: Tagged sets of U937 cells used for flow cytometric and IP analysis.

U937 HLA-A2-GFP CD8L-HA-US2
U937 HLA-A2-GFP CD8L-HA-US2 StrepII-HA-Sec61α1
U937 HLA-A2-GFP wt-US2 StrepII-HA-Sec61α1
U937 HLA-A2-GFP StrepII-HA-Sec61α1 (Control)
U937 HLA-A2-GFP CD8L-HA-US2
U937 HLA-A2-GFP CD8L-HA-US2 Strep-Flag-TRC8
U937 HLA-A2-GFP wt-US2 Strep-Flag-TRC8
U937 HLA-A2-GFP Strep-Flag-TRC8 (Control)

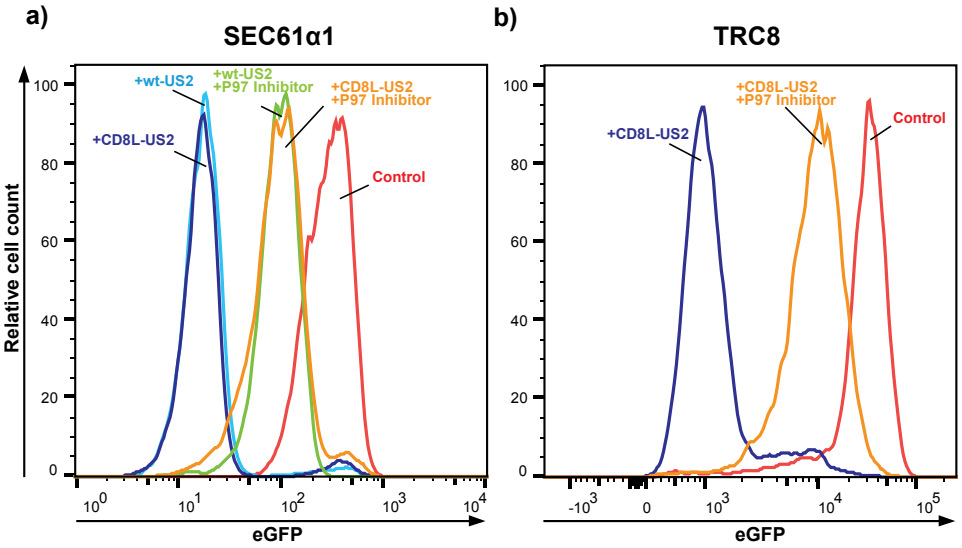

Figure 1: HCMV US2-expressing cells have lower HLA-A2-GFP levels compared to control cells. Flow cytometric analysis of U937 cells expressing HLA-A2-GFP and the constructs StrepII-HA-SEC61α1 (a) and StrepII-Flag-TRC8 (b). HLA-A2-GFP levels were measured by assessing eGFP-expression in the presence or absence of the HCMV protein US2. P97 inhibition with CB5083 partially rescues HLA-A2-GFP levels.

fluorescence intensity compared to the control cells can be observed (Fig. 1a blue and orange peak, Fig. 1b blue peak). Therefore, the introduced US2 proteins are functional and able to target the fusion protein HLA-A2-GFP for degradation. Cells containing the tagged proteins SEC61β and SEC61γ showed similar results (data not shown).

To stall the degradation process and partially rescue HLA, the cells were incubated with the P97 inhibitor CB5083 (1 μM) for 4h. This prevents the ATPase P97 from pulling HLA class I molecules out of the ER, and potentially allow for a stable interaction between HLA class I and the dislocation channel to occur. Indeed, P97 inhibition resulted in increased levels of HLA-A2-eGFP (Fig. 1a green peak and orange peak, Fig. 1b orange peak) and total HLA surface levels (data not shown). Similar results were obtained for cells transduced with the proteins SEC61β, SEC61γ (data not shown).

3.2 SEC61a1 interacts with the proteasome, P97, UBXD8, Derlin1 and HRD1

The composition of ERAD complexes involved in degradation of misfolded HLA class I molecules remains unclear. In addition, expression of the viral evasin US2 could induce changes in the composition of these complexes. Here, we investigated interacting proteins in the presence or absence of US2 in cells expressing a tagged SEC61a1 by co-immunoprecipitation studies (Fig. 2, right panel). We probed the interaction of SEC61a1

with proteins involved in ERAD, specifically HRD1, UBXD8, P97, the proteasome, and Derlin1. SEC61a1 expression was similar in US2-expressing cells (wt- or CD8L-HA-US2) and in cells lacking US2 (Fig. 2, upper panels). Although our anti-US2 antibody was not able to detect wt and HA-tagged US2 (data not shown), we could readily observe potent expression of HA-tagged US2 using an anti-HA antibody (Fig. 2, lanes 1, 4, 8, 9, 12, and 16). Expression of the proteins of interest was comparable in all cell lines (Fig. 2, staining of total cell lysate (Input)). Upon immunoprecipitation of SEC61α1, we observed interactions with the proteasome, UBXD8 and HRD1, whereas transferrin receptor (TfR) did not co-precipitate, highlighting the specificity of the IP. In addition, CD8L-HA-US2 interacted with this complex. Wt-US2 most likely shares this interaction, but could not be visualized due to a lack of a specific antibody.

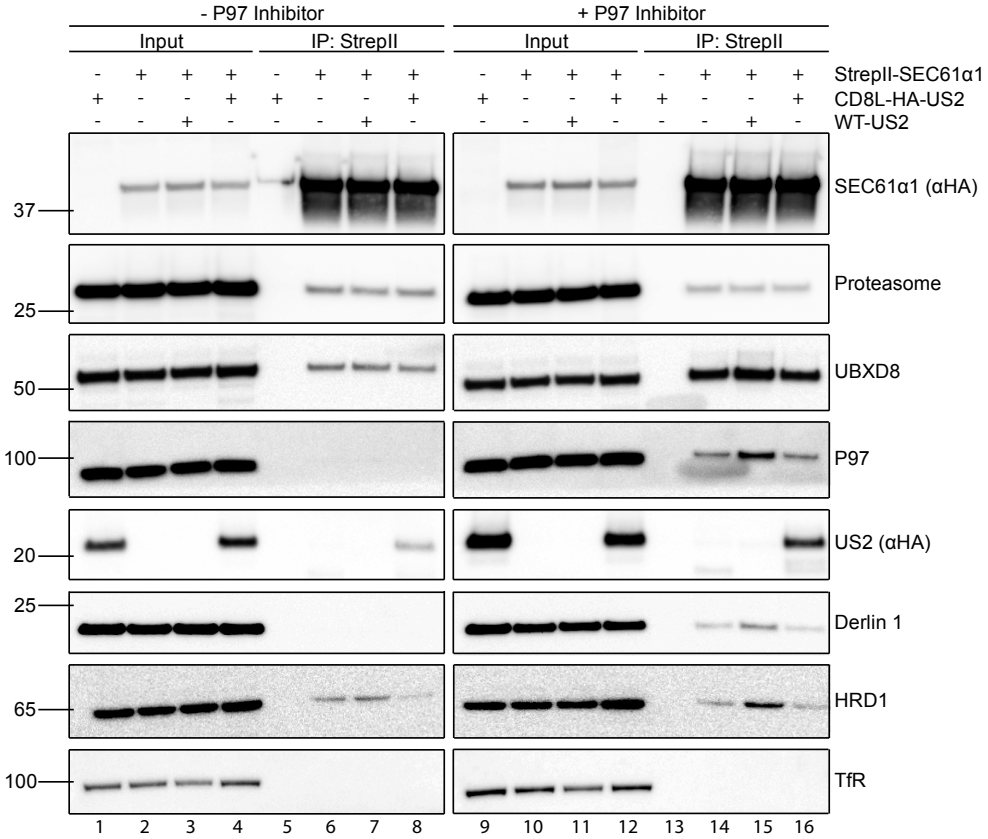

Figure 2: Interactions between-SEC61α1 and other tested proteins are enhanced upon P97 inhibitor treatment. U937-HLA-A2-GFP cells expressing a TwinStrep-HA-tagged SEC61α1 and either wt-US2 or CD8L-HA-US2 were used. TwinStrep-HA-SEC61α1 was immunoprecipitated using StrepTactin beads and 1% LMNG lysates. Immunoprecipitated proteins were eluted with 2.5mM d-Desthiobiotin. Immunoblot analysis was performed on Input (total cell lysates) and IP samples for the indicated proteins. Transferrin (TfR) was used as a loading control. One representative experiment from three replicates (N=3) is shown.

Inhibition of the ATPase P97 with CB5083 allowed the detection of additional interactions of SEC61a1 with Derlin1 and P97 (Fig. 2, right panel, +P97 inhibitor). Furthermore, P97 inhibition resulted in enhanced interactions of SEC61a1 with UBXD8 and CD8L-HA-US2. Co-immunoprecipitations of UBXD8, P97, Derlin1 and HRD1 are slightly higher in cells expressing the wt-US2 compared to cells expressing the CD8L-HA-US2. Endogenous HLA, HLA-A2-GFP and TRC8 could not be found to interact with SEC61α1 with our experimental conditions (data not shown).

The same interactions with proteins were found upon immunoprecipitations with cells expressing TwinStrep-HA-tagged SEC61β (data not shown). In contrast, no interaction was observed between SEC61γ and Derlin1 and between SEC61γ and HRD1 (data not shown).

3.3 Purification and separation of SEC-Proteasome-P97 complexes from SEC-Ribosome complexes for Cryo-EM

Contrary to the known interaction between the proteasome and the ER, complexes between SEC61α1 and proteasome, P97, UBXD8, Derlin1 or HRD1 have thus far not been described. Accordingly, no information about the structural layout of these complexes

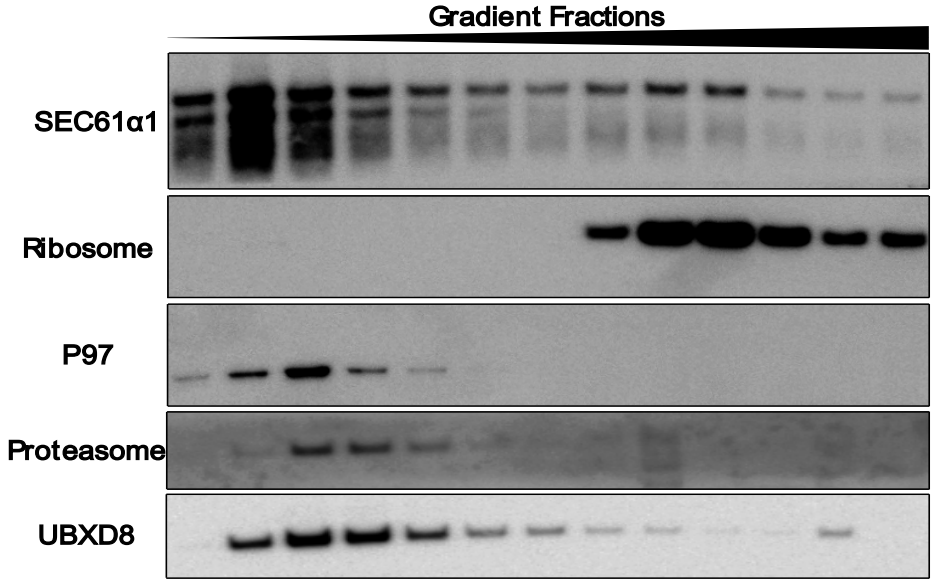

Figure 3: Glycerol gradient of SEC61α1-immunoprecipitated samples resulted in separation of ribosome-bound SEC61α1 from P97 and proteasome-bound SEC61α1. A 10-40% Glycerol gradient is showing P97-inhibitor treated SEC61α1 post-IP samples. Thirteen fractions were used for immunoblotting. P97, SEC61α1, Proteasome and UBXD8 appear to be present in the same fractions whereas a signal of ribosomes is separated and only overlaps with a signal from SEC61α1. One representative gradient from three replicates (N=3) is shown.

is known. We reasoned that our co-immunoprecipitation samples could be subjected to Cryo-EM to obtain information about the stoichiometry and structure of these complexes. Because of the function of Sec61 as a translocon, we expected that the majority of the Sec61 population would be bound to ribosomes. To remove those from our samples and focus on newly described complexes such as a possible complex with the proteasome, we subjected the co-immunoprecipitation samples to density gradient ultracentrifugation spanning a 10-40% glycerol gradient. After ultracentrifugation, samples were fractionated and subjected to electrophoresis and immunoblotting. A clear separation of SEC61-ribosome complexes and SEC61-Proteasome-P97-UBXD8 complexes was observed (Fig. 3). By changing the percentages of the glycerol gradient, SEC61-ribosome complexes were pelleted and a better separation of the remaining protein fractions and complexes was achieved. Fractions containing all proteins of interest were snap-frozen and stored for initial negative-stain electron microscopy. We are currently confirming the reproducibility of these preparations and are further optimizing the purification method, to further reduce the heterogeneity in the sample. The goal is to use these samples for Cryo-EM to unravel the structural architecture of the complex.

3.4 TRC8 interacts with ubiquitinated HLA class I

We were unable to confirm an interaction of HLA class I molecules with components of the SEC-complex. Therefore, we investigated the role of TRC8 in US2-mediated HLA class I downregulation upon P97 inhibition. Cells overexpressing TRC8 showed detectable endogenous HLA molecules as well as HLA-A2-GFP (45kDa and 75kDa, respectively); the signal was visibly lower in cells co-expressing US2 (Fig. 4, compare lanes 1 and 2). Next, we immunoprecipitated TRC8 and stained for candidate interacting proteins. We did not detect an interaction of TRC8 with Derlin1 (Fig. 4, IP) or any of the SEC-components (data not shown). TRC8 was associated with UBXD8 and to a lesser extent with P97, both in the presence and absence of US2 (lane 3 and 4). Also, TRC8 interacted with US2, (lane 4). In addition, the signal for HLA-A2-GFP in US2-expressing cells was reduced and the endogenous HLA could not be detected anymore (lane 2). Interestingly, in the StrepII-TRC8 immunoprecipitation, multiple bands were visible at around 100kDa in cells co-expressing US2 (lane 4). Ubiquitin staining suggests that the proteins at 100kDa are ubiquitinated HLA molecules (lane 4). HLA class I interaction with TRC8 could not be observed in cells that do not express US2 (lane 3). These data suggest a US2-mediated interaction of TRC8 and HLA class I molecules for the direct extraction of HLA class I molecules towards the cytosol.

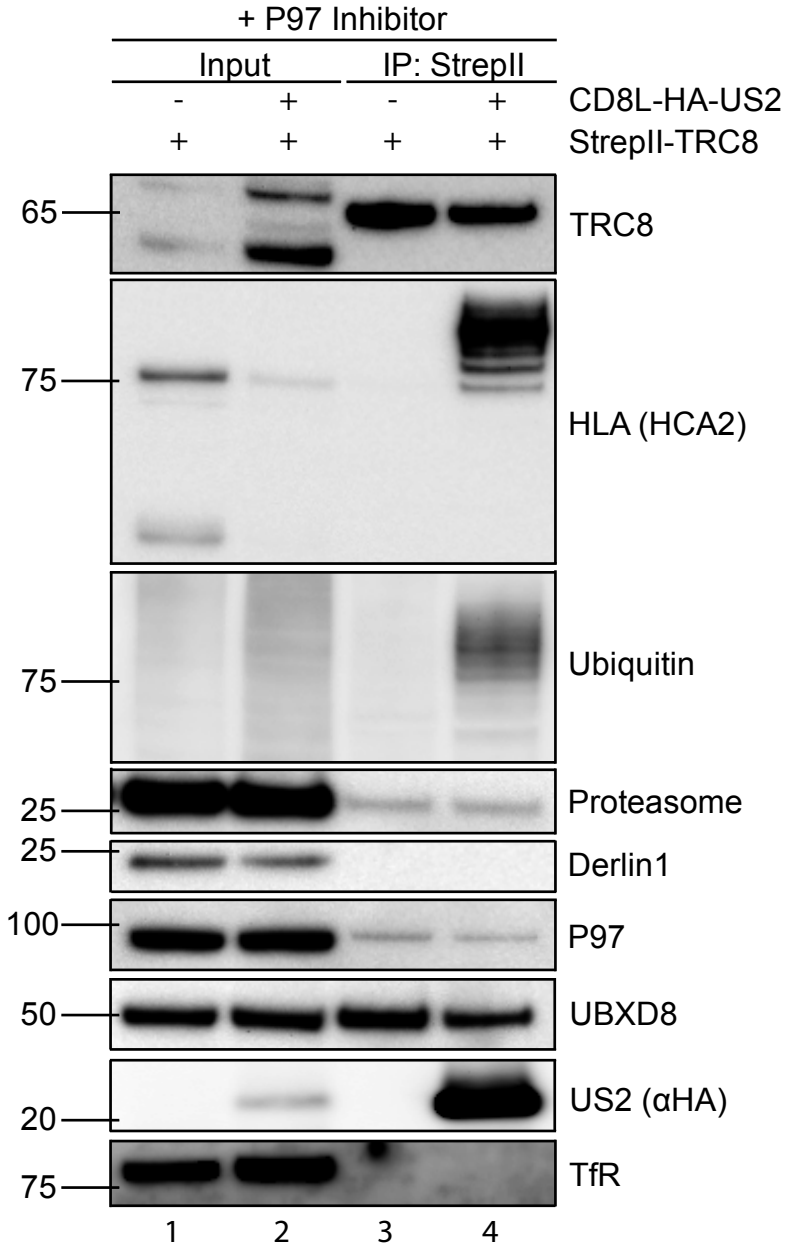

Figure 4: Immunoprecipitation of StrepII-TRC8 in the presence of US2 reveals interaction between TRC8 and ubiquitinated HLA class I. U937-HLA-A2-GFP cells expressing a TwinStrep-Flag-tagged TRC8 and either CD8L-HA-US2 or empty vector (EV) were subjected to immunoprecipitated using StrepTactin beads in 1% LMNG lysates. Immunoprecipitated proteins were eluted with 2.5mM d-Desthiobiotin. Immunoblot analysis was performed on Input (total cell lysates) and IP samples for the indicated proteins. Transferrin (TfR) was used as a loading control. TRC8 was stained with an anti-Flag antibody. One representative experiment from two replicates (N=2) is shown.

4 Discussion

It remains elusive how proteins targeted for ERAD cross the ER-membrane to reach the cytosol. Furthermore, it is unknown whether misfolded or HCMV-US2 targeted HLA class I molecules use the same channel. As multiple diseases are associated with ERAD, it is of critical importance to identify the constituents of dislocon channels and to understand the molecular mechanisms of retrotranslocation.

The SEC61 protein channel mediates the import of proteins into the ER. Potentially, this protein can function as a two-way channel for import and export of proteins. Here, we show that SEC61a1 can interact with both ribosomes and proteins involved in ERAD in a mutually exclusive manner. We identified interactions between SEC61α1, the proteasome and P97 upon P97-inhibitor treatment. Binding of SEC61a1 to P97 and the proteasome could suggest that the protein is used for export of substrates across the ER membrane. Hypothetically, a protein complex consisting of SEC-proteins, P97, the proteasome, UBXD8 and HRD1 could mediate the degradation of misfolded HLA class I molecules in an US2-independent manner and possibly also mediate the export of other ERAD substrates to the cytosol. We aim to study the structural properties of involved complexes by Cryo-EM, for which we are currently optimizing the protocols to increase the amount and purity of SEC complexes. For this we are also considering tagging a second protein in the complex to allow tandem affinity purification, thereby obtaining a more homogenous preparation for Cryo-EM.

We were unable to confirm SEC61 as a dislocon in US2-mediated HLA class I ERAD, as we could not identify direct interactions between HLA class I and SEC61. However, this does not exclude the possibility that the SEC-complex acts as a dislocon in US2-mediated downregulation of HLA class I molecules. Of note, the previously reported interaction with HLA class I was observed for the deglycosylated HLA class I degradation intermediate that occurs in the cytosol upon treatment of cells with proteasome inhibitor [18].

The E3 ubiquitin ligase TRC8 was identified by independent studies to be essential for US2-mediated HLA class I downregulation [12],[21],[30]. Interestingly, TRC8 is located in the ER membrane and has, similarly to the trimer SEC61α1/β/γ, 12 transmembrane domains. Therefore, TRC8 could be large enough to form a pore in the ER membrane through which polypeptides could be exported. Furthermore, the TM3-TM8 region of TRC8 was shown to have sequence similarities with yeast HRD1, which was previously identified to form a homo-dimeric dislocation channel for the export of misfolded proteins [31]. The interaction between TRC8, P97, the proteasome and ubiquitinated HLA class I in the presence of the viral protein US2 suggests a dual role of TRC8 as the E3 ligase as well as a component

of the dislocon-complex in US2-dependent HLA class I downregulation. Also here, a structural elucidation of the interacting proteins by Cryo-EM could help confirming a role of TRC8 as a dislocation channel. Structural insights into protein complexes mediating ERAD, as well as the identification of a dislocation channel for US2-mediated HLA class I downregulation, could lead to the development of new strategies to treat a variety of protein degradation-related diseases.

Funding

This work was funded by the European Commission under the Horizon2020 program H2020 MSCA-ITN GA 675278 EDGE.

References

1. Chen, X., Karnovsky, A., Sans, M. D., Andrews, P. C. & Williams, J. A. Molecular characterization of the endoplasmic reticulum: Insights from proteomic studies. *Proteomics* **10**, 4040–4052 (2010).
2. Kalies, K.-U., Stokes, V. & Hartmann, E. A single Sec61-complex functions as a protein-conducting channel. *Biochim. Biophys. Acta - Mol. Cell Res.* **1783**, 2375–2383 (2008).
3. Meyer, H. A. *et al.* Mammalian Sec61 is associated with Sec62 and Sec63. *J. Biol. Chem.* **275**, 14550–14557 (2000).
4. Linxweiler, M., Schick, B. & Zimmermann, R. Let's talk about Secs: Sec61, Sec62 and Sec63 in signal transduction, oncology and personalized medicine. *Signal Transduct. Target. Ther.* **2**, 17002 (2017).
5. Blobel, G. & Dobberstein, B. Transfer of proteins across membranes. I. Presence of proteolytically processed and unprocessed nascent immunoglobulin light chains on membrane-bound ribosomes of murine myeloma. *J. Cell Biol.* **67**, 835–851 (1975).
6. Araki, K. & Nagata, K. Protein folding and quality control in the ER. *Cold Spring Harb. Perspect. Biol.* **3**, a007526 (2011).
7. Olzmann, J. A., Kopito, R. R. & Christianson, J. C. The Mammalian Endoplasmic Reticulum-Associated Degradation System. *Cold Spring Harb. Perspect. Biol.* **5**, a013185–a013185 (2013).
8. Christianson, J. C. *et al.* Defining human ERAD networks through an integrative mapping strategy. *Nat. Cell Biol.* **14**, 93–105 (2012).
9. Omura, T., Kaneko, M., Okuma, Y., Matsubara, K. & Nomura, Y. Endoplasmic reticulum stress and Parkinson's disease: the role of HRD1 in averting apoptosis in neurodegenerative disease. *Oxid. Med. Cell. Longev.* **2013**, 239854 (2013).
10. ARIDOR, M. Visiting the ER: The endoplasmic reticulum as a target for therapeutics in traffic related diseases . *Adv. Drug Deliv. Rev.* **59**, 759–781 (2007).
11. Vembar, S. S. & Brodsky, J. L. One step at a time: Endoplasmic reticulum-associated degradation. *Nat. Rev. Mol. Cell Biol.* **9**, 944–957 (2008).
12. Van den Boomen, D. J. H. & Lehner, P. J. Identifying the ERAD ubiquitin E3 ligases for viral and cellular targeting of MHC class I. *Mol. Immunol.* **68**, 106–111 (2015).
13. Burr, M. L. *et al.* HRD1 and UBE2J1 target misfolded MHC class I heavy chains for endoplasmic reticulum-associated degradation. *Proc. Natl. Acad. Sci.* **108**, 2034–2039 (2011).

14. Ahn, K. *et al.* The ER-luminal domain of the HCMV glycoprotein US6 inhibits peptide translocation by TAP. *Immunity* **6**, 613–21 (1997).

15. Jones, T. R. *et al.* Human cytomegalovirus US3 impairs transport and maturation of major histocompatibility complex class I heavy chains. *Proc. Natl. Acad. Sci.* **93**, 11327–11333 (1996).

16. Park, B., Spooner, E., Houser, B. L., Strominger, J. L. & Ploegh, H. L. The HCMV membrane glycoprotein US10 selectively targets HLA-G for degradation. *J. Exp. Med.* **207**, 2033–41 (2010).

17. Wiertz, E. J. *et al.* The human cytomegalovirus US11 gene product dislocates MHC class I heavy chains from the endoplasmic reticulum to the cytosol. *Cell* **84**, 769–79 (1996).

18. Wiertz, E. J. H. J. *et al.* Sec6l-mediated transfer of a membrane protein from the endoplasmic reticulum to the proteasome for destruction. *Nature* **384**, 432–438 (1996).

19. Gewurz, B. E., Ploegh, H. L. & Tortorella, D. US2, a Human Cytomegalovirus-encoded Type I Membrane Protein, Contains a Non-cleavable Amino-terminal Signal Peptide. *J. Biol. Chem.* **277**, 11306–11313 (2002).

20. Rehm, A., Stern, P., Ploegh, H. L. & Tortorella, D. Signal peptide cleavage of a type I membrane protein, HCMV US11, is dependent on its membrane anchor. *EMBO J.* **20**, 1573–82 (2001).

21. Stagg, H. R. *et al.* The TRC8 E3 ligase ubiquitinates MHC class I molecules before dislocation from the ER. *J. Cell Biol.* **186**, 685–92 (2009).

22. van den Boomen, D. J. H. *et al.* TMEM129 is a Derlin-1 associated ERAD E3 ligase essential for virus-induced degradation of MHC-I. *Proc. Natl. Acad. Sci.* **111**, 11425–11430 (2014).

23. van de Weijer, M. L. *et al.* A high-coverage shRNA screen identifies TMEM129 as an E3 ligase involved in ER-associated protein degradation. *Nat. Commun.* **5**, 3832 (2014).

24. Tretter, T. *et al.* ERAD and protein import defects in a sec61 mutant lacking ER-lumenal loop 7. *BMC Cell Biol.* **14**, 56 (2013).

25. Kalies, K.-U., Allan, S., Sergeyenko, T., Kröger, H. & Römisch, K. The protein translocation channel binds proteasomes to the endoplasmic reticulum membrane. *EMBO J.* **24**, 2284–93 (2005).

26. Greenblatt, E. J., Olzmann, J. A. & Kopito, R. R. Derlin-1 is a rhomboid pseudoprotease required for the dislocation of mutant α-1 antitrypsin from the endoplasmic reticulum. *Nat. Struct. Mol. Biol.* **18**, 1147–1152 (2010).

27. Y, Y., Y, S., C, Y., D, R. & TA, R. A membrane protein complex mediates retro-translocation from the ER lumen into the cytosol. *Nature* **429**, 841–847 (2004).

28. Nadav, E. *et al.* A novel mammalian endoplasmic reticulum ubiquitin ligase homologous to the yeast Hrd1. *Biochem. Biophys. Res. Commun.* **303**, 91–97 (2003).

29. Fiebiger, E., Story, C., Ploegh, H. L. & Tortorella, D. Visualization of the ER-to-cytosol dislocation reaction of a type I membrane protein. *EMBO J.* **21**, 1041–1053 (2002).

30. Hsu, J. L. *et al.* Plasma Membrane Profiling Defines an Expanded Class of Cell Surface Proteins Selectively Targeted for Degradation by HCMV US2 in Cooperation with UL141. *PLoS Pathog.* **11**, 1–24 (2015).

31. Schoebel, S. *et al.* Cryo-EM structure of the protein-conducting ERAD channel Hrd1 in complex with Hrd3. *Nature* **548**, 352–355 (2017).

8

Summarizing discussion

P. Praest

Herpesviruses escape immune surveillance through the use of multiple immune-modulatory mechanisms, thereby facilitating lifelong infections. The longstanding evolutionary race between pathogen and host has resulted in large number of immune evasins. In this thesis, we study the interactions between viral evasins and host proteins and aim to understand how these impact host cellular pathways. We highlight approaches to identify viral proteins interfering with the MHC class I antigen presentation pathway (**chapter 2 and 3**)**,** give insight into the structural composition of the peptide loading complex and its manipulation by viral immune evasins (**chapters 4**)**,** aim to elucidate the structures of herpesvirus TAP inhibitors (**chapter 5**)**,** identify a peptide with antiviral activity (**chapter 6**), and elucidate key players in HCMV-mediated MHC class I downregulation (**chapter 7)**.

Viral interference with the MHC class I antigen presentation pathway

RNA viruses, such as HIV, have a high mutation rate that leads to immune evasion by antigenic variation [1]–[3]. DNA viruses, in contrast, have a relatively low mutation rate and therefore rely on alternative evasion mechanisms. The large genome of pox- and herpesviruses allows them to carry a broad range of immune evasion genes that efficiently inhibit host immune responses, such as those elicited by the MHC class I antigen presentation pathway (**chapter 3**). MHC class I molecules are displayed on most nucleated cell and present peptides to the immune system. Upon viral infection, peptides derived from endogenous proteins are replaced by virus-derived peptides. Recognition of MHC I complexes presenting viral peptides by specific $CD8^+$ cytotoxic T-cells, will result in killing of the target cell. To hide from the immune system, herpesviruses have evolved several strategies to counteract immune responses (see **chapter 3**, Figure 1), allowing them to persist in the host for life.

The importance of the MHC class I antigen presentation pathway in anti-viral immunity is highlighted by the observations that nearly every step in this pathway is targeted by viral immune evasion proteins, ultimately resulting in the downregulation of cell surface MHC class I expression. We describe a method to identify candidate gene products that are potentially responsible for evasion from MHC class I-restricted antigen presentation (**chapter 3**). In combination with other previously described assays, our method might help narrow down the exact step of interference and possibly identify new proteins responsible for manipulation of the MHC class I pathway. Indeed, we show strong phenotypes by individual viral TAP inhibitors, such as the TAP-inhibitor CPXV012 from cowpox virus [4].

Does the genetic variation of TAP influence peptide transport and/or inhibition of TAP by viral immune evasion proteins?

The transport of peptides into the ER by the transporter associated with antigen processing (TAP) is a key step for virus-derived peptide-MHC class I complexes to be presented at the cell surface. As multiple single nucleotide polymorphisms (SNPs) in TAP have been reported, we asked whether these could affect the activity of TAP or impact the inhibitory potential of viral immune evasins. To address this question, we analyzed several combinations of naturally occurring TAP SNPs and probed their ability to transport peptides across the ER membrane and allow presentation of peptide-MHC class I complexes on the cell surface (**chapter 2**). However, none of the SNPs affected peptide transport and MHC class I surface expression, nor did they impact the activity of viral TAP inhibitors. These results suggest that herpesviruses likely did not contribute to selection of inhibitor-resistant TAP variants in the human population. Nevertheless, as we have only tested several SNPs in our assays, we cannot exclude that a certain combination might result in a TAP variant resistant to viral inhibition. In a future study, the remaining TAP inhibitors could be tested, including the cowpox virus protein CPXV012 [4].

Even though SNPs were present in close proximity to the nucleotide binding regions of TAP1 and TAP2, we saw no or limited effects on the peptide transport activity by this complex. This might suggest that, if herpesviruses were not the driving force for the selection of SNPs in TAP, other pathogens might have played a role in this evolutionary step. Polymorphisms in TAP occur in different populations across the world and are being actively studied in multiple fields of research. TAP1 and TAP2 play an important role in endogenous antigen processing, interact with HLA molecules and are located within the HLA class II region between HLA-DP and -DQ loci [5]. Therefore, it is not surprising that several experimental models and human case studies implicated a role for TAP polymorphisms in viral and bacterial diseases, as well as autoimmunityand different cancers [6]–[11]. Up to date, it is unknown what factors gave rise to the polymorphisms in the TAP genes.

Insights into the structure of the peptide-loading complex (PLC) obtained by Cryo-EM

The mechanisms by which TAP mediates peptide translocation into the ER and subsequently loads peptides on newly synthesized MHC class I molecules are not fully understood. Several studies identified crucial proteins of the peptide loading complex and defined the length of the peptide substrates that are transported into the ER [12],[13]. A detailed picture of the structural composition of this complex and its structural

rearrangements that occur during a full peptide translocation cycle is still missing. Recently, the structure of TAP1 and TAP2 in complex with HSV ICP47 was solved by Cryo-EM, providing a first structural insight into viral inhibition of peptide translocation[14]. We build upon this study and constructed a model for the most likely stoichiometry of the PLC based on literature (**chapter 4**), which was confirmed by a subsequent study that determined the native structure of the human PLC by Cryo-EM [15]. Two editing modules are connected to the ER-luminal part of the TAP1/2 heterodimer (see **chapter 4**, Figure 1). MHC class I associates to these editing modules that each consist of the proteins tapasin, calreticulin and ERp57. This arrangement facilitates loading of MHC class I with newly imported peptides. For the isolation of the whole PLC, the authors made use of the ability of the herpesvirus inhibitor ICP47 from HSV to arrest and stabilize the TAP complex [16].

Structural studies on other ATP-binding cassette (ABC) transporters suggest that TAP undergoes major conformational changes during the peptide transport cycle (**chapter 4**). This theory is supported by observations that viral TAP-inhibitors bind to the complex during distinct steps of the peptide transport cycle and are mutually exclusive [17]. We aim to shed light on the TAP-mediated peptide translocation cycle and the structural composition of the TAP inhibitors by co-expressing the herpes and poxvirus-encoded TAP inhibitors together with TAP1 and TAP2 in HEK293 cells, followed by isolation of the complex and Cryo-EM (**chapter 5**).

Recently, eight high resolution structures of the ABC exporter TmrAB were elucidated that together appeared to represent a full transport cycle of an asymmetric ABC exporter in a lipid environment [18]. TmrAB is a functional homolog of TAP and was reported to be able to restore antigen presentation in human TAP-deficient cells [19],[20]. Structural insights on the heterodimeric ABC exporter TmrAB from *thermus thermophilus* could be used to extrapolate details of the TAP mediated peptide transport which at a later stage can be confirmed by the different structures of the TAP-Inhibitor complexes.

Solving the structure of viral TAP inhibitors and elucidating their binding characteristics to the TAP heterodimer might aid in the development of therapeutic intervention strategies. Some of these inhibitors interact with TAP outside of the peptide binding site of TAP. Possibly the interaction of these inhibitors with TAP can be blocked by chemical compounds. A combination of these compounds with other currently used drugs against herpesviruses could aid in the fight against these persistent viruses. Furthermore, a current investigation is testing the immune suppressive potency of the viral TAP inhibitors as a tool for fighting host-versus-graft disease in solid organ transplantation.

Degradation of TAP by BoHV-1 UL49.5

The protein UL49.5 from BoHV-1 is unique amongst the TAP inhibitors discovered thus far. This evasin inhibits TAP function by two independent mechanisms: by inducing a conformational arrest of the transporter and by targeting TAP for proteasomal degradation [21],[22]. To elucidate the mechanism of action of UL49.5, researchers have used a GFP-tagged TAP1 construct, for easier tracking of the transporter. The addition of the GFP-tag made TAP resistant for proteasomal degradation mediated by the BoHV-1 encoded protein UL49.5 [21]. Therefore, an alternative tagging-approach is needed to investigate the mechanism of the proteasomal degradation of TAP. The tagged version of TAP should retain its ability to: (1) be functional in peptide transport across the ER-membrane, (2) be targeted by the immune evasin UL49.5 and (3) be ultimately targeted for proteasomal degradation (**Addendum 1**). Among different approaches to fuse GFP to TAP1 or TAP2, fusing GFP to the N-terminus of TAP2 yielded the most promising results. This fusion protein allowed peptide transport into the ER in absence of a viral TAP inhibitor and showed a strong decrease in transport by introducing any of the known viral TAP inhibitors. Most importantly, and contrary to the previously used TAP1-GFP fusion protein, TAP2-GFP was still targeted for degradation by BoHV-1 UL49.5. Next, TAP degradation was identified to be P97-dependent. The ATPase P97 has been described to be the pulling force in extracting ubiquitinated substrates in ERAD [23]. Therefore, it could be hypothesized that UL49.5 uses an ERAD or ERAD-related pathway for the degradation of TAP, similar to the degradation of MHC class I molecules by the HCMV proteins US2 and US11 [24].

ERAD – how are proteins exported from the ER?

ER-associated protein degradation has been studied extensively over the last decades. Although key players responsible for the recognition of degradation substrates, their ubiquitination and their proteasomal degradation are well described [25],[26], it remains elusive how ERAD-substrates cross the ER membrane. Several different proteins containing at least six transmembrane domains have been suggested to act as a dislocation channel individually, or in complex with other proteins. These proteins are SEC61α/β/γ, Derlin1, TRC8 and Hrd1 [27]–[30].

Pulse-chase studies showed that deglycosylated HLA class I molecules associates with SEC61 in the presence of the HCMV protein US2 [27]. Dislocation of HLA class I molecules to the cytosol was observed within five minutes, suggesting that newly synthesized HLA class I molecules may not be released from the SEC61 complex before rerouting to the cytosol for degradation. This hints to a potential dual role of the SEC61 protein-complex, acting as a two-way channel facilitating both protein import in and export from the ER.

In agreement, we observed US2-independent interactions between SEC61 and the ERAD factors Hrd1, Derlin1, P97, UBXD8, and the proteasome (**see chapter 7**). These results confirm the previously described interaction between SEC61 and the proteasome and identify more interaction partners in this complex [30],[31].

The complex identified consists of proteins that mediate the degradation of ERAD substrates: the latter would be ubiquitinated by the E3 ligase Hrd1 and extracted by the ATPase P97 and its recruitment factor UBXD8 upon export through the SEC61 channel, to ultimately be degraded by the proteasome. By performing immunoprecipitations (IPs) on SEC61α/β/γ while inhibiting the ATPase P97 with the chemical CB5083, we aimed to stall the process of HLA class I dislocation and trap HLA class I molecules interacting with the SEC61-complex. Due to the absence of an interaction between HLA class I and SEC61 in the performed IP experiments, a role of SEC61 as a dislocon for US2-mediated HLA class I degradation cannot be confirmed nor ruled out at this stage.

Our studies show that the binding of proteasomes and ribosomes to SEC61 are mutually exclusive. Since the ATPase P97 and the proteasome form a stable complex with SEC61, it is tempting to hypothesize that the SEC61-complex directly feeds substrates into the proteasome, acting as a dislocation channel for substrates leaving the ER in an US2-independent manner. Using Cryo-EM, we aim to determine the structural architecture of this complex and to explore how the proteins interact. To obtain high-resolution structures, the current purification methods need to be optimized to obtain a homogenous sample with a sufficient concentration of complex.

While searching for a way for HLA class I molecules to exit the ER in US2-mediated degradation, we focused on interactions of proteins with the multi-transmembrane domain containing E3 ligase TRC8. We observed an interaction between TRC8 and ubiquitinated HLA class I molecules upon presence of HCMV US2 and inhibition of the ATPase P97. We confirm the previously described interaction of TRC8 with HLA class I molecules [28], but also found UBXD8, P97 and the proteasome to be interacting partners of TRC8. These interactions hint towards a dual function of TRC8 in the ubiquitination and channeling of HLA class I towards the cytosol. Another possibility is that a yet unknown transmembrane protein forms the HLA class I dislocation channel and interacts with TRC8, as was observed for the E3 ligase Hrd1 with SEC61. The multiple transmembrane domains of both, TRC8 and HRD1, could either form or contribute to the dislocation channel.

Our current knowledge hints towards the occurrence of different substrate-dependent dislocation complexes. The Hrd1-SEC61-complex could be responsible for the degradation of misfolded proteins, whereas the TRC8-complex could be responsible for the US2-

mediated degradation of HLA class I molecules. It awaits clarification whether TRC8 holds a dual function as a ubiquitin ligase and a protein dislocation channel on its own, and if additional proteins are needed to support the latter function. Besides US2, HLA class I degradation is also promoted by HCMV protein US11. This viral immune evasion protein depends on TMEM129 as the E3 ubiquitin ligase [32]. Interestingly, like TRC8, the E3 ligase TMEM129 was found to interact with ERAD-related proteins in the absence of the viral inhibitor [33]. Therefore, it is likely that TMEM129 is also responsible for the ubiquitination of endogenous ERAD substrates in the context of protein quality control in the ER. TMEM129 was identified as the 10th mammalian ER membrane-anchored ubiquitin ligase, next to Hrd1, Gp78, RMA1, TEB4, RFP2, TRC8, Kf-1, RNF170 and ZNRF4 [34]. This leads to the question if there are additional ERAD-related complexes for the degradation of substrates. In contrast to other E3 ligases, TMEM129 was reported to only have three transmembrane domains [35], so it is questionable if this E3 ligase could act as protein translocation channel on its own.

A dual mechanism of CPXV012?

For cowpox virus (CPXV), both CPXV203 and CPXV012 interfere with MHC class I-restricted antigen presentation. Whereas CPXV203 retains peptide-loaded MHC class I molecules in the ER, CPXV012 inhibits TAP function [4],[36]. CPXV012 is the only known viral TAP inhibitor outside the herpesvirus family to date. It is assumed that this protein resulted from a 5-nucleotide frameshift of its homologue D10L, leading to a truncated ER-luminal protein present in CPXV012 [37].

A peptide corresponding to the active domain of CPXV012 is a potent inhibitor of cross-presentation in a vaccinia virus (VACV) infection model [38]. Intriguingly, the peptide also holds potent antiviral activity towards several viruses (**see chapter 6**). The cationic CPXV012 peptide can interact with negatively charged phospholipids such as phosphatidylserine (PS) in viral membranes. Viral membranes composed of PS are damaged by the peptide and the infection is hindered. This action of the peptide opens possibilities for application as antiviral therapy or prophylactic treatment, as shown previously for the chimeric antibody bavituximab that can also interact with PS in the viral membrane [39]. In the current study we used an unmodified peptide derived from the full-length protein CPXV012. Future research could help designing a peptide with even lower toxicity while increasing its efficiency.

So far, the antiviral activity of the peptide was only studied by adding the peptide exogenously to cell cultures. It's unclear whether the peptide is produced during cowpox virus infection. If this is the case, the peptide could block viral infection, either by CPXV

itself, or by other viruses. An emerging and unresolved question would be if this mode of action could occur without hindering a CPXV infection itself. On the other hand, this feature could theoretically be profitable for the cowpox virus, as it could prevent the cell from a superinfection by other pathogens. This would grant the cowpox virus exclusive use of cellular resources and a more effective reproduction. A prevention from superinfection has been described for a variety of other viruses including influenza, HSV-1, VACV and HIV [40]–[43].

Concluding remarks

Viruses have evolved sophisticated mechanisms to interfere with the hosts' immune system and to escape immune surveillance thereby allowing them to persist for life. In this thesis we elucidate how viruses interfere with TAP mediated transport of peptides and our results contribute to our general knowledge about the ER-associated degradation of proteins and US2-dependent HLA class I downregulation. The findings on these host-pathogen interactions and their influence on biological processes may be usurped to develop new antiviral drugs, vaccines and therapies for a wide range of herpes and poxviruses.

References

1. Duffy, S. Why are RNA virus mutation rates so damn high? *PLOS Biol.* **16**, e3000003 (2018).
2. Elena, S. F. & Sanjuán, R. Adaptive value of high mutation rates of RNA viruses: separating causes from consequences. *J. Virol.* **79**, 11555–8 (2005).
3. Finlay, B. B. & McFadden, G. Anti-Immunology: Evasion of the Host Immune System by Bacterial and Viral Pathogens. *Cell* **124**, 767–782 (2006).
4. Alzhanova, D. *et al.* Cowpox Virus Inhibits the Transporter Associated with Antigen Processing to Evade T Cell Recognition. *Cell Host Microbe* **6**, 433–445 (2009).
5. Abitew, A. M., Sobti, R. C., Sharma, V. L. & Wanchu, A. Analysis of transporter associated with antigen presentation (TAP) genes polymorphisms with HIV-1 infection. *Mol. Cell. Biochem.* **464**, 65–71 (2020).
6. Correa, P. A. *et al.* TAP1 and TAP2 polymorphisms analysis in northwestern Colombian patients with systemic lupus erythematosus. *Ann. Rheum. Dis.* **62**, 363–365 (2003).
7. Wang, D. *et al.* Association of LMP/TAP Gene Polymorphisms with Tuberculosis Susceptibility in Li Population in China. *PLoS One* **7**, e33051 (2012).
8. Sunder, S. R., Hanumanth, S. R., Gaddam, S., Jonnalagada, S. & Valluri, V. L. Association of TAP 1 and 2 gene polymorphisms with human immunodeficiency virus–tuberculosis co-infection. *Hum. Immunol.* **72**, 908–911 (2011).
9. Aquino-Galvez, A. *et al.* Transporter associated with antigen processing (TAP) 1 gene polymorphisms in patients with hypersensitivity pneumonitis. *Exp. Mol. Pathol.* **84**, 173–177 (2008).
10. Xu, C. *et al.* Genetic Polymorphisms of LMP/TAP Gene and Hepatitis B Virus Infection Risk in the Chinese Population. *J. Clin. Immunol.* **27**, 534–541 (2007).
11. Gomez, L. M. *et al.* Analysis of IL1B, TAP1, TAP2 and IKBL polymorphisms on susceptibility to tuberculosis. *Tissue Antigens* **67**, 290–296 (2006).
12. Koopmann, J. O., Post, M., Neefjes, J. J., Hämmerling, G. J. & Momburg, F. Translocation of long peptides by transporters associated with antigen processing (TAP). *Eur. J. Immunol.* **26**, 1720–8 (1996).
13. Abele, R. & Tampé, R. Function of the transport complex TAP in cellular immune recognition. *Biochimica et Biophysica Acta - Biomembranes* (1999) doi:10.1016/S0005-2736(99)00171-6.
14. Oldham, M. L. *et al.* A mechanism of viral immune evasion revealed by cryo-EM analysis of the TAP transporter. *Nature* **529**, 537–40 (2016).
15. Blees, A. *et al.* Structure of the human MHC-I peptide-loading complex. *Nature* **551**, 525–528 (2017).
16. Herbring, V., Bäucker, A., Trowitzsch, S. & Tampé, R. A dual inhibition mechanism of herpesviral ICP47 arresting a conformationally thermostable TAP complex. *Sci. Rep.* **6**, 36907 (2016).
17. Matschulla, T. *et al.* A highly conserved sequence of the viral TAP inhibitor ICP47 is required for freezing of the peptide transport cycle. *Sci. Rep.* **7**, 2933 (2017).
18. Hofmann, S. *et al.* Conformation space of a heterodimeric ABC exporter under turnover conditions. *Nature* **571**, 580–583 (2019).
19. Zutz, A. *et al.* Asymmetric ATP hydrolysis cycle of the heterodimeric multidrug ABC transport complex TmrAB from Thermus thermophilus. *J. Biol. Chem.* **286**, 7104–15 (2011).

20. Nöll, A. *et al.* Crystal structure and mechanistic basis of a functional homolog of the antigen transporter TAP. *Proc. Natl. Acad. Sci.* 201620009 (2017) doi:10.1073/pnas.1620009114.

21. Koppers-Lalic, D. *et al.* Varicelloviruses avoid T cell recognition by UL49.5-mediated inactivation of the transporter associated with antigen processing. *Proc. Natl. Acad. Sci.* **102**, 5144–5149 (2005).

22. Koppers-Lalic, D. *et al.* Varicellovirus UL49.5 Proteins Differentially Affect the Function of the Transporter Associated with Antigen Processing, TAP. *PLoS Pathog.* **4**, e1000080 (2008).

23. Rabinovich, E., Kerem, A., Fröhlich, K.-U., Diamant, N. & Bar-Nun, S. AAA-ATPase p97/Cdc48p, a cytosolic chaperone required for endoplasmic reticulum-associated protein degradation. *Mol. Cell. Biol.* **22**, 626–34 (2002).

24. van de Weijer, M. L., Luteijn, R. D. & Wiertz, E. J. H. J. Viral immune evasion: Lessons in MHC class I antigen presentation. *Semin. Immunol.* **27**, 125–137 (2015).

25. Olzmann, J. A., Kopito, R. R. & Christianson, J. C. The Mammalian Endoplasmic Reticulum-Associated Degradation System. *Cold Spring Harb. Perspect. Biol.* **5**, a013185–a013185 (2013).

26. Christianson, J. C. *et al.* Defining human ERAD networks through an integrative mapping strategy. *Nat. Cell Biol.* **14**, 93–105 (2012).

27. Wiertz, E. J. H. J. *et al.* Sec6l-mediated transfer of a membrane protein from the endoplasmic reticulum to the proteasome for destruction. *Nature* **384**, 432–438 (1996).

28. Stagg, H. R. *et al.* The TRC8 E3 ligase ubiquitinates MHC class I molecules before dislocation from the ER. *J. Cell Biol.* **186**, 685–92 (2009).

29. Tretter, T. *et al.* ERAD and protein import defects in a sec61 mutant lacking ER-lumenal loop 7. *BMC Cell Biol.* **14**, 56 (2013).

30. Kalies, K.-U., Allan, S., Sergeyenko, T., Kröger, H. & Römisch, K. The protein translocation channel binds proteasomes to the endoplasmic reticulum membrane. *EMBO J.* **24**, 2284–93 (2005).

31. Ng, W., Sergeyenko, T., Zeng, N., Brown, J. D. & Römisch, K. Characterization of the proteasome interaction with the Sec61 channel in the endoplasmic reticulum. *J. Cell Sci.* **120**, 682–691 (2007).

32. van de Weijer, M. L. *et al.* A high-coverage shRNA screen identifies TMEM129 as an E3 ligase involved in ER-associated protein degradation. *Nat. Commun.* **5**, 3832 (2014).

33. van den Boomen, D. J. H. *et al.* TMEM129 is a Derlin-1 associated ERAD E3 ligase essential for virus-induced degradation of MHC-I. *Proc. Natl. Acad. Sci.* **111**, 11425–11430 (2014).

34. Claessen, J. H. L., Kundrat, L. & Ploegh, H. L. Protein quality control in the ER: Balancing the ubiquitin checkbook. *Trends Cell Biol.* **22**, 22–32 (2012).

35. van de Weijer, M. *et al.* The E3 Ubiquitin Ligase TMEM129 Is a Tri-Spanning Transmembrane Protein. *Viruses* **8**, 309 (2016).

36. Byun, M., Wang, X., Pak, M., Hansen, T. H. & Yokoyama, W. M. Cowpox virus exploits the endoplasmic reticulum retention pathway to inhibit MHC class I transport to the cell surface. *Cell Host Microbe* **2**, 306–15 (2007).

37. Luteijn, R. D. *et al.* Cowpox Virus Protein CPXV012 Eludes CTLs by Blocking ATP Binding to TAP. *J. Immunol.* **193**, 1578–1589 (2014).

38. Spel, L. *et al.* Endocytosed soluble cowpox virus protein CPXV012 inhibits antigen cross-presentation in human monocyte-derived dendritic cells. *Immunol. Cell Biol.* **96**, 137–148 (2018).

39. Soares, M. M., King, S. W. & Thorpe, P. E. Targeting inside-out phosphatidylserine as a therapeutic strategy for viral diseases. *Nat. Med.* **14**, 1357–62 (2008).

40. Doceul, V., Hollinshead, M., van der Linden, L. & Smith, G. L. Repulsion of superinfecting virions: a mechanism for rapid virus spread. *Science* **327**, 873–876 (2010).

41. Huang, I.-C. *et al.* Influenza A virus neuraminidase limits viral superinfection. *J. Virol.* **82**, 4834–43 (2008).

42. Criddle, A., Thornburg, T., Kochetkova, I., DePartee, M. & Taylor, M. P. gD-Independent Superinfection Exclusion of Alphaherpesviruses. *J. Virol.* **90**, 4049–4058 (2016).

43. Sloan, R. D., Donahue, D. A., Kuhl, B. D., Bar-Magen, T. & Wainberg, M. A. Expression of Nef from unintegrated HIV-1 DNA downregulates cell surface CXCR4 and CCR5 on T-lymphocytes. *Retrovirology* **7**, 44 (2010).

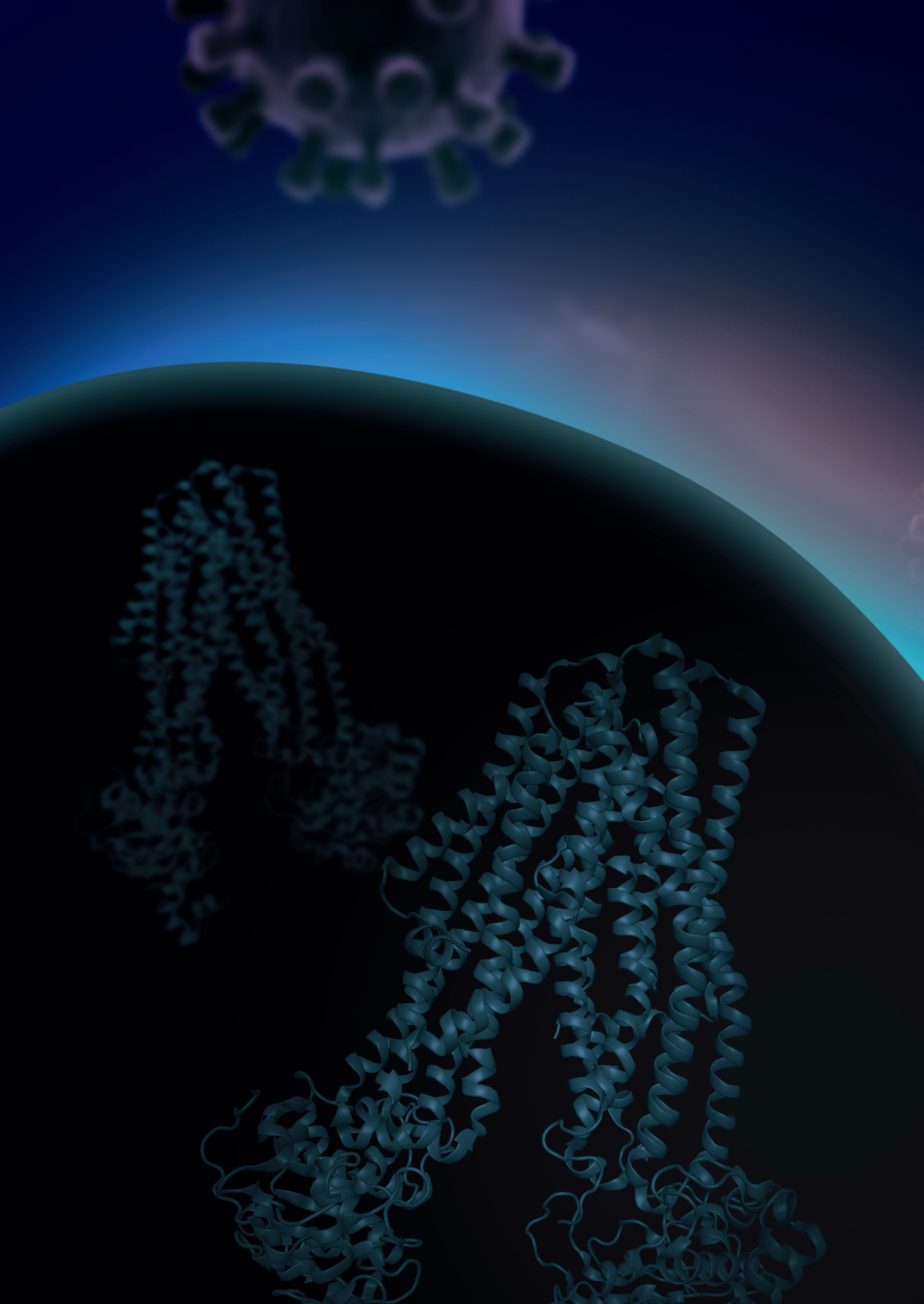

Addendum 1

Fluorescent TAP as a model for virus-induced degradation of the antigenic peptide transporter

M. Wachalska, M. Graul, P. Praest,
K. Bienkowska-Szewczyk, R.D. Luteijn,
A.W. Babnis, E.J.H.J. Wiertz, A.D. Lipinska

Published in Cells , Cell Biology of Viral Infections
(2019) 8(12),1590

Abstract

Transporter associated with antigen processing (TAP), a key player in the major histocompatibility complex class I-restricted antigen presentation, makes an attractive target for viruses that aim to escape the immune system. Mechanisms of TAP inhibition vary among virus species. Bovine herpesvirus 1 (BoHV-1) is unique in its ability to target TAP for proteasomal degradation following conformational arrest by the UL49.5 gene product. The exact mechanism of TAP removal still requires elucidation. For this purpose, a TAP-GFP (green fluorescent protein) fusion protein is instrumental, yet GFP-tagging may affect UL49.5-induced degradation. Therefore, we constructed a series of TAP-GFP variants using various linkers to obtain an optimal cellular fluorescent TAP platform. Mel JuSo (MJS) cells with CRISPR/Cas9 TAP1 or TAP2 knockouts were reconstituted with TAP-GFP constructs. Our results point towards a critical role of GFP localization on fluorescent properties of the fusion proteins and, in concert with the type of a linker, on the susceptibility to virally-induced inhibition and degradation. The fluorescent TAP platform was also used to re-evaluate TAP stability in the presence of other known viral TAP inhibitors, among which only UL49.5 was able to reduce TAP levels. Finally, we provide evidence that BoHV-1 UL49.5-induced TAP removal is p97-dependent, which indicates its degradation via endoplasmic reticulum-associated degradation (ERAD).

1. Introduction

The co-existence of a host and a virus depends on a subtle balance between the pathogen replication and the host immune response. Virus-derived peptides, originating mainly from the proteasomal degradation, are presented by the major histocompatibility complex class I (MHC I) molecules, leading to the recognition of an infected cell by cytotoxic $CD8^+$ T lymphocytes (CTLs) (reviewed in [1]). The transporter associated with antigen processing (TAP) plays a pivotal role in MHC I-restricted antigen presentation, which makes it an attractive target for viruses that aim to escape the immune system.

TAP is a heterodimer belonging to the ATP-binding cassette (ABC) family transporters. It consists of two subunits, TAP1 (ABCB2) and TAP2 (ABCB3) [2]. The core of each subunit is formed by an N-terminally-located transmembrane domain (TMD), composed of six transmembrane helices (TMs), responsible for peptide recognition and binding [3], and a highly conserved C-terminal nucleotide-binding domain (NDB), which can bind and hydrolyze ATP [4]. Acquiring both substrates, ATP and the peptide, occurs independently [3]. This induces conformational rearrangements within TAP, resulting in a switch from an inward-open to an outward-facing conformation and release of the peptide into the lumen of endoplasmic reticulum (ER). Afterward, ATP hydrolysis triggers the release of phosphate and restores the resting state of TAP [5]. The presence of core-flanking TMD0 domains (four TMs in TAP1 and three TMs in TAP2) at the N termini of TAP1/TAP2 is not necessary for peptide transport; however, it is crucial for assembly of the peptide-loading complex (PLC) and subsequent exposure of antigenic peptides to CTLs [6].

During co-evolution with their hosts, several herpesviruses and a single known (to date) poxvirus have specialized in TAP inhibition via diverse mechanisms (reviewed in [7]). Herpes simplex virus 1 and 2 (HSV-1 and HSV-2) encode the ICP47 protein, which competes for the peptide-binding site and, through its characteristic structure, tethers the TAP-ICP47 complex in an inward-facing conformation [8–10]. In contrast, the US6 protein of human cytomegalovirus (HCMV) [11–13] and the cowpox virus (CPXV) strain Brighton Red-encoded CPXV012 protein can inhibit ATP binding to NDBs while leaving peptide binding unaffected [14–16]. Mechanisms of TAP inhibition by herpesvirus UL49.5 protein family encoded by members of the *Varicellovirus* genus are still not fully understood and seem to differ in detail between virus species. Most of the UL49.5 orthologs inhibit conformational rearrangements within TAP [17]. Bovine herpesvirus 1 (BoHV-1) UL49.5 seems to be unique in its ability to target bovine, human, and murine TAP for proteasomal degradation following the conformational arrest [7,18,19]. Varicella-zoster virus (VZV)-encoded UL49.5 can bind TAP, yet it exhibits no inhibitory properties [20]. TAP degradation activity was also described for the murine gammaherpesvirus-68 MK3 protein [21] and the rodent herpesvirus Peru

pK3 ortholog [22], which both carry a cytoplasmic RING (really interesting new gene) finger domain and can act towards the murine transporter. The recently described poxvirus molluscum contagiosum virus MC80 protein can destabilize human TAP; however, in contrast to BoHV-1 UL49.5, the transporter is not the primary target of the inhibitor [23].

Recently, fluorescent tags and gene fusion technology have become indispensable in a wide range of biochemical and cell biology applications, nevertheless in some circumstances designing a functional fluorescent fusion protein remains challenging. Numerous studies have shown that a choice of a linker may have a significant impact on proper folding, yield, and functionality of the fusion protein and its interaction with other proteins. Flexible linkers are usually applied to provide a certain degree of movement, while rigid linkers are preferable to separate two bioactive domains spatially [24].

To investigate the mechanism of TAP inhibition or removal, a TAP-GFP (green fluorescent protein) fusion protein was instrumental, yet GFP-tagging was observed to abolish the susceptibility of TAP to degradation induced by the BoHV-1-encoded UL49.5 [18]. Here, we report the construction of a series of full-length TAP1 and TAP2 variants carrying either N- or C-terminal GFP with different types of linkers and evaluate the impact of the TAP-GFP fusion design on their fluorescence and functionality, as well as susceptibility to virus-induced inhibition and degradation. Such a fluorescent TAP platform may constitute a platform to explain the molecular mechanism of UL49.5 activity and potentially contribute to better characterization of the transporter itself.

2. Materials and Methods

2.1. Cells and viruses

Madin-Darby bovine kidney (MDBK) cells (ATCC, Manassas, VA, USA, CCL-22), human melanoma Mel JuSo (MJS) cells, MJS TAP1 CRISPR/Cas9 knock-out (TAP1 KO), MJS TAP2 CRISPR/Cas9 knock-out (TAP2 KO) [25], and U937 (ATCC, CRL-1593) were cultured in RPMI 1640 (Corning, Corning, NY, USA) supplemented with 10% fetal bovine serum (FBS, Thermo Scientific, (Thermo Scientific, Waltham, MA, USA,)) and Antibiotic Antimycotic Solution (Thermo Scientific). Lenti-X HEK293T and GP2-293 cells (both from Takara/Clontech, Kusatsu, Japan) used for lentivirus and retrovirus production, respectively, were cultured in Iscove's modified Dulbecco's medium (IMDM, Lonza, Basel, Switzerland) supplemented as above. HEK293T (ATCC, CRL-3216) cells were cultured in Dulbecco's modified Eagle's medium (DMEM, high glucose, Lonza) supplemented as above. BoHV-1 field strain Lam (Institute for Animal Health and Science, Lelystad, the Netherlands) was propagated and titrated on MDBK cells.

2.2. DNA constructs

All TAP constructs were cloned in lentiviral vectors downstream of an EF1α promoter.

For unmodified (wild-type, wt) TAP1 or TAP2 reconstitution, dual promoter lentiviral vectors described in [25] (pPuroR-GFP-TAP1 and pZeoR-mAmetrine-TAP2) were used. mAmetrine and marker GFP genes were removed from these vectors. Fragments of TAP1 and TAP2 sequences were ordered as synthetic genes designed for cloning in pEGFP-N3 or pEGFP-C1 (Takara/Clontech). For TAP1-N-GFP (TAP1 with the N-terminal GFP, random linker), TAP1-C-GFP (TAP1 with the C-terminal GFP, random linker), TAP2-N-GFP (TAP2 with the N-terminal GFP, random linker), and TAP2-C-GFP (TAP2 with the C-terminal GFP, random linker), fusion genes were re-cloned in the original lentiviral vectors. The amino acid sequences of random linkers resulting from the cloning procedure are depicted in Figure 1A. Fragments coding for TAP1 with helical linker sequences were ordered as synthetic genes designed for cloning in pEGFP-N3 or pEGFP-C1. TAP1-HN-GFP (TAP1 with the N-terminal GFP, helical linker) or TAP1-HC-GFP (TAP1 with the C-terminal GFP, helical linker) were re-cloned in the lentiviral vector pCDH-EF1α-MCS-(PGK-Puro) (System Biosciences, Palo Alto, CA, USA).

Genes coding for viral TAP inhibitors were cloned in retroviral vectors downstream of a retroviral promoter. The BoHV-1 UL49.5 gene was cloned from pLZRS-BoHV-1 UL49.5-IRES-GFP [18] in BamHI-EcoRI sites of pLZRS-IRES-ΔNGFR [26]. The VZV UL49.5 gene was amplified from the pLZRS-VZV UL49.5-IRES-GFP vector [20] using KOD Hot Start DNA polymerase (Merck, Darmstadt, Germany) and the following primers: forward 5′-CGGGATCCCACCATGGGATCAATTACC-3′ and reverse 5′-CCGGAATTCTTACCACGTGCTGCGTAATAC-3′. The PCR product was verified by DNA sequencing and introduced into BamHI and EcoRI sites of the pBABEpuro vector [27]. Synthetic genes encoding: myc-tagged HSV-1 ICP47 (Gene ID: 2703441), myc-tagged HCMV US6 (Gene ID: 3077555), or the FLAG-N-CPXV012 (Gene ID: 1485887) variantlacking six N-terminal amino acid residues [28] were introduced into BamHI and EcoRI restriction sites of pBABEpuro.

2.3. Retroviral and lentiviral transduction

For the production of recombinant lentiviruses, third-generation packaging vectors based on the pRSV-Rev and pCgpV plasmids (Cell Biolabs, San Diego, CA, USA), the obtained lentiviral expression vectors, and pCMV-VSV-G (Cell Biolabs) for pseudotyping were co-transfected into Lenti-X HEK293T cells using CalPhos mammalian transfection kit (Takara/Clontech). For recombinant retroviruses, a transfer plasmid (pBABEpuro-based or pLZRS-

IRES-ΔNGFR-based) and pCMV-VSV-G were co-transfected into GP2-293 packaging cells as above. Twenty-four hours after transfection the medium was refreshed; for lentiviruses it was supplemented with 1 mM sodium butyrate (Sigma-Aldrich, Saint Louis, MO, USA). Virus-containing supernatants were collected after 48 h, concentrated with PEGit (System Biosciences), and used for transduction in the presence of 0.01 mg mL^{-1} polybrene (Sigma-Aldrich). MJS cells with TAP1 or TAP2 knock-outs were stably reconstituted with the wt or fluorescent TAP1 or TAP2 constructs using lentivirus vectors and cell-sorting for GFP- and MHC I-positive cells. The cells were subsequently transduced with a retrovirus coding for BoHV-1 UL49.5 and sorted for nerve growth receptor (NGFR)-positive cells or with a retrovirus coding for HSV-1 ICP47, HCMV US6, VZV UL49.5, or CPXV012, and selected with puromycin (2 µg mL^{-1}) (Sigma-Aldrich).

2.4. Plasmid transfection

HEK293T cells were transfected with plasmids encoding fluorescent TAP variants using JetPRIME (Polyplus-transfection, Illkirch, France) according to the manufacturer's protocol and analyzed after 24 h by flow cytometry.

2.5. Generation of TAP1/TAP2 double knock-out U937 cells for Reconstitution with fluorescent TAP variants

U937 TAP1/TAP2 KO cells were generated with a strategy described for MJS TAP1/TAP2 KO in [25] Briefly, U937 cells were transfected with pSico-CRISPR-PuroR containing the TAP2-targeting crRNA sequence 5'-GGAAGAAGAAGGCGGCAACG-3'. The cells were selected with puromycin (4 µg mL^{-1}), and cloned by limiting dilution. Individual clones were analyzed by flow cytometry to identify clones with low cell surface MHC I expression, followed by immunoblotting and DNA sequencing of the genomic target site. A clone lacking TAP2 was subsequently transfected with a pSicoR-CRISPR-PuroR vector containing the TAP1-targeting crRNA sequence 5'-GGGGTCCTCAGGGCAACGGT-3'. After selection with puromycin and cell cloning, the clones were analyzed for TAP1 expression by immunoblotting and DNA sequencing of the genomic target site. Genomic DNA sequence analysis revealed a 16-bp deletion around the TAP2 gRNA target site and multiple short deletions altering the whole TAP1 gene sequence downstream of the target site. A monoclonal cell line lacking TAP1 and TAP2 was used for reconstitution with a combination of unmodified and fluorescent TAP-encoding sequences delivered by lentivirus vectors. Reconstituted U937 cells were sorted for GFP and high MHC I expression. The cells were subsequently transduced with the BoHV-1 UL49.5-encoding retrovirus and sorted for NGFR.

2.6. Antibodies

Antibodies used for immunoblotting: mouse anti-TAP1 monoclonal antibody MAb 143.5 (kindly provided by R. Tampé, Institute of Biochemistry, The Johann Wolfgang Goethe University, Frankfurt, Germany); mouse anti-TAP2 MAb 435.3 (a kind gift from P. van Endert, INSERM U25, Institute Necker, Paris, France); rabbit anti-TAP1 (Enzo Life Sciences, Farmingdale, NY, USA); rat anti-GFP 3H9 (Chromotek, Planegg, Germany); mouse anti-myc tag 9B11 (Cell Signaling, Danvers, MA, USA); rabbit anti-β-actin (Novus Biologicals, Centennial, CO, USA); rabbit anti-β-catenin (Santa Cruz Biotechnology, Dallas, TX, USA); rabbit antibodies (H11) against a synthetic peptide derived from the N-terminal domain of BoHV-1 UL49.5 [26] and mouse anti-OctA (FLAG) G-8 (Santa Cruz Biotechnology); and mouse anti-HC10 [19] and rabbit anti-ERp57 H-220 (Santa Cruz Biotechnology). Probes used for immunofluorescence: Alexa 633-conjugated concanavalin A (ConA) (Thermo Scientific). Antibodies used for flow cytometry: mouse anti-MHC I W6/32 (Novus Biologicals); mouse anti-NGFR (Sigma-Aldrich); and Alexa 633-conjugated goat anti-mouse IgG (Thermo Scientific).

2.7. Flow cytometry

Cell surface expression of MHC I was determined by indirect immunofluorescence using primary anti-MHC I antibodies (1:1000) and secondary antibodies (1:1000), all in phosphate buffered saline (PBS) buffer containing 1% bovine serum albumin and 0.02% sodium azide. For cell sorting, anti-NGFR antibodies (1:1000) and secondary antibodies were used. Cells were analyzed using a FACS Calibur flow cytometer (Becton Dickinson, Franklin Lakes , NJ, USA) and CellQuest software (version 5.2.1, Becton Dickinson)); for cell sorting, the sorting option of FACS Calibur was applied.

2.8. Immunoblotting and immunoprecipitation

For immunoblotting, the cells were lysed in Cell Lytic M buffer (Sigma-Aldrich); for immunoprecipitation, the cells were lysed in a buffer containing 1% digitonin (Merck), 50 mM Tris-HCl, pH 7.5, 5 mM $MgCl_2$, and 150 mM NaCl. The buffers were supplemented with the cOmplete mini protease inhibitor cocktail (Roche, Basel, Switzerland). Cell lysates were analyzed by SDS-PAGE and immunoblotting as previously described [26] or incubated with GFP-Trap (Chromotek) according to the manufacturer's protocol to isolate protein complexes.

2.9. Peptide transport assay

The peptide transport assay was performed as described before [26]. Briefly, the cells were permeabilized with 2 IU ml^{-1} of Streptolysin O (Sigma-Aldrich) at 37 °C for 15 min. The cells (2×10^6 cells/sample) were subsequently incubated with 600 pmol of the fluorescein-conjugated synthetic peptide CVNKTERAY (JPT Peptide Technologies, Berlin, Germany) in the presence or absence of ATP (10 mM final concentration) at 37 °C for 10 min. Peptide translocation was terminated by adding 1 mL of ice-cold lysis buffer containing 1% Triton X-100. After 20 min of lysis, cell debris was removed by centrifugation, and supernatants were collected and incubated with 100 µL of concanavalin A (ConA)-Sepharose (Sigma-Aldrich) at 4 °C for 1 h to isolate the glycosylated peptides. After extensive washing of the beads, the peptides were eluted with elution buffer (500 mM mannopyranoside, 10 mM EDTA, 50 mM Tris-HCl, pH 8.0) by rigorous shaking for 1 h at 25 °C. Eluted peptides were separated from ConA by centrifugation at 12,000× *g*. The fluorescence intensity was measured using a fluorescence plate reader (EnVision, PerkinElmer, Waltham, USA) with excitation and emission wavelengths of 485 nm and 530 nm, respectively.

2.10. Immunofluorescence

MJS cells were grown on microcover glass, fixed with 4% paraformaldehyde in PBS, permeabilized with 0.2% Triton X-100 in PBS, and stained with Alexa 633-ConA (1:1000), prepared in PBS containing 1% bovine serum albumin (Sigma-Aldrich). GFP booster (1:100, Chromotek) was used for MJS-TAP2-C-GFP to enhance the green fluorescence. The blue signal was electronically converted into the red during the analysis of images using Leica TCS SP8X confocal laser scanning microscope (Leica, Wetzlar, Germany).

3. Results

3.1. Construction and characterization of fluorescent TAP-GFP variants

In order to develop a universal fluorescent platform for virus-induced TAP degradation, we constructed six versions of TAP-GFP fusion: four with two types of linkers, a random linker or a helical one, placed at the N- or C-terminus of TAP1, and two with a random linker at the N- or C-terminus of TAP2 (Figure 1A). A number of studies regarding fusion protein linker design have suggested that the most important features of a proper linker are its hydrophilicity and flexibility [24]. The random linkers used to join TAP and GFP have resulted from the cloning procedure into one of the pEGFP plasmid series. The analysis of their amino acid sequence revealed they were unstructured; thus, they should be more flexible. In some cases, flexible linkers may result in undesired interactions or interference

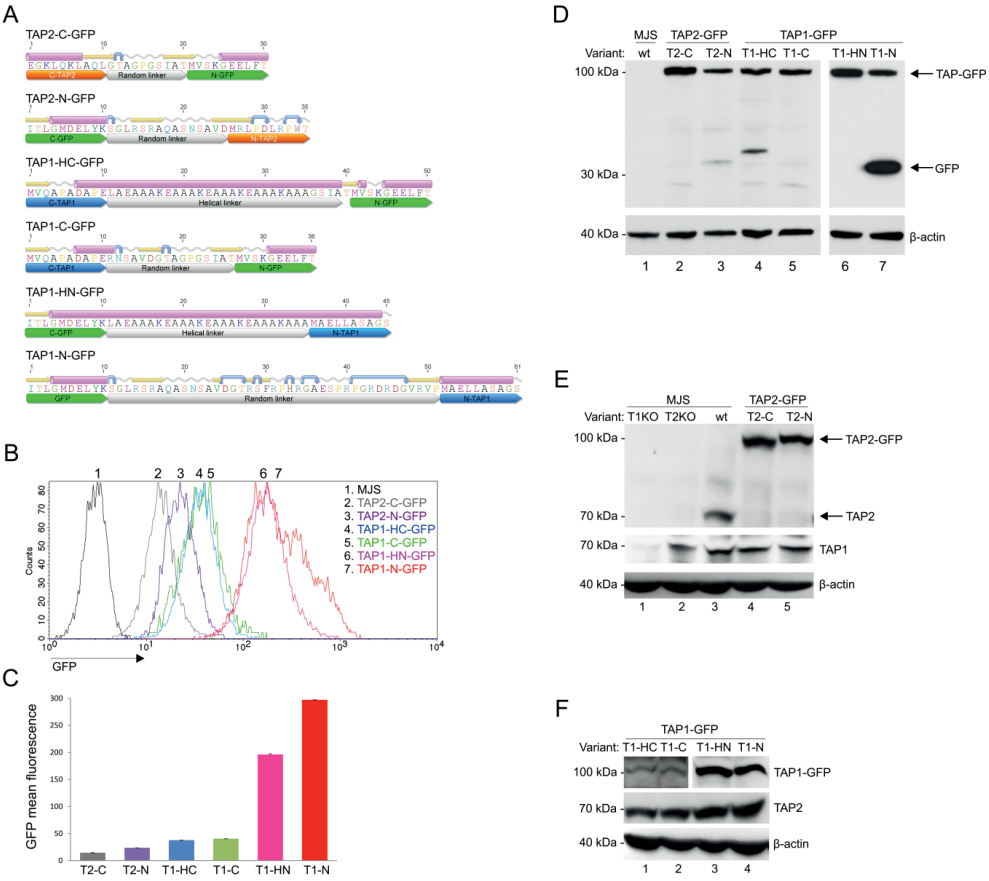

Figure 1: Construction and characterization of fluorescent transporter associated with antigen processing (TAP)-green fluorescent protein (GFP) variants. Mel JuSo (MJS) cells with CRISPR/Cas9 TAP1 or TAP2 knockouts (T1KO, T2KO) were stably reconstituted with fluorescent TAP1 or TAP2 constructs using lentivirus vectors and cell sorting. (A) Schematic representation of TAP-GFP constructs. Secondary structures of linkers flanked by ten amino acid residues of fused proteins were determined by the Geneious software; α-helices are depicted in pink, coiled regions in gray, β-strands in yellow, and turns in blue. (B) Representative histograms of TAP-GFP fluorescence intensity. (C) Comparative TAP-GFP analysis by flow cytometry. The mean fluorescence intensity of three independent measurements is represented as bars with standard deviations. The statistical significance was assessed by t-test; $p \leq 0.001$. (D–F) Expression of TAP-GFP variants in stable cell lines was determined by SDS-PAGE and immunoblotting using: (D) anti-GFP monoclonal antibody (Mab) (E) anti-TAP2 MAb (F) anti-TAP1 MAb. β-actin was used as a loading control. Abbreviations: T2-C: TAP2-C-GFP (TAP2 with the C-terminal GFP, random linker); T2-N: TAP2-N-GFP (TAP2 with the N-terminal GFP, random linker); T1-C: TAP1-C-GFP (TAP1 with the C-terminal GFP, random linker); T1-HC: TAP1-HC-GFP (TAP1 with the C-terminal GFP, helical linker); T1-N: TAP1-N-GFP (TAP1 with the N-terminal GFP, random linker); T1-HN: TAP1-HN-GFP (TAP1 with the N-terminal GFP, helical linker)

between the fusion partners. In such cases, rigid linkers are preferable to separate two independently active domains spatially. An example of a rigid linker is the α helix-forming peptide AEAAAKEAAAKEAAAKA, stabilized by salt bridges between glutamate and lysine residues [29]. The distance between two separated domains can be regulated by changing the number of EAAAK motif repetitions. By using fluorescence resonance energy transfer (FRET) measurement, the helical linker with four repetitions of this motif has been demonstrated as the most efficient in separating two fluorescent proteins [30]. Therefore, this linker was selected for our studies to generate N- and C-terminal fusion of TAP1 and GFP. To introduce fluorescent TAP-GFP into human melanoma MJS cells, we first generated, by using CRISPR/Cas9-based technology, TAP1 or TAP2 knock-outs (KO). This enabled stable reconstitution of the cells with a fluorescent TAP1 or TAP2 using lentiviral vectors. The cells were subsequently sorted based on GFP to high purity (>98%). MJS cells have been shown to be permissive for BoHV-1 infection and are widely used in the research on modulation of antigen presentation by viruses [31–33].

First, we analyzed the GFP fluorescence intensity of our constructs (Figure 1B,C). Flow cytometry analysis revealed that N-terminal fusions of GFP to TAP1 exhibited the highest fluorescence, followed by TAP1 C-terminal fusion constructs. The type of linker seemed to have no crucial impact on the fluorescence intensity, although, for TAP1-N-GFP, a population of brighter green fluorescent cells could be observed when compared to TAP1-HN-GFP. TAP2 constructs exposed the lowest fluorescence, with a similar tendency of N-terminal fusion outperforming the C-terminal one. In addition, for TAP1-N-GFP, we

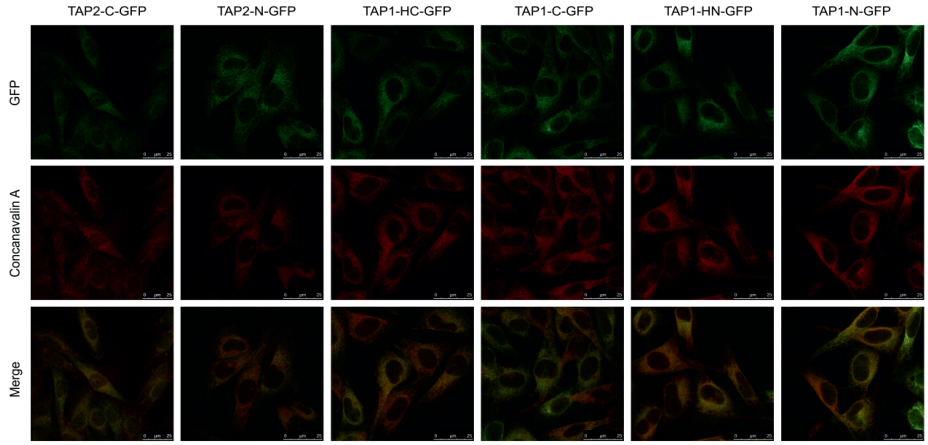

Figure 2: TAP-GFP variants demonstrate endoplasmic reticulum (ER) localization. MJS cells reconstituted with TAP-GFP variants were fixed, permeabilized, and stained with Alexa 633-conjugated concanavalin A (ER marker). Colocalization with GFP was analyzed using fluorescent confocal microscopy. For MJS TAP2-C-GFP, the GFP booster was used to enhance very weak green fluorescence.

could observe a more heterogeneous distribution of GFP fluorescence than for the other variants.

During the transient expression of fluorescent constructs in plasmid-transfected HEK293T cells, we could observe a similar range of GFP fluorescence, which indicates that differences in GFP fluorescence depend on the properties of individual fusion proteins rather than result from random incorporation of a lentivirus into a host genome (Figure S1). TAP2-C-GFP was performing noticeably better in transfected HEK293T than in the stable MJS cell line, and this time TAP1-HN-GFP slightly outperformed TAP1-N-GFP.

Next, we characterized the expression of TAP-GFP constructs by SDS-PAGE and immunoblotting. TAP1 and TAP2 have a similar apparent molecular mass of approximately 75 kDa. The fusion to GFP should yield a single protein at 100 kDa. All constructs were detected in cell lysates with anti-GFP antibodies at the predicted molecular weight of 100 kDa; only for TAP1-N-GFP did we observe an additional 30-kDa band corresponding to, most probably, cleaved free GFP or cleaved TAP-GFP fragment (Figure 1D). Fluorescent TAP could also be detected with anti-TAP1 or anti-TAP2 antibodies (Figure 1E,F). The reconstitution of TAP1KO cells with a fluorescent variant of TAP1 resulted in increased stability of endogenous TAP2 as it could be detected in higher amounts than in TAP1KO cells (compare lane 1 in Figure 1E with lanes 1–4 in Figure 1F). This is in agreement with a previous study reporting that unlike TAP1, TAP2 is unstable when expressed without the other half of the transporter [34]. The higher sensitivity of TAP2 can most probably explain why no band corresponding to TAP2 could be identified in MJS TAP1KO cells (Figure 1E, lane 1), while TAP1 could be easily detected in MJS TAP2KO cells (Figure. 1E, lane 2).

3.2. TAP-GFP localizes in the ER and forms a functional transporter

TAP localizes in the cells predominantly in the ER [35]. To assess if the fluorescent TAP constructs acquired their proper localization, we stained the cells with Alexa 633-conjugated concanavalin A (ConA), an ER-cis Golgi marker, and analyzed fluorescence distribution by confocal laser scanning microscopy (Figure 2). In all cell lines, TAP-GFP (green) localized predominantly in the ER (red), as it co-localized with the ER marker (yellow). No granular localization patterns that would indicate TAP aggregates could be visualized.

Based on the currently available evidence, a lack of at least one fully functional TAP subunit results in a suppressed peptide translocation and production of empty or suboptimally loaded unstable MHC I molecules, mostly retained in the ER [36]. GFP fusion could potentially affect TAP structure and activity. Therefore, the functionality of fluorescent TAP

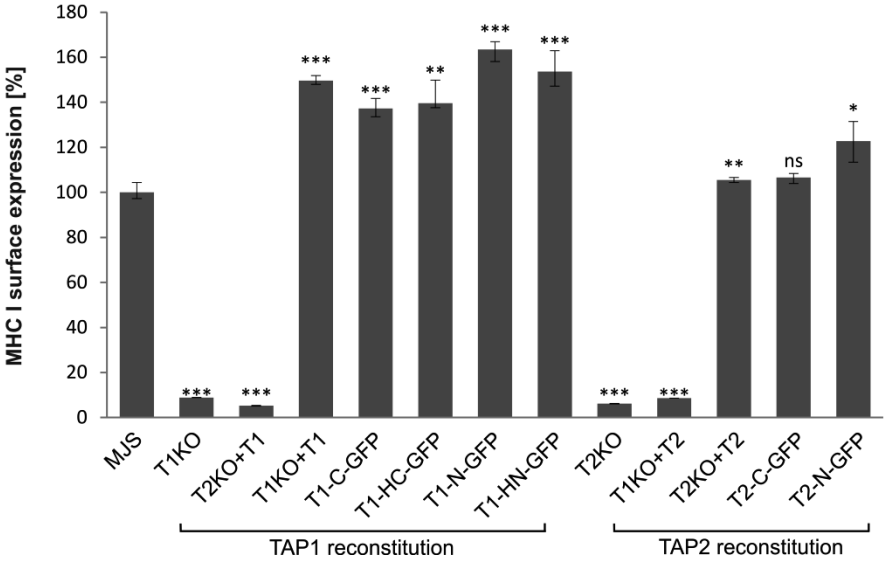

Figure 3: TAP-GFP forms a functional transporter. MJS cells with CRISPR/Cas9 TAP1 or TAP2 knockouts (T1KO or T2KO) were stably reconstituted with wild-type or fluorescent TAP1 or TAP2 variants. Surface expression of major histocompatibility complex class I (MHC I) was assessed by flow cytometry using specific antibodies (W6/32). MHC I expression on MJS cells with TAP reconstitution is presented as the percentage of MHC I mean fluorescence intensity on MJS cells (set as 100%). The analysis was performed in triplicates. The statistical significance of differences between MHC I on MJS cell with TAP reconstitution and MJS wild-type (wt) cells was estimated by t-test; *** $p \leq 0.001$, ** $p \leq 0.01$, * $p \leq 0.05$, ns: not significant.

constructs was tested by measuring cell surface expression of MHC I by flow cytometry (Figure 3). As expected, MJS cells with TAP1KO or TAP2KO exhibited strongly reduced levels of MHC I. To have a proper control for testing the effect of fluorescent tagging on TAP performance, especially during overexpression of a TAP subunit, we generated control cell lines reconstituted with unmodified TAP subunits (MJS TAP1KO + TAP1 and MJS TAP2KO + TAP2). Overexpression of individual TAP subunits might result in the formation of their homodimers, affecting the interpretation of our further experiments [19,37]. Therefore, as an additional control, we transduced TAPKO cells with vectors enabling overexpression of the existing half-transporter (MJS TAP1KO + TAP2 and MJS TAP2KO + TAP1). As expected, MHC I surface levels were reduced in those cells to a similar extent as in TAP1KO or TAP2KO cells. On the other hand, reconstitution of the missing TAP subunit with its fluorescent variant rescued surface MHC I to levels slightly higher than on parental ("wild-type") MJS cells, but similar to the ones observed on the cells reconstituted with the non-fluorescent TAP.

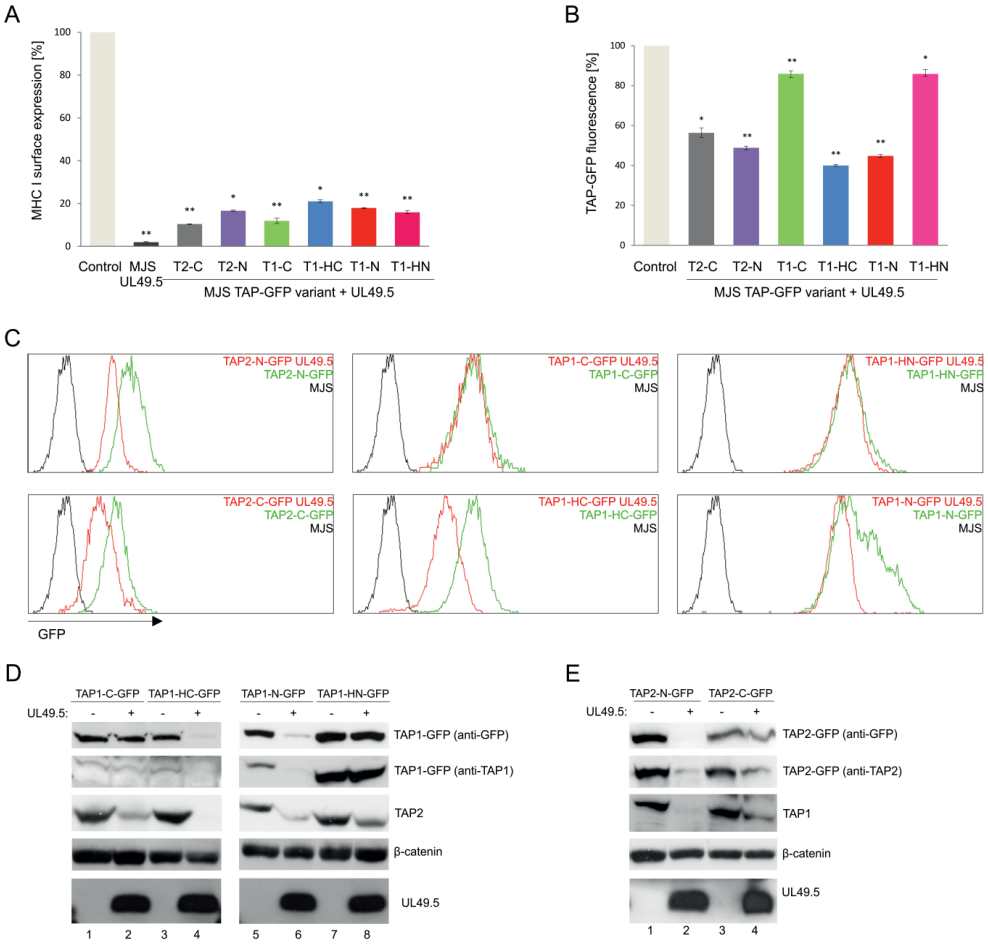

Figure 4: TAP-GFP variants differ in their sensitivity to UL49.5-mediated inhibition and degradation. MJS cells with fluorescent TAP1 or TAP2 variants were transduced with a retrovirus encoding bovine herpesvirus 1 (BoHV-1) UL49.5. (A) Surface expression of MHC I was assessed by flow cytometry using specific antibodies (W6/32). MHC I expression is presented as the percentage of mean fluorescence intensity; fluorescence of parental cells without UL49.5 was set as 100%. The analysis was performed in triplicates. The statistical significance of differences between MJS TAP-GFP and MJS TAP-GFP UL49.5 cell lines was estimated by t-test; ** $p \leq 0.001$ * $p \leq 0.005$. (B) GFP mean fluorescence intensity is presented as the percentage of GFP fluorescence of parental cells (set as 100%). The analysis was performed in triplicates. The statistical significance of differences between MJS TAP-GFP and MJS TAP-GFP UL49.5 cell lines was estimated by t-test; ** $p \leq 0.001$ * $p \leq 0.005$. (C) The effect of UL49.5 on GFP level in MJS TAP-GFP cells was assessed by flow cytometry. (D,E) Degradation of TAP-GFP variants in the presence of BoHV-1 UL49.5 in stable cell lines was determined by SDS-PAGE and immunoblotting using: anti-GFP, anti-TAP1, anti-TAP2, or anti-UL49.5 antibodies. β-catenin was used as a loading control.

3.3. The sensitivity of TAP-GFP variant to UL49.5-Mediated MHC I downregulation and TAP degradation

To examine the sensitivity of fluorescent TAP to BoHV-1-encoded UL49.5-mediated inhibition, UL49.5 was introduced to stable cell lines with TAP-GFP variants using a retrovirus vector. The cells were subsequently sorted for high purity based on the expression of truncated NGFR as a marker, and analyzed by flow cytometry for surface expression of MHC I (Figure 4A). According to the obtained data, all fluorescent transporters were prone to UL49.5-induced inhibition, which was illustrated as the downregulation of MHC I, to a similar extent for all the tested variants.

Next, we analyzed the susceptibility of TAP-GFP variants to UL49.5-triggered degradation (Figure 4B,C). Flow cytometry analysis revealed a reduction of GFP mean fluorescence intensity by approximately 50% in the cells co-expressing UL49.5 with TAP1-N-GFP, TAP1-HC-GFP, and both TAP2 variants, in comparison to the control cells expressing the fluorescent transporter without UL49.5. There were no significant changes in GFP fluorescence observed in the cells expressing TAP1-C-GFP or TAP1-HN-GFP with UL49.5.

Susceptibility of TAP1-HC-GFP and TAP2-N-GFP constructs to UL49.5-dependent TAP inhibition and degradation was also confirmed in a reconstituted U937 cell line (Figure S2), where downregulation of surface MHC I, as well as a decrease of mean GFP fluorescence to the similar extent as in MJS cells, could be denoted.

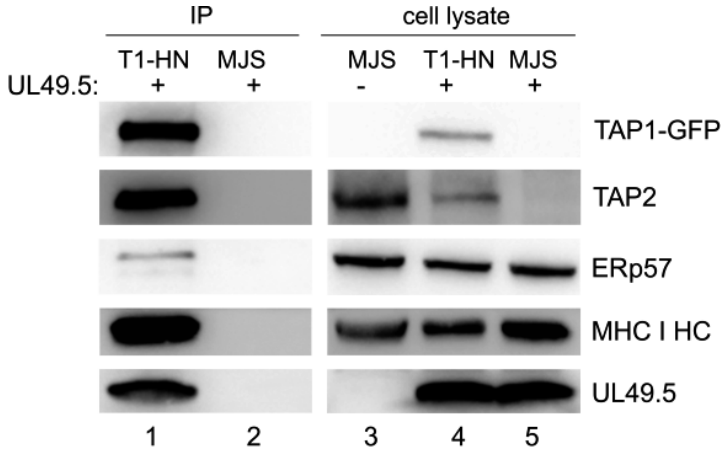

Figure 5: TAP1-GFP interacts with UL49.5 and the peptide-loading complex. TAP1-HN-GFP (T1-HN) was immunoprecipitated by GFP-Trap from lysates of MJS cells expressing TAP1-HN-GFP and UL49.5 or wt MJS with UL49.5 only. Co-precipitating proteins were analyzed by SDS-PAGE and immunoblotting using antibodies against GFP, TAP2, ERp57, MHC I HC, and UL49.5. Right panel: cell lysates were loaded on SDS-PAGE directly and analyzed by immunoblotting.

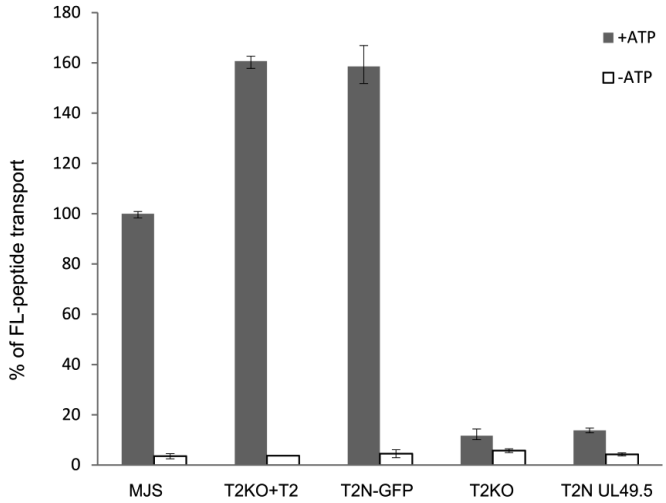

Figure 6: UL49.5-induced inhibition of peptide transport. MJS cells with CRISPR/Cas9 TAP2 knockout (T2KO) were stably reconstituted with wild-type TAP2 (T2KO+T2) or fluorescent TAP2 (T2N-GFP), subsequently transduced with a retrovirus encoding BoHV-1 UL49.5, and sorted (T2N UL49.5). Transport activity of TAP was analyzed using fluorescein-labeled peptide CVNKTERAY in the presence of ATP (gray bars) or EDTA (white bars). Peptide transport is expressed as a percentage of translocation, relative to the translocation observed in control MJS cells (set at 100%). The experiment was performed in triplicates. The statistical significance of differences between MJS controls and reconstituted or KO variants was estimated by t-test; for all the samples $p \leq 0.005$.

To verify if changes in GFP fluorescence correspond with the decreased TAP protein level, immunoblotting analysis of cell lysates was performed (Figure 4D,E). A similar level of BoHV-1 UL49.5 protein could be observed in all cell lines. Decreased amounts of TAP1-N-GFP, TAP1-HC-GFP, and both TAP2-GFP fusion proteins could be detected in the presence of UL49.5, with the use of both anti-GFP and specific anti-TAP antibodies. Of note, in the case of non-degradable fluorescent TAP1 constructs (TAP1-HN-GFP and TAP1-C-GFP), the level of endogenous TAP2 was decreased (compare TAP2 in Figure 4D in lanes 1–2 and 5–6), what may suggest partial degradation of the untagged TAP subunit only. Degradation in TAP1-HC-GFP and TAP2-N-GFP cell lines was observed for both, exogenous fluorescent and endogenous TAP subunits. TAP1-N-GFP and TAP2-C-GFP characterized with only partial degradation.

3.4. Interaction of TAP-GFP with UL49.5 and the Peptide-Loading Complex

To assess the interaction of a non-degradable TAP with BoHV-1-encoded UL49.5 and selected components of PLC, we chose the TAP1-HN-GFP construct as demonstrating high expression. Among proteins co-immunoprecipitating with the fluorescent transporter (using GFP-Trap), we could identify UL49.5 and endogenous TAP2, as well as the known

components of PLC: MHC I heavy chain and ERp57 (Figure 5). These results highlight the fact that UL49.5 is still capable of interacting with the non-degradable TAP1-HN-GFP. Unspecific binding of UL49.5 was excluded by immunoprecipitation from MJS wt cell lysate (with unmodified TAP) expressing UL49.5.

3.5. Application of the TAP2-N-GFP variant as a platform to study BoHV-1 UL49.5 activity in virus-infected cells

In the more detailed studies on our fluorescent TAP platform, we focused on a single TAP-GFP variant, selecting TAP2-N-GFP. TAP1-N-GFP was excluded based on the presence of a free form of GFP. The constructs resistant to UL49.5-triggered degradation were eliminated as well, as was TAP2-C-GFP due to its very week, nearly undetectable basic green fluorescence and only partial degradation in the presence of UL49.5.

First, we confirmed that UL49.5-mediated MHC I downregulation relies on the inhibition of antigenic peptide translocation. TAP transport assay was performed in TAP2-N-GFP MJS cells and TAP2-N-GFP cells expressing UL49.5 or (as controls) in MJS wt, MJS TAP2KO cells, and MJS TAP2KO cells reconstituted with a non-fluorescent TAP2. The assay was based on cytoplasm-to-ER translocation of fluorescein-conjugated substrate peptides,

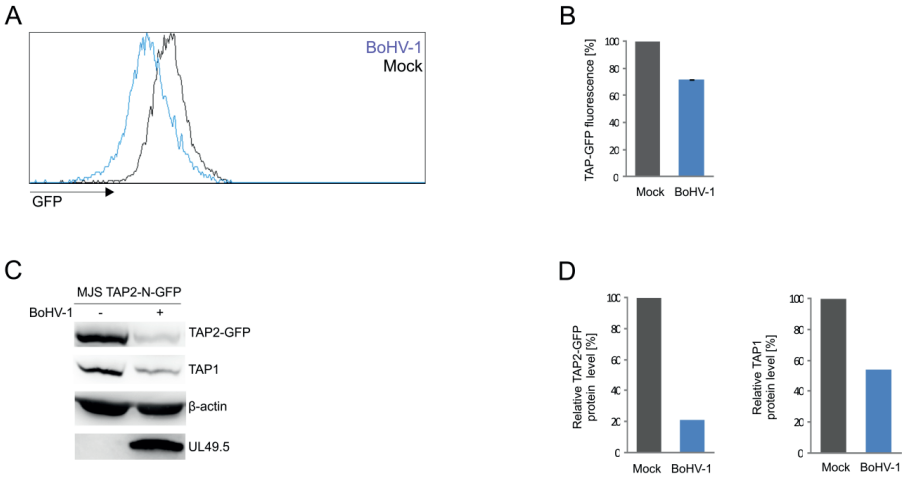

Figure 7: BoHV-1 infection results in TAP2-GFP degradation. MJS TAP2-N-GFP cells were infected with BoHV-1 at a multiplicity of infection (moi) = 10. Twenty-four hours post-infection, cells were collected and analyzed. (A) TAP2-GFP fluorescence was assessed by flow cytometry; histograms from a representative analysis are shown, and (B) depicted as the percentage of fluorescence in mock-infected MJS TAP2-N-GFP cells (set as 100%). The analysis was performed in triplicates. The statistical significance was assessed by t-test; $p \leq 0.0005$ (C) TAP2-GFP degradation was determined by SDS-PAGE and immunoblotting using anti-GFP, anti-TAP1, or anti-UL49.5 antibodies; β-actin was used as a loading control. (D) The relative amount of TAP2-GFP detected by immunoblotting was normalized to β-actin.

in the presence of ATP or EDTA, as a passive diffusion control (Figure 6). Reconstitution with fluorescent TAP restored peptide transport when compared to the parental TAP2KO cells to a level of almost 50% higher than for MJS wt cells. This might result from high expression of exogenous TAP2 as a very similar transport activity was denoted for the non-fluorescent TAP2 reconstitution. The presence of UL49.5 inhibited peptide translocation to the level of TAP2KO cells.

Finally, to test whether we can apply our fluorescent TAP platform to quantify the TAP level during virus infection, we infected MJS TAP2-N-GFP cells with BoHV-1 and analyzed TAP-derived GFP fluorescence by flow cytometry (Figure 7A,B). TAP2-N-GFP and endogenous TAP1 levels were assessed in infected cell lysates by immunoblotting (Figure

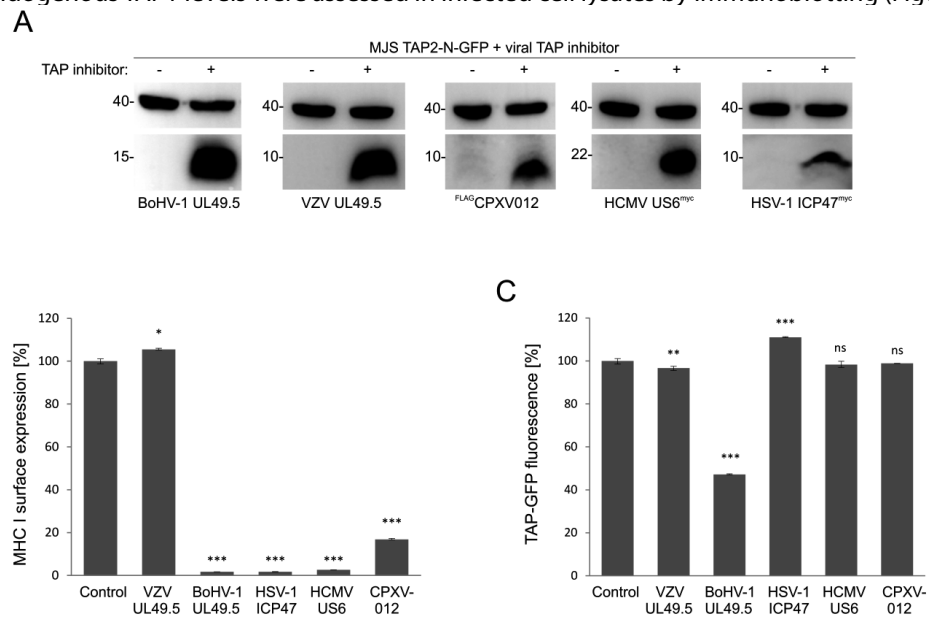

Figure 8: BoHV-1 UL49.5-mediated TAP degradation is unique among viral inhibitors of human TAP. MJS TAP2-N-GFP cells were transduced with a retrovirus encoding BoHV-1 UL49.5, varicella-zoster virus (VZV) UL49.5, human cytomegalovirus (HCMV) US6, herpes simplex virus 1 (HSV-1) ICP47, and cowpox virus CPXV012 and selected with puromycin. (A) The presence of viral TAP inhibitors was confirmed by SDS-PAGE and immunoblotting using anti-β, anti-BHV-1 UL49.5, anti-VZV UL49.5, anti-c-myc for HSV-1 ICP47, and HCMV US6 or anti-FLAG antibodies for CPXV012; β-actin (upper panels) was used as a loading control. Size markers are in kDa. (B) Surface expression of MHC I was assessed by flow cytometry using specific antibodies (W6/32). MHC I expression is presented as the percentage of MHC I on MJS TAP2-N-GFP cells (set as 100%). The analysis was performed in triplicates. The statistical significance of differences between MJS TAP2-N-GFP cells and cells with viral inhibitor was assessed by t-test; *** $p \leq 0.001$ * $p \leq 0.05$. (C) The mean fluorescence intensity of GFP was analyzed by flow cytometry and presented as the percentage of GFP fluorescence of MJS TAP2-N-GFP cells (set as 100%). The analysis was performed in triplicates. The statistical significance of differences between MJS TAP2-N-GFP cells and cells with a viral inhibitor was assessed by t-test; *** $p \leq 0.001$ ** $p \leq 0.01$ ns: not significant.

7C,D). The viral infection resulted in a 30% decrease of mean GFP fluorescence intensity, while approximately 70% and 50% reduction of TAP2-N-GFP and TAP1 protein levels, respectively, could be demonstrated by immunoblotting.

3.6. Only UL49.5 among different viral TAP inhibitors can induce human TAP degradation

The effect of viral TAP inhibitors on TAP stability was reported, usually, in separate studies. TAP levels were analyzed in those reports by immunoblotting. To compare the sensitivity of fluorescent TAP to different viral inhibitors, we selected several representatives with distinct modes of action. Those were: competition for peptide (HSV-1 ICP47) or ATP

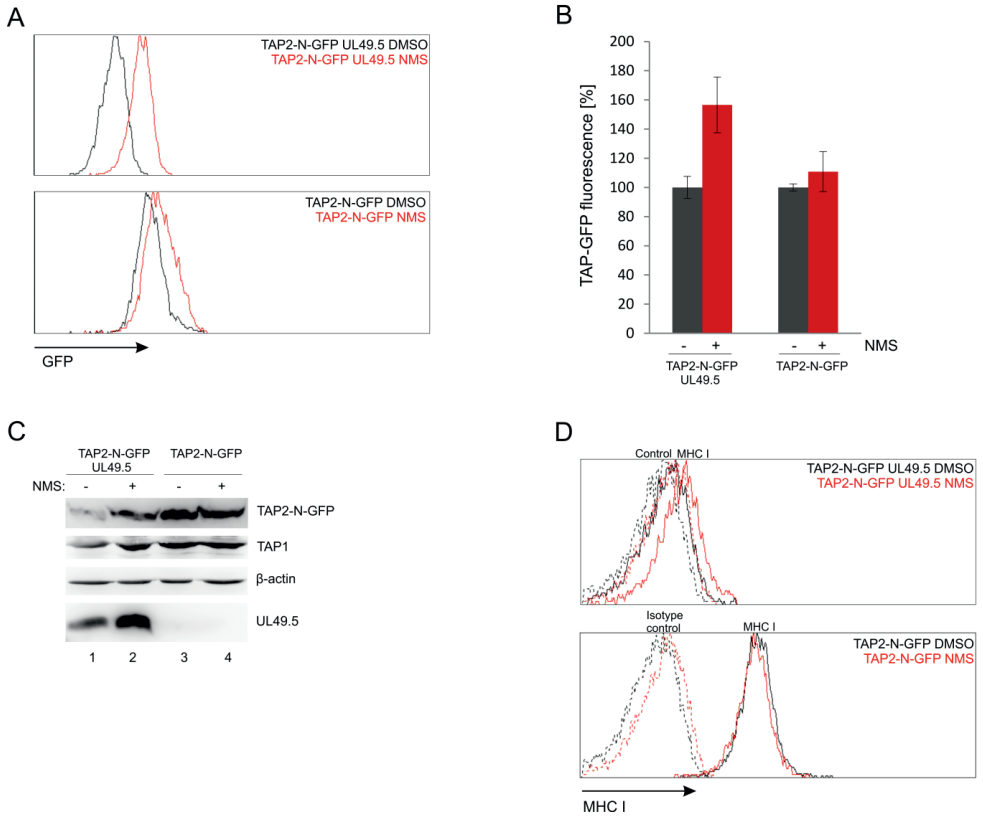

Figure 9. UL49.5 induced TAP-GFP degradation is p97-dependent. MJS TAP2-N-GFP UL49.5 cells were treated with p97 inhibitor NMS-873 (NMS) at 2 μM concentration for 24 hours. (A) Flow cytometry analysis of GFP fluorescence in NMS-treated and control (DMSO-treated) cells. (B) Relative GFP fluorescence in NMS-treated cells calculated as a percentage of GFP fluorescence in the control cells. The analysis was performed in triplicates. (C) The level of TAP-GFP in the presence of p97 inhibitor was determined by SDS-PAGE and immunoblotting using anti-GFP, anti-TAP1 or anti-UL49.5 antibodies; β-actin was used as a loading control. (D) Surface expression of MHC I assessed by flow cytometry using specific antibodies (W6/32).

(HCMV US6 and CPXV012) binding, as well as conformational arrest and degradation (BoHV-1 UL49.5) or a TAP-binding protein with no activity towards the transporter (VZV-encodedUL49.5). MJS TAP2-N-GFP cells were transduced with a retrovirus vector encoding a viral TAP inhibitor and subsequently selected to high purity. The presence of inhibitors was determined by immunoblotting (Figure 8A). Downregulation of MHC I surface expression could be observed during flow cytometry analysis, as expected, for all but the VZV-encoded protein (Figure 8B). Mean GFP fluorescence intensity measurement illustrated that BoHV-1 UL49.5 was unique in causing TAP-GFP degradation. ICP47 even seemed to slightly stabilize TAP-GFP (Figure 8C).

3.7. UL49.5-induced TAP-GFP degradation is p97-dependent

The fluorescent TAP platform can be potentially applied to search for cellular proteins involved in the activity of BoHV-1 UL49.5. According to previous studies, UL49.5-induced TAP degradation is proteasome-dependent [18]. Since TAP is an ER-resident protein, it is presumed to be removed via one of the endoplasmic reticulum-associated degradation (ERAD) pathways. To verify this hypothesis, we used NMS-873 (NMS), an allosteric inhibitor of p97/VCP (valosin-containing protein) a major AAA ATPase belonging to ERAD [38]. MJS TAP2-N-GFP cells with or without UL49.5 were treated with a 2 μM concentration of NMS for 24 h and analyzed by flow cytometry. Inhibition of p97 drastically rescued the mean fluorescence intensity of TAP2 in the presence of UL49.5 to 170% of mean fluorescence intensity in cells treated with DMSO, while in TAP2-N-GFP cells without UL49.5 we could observe only minimal increase to 115% (Figure 9A,B). Compatible results were obtained during immunoblotting analysis of cell lysates (Figure 9C, compare TAP2-GFP in lanes 1–2 and 3–4). Interestingly, inhibition of p97 seemed to stabilize also the expression of UL49.5 (Figure 9C, lanes 1–2). However, apparently, this did not result in a more pronounced TAP-GFP degradation when p97 was blocked.

Next, by using flow cytometry, we determined how inhibition of p97 influences MHC I cell surface expression in the presence (and also absence) of UL49.5. NMS-873-treated cells had only slightly improved surface MHC I levels (Figure 9D). This effect was reminiscent of MHC I levels in the presence of some UL49.5 point mutants, which lost the ability to induce TAP degradation, like, for instance, mutants in the C-terminal RGRG motif [32].

4. Discussion

Quantitative studies on protein stability and degradation may require proper tools and platforms that grant full functionality of the protein of interest and, at the same time, assess the protein levels accurately. Here, we tested the application potential of various

full-length TAP to GFP fusion constructs for the studies on TAP stability in the presence of four inhibiting proteins encoded by viruses, to obtain the most suitable fluorescent TAP platform. All the tested TAP-GFP variants were functional. Nevertheless, our results point toward a critical role of GFP localization on fluorescence intensity of the tagged transporter, which in concert with the type a linker used to separate TAP and GFP may regulate its susceptibility to virally induced degradation. By using this platform, we also provide evidence that BoHV-1 UL49.5-induced TAP degradation is p97-dependent.

In a study on HSV-1 ICP47, a truncated fluorescent TAP complex (the so-called 6+6 transmembrane TAP core C-terminally fused to mVenus or mCerulean) was used to determine the effect of the viral protein on TAP thermostability [39]. However, for the studies on UL49.5, which was our primary protein of interest, the full-length TAP should constitute a better platform, as N-terminal TMD0s are required for maximum efficiency of UL49.5 binding and inhibition [19]. Full-length fluorescent TAP has been successfully used in several basic studies, some of which were to elucidate the association of $H2L^d$ molecules with the TAP complex [40], follow lateral mobility of TAP in living cells [41], or illustrate its cellular distribution [42,43]. In those reports, the addition of a relatively large GFP tag to a much larger multiple membrane-spanning partner protein was tolerated to grant proper localization and functionality of the transporter. However, when exploited in a study on varicellovirus immune evasion, GFP-tagged TAP (C-terminal fusion using a random linker) failed to be degraded by BoHV-1 UL49.5, contrary to non-fluorescent wt TAP [18]. Since BoHV-1-encoded UL45.9 has been, so far, the only known viral inhibitor which can cause human TAP degradation apart from its inhibition, further investigation into this mechanism seemed very intriguing, and for this purpose, construction of fluorescent TAP was instrumental.

Designing an optimal fluorescent TAP construct was hampered by the lack of complete structural information about TAP-UL49.5 interaction, and thus, it required an experimental evaluation of different TAP-GFP variants. The latest structural study on BoHV-1 UL49.5 revealed its 3D structure, while subsequent molecular docking experiments proposed three different possible orientations of TAP-UL49.5 complex in which UL49.5 was suggested to interact simultaneously with both TAP subunits [44]. However, these models were predicted based on the structure of ICP47-arrested TAP conformation [10], and therefore the actual UL45.9-TAP binding model needs to be further confirmed.

Fluorescence analysis of constructed TAP-GFP variants in stable MJS cell lines provides evidence that the tag location, rather than the type of a linker used to separate TAP and GFP, has a pivotal impact on fluorescence intensity. N-terminal fusions generally granted stronger fluorescence (Figure 1B,C and S1). It is worth mentioning here that both ends

of TAP1 are present in the cytoplasm, while TAP2 incorporates its C terminus in the cytoplasm, and the N terminus localizes to the ER lumen [45,46]. Together with the fact that fluorescence of both TAP1 fusions was more intense than of TAP2, our results lead to speculations that it is the structure of both TMD0 and C-terminal NBDs that determines the fluorescent potential of the tagged constructs. For some constructs, especially for TAP1-N-GFP, we could observe additional protein products reacting with GFP-specific antibodies (Figure 1D), which might correspond to cleaved GFP and could also, most probably, explain higher and heterogeneous GFP signal of this construct observed by flow cytometry. The reason for the presence of free GFP in the case of TAP1-N-GFP is not fully understood. The length of this linker exceeds the size of other tested linkers, so it has a higher chance of affecting the stability of the protein. Another explanation might be the presence of a sequence recognized by cellular proteases, but ExPASy PeptideCutter software analysis (https://web.expasy.org/peptide_cutter) did not reveal any significant candidates.

Fluorescent tagging did not affect the subcellular localization and function of the transporter, even upon overexpression of only one TAP subunit (Figures 2 and 3). Both TAP1 and TAP2 lack an N-terminal signal sequence for ER targeting [47], and the exact ER-targeting or ER-retention signals have not been identified to date. This encouraged us to design N-terminal GFP fusions with no additional signaling sequences preceding the tag. The localization of our constructs resembles patterns previously described for other recombinant fluorescent TAP proteins [38–41]. Our results stay in line with the studies on truncated TAP1/TAP2 [43] or functional dissection of transmembrane regions of TAP [6], which have indicated that the transmembrane segments themselves determine ER-localization. It is interesting that even genetically separated TMD0 and the core domains of TAP1 and TAP2 were previously found in the ER (TMD0 additionally localizing to the ER-Golgi intermediate compartment (ERGIC)), when co-expressed [6].

Replacing endogenous TAP1 or TAP2 with TAP-GFP or the untagged subunit restored MHC I on a cell surface equally well and to a level higher than on MJS wt cells (especially in the case of TAP1 constructs). One possible explanation could be the stronger stabilization of endogenous TAP2 by overexpression of TAP1. This effect might be especially noticeable in MJS cells since many melanoma-derived lines have lower endogenous expression of TAP, normally limiting MHC I surface levels [48]. Transduction of MJS TAP1KO or TAP2KO cells with the endogenously present subunit of the transporter did not increase MHC I level, which stays in line with the current view that although TAP1 and TAP2 can form homodimers under certain conditions, they are not functional in antigen presentation [19,35].

One of the most important results of this work provides evidence that all TAP-GFP variants were susceptible to UL49.5-induced inhibition to a similar extent, as assessed by surface MHC I downregulation (Figure 4A). However, only some of them were prone to degradation (both TAP2 fusions, TAP1-N-GFP and TAP1-HC-GFP, Figure 4B,D,E). TAP1-C-GFP remained resistant to UL49.5 what stays in agreement with the previous report [18]. As an interpretation of these data, we can suggest that the helical linker, in contrast to the random one, located at the C terminus of TAP1, effectively separates TAP from GFP to enable undisturbed TAP-UL49.5 interaction, resulting eventually in TAP degradation. Alternatively, it may also permit better access to ERAD components. In the case of the fluorescent TAP2 subunit, the location of GFP, despite the presence of random linkers, did not affect degradation, which could arise from structural differences between the TAP subunits. The TAP2 construct with GFP located in the ER lumen (TAP2-N-GFP) manifested more prominent degradation than the one with GFP in the cytoplasm. An additional observation from this experiment demonstrates that even in the case of a non-degradable fluorescent TAP variant, the second untagged endogenous TAP subunit seems to be sensitive to UL49.5-induced degradation (Figure 4D,E). This, in our opinion, supports the idea of reduced access to ERAD components in TAP1-C-GFP, whereas the access of the second untagged destabilized subunit remains, in this case, undisturbed. It is still unsolved whether UL49.5 can bind single TAP subunits, and the current mechanism points out at the heterodimer as the primary target [19]. As in MJS cells with non-degradable TAP variants, we could observe very efficient MHC I reduction, and the PLC composition in those cells seemed to be intact (Figure 5), at least with regard to the interaction of TAP with ERp57 and MHC I; our data confirm the previous report by [18], demonstrating that abolished degradation does not exclude inhibition. It even seems that TAP degradation might be only an auxiliary event, a "finish-off" effect, in the mechanism of UL49.5 action.

For further studies, we selected and validated TAP2-N-GFP as the most promising variant. TAP transport assay performed on this cell line confirmed that changes in MHC I surface levels reflect TAP transport efficiency (Figure 6). TAP transport in reconstituted cell lines, either with wt or a fluorescent version of the TAP subunit, was higher than in wt MJS. Then we demonstrated that results obtained in a stable cell line model system reflect a situation that occurs upon BoHV-1 infection, which was illustrated as loss of GFP fluorescence observed by flow cytometry and reduction of protein level shown by immunoblotting (Figure 7).

A former pulse-chase experiment with the use of proteasome inhibitor postulated co-degradation of TAP with UL49.5 [18]. In line with this working model, our data show that inhibition of p97 increases levels of both TAP and UL49.5, and demonstrate for the first

time that UL49.5-induced TAP degradation requires functional p97. Most of known ER-resident substrates of this ATPase, which retrotranslocates proteins back to the cytoplasm, are ubiquitinated and targeted for proteasomal degradation [38], indicating that UL49.5 mediated TAP degradation occurs via ERAD.

Finally, the TAP2-N-GFP construct was verified as a platform for different viral TAP inhibitors, representing distinct mechanisms of transport inhibition and, most probably, binding another TAP conformation [28,39,49]. BoHV-1, HSV-1, and HCMV-encoded proteins were capable of drastic reduction of surface MHC I; CPXV012 contributed to a slightly weaker but still significant downregulation of MHC I, whereas VZV UL49.5, as expected, did not cause any changes. In terms of degradation, only BoHV-1 UL49.5 was able to decrease TAP-GFP levels, while ICP47 seemed even to stabilize TAP, which is in accordance with its reported effect on TAP thermostability. We believe that the fluorescent TAP platform provides more quantitative data in this respect when compared to previous immunoblotting analyses, which generally are more technically error-prone.

5. Conclusions

In this study, we were able to validate the application potential of fluorescent TAP as a platform for viral immune evasion studies. Our results indicate TAP-GFP variants susceptible to BoHV-1 UL49.5-induced degradation, demonstrate that this degradation is p97-dependent, and emphasize the importance of linker design in fusion protein construction. The fluorescent TAP platform can be now applied in further research on BoHV-1 UL49.5, for instance in the genome-wide search for cellular proteins responsible for UL49.5-induced degradation, where the fluorescent signal can be measured and indicate even small changes in TAP levels. TAP-GFP could be also exploited to identify the active motifs or amino acid residues of UL49.5 affecting TAP stability. The same platform with viral inhibitors can be applied, in a similar way as in the study by [28], to identify TAP conformation recognized by UL49.5.

Author Contributions

conceptualization, M.W. and A.D.L.; methodology, M.W. and A.D.L.; investigation, M.W., M.G, P.P., A.W.B., R.D.L., and A.D.L.; resources, A.D.L. and E.J.H.J.W.; writing—original draft preparation, A.D.L. and M.W.; writing—review and editing, A.D.L., P.P., K.B.S., and E.J.H.J.W.; visualization, M.W. and A.D.L.; supervision, A.D.L., K.B.S., and E.J.H.J.W.; project administration, A.D.L.; funding acquisition, P.P. and A.D.L.

Funding

This study was funded by Polish National Science Center, grant number UMO-2014/14/E/NZ6/00164 to A.D.L. P.P. was funded by the European Commission under the Horizon2020 program H2020 MSCA-ITN GA 675278 EDGE.

Acknowledgments

We would like to thank Dr. Michał Rychłowski, Laboratory of Virus Molecular Biology, University of Gdańsk, Poland, for help with fluorescent confocal microscopy and Dr. Robert-Jan Lebbink, Department of Medical Microbiology, University Medical Center Utrecht, The Netherlands, for help in preparation of this manuscript.

References

1. Jensen, P.E. Recent advances in antigen processing and presentation. Nat. Immunol. 2007, 8, 1041–1048.
2. Dean, M.; Annilo, T. Evolution of the ATP-binding cassette (ABC) transporter superfamily in vertebrates. Annu. Rev. Genom. Hum. Genet. 2005, 6, 123–142.
3. van Endert, P.M.; Tampé, R.; Meyer, T.H.; Tisch, R.; Bach, J.-F.; McDevitt, H.O. A sequential model for peptide binding and transport by the transporters associated with antigen processing. Immunity 1994, 1, 491–500.
4. Neefjes, J.J.; Momburg, F.; Hämmerling, G.J. Selective and ATP-dependent translocation of peptides by the MHC-encoded transporter. Science 1993, 261, 769–771.
5. Geng, J.; Sivaramakrishnan, S.; Raghavan, M. Analyses of conformational states of the transporter associated with antigen processing (TAP) protein in a native cellular membrane environment. J. Biol. Chem. 2013, 288, 37039–37047.
6. Koch, J.; Guntrum, R.; Heintke, S.; Kyritsis, C.; Tampé, R. Functional dissection of the transmembrane domains of the transporter associated with antigen processing (TAP). J. Biol. Chem. 2004, 279, 10142–10147.
7. Verweij, M.C.; Horst, D.; Griffin, B.D.; Luteijn, R.D.; Davison, A.J.; Ressing, M.E.; Wiertz, E.J.H.J. Viral Inhibition of the transporter associated with antigen processing (TAP): A striking example of functional convergent evolution. PLoS Pathog. 2015, 11, e1004743.
8. Früh, K.; Ahn, K.; Djaballah, H.; Sempé, P.; Peter, M. van Endert, P.M.; Tampé, R.; Peterson, P.A.; Yang, Y. A viral inhibitor of peptide transporters for antigen presentation. Nature 1995, 375, 415–418.
9. Tomazin, R.; Hill, A.B.; Jugovic, P.; York, I.; van Endert, P.; Ploegh, H.L.; Andrews, D.W.; Johnson, D.C. Stable binding of the herpes simplex virus ICP47 protein to the peptide binding site of TAP. EMBO J. 1996, 15, 3256–3266.
10. Oldham, M.L.; Grigorieff, N.; Chen, J. Structure of the transporter associated with antigen processing trapped by herpes simplex virus. eLife 2016, 5, e21829.

11. Ahn, K.; Gruhler, A.; Galocha, B.; Jones, T.R.; Wiertz, E.J.H.J.; Ploegh, H.L.; Peterson, P.A.; Yang, Y.; Früh, K. The ER-luminal domain of the HCMV glycoprotein US6 inhibits peptide translocation by TAP. Immunity 1997, 6, 613–621.

12. Kyritsis, C.; Gorbulev, S.; Hutschenreiter, S.; Pawlitschko, K.; Abele, R.; Tampé, R. Molecular mechanism and structural aspects of transporter associated with antigen processing inhibition by the cytomegalovirus protein US6. J. Biol. Chem. 2001, 276, 48031–48039.

13. Halenius, A.; Momburg, F.; Reinhard, H.; Bauer, D.; Lobigs, M.; Hengel, H. Physical and functional interactions of the cytomegalovirus US6 glycoprotein with the transporter associated with antigen processing. J. Biol. Chem. 2006, 281, 5383–5390.

14. Alzhanova, D.; Edwards, D.M.; Hammarlund, E.; Scholz, I.G.; Horst, D.; Wagner, M.J.; Upton, C.; Wiertz, E.J.; Slifka, M.K.; Früh, K. Cowpox virus inhibits the transporter associated with antigen processing to evade T cell recognition. Cell Host Microbe 2009, 6, 433–445.

15. Byun, M.; Verweij, M.C.; Pickup, D.J.; Wiertz, E.J.H.J.; Hansen, T.H.; Yokoyama, W.M. Two mechanistically distinct immune evasion proteins of cowpox virus combine to avoid antiviral CD8 T Cells. Cell Host Microbe 2009, 6, 422–432.

16. Luteijn, R.D.; Hoelen, H.; Kruse, E.; van Leeuwen, W.F.; Grootens, J.; Horst, D.; Koorengevel, M.; Drijfhout, J.W.; Kremmer, E.; Früh, K.; et al. Cowpox virus protein CPXV012 eludes CTLs by blocking ATP binding to TAP. J. Immunol. 2014, 193, 1578–1589.

17. Verweij, M.C.; Lipinska, A.D.; Koppers-Lalic, D.; van Leeuwen, W.F.; Cohen, J.I.; Kinchington, P.R.; Messaoudi, I.; Bienkowska-Szewczyk, K.; Ressing, M.E.; Rijsewijk, F.A.M.; et al. The capacity of UL49.5 proteins to inhibit TAP is widely distributed among members of the genus varicellovirus. J. Virol. 2011, 85, 2351–2363.

18. Koppers-Lalic, D.; Reits, E.A.J.; Ressing, M.E.; Lipinska, A.D.; Abele, R.; Koch, J.; Rezende, M.M.; Admiraal, P.; van Leeuwen, D.; Bienkowska-Szewczyk, K.; et al. Varicelloviruses avoid T cell recognition by UL49.5-mediated inactivation of the transporter associated with antigen processing. Proc. Natl. Acad. Sci. USA 2005, 102, 5144–5149.

19. Verweij, M.C.; Koppers-Lalic, D.; Loch, S.; Klauschies, F.; de la Salle, H.; Quinten, E.; Lehner, P.J.; Mulder, A.; Knittler, M.R.; Tampé, R.; et al. The varicellovirus UL49.5 protein blocks the transporter associated with antigen processing (TAP) by inhibiting essential conformational transitions in the 6+6 transmembrane TAP core complex. J. Immunol. 2008, 181, 4894–4907.

20. Koppers-Lalic, D.; Verweij, M.C.; Lipińska, A.D.; Wang, Y.; Quinten, E.; Reits, E.A.; Koch, J.; Loch, S.; Rezende, M.M.; Daus, F.; et al. Varicellovirus UL49.5 proteins differentially affect the function of the transporter associated with antigen processing, TAP. PLoS Pathog. 2008, 4, e1000080.

21. Boname, J.; May, J.; Stevenson, P. The murine gamma-herpesvirus-68 MK3 protein causes TAP degradation independent of MHC class I heavy chain degradation. Eur. J. Immunol. 2005, 35, 171–179.

22. Herr, R.A.; Wang, X.; Loh, J.; Virgin, H.W.; Hansen, T.H. Newly discovered viral E3 ligase pK3 induces endoplasmic reticulum-associated degradation of class I major histocompatibility proteins and their membrane-bound chaperones. J. Biol. Chem. 2012, 287, 14467–14479.

23. Harvey, I.B.; Wang, X.; Fremont, D.H. Molluscum contagiosum virus MC80 sabotages MHC-I antigen presentation by targeting tapasin for ER-associated degradation. PLoS Pathog. 2019, 15, e1007711.

24. Chen, X.; Zaro, J.L.; Shen, W.-C. Fusion protein linkers: Property, design and functionality. Adv. Drug. Deliver. Rev. 2013, 65, 1357–1369.

25. Praest, P.; Luteijn, R.D.; Brak-Boer, I.G.J.; Lanfermeijer, J.; Hoelen, H.; Ijgosse, L.; Costa, A.I.; Gorham, R.D.; Lebbink, R.J.; Wiertz, E.J.H.J. The influence of TAP1 and TAP2 gene polymorphisms on TAP function and its inhibition by viral immune evasion proteins. Mol. Immunol. 2018, 101, 55–64.

26. Lipińska, A.D.; Koppers-Lalic, D.; Rychlowski, M.; Admiraal, P.; Rijsewijk, F.A.M.; Bienkowska-Szewczyk, K.; Wiertz, E.J.H.J. Bovine herpesvirus 1 UL49.5 protein inhibits the transporter associated with antigen processing despite complex formation with glycoprotein M. J. Virol. 2006, 80, 5822–5832.

27. Morgenstern, J.P.; Land, H. Advanced mammalian gene transfer: High titre retroviral vectors with multiple drug selection markers and a complementary helper-free packaging cell line. Nucleic Acid Res. 1990, 18, 3587–3596.

28. Lin, J.; Eggensperqer, S.; Hank, S.; Wycisk, A.I.; Wieneke, R.; Mayerhofer, P.U.; Tampé, R. A negative feedback modulator of antigen processing evolved from a frameshift in the cowpox virus genome. PLoS Pathog. 2014, 10, e1004554.

29. Marqusee, S.; Baldwin, R.L. Helix stabilization by Glu-Lys+ salt bridges in short peptides of de novo design. Proc. Natl. Acad. Sci. USA 1987, 84, 8898–902.

30. Arai, R.; Ueda, H.; Kitayama, A.; Kamiya, N.; Nagamune, T. Design of the linkers which effectively separate domains of a bifunctional fusion protein. Protein Eng. Des. Sel. 2001, 14, 529–532.

31. Koppers-Lalic, D.; Rychlowski, M.; van Leeuwen, D.; Rijsewijk, F.A.M.; Ressing, M.E.; Neefjes, J.J.; Bienkowska-Szewczyk, K.; Wiertz, E.J.H.J. Bovine herpesvirus 1 interferes with TAP-dependent peptide transport and intracellular trafficking of MHC class I molecules in human cells. Arch. Virol. 2003, 148, 2023–2037.

32. Verweij, M.C.; Lipińska, A.D.; Koppers-Lalic, D.; Quinten, E.; Funke, J.; van Leeuwen, H.C.; Bieńkowska-Szewczyk, K.; Koch, J.; Ressing, M.E.; Wiertz, E.J.H.J. Structural and functional analysis of the TAP-inhibiting UL49.5 proteins of varicelloviruses. Mol. Immunol. 2011, 48, 2038–2051.

33. Praest, P.; de Buhr, H.; Wiertz, E.J.H.J. A flow cytometry-based approach to unravel viral interference with the MHC class I antigen processing and presentation pathway. In Antigen Processing; van Endert, P., Ed.; Springer: New York, NY, USA, 2019; Volume 1988, pp. 187–198.

34. Keusekotten, K.; Leonhardt, R.M.; Ehses, S.; Knittler, M.R. Biogenesis of functional antigenic peptide transporter TAP requires assembly of pre-existing TAP1 with newly synthesized TAP2. J. Biol. Chem. 2006, 281, 17545–17551.

35. Kleijmeer, M.J.; Kelly, A.; Geuze, H.J.; Slot, J.W.; Townsend, A.; Trowsdale, J. Location of MHC-encoded transporters in the endoplasmic reticulum and cis-Golgi. Nature 1992, 357, 342–344.

36. Van Kaer, L.; Ashton-Rickardt, P.G.; Ploegh, H.L.; Tonegawa, S. TAP1 mutant mice are deficient in antigen presentation, surface class I molecules, and CD4−8+ T cells. Cell 1992, 71, 1205–1214.

37. Antoniou, A.N.; Ford, S.; Pilley, E.S.; Blake, N.; Powis, S.J. Interactions formed by individually expressed TAP1 and TAP2 polypeptide subunits. Immunology 2002, 106, 182–189.

38. Xia, D.; Tang, W.K.; Ye, Y. Structure and function of the AAA+ ATPase p97/Cdc48p. Gene 2016, 583, 64–77.

39. Herbring, V.; Bäucker, A.; Trowitzsch, S.; Tampé, R. A dual inhibition mechanism of herpesviral ICP47 arresting a conformationally thermostable TAP complex. Sci. Rep. 2016, 6, 36907.

40. Marguet, D.; Spiliotis, E.T.; Pentcheva, T.; Lebowitz, M.; Schneck, J.; Edidin, M. Lateral diffusion of GFP-tagged H2Ld molecules and of GFP-TAP1 reports on the assembly and retention of these molecules in the endoplasmic reticulum. Immunity 1999, 11, 231–240.

41. Reits, E.A.J.; Vos, J.C.; Grommé, M.; Neefjes, J. The major substrates for TAP in vivo are derived from newly synthesized proteins. Nature 2000, 404, 774–778.

42. Kobayashi, A.; Maeda, T.; Maeda, M. Membrane localization of transporter associated with antigen processing (TAP)-like (ABCB9) visualized in vivo with a fluorescence protein-fusion technique. Biol. Pharm. Bull. 2004, 27, 1916–1922.

43. Ghanem, E.; Fritzsche, S.; Al-Balushi, M.; Hashem, J.; Ghuneim, L.; Thomer, L.; Kalbacher, H.; van Endert, P.; Wiertz, E.; Tampe, R.; et al. The transporter associated with antigen processing (TAP) is active in a post-ER compartment. J. Cell Sci. 2010, 123, 4271–4279.

44. Karska, N.; Graul, M.; Sikorska, E.; Zhukov, I.; Ślusarz, M.J.; Kasprzykowski, F.; Lipińska, A.D.; Rodziewicz-Motowidło, S. Structure determination of UL49.5 transmembrane protein from bovine herpesvirus 1 by NMR spectroscopy and molecular dynamics. BBA Biomembr. 2019, 1861, 926–938.

45. Vos, J.C.; Spee, P.; Momburg, F.; Neefjes, J. Membrane topology and dimerization of the two subunits of the transporter associated with antigen processing reveal a three-domain structure. J. Immunol. 1999, 163 6679–6685.

46. Schrodt, S.; Koch, J.; Tampé, R. Membrane topology of the transporter associated with antigen processing (TAP1) within an assembled functional peptide-loading complex. J. Biol. Chem. 2006, 281, 6455–6462.

47. Lankat-Buttgereit, B.; Tampé, R. The transporter associated with antigen processing (TAP): A peptide transport and loading complex essential for cellular immune response. In ABC Proteins: From Bacteria to Man; Holland, B., Cole, S.P.C., Kuchler, K., Higgins, C.F., Eds.; Academic Press, Cambridge, MA, USA: 2003; pp. 533–550.

48. Kageshita, T.; Hirai, S.; Ono, T.; Hicklin, D.J.; Ferrone, S. Down-regulation of HLA class I antigen-processing molecules in malignant melanoma. Am. J. Pathol. 1999, 154, 745–754.

49. Matschulla, T.; Berry, R.; Gerke, C.; Döring, M.; Busch, J.; Paijo, J.; Kalinke, U.; Momburg, F.; Hengel, H.; Halenius, A. A highly conserved sequence of the viral TAP inhibitor ICP47 is required for freezing of the peptide transport cycle. Sci, Rep. 2017, 7, 2933.

Supplementary Material

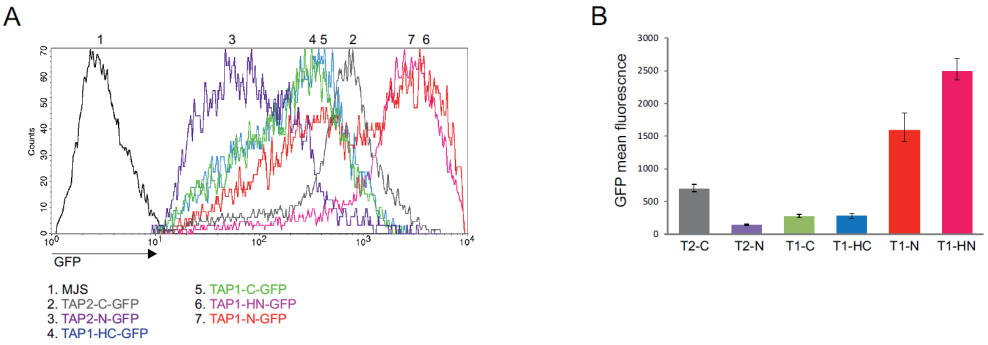

Figure S1: Comparison of GFP fluorescence of TAP-GFP variants in HEK293T cells. HEK293T cells were transfected with plasmids encoding different TAP-GFP variants. A. Fluorescence intensity was analyzed by flow cytometry. B. GFP mean fluorescence was analyzed by flow cytometry; the statistical significance was assessed by t-test; p≤0,01.

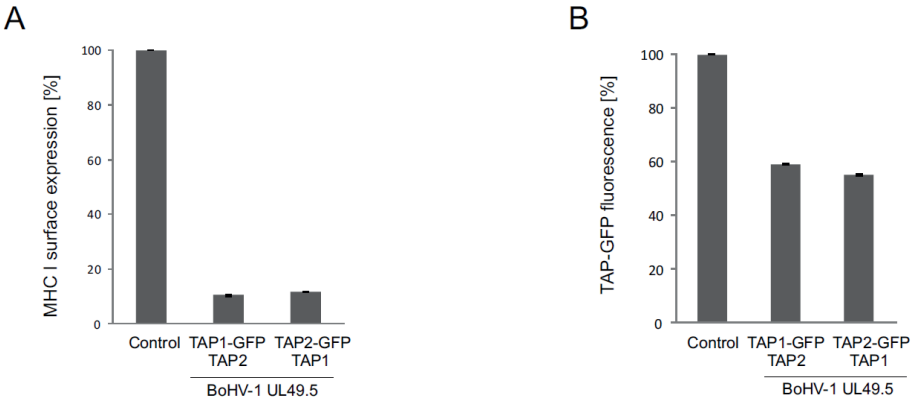

Figure S2: Susceptibility of TAP-GFP expressed in reconstituted U937 cells to UL49.5-mediated inhibition and degradation. U937 TAP1 and TAP2 KO cells reconstituted with a combination of a fluorescent and an unmodified TAP subunit were transduced with a retrovirus encoding BoHV-1 UL49.5. A. Surface expression of MHC I was assessed by flow cytometry using specific antibodies (W6/32). MHC I expression is presented as the percentage of mean fluorescence intensity; fluorescence of parental cells without UL49.5 was set as 100%. The analysis was performed in triplicates. The statistical significance of differences between U937 TAP-GFP and U937 TAP-GFP UL49.5 cell lines was estimated by t-test; p≤0,001. B. GFP mean fluorescence intensity is presented as the percentage of GFP fluorescence of parental cells (set as 100%). The analysis was performed in triplicates. The statistical significance of differences between U937 TAP-GFP and U937 TAP-GFP UL49.5 cell lines was estimated by t-test; p≤0,001. Abbreviations:TAP1-GFP – TAP1-HC-GFP; TAP2-GFP – TAP2- N-GFP.

Appendices

Dutch Summary
Acknowledgements
About the author
List of Publications

Nederlandse Samenvatting

Herpesvirussen gebruiken een breed scala aan immuunmodulerende mechanismen om te ontsnappen aan het afweersysteem, waardoor levenslange infecties ontstaan met deze virussen. Momenteel zijn er negen herpesvirussen waarvan de mens de natuurlijke gastheer is: herpes simplex-virus type 1 en 2 (HSV-1 en HSV-2, ook wel humaan herpesvirus 1 en 2 (HHV-1 en HHV-2) genoemd), varicella-zoster virus (VZV of HHV-3), Epstein-Barr-virus (EBV of HHV-4), humaan cytomegalovirus (HCMV of HHV-5), humaan herpesvirus 6A, 6B en 7 (HHV-6A / B en HHV-7) en Kaposi-sarcoom-geassocieerd herpesvirus (KSHV of HHV-8). Deze menselijke herpesvirussen worden geassocieerd met een grote verscheidenheid aan ziekten. Meestal verlopen primaire infecties asymptomatisch en worden ze vaak niet opgemerkt bij gezonde personen. Reactivatie bij gezonde personen en infecties bij immuungecompromitteerde mensen kunnen echter tot ernstige ziekten leiden.

De langdurige co-evolutie van ziekteverwekker en gastheer heeft geresulteerd in een groot aantal virale eiwitten die fungeren als "immuunontduikers" (*evasins*). In dit proefschrift bestuderen we de interacties tussen virale *evasins* en gastheereiwitten en proberen we te begrijpen hoe deze *evasins* essentiële processen in de gastheer beïnvloeden.

De "Transporter associated with antigen processing" (TAP) is vaak een doelwit van virale immuunontwijkingsstrategieën. Deze ER-residente transporter is samengesteld uit de eiwitten TAP1 en TAP2 (TAP heterodimeer). TAP speelt een cruciale rol bij het laden van virale peptiden op MHC klasse I-moleculen. Deze MHC klasse I moleculen presenteren peptiden aan witte bloedlichaampjes (zogenaamde cytotoxische T-lymfocyten); als deze cellen een virus-gecodeerd peptide herkennen zullen zij de virus-geïnfecteerde cel opruimen. Er bestaan verschillende varianten (polymorfismen) van TAP1 en TAP2 in de menselijke populatie. Sommige varianten zijn eerder in verband gebracht met auto-immuunziekten en gevoeligheid voor infecties. In **hoofdstuk 2** hebben we de invloed van natuurlijk voorkomende TAP-varianten ("polymorfismen") op peptidetransport en MHC klasse I-expressie bestudeerd.

Daarnaast hebben we het remmend vermogen van drie virale immuunontduikingseiwitten getest: de TAP-remmers US6 van HCMV, ICP47 van HSV-1 en BNLF2a van EBV, voor een reeks TAP1- en TAP2-varianten. Onze resultaten suggereren dat deze TAP-polymorfismen geen of een beperkt effect op peptidetransport of MHC klasse I-expressie hebben. Bovendien geeft onze studie aan dat de door herpesvirus gecodeerde TAP-remmers zich op een breed spectrum van TAP-varianten richten; remming van TAP wordt niet beïnvloed door de polymorfismen van TAP die in deze studie zijn getest. Op grond van deze bevindingen zou men kunnen speculeren over (het ontbreken van) een bijdrage van herpesvirussen

aan de selectie van TAP varianten tijdens de langdurige co-evolutie van deze virussen met hun gastheer.

In **Hoofdstuk 3** beschrijven we een methode die kan worden gebruikt voor de identificatie van virale genproducten die mogelijk verantwoordelijk zijn voor ontwijking van MHC klasse I-specifieke antigeenpresentatie. De genen die van belang zijn worden in het lab in cellijnen tot expressie gebracht door middel van lentivirale transductie. Vervolgens wordt MHC I expressie op het celoppervlak gemeten met MHC klasse I-specifieke antilichamen, door middel van flowcytometrie. Zodra een virale genproduct dat verantwoordelijk is voor MHC I-downregulatie is geïdentificeerd, kunnen dezelfde cellen worden gebruikt om het werkingsmechanisme op te helderen. Met behulp van specifieke assays kunnen we uitzoeken in welk stadium van de antigeenverwerking de storing plaatsvindt. Virussen richten zich vaak op een essentiële stap: de translocatie van peptiden van het cytoplasma naar de ER via TAP.

De TAP-functie kan worden gemeten met behulp van een zeer specifieke *in vitro* flowcytometrische assay, waarbij de import van een fluorescend peptidesubstraat wordt gemeten. Virus-gecodeerde MHC klasse I-remmers die de verwerking en presentatie van antigeen belemmeren kunnen worden geïdentificeerd met deze methode. Vervolgens kan hun werkingsmechanisme worden ontrafeld; deze kennis kan onder meer worden gebruikt om stoffen te ontwikkelen waarmee de afweer actief kan worden geremd. Op TAP gelijkende transporters spelen ook een rol bij de resistentie van bacteriën tegen antibiotica en de resistentie van kankercellen tegen cytostatica. Kennis over de remming van de "peptidenpomp" TAP door viruseiwitten kan van nut zijn voor het ontwerpen van remmers die selectief vergelijkbare "pompen" remmen in bacteriën en kankercellen .

In **Hoofdstuk 4** vatten we recente structurele en functionele inzichten in de moleculaire architectuur van het PLC samen. We schetsen hoe TAP het transport van peptiden over het ER-membraan bewerkstelligt en hoe herpes- en pokkenvirussen het peptidentransport door TAP en daaropvolgende antigeenpresentatie remmen. Huidige structurele informatie werd gecombineerd in een model voor het PLC. Dit model werd later bevestigd via cryo-elektronenmicroscopie in een onafhankelijk onderzoek. Verder hebben we op basis van de structuren van andere transporters structurele informatie over de transportcyclus van TAP kunnen extrapoleren.

Hoewel de moleculaire mechanismen die ten grondslag liggen aan virale targeting van het PLC eerder zijn bestudeerd, ontbreekt het veelal aan gedetailleerde structurele studies over deze interacties. In **Hoofdstuk 5** willen we de moleculaire interacties tussen TAP en TAP-remmers van verschillende grote DNA-virussen bestuderen, waaronder

ICP47 van het HSV-1, BNLF2a van het EBV en US6 van het HCMV. Met behulp van *single-particle* cryo-elektronenmicroscopie (cryo-EM) willen we onderzoeken waar de interactie plaatsvindt, en hoe de peptidetransportcyclus op structureel niveau wordt beïnvloedt. In dit hoofdstuk wordt de aanpak voor dit onderzoek beschreven.

In **Hoofdstuk 6** identificeren we een peptide afkomstig van het koepokkenvirus-eiwit CPXV012 als een breed-spectrum antiviraal peptide. We ontdekten dat dit CPXV012-peptide de infectie door een groot aantal klinisch en economisch belangrijke virussen belemmert, waaronder pokkenvirussen, herpes simplex-virus-1, hepatitis B-virus, HIV-1 en Rift Valley-koortsvirus. Het gemeenschappelijk kenmerk van deze visussen is de aanwezigheid van een omhulsel of mantel. Infecties door virussen zonder mantel, zoals het Coxsackie B3-virus en adenovirus, worden niet beïnvloed. De resultaten duiden erop dat directe interacties met het CPXV012-peptide de virale deeltjes kunnen neutraliseren. Er zijn ook aanwijzingen dat dit kationische peptide specifiek kan binden aan membranen samengesteld uit het anionische fosfolipide fosfatidylserine (fosfatidylserine is een belangrijk bestanddeel van veel virale membranen). Onze resultaten wijzen er sterk op dat het CPXV012-peptide virusinfecties kan remmen door directe interacties met fosfatidylserine in de virale envelop. Deze resultaten laten de potentie zien van kationische peptiden als breedwerkende virusremmers.

In **Hoofdstuk 7** hebben we twee HCMV *evasins* nader bekeken. De eiwitten US2 en US11 "kapen" het ER-geassocieerde proteïneafbraakproces om nieuw gesynthetiseerde HLA klasse I-moleculen af te breken (HLA is hetmenselijke MHC klasse I). Omdat antigeenpresentatie verhinderd wordt, kan het virus T-celherkenning van virus-geïnfecteerde cellen ontwijken. Meerdere cellulaire eiwitten zijn cruciaal voor US2- en US11-gemedieerde HLA klasse I-afbraak. Echter, de eiwitkanalen waar doorheen HLA-I-moleculen van het ER naar het cytosol worden geleid - retrotranslocatie of dislocatie genoemd - zijn nog niet geïdentificeerd. Ook zijn de *dislocon*-kanalen, die betrokken zijn bij de dislocatie van endogene substraten in een fysiologische setting, nog onbekend.

In deze studie willen we de eiwitten die het dislocon-kanaal vormen identificeren aan de hand van co-immunoprecipitatie-onderzoeken. We hebben eiwit-eiwitinteracties tussen het SEC-translocatiecomplex, P97, HRD1, Derlin1 en het proteasoom kunnen identificeren. Deze interacties suggereren dat het SEC61-complex zelf betrokken zou kunnen zijn bij eiwitdislocatie. We hebben echter geen interactie van SEC61 met HLA klasse I-moleculen kunnen bevestigen, ongeacht de afwezigheid of aanwezigheid van US2. Dit houdt mogelijk verband met de cellijnen die voor dit onderzoek zijn gebruikt: in deze cellen is het afbraakintermediair van HLA klasse I, dat eerder in een complex met SEC61 werd waargenomen, niet gevonden. Het onderzoek zal daarom moeten worden

herhaald in cellijnen waarin dit afbraakintermediair wel kan worden aangetroffen. Het is ook mogelijk dat de HLA klasse I-moleculen via een alternatief kanaal het ER verlaten. In aanwezigheid van US2 bleek geübiquitineerd HLA klasse I te binden aan het E3-ligase TRC8, het ATPase P97 en het proteasoom. Deze bevindingen suggereren dat TRC8 een dubbele rol speelt: het kan als E3-ligase fungeren, en als een component van het *dislocon* bij US2-afhankelijke afbraak van HLA klasse I.

In **Hoofdstuk 8** worden alle bevindingen van dit proefschrift samengevat en wordt besproken hoe toekomstig onderzoek kan leiden tot een beter begrip van de immuunontduiking van herpesvirussen en de ontwikkeling van nieuwe behandelmethoden.

Dankwoord / Acknowledgements

Emmanuel, I met you right in the best moment. My interest in the field of virology was growing and during my internship at the MMB in 2015 I got the opportunity to learn a lot of new techniques. Apparently, I made a not too bad impression and I was 'allowed' to come back for a little longer. This PhD position gave me the chance to build up a network and get to know many nice people. You gave me the freedom of working on a slightly different subject than initially planned and always supported my ideas and suggestions. Your positive energy and happy mood helped a lot, also in times when the experiments didn't go as planned.

Robert Jan, thank you so much for all the (scientific and non-scientific) talks we had from time to time. You taught me how to use certain methods and you were patient when people didn't understand things in the first place. You always aim for new techniques and alternative experiments to get to certain results. Your realistic and always critical attitude helped a lot during my PhD and I am happy that I got the chance to learn so many things from you.

Ingrid, thank you so much for all your help and patience during my PhD. Some of these chapters would not have been possible without your super efficient planning and persistence of getting the perfect blots. I am thankful for the time we worked together and for your honest and direct way of saying and handling things. I was always surprised about the amount of results you showed me for our projects while working only three days a week plus the coffee time in between, supervising students and solving general lab issues.

Ana, I will miss it to quickly drop by at your office and have a chat. You did so much for me at the end of my PhD and also for this book. You helped me getting the right statistics for publications, you rewrote manuscript to address reviewer comments, you arranged so many small things on the side for me…I think I could make an endless list of things where you supported me. I wish you all the best for the future and I really hope we will stay in contact =)

Hendrik, danke für nichts! (den werden so einige glaube ich nicht verstehen haha) Ok, Spaß beiseite…Ich bin wirklich froh, dass du bei uns in der Gruppe angefangen hast. Wir haben durch Meetings, Konferenzen und private Events schon so diverse Eckchen von der Welt zusammen bereist und gesehen. Dabei haben wir so einige lustige, verrückte und spaßige Dinge erlebt. Vielleicht sollten wir 2028 noch einmal den West Coast Trail machen um unsere Bojen wieder zu suchen und natürlich für die romantischen Nächte zusammen

im Zelt ;) Danke für die gemeinsame Zeit und die gemeinsamen Momente, die wir bisher hatten, als Arbeitskollegen, Travelbuddy's und Freunde.

Lisette, I hope you still have that lovely bacteria plate that I made for you. It took me some attempts go get it so nice haha. I will really miss sitting next to you in the lab. I will miss all the serious scientific talks we had for sure (did we even have some?) and the 'non-scientific' fun discussions every now and then as well. I really hope that the German flag will stay on top of the Dutch one. I will come by and check!

Ingo, ohne dich wäre ich nie am UMCU gelandet. Du hast mir damals die Chance gegeben, während meines Master Studiums ins „Ausland" für ein Praktikum zu gehen. Die Zeit in der Virologie in Düsseldorf hat mir viel Erfahrung eingebracht, die ich hoffentlich noch weiterhin in meinem Leben nutzen kann. Ich hoffe, die gute Zusammenarbeit zwischen den beiden Arbeitsgruppen hält noch lange an und dass ihr noch einige spannende Entdeckungen in der Pocken-, Herpes- und TAP-Welt haben werdet.

The RON, wRONg, ROW or what so ever room: My (ex)roomies Jasper, Nienke, Seline, Dani, Ron, Leire, Hendrik, Sjors, Guus, Coco…we had so much fun in the office together. Too bad that we couldn't dress up one last time together to win another best group-costume price. I will really miss the inspiring sound and the vibrations of the centrifuge next door; it really helped me concentrating a lot during work. Thanks for all the support, the fun moments, the 'dog of the day' discussions, the 'monkey on the car', all the treats you guys brought into the office and many, many more things!

Friedrich, thank you for the collaboration on different projects and for many helpful meetings and suggestions for our experiments. My fingers are crossed that we will obtain nice structures from the different TAP inhibitors!

Rutger, too bad you already left so early after I started my PhD…thank you for your time and patience during my internship and for all the tips (yes, also the pipet tips) and tricks in the lab! With our first project together you had paved the way for my future research and other projects from this thesis.

Wiertz Group and Ex-Wiertz Group Members (Jasper, Ferdy, Anouk, Rutger, Michiel, Hendrik, Shu, Anouk, Ingrid, Ana, Elisabeth and all students over the time), thank you for all your support, help with experiments, fruitful (like Emmanuel would say) meetings and time together.

My Students, thank you for your time, effort and enthusiasm. Your work contributed to different chapters of this book. **Jet**, my first student. You always brought a happy and

funny mood to work and I must admit I was a bit scared of supervising my first student. Even though it was only for a short time I hope that you also enjoyed it (I think you did, otherwise you wouldn't have been back for almost another year ;)). **Klasina**, I must say I never heard your name before in my life. Thank you for your contribution on the ERAD chapter! I hope you're doing alright on the other side of the world. I already miss all the 'bullshit' talks we had. Happy partying in Australia (and also good luck for the internship for sure). **Sara**, you brought quite some fresh energy into our group. I think Emmanuel, Ingrid and I were all surprised how fast and well you worked independently and also showed us publication grade figures with your own data. Keep on going that way and good luck for your future!

Axel, thanks for suffering with me in the last weeks of the writing and the submission of the thesis as well as getting through all that 'deadline jungle'.

Manuel, danke für eine so tolle Zusammenarbeit. Ich hoffe, dass die Projekte weiterhin gut weiterlaufen und dass wir noch die eine oder andere Struktur zu Gesicht bekommen werden. Genauso wie wir, seid Susi und du gerne am erkunden der Welt; deswegen bin ich schon gespannt, in welches außergewöhnliche Land eure nächste Reise geht.

Panos and Hanneke, a big thanks to all the work and effort you put into the TAP project. Without all these optimization steps over and over again we wouldn't be so far. I wish you good luck for your future careers!

Juliette, thanks a lot for working with me/us on some initial experiments on the ERAD story. I would be very happy if the collaboration will continue, also without me.

Jelle and Piet, I will really miss all your stupid but super funny word jokes and comments. I hope you will always continue with them because the whole department benefits from your good mood and positive energy.

All OIO's and other colleagues from the MMB, thank you for a great time in the department, during meetings, on conferences and other events. I will miss the 'coffee is ready in 10 minutes' and the cakes every now and then on Thursday's.

The TC de Uithof, a club that not only offered me a position in one of their teams, but also gave me the opportunity to get to know many people who I can call my friends now. I enjoyed all the activities on and also off the court with you guys. **Irene**, you made it possible for me to join the club. **Simon**, you asked me for a 'double-date' right away and we had some awesome tournaments together. **Teamies**, the spring and also fall competition were always the highlight of the year, I will miss these.

Patrick und Björn, in den letzten Jahren haben wir einiges zusammen unternommen, konnten über alles quatschen und haben immer versucht, uns regelmäßig zu sehen. Ich bin froh, euch damals an der Uni in Düsseldorf kennen gelernt zu haben und hoffe auf noch die ein oder anderen Events, Reisen oder sonstige Sachen (Bierchen) zusammen!

Liebe Familie (Oma('s), Waltraud, Sigrid, Oliver, Lennart, Marco, Astrid, Phillip und Simon), ich habe mich wahnsinnig darüber gefreut, dass ihr alle sofort zugesagt habt, als ich euch für meine Doktorverteidigung eingeladen habe. Vielen Dank für jegliche Unterstützung in den letzten Jahren, die ich in vielerlei Formen von euch erhalten habe.

Ulfert und Gabi, ich habe euch vor 7 Jahren kennen gelernt und wurde direkt mit einem Schnaps begrüßt. Dieser sympathische erste Eindruck bleibt bis heute bestehen (auch ohne Alkohol ;))! Ihr habt mir gleich das Gefühl gegeben, Teil eurer Familie zu sein und behandelt alle Schwiegerkinder wie eure eigenen. Ich bin dankbar für all die tollen Momente, die wir zusammen erlebt haben, und werde sie für immer in Erinnerung behalten. Der starke Zusammenhalt in der Familie ist etwas sehr Tolles, was auch für immer so bleiben sollte, auch wenn du, Gabi, unglaublich fehlst.

Mama und Papa, ich weiß gar nicht, wo ich anfangen soll mich zu bedanken. Ihr habt mich immer unterstützt, egal ob es sportlich, privat oder beruflich ist/war. Ihr habt mir die Chance gegeben, das zu machen, was ich wollte. Kein Weg war zu weit, um etwas für mich zu erledigen, oder mich irgendwo hin zu fahren. Ich bin stolz, euch meine Eltern nennen zu dürfen und dass ihr mir all dies ermöglicht habt.

Svenja, wir kennen uns nun schon ein gefühltes halbes Leben lang. Wir haben schon viel erlebt, viele Orte bereist und auch schwierige Zeiten zusammen überstanden. Du hast mich immer unterstützt und mich immer motiviert, falls ich gerade mal nicht so wirklich aus dem Quark kam. Selbst bei meiner Doktorarbeit hast du mitgeholfen, indem du Kapitel Korrektur gelesen hast oder mich daran erinnert hast, dass es doch mal wieder Zeit ist, etwas mehr zu schreiben, um Deadlines einzuhalten. Ich genieße die Zeit mit dir an meiner Seite und hoffe, dass wir noch ein langes Leben miteinander verbringen können. Ik hou van jou!

About the author

Thomas Patrique Praest was born on 15th October 1991 in Bocholt, Germany. In summer 2010 he graduated from the high school Gymnasium Aspel (Rees, Germany) and started the bachelor's program in informatics at Heinreich Heine University Düsseldorf. In 2011 he changed the course of study and continued with the bachelor's program in Biology. Patrique discovered his interest in the field of virology when working on his bachelor's thesis in the working group of Prof. Dr. Ingo Drexler (Molecular Virology) at the Department of Virology (University Hospital Düsseldorf). The topic of his bachelor's thesis was 'The characterization of recombinant MVA vectors with different expression kinetics of the fusion protein mCherry/ovalbumin'. In 2014 Patrique obtained the Bachelor of Science degree in Biology and continued with the master's degree course in Biology. During his studies he received an Erasmus+ grant and performed an internship in the department of Medical Microbiology at the University Medical Center Utrecht in the Netherlands. Under the supervision of Prof. Dr. Ingo Drexler, Prof. Dr. Emmanuel Wiertz and Dr. Rutger Luteijn he started his research for his master's thesis with the topic 'The role of the ABCB9 transporter associated with antigen processing-like (TAPL) in presentation of viral antigens'. Patrique was awarded the Master of Science degree in Biology on 26th of September 2016 and subsequently started his PhD position on 1st October at the Department of Medical Microbiology at the University Medical Center Utrecht in the Netherlands. This PhD position was part of the Marie Skłodowska-Curie Innovative Training Network 'EDGE' for early stage researchers funded by the European Commission under the H2020 program. Patrique was supervised by Prof. Dr. Emmanuel Wiertz and Dr. Robert Jan Lebbink and the results of this research are described in this thesis and parts have been published in various international scientific journals.

List of Publications

Praest P., Luteijn R.D., Brak-Boer I.G.J., Lanfermeijer J., Hoelen H., Ijgosse L., Costa A.I., Gorham R.D., Lebbink R.J., & Wiertz E.J.H.J. (2018). The influence of TAP1 and TAP2 gene polymorphisms on TAP function and its inhibition by viral immune evasion proteins. Molecular Immunology, 101. https://doi.org/10.1016/j.molimm.2018.05.025

Praest P., Liaci A.M., Förster F., & Wiertz E.J.H.J. (2019). New insights into the structure of the MHC class I peptide-loading complex and mechanisms of TAP inhibition by viral immune evasion proteins. Molecular Immunology, 113, 103–114. https://doi.org/10.1016/j.molimm.2018.03.020

Praest P., de Buhr H., & Wiertz E.J.H.J. (2019). A flow cytometry-based approach to unravel viral interference with the MHC class I antigen processing and presentation pathway. In Methods in Molecular Biology (Vol. 1988). https://doi.org/10.1007/978-1-4939-9450-2_14

Wąchalska M., Graul M., **Praest P.,** Luteijn R. D., Babnis A. W., Wiertz E.J.H.J., Bieńkowska-Szewczyk K., & Lipińska A. D. (2019). Fluorescent TAP as a Platform for Virus-Induced Degradation of the Antigenic Peptide Transporter. Cells, 8(12), 1590. https://doi.org/10.3390/cells8121590

Saravanan M.S., Ryazanov S., Leonov A., Nicolai J., **Praest P.,** Giese A., Winter R., Khemtemourian L., Griesinger C., & Killian J.A. (2019). The small molecule inhibitor anle145c thermodynamically traps human islet amyloid peptide in the form of non-cytotoxic oligomers. Scientific Reports, 9(1), 1–12. https://doi.org/10.1038/s41598-019-54919-z

Praest P., Liaci A.M., Leegwater H., Drougkas P., Lebbink R.J., Foerster F., Wiertz E.J.H.J. Paving the road to a structural elucidation of the TAP mediated peptide transport cycle by Cryo-EM. Manuscript in preparation.

Luteijn R.D., Thiele F., **Praest P.,** Sadasivam S.M., Singethan K., Drijfhout J.W., Bach C., de Boer S.M., van Kuppeveld F.J., Tao S., Helfer M., Bach N., Protzer U., Costa A.I., Killian J.A., Drexler I., Wiertz E.J.H.J. A broad-spectrum antiviral peptide blocks infection of viruses by binding to phosphatidylserine in the viral envelope. Submitted for publication.

Praest P., Brak-Boer I.G.J., Blanken S.L., Fedry J., Chappin K., Schuren A.B.C., Costa A.I., Foerster F., Lebbink R.J., Wiertz E.J.H.J. Identifying Sec61 and TRC8 as components of a dislocation complex involved in ER-associated degradation (ERAD). Manuscript in preparation.